



UNIVERSITA' DEGLI STUDI DI MILANO
FACOLTA' DI SCIENZE DEL FARMACO
Department of Pharmaceutical Sciences
PhD Course in Pharmaceutical Sciences (XXX Cycle)

**Constrained β -amino acids as molecular tools for the
preparation of foldamers**

Tutor: Prof. Maria Luisa GELMI

Coordinator: Prof. Giancarlo ALDINI

PhD Thesis of:
Raffaella Bucci
R10893

Academic year 2016/2017

*'No longer scared of the dark, because sun comes back;
it was Copernicus who explained this'*

Jacques Dubochet,
Nobel Prize in Chemistry, 2017

Acknowledgement

I want to express my deeply-felt thanks to my Supervisor, Prof. Maria Luisa Gelmi, for her warm encouragement and guidance. I would also like to express my gratitude to Dr. Sara Pellegrino for her constant support in these three years. I appreciated all their contributions of time, ideas and teaching, that made my PhD experience productive and stimulating.

A special thanks is given to all my colleagues and students who worked with me. In these 3 years the group has been a source of friendship and collaborative support.

I wish to sincerely thank Helma Wennemers for accepting me in her group at ETH Zurich as a visiting PhD student. Spending seven months in such a multidisciplinary environment has been an amazing experience, which will inspire my future in science.

A grateful acknowledgement to all my collaborators, mentioned in this thesis, who supported my research activity: Dr. Alessandro Contini and Prof. Gandolfi, from Università degli Studi di Milano, Prof. Meital Reches, from University of Jerusalem and Dr. Marco Feligioni, from EBRI, Rome.

Finally, I would like to thank my family: my parents for all their support, my roommate and sister for having been my light that has always guided me home and my love Alberto for giving me all the faithful support that I needed and for being to me an example of dedication in the scientific research.

Contents

Table of Abbreviations.....	7
General introduction	1
β -Amino Acids.....	13
Acyclic β-amino acids	13
Cyclic β-amino acids	15
β-Peptides and α,β-Hybrid Peptides Secondary Structure	16
Biological and pharmaceutical applications	22
Nanomaterial applications.....	24
Aim of the thesis.....	27
Tetrahydroisoquinoline-4-carboxylic Acid/β-Alanine as flexible reverse turn mimic	29
Aim of the project.....	31
Synthesis.....	33
β-TIC synthesis	33
Enzymatic resolution of N-Boc derivative 5.....	34
Peptide synthesis	36
NMR study and computational analysis of (+)-13 and (-)-14 model peptides	38
Experimental part.....	44
Synthesis of ethyl isoquinoline-4-carboxylate (3)	44
Synthesis of ethyl 1,2,3,4-tetrahydroisoquinolin-4-carboxylate AcOH (4)....	44
Synthesis of 1,2,3,4-Tetrahydroisoquinoline-2-carboxylic Acid ·HCl (1).....	45
Synthesis of Ethyl N-Boc-1,2,3,4-tetrahydroisoquinolin-4-carboxylate (5)...	45
Enzymatic resolution of compound 5 with Pronase.....	46
Recycle of the enantio-enriched acid (+) 6 to racemic 5	47
Synthesis of Ethyl (R)-1,2,3,4-tetrahydroisoquinolin-4-carboxylates CF ₃ CO ₂ H (-)4.....	47
Synthesis of Fmoc-(L)-Ala-(R)-TICOEt (-)-11	48
Synthesis of Fmoc(L)Ala-(R)TIC-OH (-)-12	49

Synthesis of β -Ala-(L)ValOBn (10)	50
Synthesis of Fmoc(L)Ala-TIC- β Ala-(L)Val-OBn (+)-13.....	51
Synthesis of Fmoc(L)Ala-TIC- β Ala-(L)Val-OBn (+)-13 and (-)-14.	56
Morpholine β -amino acid as γ -turn inducer.....	61
Aim of the project.....	63
γ -turn	66
Synthesis.....	68
Morph β -AA synthesis.....	68
Peptide synthesis	70
Computational analysis and NMR study of compounds 8, 8a, 10, 13.....	73
Computational analysis of compound 17.....	73
NMR analysis of tripeptide 17	74
NMR analysis of tripeptide 17a	76
NMR analysis of pentapeptide 19.....	78
NMR analysis of hexapeptide 13	80
Experimental part.....	83
Synthesis of ‘3-hydroxy-2-(1-methoxy-2-oxoethoxy)propanal’ (12).....	83
Synthesis of ‘2S,6S-(4-benzyl-6-methoxymorpholin-2-yl)methanol’ (13)	83
Synthesis of 2S,6S-(4-Boc-6-methoxymorpholin-2-yl)methanol’ (15).....	84
Synthesis of ‘2S,6S-(4-Boc-6-methoxymorpholin-2-yl)carboxylic Acid (1) .	84
Synthesis of ‘N-Boc-Leu-Val-CONH ₂ ’	85
Synthesis of ‘NH ₂ -Leu-Val-CONH ₂ ’ (16).....	86
Synthesis of ‘N-Boc-Morph β -Leu-Val-CONH ₂ ’ (17).....	86
Synthesis of ‘CF ₃ COO ⁻ (NH ₃ -Morph β -Leu-Val-CONH ₂)’ (18)	91
Synthesis of ‘N-Boc-Val-Gly-OBn’	91
Synthesis of ‘N-Boc-Val-Gly-OH’	92
Synthesis of ‘N-Boc-Val-Gly-Morph β -Leu-Val-CONH ₂ ’ (19)	92
Synthesis of ‘N-Boc-Leu-Val-OBn’	100
Synthesis of ‘NH ₂ -Leu-Val-OBn’ (16a)	101

Synthesis of 'N-Boc-Morph β -Leu-Val-OBn' (17a)	101
Synthesis of 'NH-Morph β -Leu-Val-OBn' (21).....	106
Synthesis of 'N-Boc-Morph β -Leu-Val-OH' (20).....	106
Synthesis of 'N-Boc-Morph β -Leu-Val-Morph β -Leu-Val-OBn' (22).....	107
2,3-Diaryl- β -amino acid for the preparation of α,β Foldamers and its use for nanomaterial application	119
Aim of the project.....	121
Peptide synthesis.....	122
Model peptide characterization	125
Solid state (X-ray analysis) of 3b-D2	125
NMR Characterization	126
Characterization of 3a-(D1) and 3b-(D2).....	126
NMR Characterization of tetrapeptide 6a-(D1)	128
NMR Characterization of hexapeptide 8a-(D1).....	130
Nanomaterial application	133
Self-assembly of an amphipathic $\alpha\beta$ -tripeptide into cationic spherical particles for intracellular delivery.....	133
Literature overview of Cationic Nanoparticles	135
Result	136
Synthesis and self-assembly studies	136
Nanoparticles characterization.....	137
Experimental part.....	147
Synthesis of amino acid syn-1	147
Synthesis of amino acid syn-2	148
Synthesis of compounds 3a-(D1) and 3b-(D2)	148
Synthesis of compound NH ₃ ⁺ -D1-OH and NH ₃ ⁺ -D2-OH	150
Synthesis of compound 4a-(D1) and 4b-(D2).....	150
Synthesis of compound 5a-(D1) and 5b-(D2).....	151
Synthesis of compound 6a-(D1) and 6b-(D2).....	152
Synthesis of 7a-(D1) and 7b-(D2).....	156

Synthesis of compound 8a-(D1) and 8b-(D2).....	156
Synthesis of compound T2R.....	160
Pronase stability of T2R.....	163
Novel bicyclic Δ^2 -isoxazoline derivatives as potential turn inducers in peptidomimetic syntheses	165
Aim of the project.....	167
Overview on [1,3]-cycloaddition reaction	168
Synthesis.....	170
Synthesis of isoxazoline containing scaffold.....	170
[1,3] Cycloaddition studies: synthesis of Δ^2 -isoxazoline-fused pyrroline derivatives	172
Preliminary studies on mechanism of the key step [1,3]- cycloaddition reaction: NMR and computational study	174
Peptide synthesis.....	179
Characterization by NMR spectroscopy of tripeptides compound 12b and 12a	181
Experimental part.....	186
Synthesis of ‘(S)-(tert-butoxycarbonyl)-L-phenylalaninate’ (2).....	186
Synthesis of ‘tert-butyl (1-oxo-3-phenylpropan-2-yl)carbamate’ (5).....	186
Synthesis of ‘tert-butyl (S)-(1-hydroxy-3-phenylpropan-2-yl)carbamate’ (4)	187
Synthesis of ‘tert-butyl (S)-(1-hydroxy-3-phenylpropan-2-yl)carbamate’ (4)	187
Synthesis of ‘tert-butyl (1-oxo-3-phenylpropan-2-yl)carbamate’ (Parikh- Doering oxidation) (5)	188
Synthesis of ‘tert-butyl (1-oxo-3-phenylpropan-2-yl)carbamate’ (Swern Oxidation) (5).....	189
Synthesis of ‘tert-butyl (1-oxo-3-phenylpropan-2-yl)carbamate’ (TEMPO Oxidation) (5).....	189
Synthesis of ‘tert-butyl (1-oxo-3-phenylpropan-2-yl)carbamate’ (Dess-Martin Oxidation) (5).....	190
Synthesis of ‘tert-butyl (1-(hydroxyimino)-3-phenylpropan-2-yl)carbamate’ (6).....	190

Synthesis of 'tert-butyl (1-chloro-1-(hydroxyimino)-3-phenylpropan-2-yl)carbamate' (7).....	191
CYCLOADDITION - Synthesis of Δ^2 -isoxazoline-fused pyrroline nuclei (9a + 9b).....	192
Characterization of tert-butyl (1-(5-benzyl-3a,5,6,6a-tetrahydro-4H-pyrrolo[3,4-d]isoxazol-3-yl)-2-phenylethyl)carbamate (9b)	195
Synthesis of '(3aR,6aS)-2,2,2-trichloroethyl 3-((S)-1-((tert-butoxycarbonyl)amino)-2-phenylethyl)-6,6a-dihydro-3aH-pyrrolo[3,4-d]isoxazole-5(4H)-carboxylate' (10a+10b)	195
Synthesis of 'tert-butyl ((S)-2-phenyl-1-((3aS,6aR)-4,5,6,6a-tetrahydro-3aH-pyrrolo[3,4-d]isoxazol-3-yl)ethyl)carbamate' (11a)	196
Synthesis of 'tert-butyl ((S)-2-phenyl-1-((3aR,6aS)-4,5,6,6a-tetrahydro-3aH-pyrrolo[3,4-d]isoxazol-3-yl)ethyl)carbamate' (11b).....	197
Synthesis of 'tert-butyl ((S)-1-((3aS,6aR)-5-((S)-2-((S)-2-acetamido-4-methylpentanamido)-3-methylbutanoyl)-4,5,6,6a-tetrahydro-3aH-pyrrolo[3,4-d]isoxazol-3-yl)-2-phenylethyl) carbamate' (12a).....	198
Synthesis of 'tert-butyl ((S)-1-((3aR,6aS)-5-((S)-2-((S)-2-acetamido-4-methylpentanamido)-3-methylbutanoyl)-4,5,6,6a-tetrahydro-3aH-pyrrolo[3,4-d]isoxazol-3-yl)-2-phenylethyl) carbamate' (12a).....	201
Effects of neighboring functionalized prolines on the stability of collagen triple helices.....	207
Introduction.....	209
Aim of the project.....	214
Design and Peptide Synthesis.....	216
Result and discussion	217
Triple helices with Azp-containing CMPs in the Xaa position (CMP 1-CMP 2-CMP 1'-CMP 2')	219
Triple helices with Amp in the Xaa position (CMP 3-CMP 4-CMP 3'-CMP 4').....	220
Triple helices with Acp-containing CMP in the Xaa position (CMP 5-CMP 6-CMP 5'-CMP 6')	221
Thermal Stability of triple helices derived from CMPs of the type -((4SAzp)-Hyp-Gly) _n -	223
Experimental part.....	225

Protocol A - General procedure for swelling	225
Protocol B - General protocol for microwave-assisted peptide synthesis	225
Protocol C – On resin N-terminal acetylation and side chain acetylation	225
Protocol D - On resin Staudinger reduction.....	226
Protocol E - Cleavage from the resin	226
Protocol F – Purification and analysis by RP HPLC	226
Protocol G	227
Ac-[ProHypGly] ₃ -(4R)AzpProGly-[ProHypGly] ₃ -NH ₂	227
Ac-[ProHypGly] ₃ -(4R)AmpProGly-[ProHypGly] ₃ -NH ₂	227
Ac-[ProHypGly] ₃ -(4R)AcpProGly-[ProHypGly] ₃ -NH ₂	228
Ac-[ProHypGly] ₃ -(4S)AzpProGly-[ProHypGly] ₃ -NH ₂	228
Ac-[ProHypGly] ₃ -(4S)AmpProGly-[ProHypGly] ₃ -NH ₂	229
Ac-[ProHypGly] ₃ -(4S)AcpProGly-[ProHypGly] ₃ -NH ₂	229
Ac-[ProHypGly] ₃ -(4R)AzpHypGly-[ProHypGly] ₃ -NH ₂	229
Ac-[ProHypGly] ₃ -(4R)AmpHypGly-[ProHypGly] ₃ -NH ₂	230
Ac-[ProHypGly] ₃ -(4R)AcpHypGly-[ProHypGly] ₃ -NH ₂	230
Ac-[ProHypGly] ₃ -(4S)AzpHypGly-[ProHypGly] ₃ -NH ₂	231
Ac-[ProHypGly] ₃ -(4S)AmpHypGly-[ProHypGly] ₃ -NH ₂	231
Ac-[ProHypGly] ₃ -(4S)AcpHypGly-[ProHypGly] ₃ -NH ₂	232
Ac-[ProHypGly] ₃ -(4R)AzpFlpGly-[ProHypGly] ₃ -NH ₂	232
Ac-[ProHypGly] ₃ -(4R)AmpFlpGly-[ProHypGly] ₃ -NH ₂	233
Ac-[ProHypGly] ₃ -(4S)AzpFlpGly-[ProHypGly] ₃ -NH ₂	233
Ac-[ProHypGly] ₃ -(4S)AmpFlpGly-[ProHypGly] ₃ -NH ₂	234
Ac-[ProHypGly] ₃ -(4S)AcpFlpGly-[ProHypGly] ₃ -NH ₂	234
Bibliography.....	236

Table of Abbreviations

AA = Amino acid

ACHC = *trans*-2-aminocyclohexanecarboxylic acid

ACP = *trans*-3-amino-pyrrolidine-4-carboxylic acid

ACPC = *trans*-2-aminocyclopentanecarboxylic acid

Ala = Alanine

Amp = Aminoproline

Arg = Arginine

Azp = Azidoproline

Bn = Benzil

Boc = tert-Butyloxycarbonyl

CMP = Collagen Model Peptide

DCHC = *trans*-2,5-diaminocyclohexanecarboxylic acid

DMSO = dimethylsulfoxide

e.e. = enantiomeric excess

Flp = Fluoroproline

Fmoc = Fluorenylmethyloxycarbonyl

Gln = Glutamine

HMBC = Heteronuclear Multiple Bond Correlation

HSQC = Heteronuclear Single Quantum Coherence

Hyp = Hydroxyproline

Ile = Isoleucine

IR = infra-red

Leu = Leucine

MS = mass spectrometry

NIP = Nipecotic Acid

NMM = N-methylmorpholine

NOE = Nuclear Overhauser effect

NOESY = Nuclear Overhauser effect spectroscopy

NP = Nanoparticle

NT = Nanotube

PBS = Phosphate buffer solution

Ph = phenyl

Phe = Phenylalanine

PPI = Protein-protein interaction

Ppm = Parts per million

Pro = Proline

ROESY = rotating frame NOESY

SEM = Electron microscopy and

TEA = Triethylamine

TEM = Transmission electron microscopy

TFA = trifluoroacetic acid

THF = tetrahydrofurane

Thr = Threonine

TIC = Tetrahydroisoquinoline-4-carboxylic acid

TOCSY = total correlation spectroscopy

Tyr = Tyrosine

Val = Valine

General introduction

Amino acids (AAs) are the building blocks of peptides and proteins and Nature has optimized their structures to absolve numerous functions in almost all the biological processes. Even if they are very simple molecules, containing at least one amino group and one carboxylic group, they can induce high molecular complexity, being at the molecular basis of the living world.

The function of the majority of proteins derives from their ability to adopt a discrete three-dimensional folded structure that is encoded by a specific sequence of amino acid side chains; extensive research have been done to understand the relationship between protein sequence, folding and function¹.

Inspired by the diversity of folded structures and functions manifested by proteins, chemists in recent years have tried to maintain the similar structure in oligomers that are analogous to proteins but with unnatural backbones. These molecules are called ‘foldamers,’ a term coined by Gellman in his Manifesto to describe ‘any polymer with a strong tendency to adopt a specific compact conformation’²

Most of the researches on foldamers are motivated by two parallel aims. The first one is the exploration of the folding behavior of unnatural backbones, proving that natural oligomers are not unique in their ability to adopt a particular conformation. The second one is providing protein-like biological functions in chemical species that overcome some of the limitations in the use of natural macromolecules for therapeutic applications.

In fact, two major problems in using peptides and proteins as drugs are: the rapid degradation in vivo by proteolytic enzymes^{3,4} and the unfavorable pharmacokinetic profile⁵.

The problem of poor biostability is overcome by almost all foldamers, as most proteases do not effectively recognize peptidic backbones that deviate from natural ones.

Regarding the issue of cell permeability, some foldamer scaffolds with reduced backbone polarity relative to polypeptides have been shown to passively cross membranes, and appropriately designed sequences can be subject to active cellular

uptake. Moreover, membrane permeability is not a prerequisite for activity due to the fact that many biomedically important targets (e.g., viral fusion proteins, growth factor receptors) are extracellular⁶.

Furthermore, nowadays, scientists are trying to develop also smart materials for a large range of the applications (biosensors, biomolecular devices and hybrid catalysts) using Aas and small peptides. The versatility of these compounds is due to their behaviour in self-assembly and self-organization. Moreover, their side chain can give rise to different physical properties, such as size, shape, charge, capacity of hydrogen bonding, hydrophilicity/hydrophobicity (hydrophobic interactions), and chemical reactivity.

Thus, scientists have developed a large variety of nanomaterials so far, such as hydrogel, organogel, nanoarchitectures, vesicles, and micelles, using standard or not natural Aas/peptides⁷⁻¹².

In conclusion, it has to be highlighted that the use of not natural Aas for the synthesis of peptidomimetics opens the door to create more stable peptide that could be used in biomedical field and for preparation of more stable materials for a wide range of application, from catalysis to electrochemistry, from biology to nanomedicine.

During my PhD I mainly focused my research activity on the synthesis and the study of new β -Aas. In the following paragraphs an overview from the literature of β -amino acids and their application in peptide synthesis is presented.

β -Amino Acids

β -Aas are commonly considered as unnatural amino acids, even if in Nature we can find some of them as secondary metabolites or as components of complex natural products. They are analogues of α -Aas in which the amino group is linked to the β -carbon instead of the α -carbon (Figure 1).

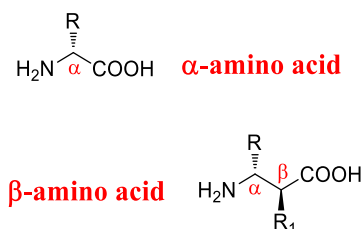


Figure 1: General Formula of α - and β -amino acid.

The main advantage in using peptides containing β -Aas is their higher stability toward proteolysis in comparison with α -peptides^{3,4}. Moreover, they have a great chemical variability that leads to the formation of different and complex secondary structures.

Acyclic β -amino acids

β -Aas nomenclature depends on the position of the side chain (*i.e.* on C_α , C_β , or both). In order to distinguish positional isomers, Seebach and co-workers¹³ proposed the terms β^2 and β^3 amino acids, where the numbers indicate the position of the side chain substitution with respect to the carboxylic function, in order to distinguish positional isomers (Figure 2).

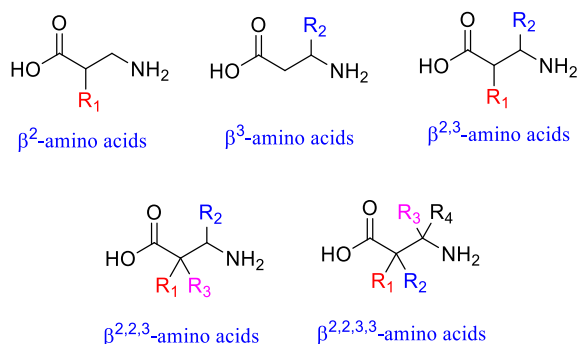


Figure 2: Nomenclature of β -amino acids

$\beta^{2,3}$ -AAs exist as a pair of diastereoisomers, generally named *syn* and *anti*, depending on the stereo-isomeric relationship of the substituents that could drive a particular conformation of peptide.

The conformation of β -peptides is described by the main chain torsional angles, which are assigned as ω , ϕ , θ , and ψ angles (Figure 3) in the convention of Balaram¹⁴.

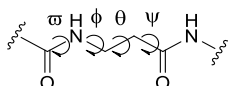


Figure 3: Main chain torsional angles of β -peptides

Substituents effect on the local conformation of a β -amino acid is summarized in Figure 4. Unsubstituted β -Aas, *i.e.* β -alanine, is highly flexible, as for Glycine for α -Aas. On the other hand, Substituents at position 2 or 3 favor a *gauche* conformation around the C^2 - C^3 bond¹⁵.

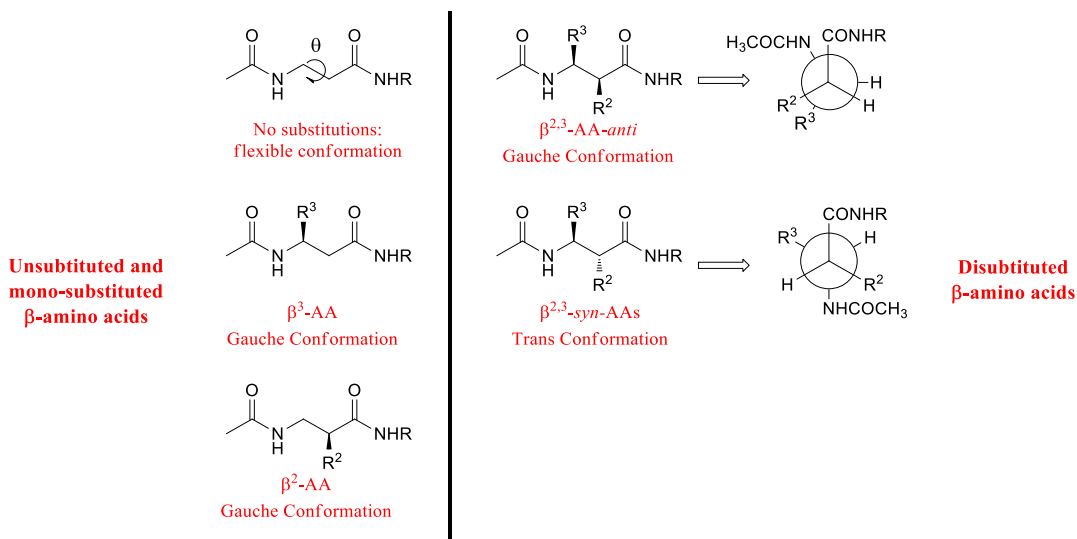


Figure 4: Substituent effects on β peptide conformation

$\beta^{2,3}$ -Aas are even more conformationally constrained. *Anti* $\beta^{2,3}$ -amino acids favors *gauche* conformation while *syn* $\beta^{2,3}$ -amino acids a *trans* conformation of β -peptides (Figure 4¹⁶).

All the above studies are supported by computational analysis that are focused on the comprehension of the substituents effect on model β -amino acids in the peptide conformation¹⁷⁻¹⁹.

Cyclic β -amino acids

Carbocyclic β -Aas are useful intermediates for the enantioselective synthesis of alkaloids²⁰. Moreover, the exploitation of cyclic β -Aas in peptide synthesis has been extensively studied in the last decades. Being conformationally constrained, they could induce very stable peptide secondary structures.

These studies are mostly focused on *trans*-2-aminocyclohexanecarboxylic acid (ACHC)^{18,21}, *trans*-2,5-diaminocyclohexanecarboxylic acid (DCHC)^{19,22}, *trans*-2-aminocyclopentanecarboxylic acid (ACPC)²³, *trans*-3-amino-pyrrolidine-4-carboxylic acid (APC)²⁴ and *cis*-pentacine (Figure 5). In this situation, *gauche*-type

conformations are more strongly promoted in comparison with acyclic β -amino acids. It was evidenced that the ring size determines the precise C^2 - C^3 torsional preference, which in turn influences the β -peptide architecture²³. These cyclic β -amino acids are known to stabilize various different secondary structure motifs in synthetic oligomers²⁵.

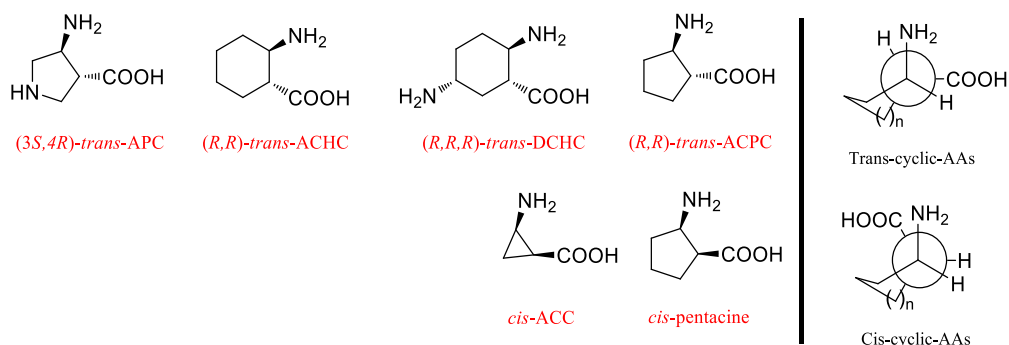


Figure 5: Newman projection of *cis* and *trans* cyclic β -amino acids.

Several other cyclic β -amino acids were reported in the literature. Their ability to induce specific conformation when inserted in peptide sequences will be illustrated in specific paragraphs of this thesis.

β -Peptides and α,β -Hybrid Peptides Secondary Structure

An increasing amount of evidence demonstrates that biomimicking β -amino acid sequences (β -peptide foldamers or α/β foldamers) are fully capable of forming residue-controlled and biologically active secondary structures, such as various types of helices, strands, and loops. The type of the secondary structure depends on both the stereochemistry and the substituents on C^2 and C^3 and their stereochemical relation²⁶.

Here an overview of peptide conformations is presented.

Helical conformation

Helix arrangement in biopolymers is generally length-dependent, with significant helix formation occurring only when a critical chain length is reached.

It's interesting to see that in organic solvents α -peptide helices require at least 8-12 residues to form stable helices, instead β -peptides need six residues.

Moreover, highly conformationally constrained β -peptides can form helices with even four residues²⁷.

To understand which is the driven force of β -AAs in the helix formation, polymers constituted by β^2 or β^3 -amino acids, which differ from the commonly occurring α -peptides by the insertion of a single methylene group at the AA-level, were studied. The increase of conformational flexibility, due to the insertion of a methylene group, is not favorable in terms of entropy with the helix formation²⁷.

On the other hand, β -hydrogen bonding, which requires the restriction of three dihedral angles, can be energetically more favorable than α -hydrogen bonding, which restricts only two torsions. As a result, a more stable hydrogen bond network was formed¹⁶. In organic solvents, β -peptides helices are quite stable in comparison with α -helical conformation of α -peptides.

β -peptide helix conformations could be classified as follows:

- ✓ 14-helix, which is stabilized by hydrogen bonding between the amide proton at position i and the main chain carbonyl at position $(i+2)$, forming a series of 14-membered rings¹⁶. Depending on the stereochemistry, either a left-handed or a right-handed 14-helix is formed. Peptides formed from β^3 -amino acids derived from naturally occurring L -amino acids adopt left-handed 14-helices.
- ✓ 12-helix, which is stabilized by a series of hydrogen bonds between amide carbonyl groups at position i and amide protons at position $(i+3)$ ¹⁶. The helix repeats approximately every 2.5 residues and shows the same polarity as the α -helix, with the amide protons exposed from the N -terminal end of the helix.

- ✓ 10/12 helix, where amides, surrounded by methylene hydrogens, bond to one another ($i, i+2$), forming the 10-membered rings, while the 12-atom rings are formed between amides surrounded by side chains ($i+1, i+3$)¹⁶ β -Peptides with alternating β^2 - and β^3 monosubstituted residues can adopt the 10/12 helix conformation. The characteristic feature of this helix is an intertwined network of 10- and 12- membered hydrogen-bonded rings. In the 10/12-helix there are two types of amide bond orientations. The 10-atom ring amides are approximately perpendicular to the helical axis, while the 12-atom ring amides are nearly aligned with the helical axis.
- ✓ *Fleet et al.* recently prepared peptides from β -amino acids with an oxetane ring constraint. Surprisingly, this β -peptide showed an unprecedented 10-helix secondary structure in organic solvent²⁸.
- ✓ The 8/helix in which two residues for one turn with eight-membered ring hydrogen bonds are present. This kind of helix was observed only in the crystal structure of short oligomer of 1-(aminomethyl)cyclopropanecarboxylic acid²⁹ and for α -aminoxy acids³⁰.

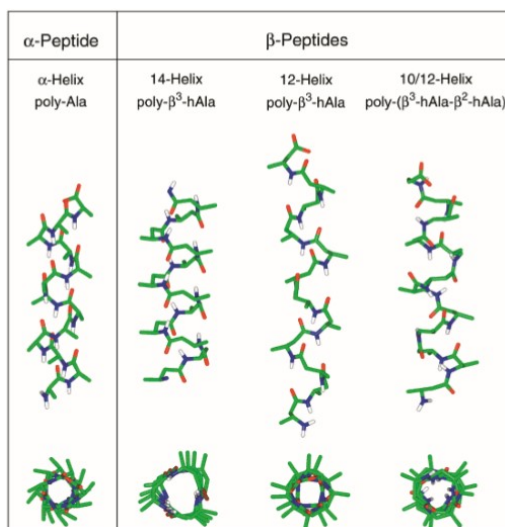


Figure 6¹⁶: Structure of the α -helix, 14-helix, 12-helix, and 10/12-helix. The hydrogens are omitted for clarity, except for the amide hydrogens (white). Carbon atoms are shown in green, nitrogen in blue, and oxygen in red.

β-Sheet-like conformations

β-Sheet like conformations are divided into two type: *anti* and *gauche* type and it depends on the C²-C³ torsion angle³¹.

The main feature of the *anti*-type *β*-peptide sheet is the formation of a net dipole, since every carbonyl group is oriented in the same direction (Figure 7).

In contrast, *β*-sheets formed by *α*-peptides have little or no net dipole because the backbone carbonyls alternate in direction along each strand. *β*-Peptide sheets formed by residues with *gauche* C²-C³ torsion angles would lack a net dipole for the same reason.

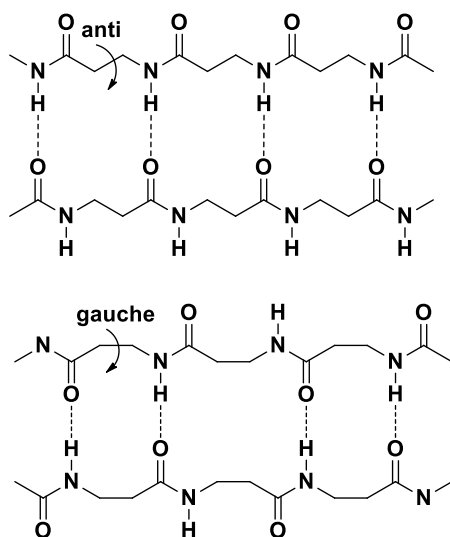


Figure 7³¹: *anti* and *gauche* type of *β*-sheet

Significant progresses have been made toward the goal of preparing *β*-peptides with sheet-like conformations. In early work poly-*β*-Ala was shown to crystallize as an extended sheet-like structure³² but it is disordered in solution³³. Sheet secondary structure has also been obtained for other poly-*β*-amino acids^{34,35}, although other studies of similar polymers have led to the conclusion that helical conformations are preferred^{36,37}.

Seebach³⁸ and Gellman³⁹ designed β -peptides that adopt a hairpin-like conformation in which the two β -amino acid residues at *C*- and *N*-termini end are engaged in antiparallel sheet-type hydrogen-bonding interactions (Figure 8)

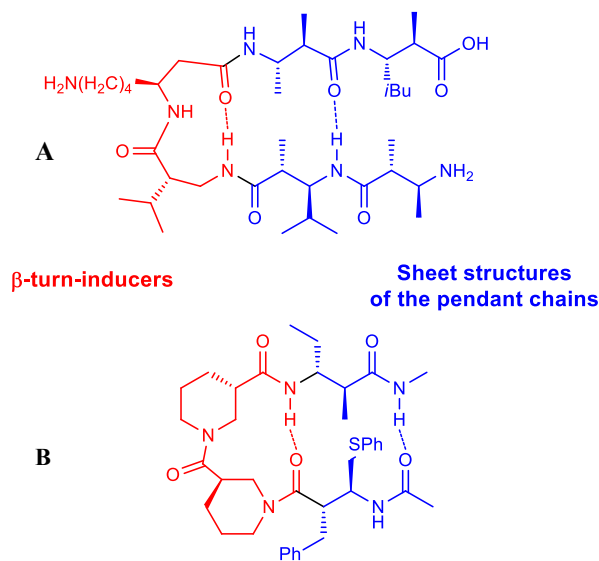


Figure 8: Example of the two hairpin mimics used by Seebach (A) and Gellman (B)

The *syn* configuration of $\beta^{2,3}$ -amino acid residue in the pendants chains favors the formation of the right N-C³-C²-C torsion angle for an *anti*-type β -sheet (180°).

The replacement of the disubstituted $\beta^{2,3}$ -amino acid residues with β -alanine led to the formation of a non-polar sheet in which residues have gauche C²-C³ torsion angles. On the other hand, the insertion of β^2 or β^3 -residues gave an equilibration between the two types of β -peptide sheet.

These results suggest that $\beta^{2,3}$ disubstituted residues with the *syn* configuration have the highest sheet-forming propensity⁴⁰.

β -turn conformations

Loops and turns are deeply studied because they are molecular tools often used to reverse the peptide backbone direction, inducing protein tertiary structure.

For the first time *Seebach et al.* reported an example of turn-like conformation: a 10-membered ring turn structures in homo tripeptides composed by 2,2- or 3,3-disubstituted β -AAs, as it is shown in the Figure 9.

In this case, double substitution at C² or C³ position sterically prevents helix formation. This conformation forces one of the two-alkyl groups into an axial position, proximal to the helical axis⁴¹ stabilizing reverse turn motifs²⁶.

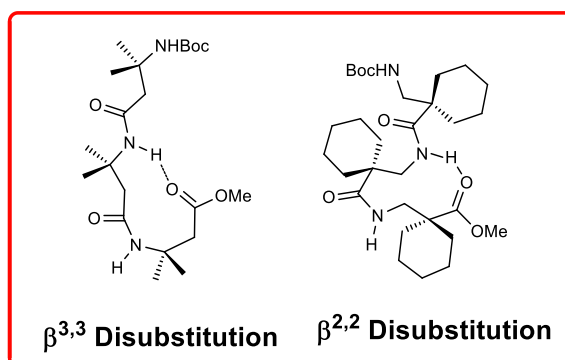


Figure 9: Ten-membered H-bonded ring proposed by Seebach in 1998

Seebach et al. also found that a dipeptide sequence containing a β^2 -AA followed by a β^3 -AA stabilized a reverse turn when inserted in a $\beta^{2,3}$ -AAs sequence (Figure 8, example A) giving a hairpin.

Later on, *Gellman et al.* used a particular scaffold, nipecotic acid (Nip), a cyclic β -amino acid, as turn inducer in peptide sequences containing β -AA (Figure 8B).

In particular, the behavior of a heterochiral (*R*, *S*)-homo-dipeptide composed by Nip (or its counterpart (*S*, *R*) homo-dipeptide) inserted as central residues in a short β -tetrapeptide (Figure 10) was found able to induce a peptide reverse turn^{39,31}. The presence of a tertiary amide was necessary at the center of the turn-forming segment and adopting an *E* conformation favored the reverse turn conformation. On the other hand, secondary amides are largely confined to *Z* conformation destabilizing turn secondary structure.

Also the configuration on the stereogenic center of Nip units is essential for inducing a reverse turn. In fact, the homochiral-dinipecotic acid with the same stereochemistry prevented the sheet interactions between the terminal residues of the peptide, avoiding the formation of an ordered hairpin structures⁴². Moreover, when a single Nip unit is matched with an acyclic β -amino acid the hairpin formation is ineffective⁴³.

Heterochiral Nip homo-dipeptide was also inserted in a short α -peptide sequence⁴², obtaining a hairpin mimic of a hybrid α/β peptide (Figure 10).

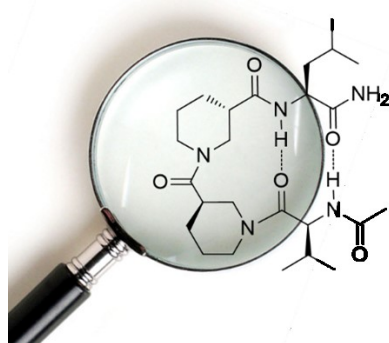


Figure 10: Heterochiral R^*,S^* homo-peptide composed by Nip, used as β -turn inducer

Biological and pharmaceutical applications

The main problem in using peptides in pharmaceutical application is their degradation by peptidases. Seebach group, performing digestion experiments using a variety of peptidases and β -peptides, demonstrated that they undergo no degradation, in contrast to their α -peptide counterparts¹³. These results are not surprising if we think about the basis of ‘recognition’ of a substrate by a peptidase and the recognition of the three-dimensional environment within the active site based on the formation of H-bonds generating a specific secondary structure⁴⁴. In fact, although both α -peptides and β -peptides have the possibility of adopting pleated sheets or helical conformations, these secondary structures are, in fact, very different.

Seebach et al. showed also that β -peptides made from acyclic building blocks with incorporated α -amino acids are stable against proteolytic attacks as well⁴⁵.

Gellman et al. studied the stability of hybrid α/β -peptides with cyclic β -amino acids using proteases trypsin, chymotrypsin and pronase. They found that oligomers containing a 1:1 alternation of α - and β -residues are highly resistant to proteolytic degradation^{46,47,48}.

All these results are very promising for the use of β -peptides or hybrid α/β -peptides in biological and pharmaceutical applications.

Moreover, there are a lot of example in literature in which β -amino acids were inserted in a natural structure for the synthesis of more stable model peptides.

As an example, Reiser group synthesized different analogues of Neuropeptide Y (Figure 11), containing β -aminocyclopropane carboxylic acids. These analogs are more rigid, but keeping the structural requirements for biological activity at the Y1 receptor⁴⁹.

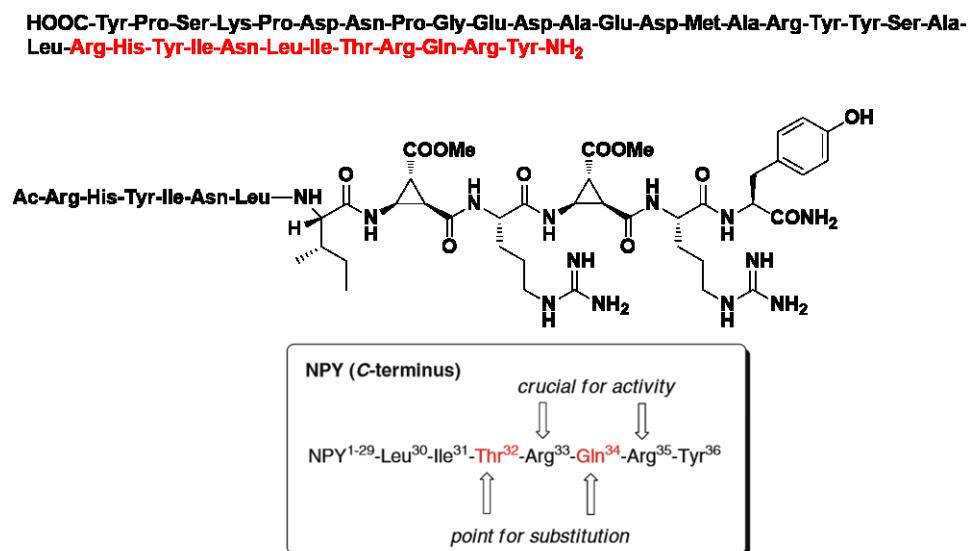


Figure 11: Reiser's Neuropeptide Y analogues

Hybrid α/β -peptides were also used in the inhibition of protein-protein interaction (PPI). Recognition of specific secondary structure motifs of a protein surface triggers

the ability of a synthetic oligomer in disrupting PPIs. Therefore, peptide structural motifs able to mimic typical helical constructs of α -peptides or other secondary structures have been developed^{50,51}.

One example is a chimeric ($\alpha/\beta+\alpha$)-peptide containing *trans*-ACPC that binds the BH3-recognition site of the anti-apoptotic protein Bcl-XL. This peptide foldamer was able to inhibit the interaction between Bcl-XL and its pro-apoptotic partner. The obtained crystal structure of the foldamer-protein complex revealed that the foldamer helix is able to mimic an α -helix⁵². Indeed, the spatial arrangement of the α -peptide side chains can be reproduced accurately as depicted in the Figure 12.

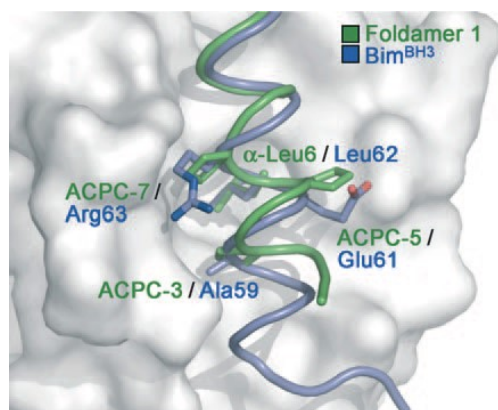


Figure 12⁵²: Overlay of the crystal structures of a BH3-recognition site with endogenous α -peptide ligand (blue ribbon) and of an $\alpha/\beta+\alpha$ chimeric peptide foldamer (green ribbon) bound to the BH3-recognition site of Bcl-xL (in gray).

Nanomaterial applications

The ability of short peptides, containing β -amino acids, to stabilize secondary structures makes them able to self-assemble or generate supramolecular architectures for nanomaterial applications⁵³.

The β -alanine, for instance, could generate different nanostructure, depending on solvent, temperature and surface functionality of the material on which it self-assembles. Indeed nanovesicles formed by *N,N*-dicyclohexylurea- β -alanine are

used as drug delivery system⁵⁴. Also β -alanine tetramers form vesicles in aqueous solution. These architectures are able to encapsulate *L*-dopa and to release it with the change of pH⁵⁵.

There are also several examples of self-assembly of β^3 -amino acids, for example β^3 -Dipeptides containing β -Phe are able to form different nanostructure, depending on pH, temperature and solvent⁵⁶.

Few example of nanostructures formed by linear disubstituted $\beta^{2,3}$ -amino acids are present in literature, one of these is from our research group. The self-assembly behavior of dipeptide containing $\beta^{2,3}$ -diarylamino acid and *L*-alanine gave proteolytic stable nanotubes, that are able to load small molecules and to enter in the cell⁴⁷ (Figure 13).

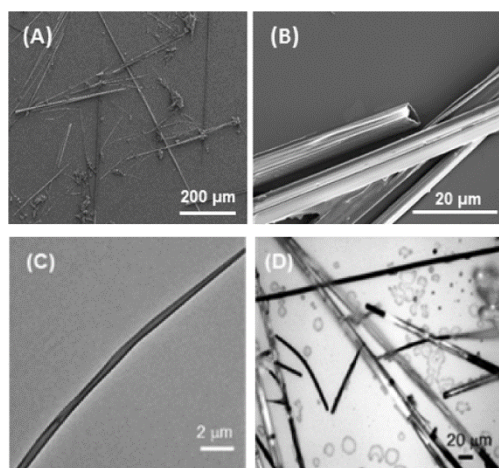


Figure 13⁴⁷: (A) HR-SEM micrograph of the tubes; (B) High magnification HR-SEM micrograph (C) TEM micrograph of an individual tube (D) optical microscopic images of the tubular assemblies

There are also several examples of supramolecular architecture given by $\beta^{2,3}$ -cyclic amino acids inserted in β - or α,β -peptides. Ortuno and co-workers deeply studied the effect of *cis/trans* stereochemistry of cyclobutene β -amino acids in molecular organization⁵⁷. β -dipeptide containing two *trans* moiety or only one *cis* cyclobutene β -amino acid forms nanoscale helical aggregates that form solid-like network⁵⁸. On

the other hand, β -dipeptide containing two *cis* moiety functionalized with π -electron rich tetrathiafulvalene form fibers able to conduct electricity⁵⁹.

In conclusion, nowadays many synthetic efforts have been already done to obtain new and different non-standard amino acids for their importance in nanomaterial application. On the other hand, due to the endless functional variability that could be inserted, it is possible to reach an infinite number of molecular combination and architectures. Moreover, the application of β -amino acids in nanomaterial field has yet to be completely exploited.

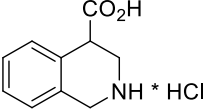
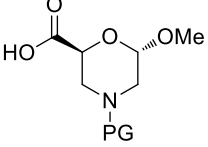
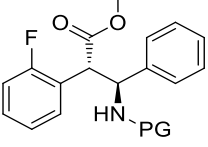
Aim of the thesis

Even if we are in the early stage of foldamer research, a lot of work on β - or α,β -foldamers has already been done.

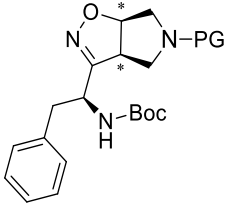
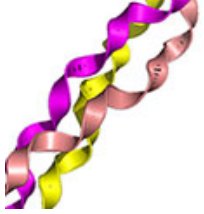
Gellman predicted in his *Manifesto*²: ‘the 20th century will come to be viewed as the period in which chemists acquired synthetic and technical mastery over small molecules, and the 21st century as the period in which that mastery was extended to heteropolymers’. Expanding the scope of the accessible secondary structures is one of the main challenges of this research field.

In my PhD thesis, I was involved in several projects regarding the synthesis of new enantiopure β -amino acids, the preparation of small α/β -peptide sequences possessing defined secondary structure.

In the first part of my thesis I will report on the:

 <p>Chapter 1</p>	synthesis of tetrahydroisoquinoline 4-carboxylic acid and its use in the preparation of α/β -peptides. This new β -amino acid, coupled with β -Ala, can stabilize a flexible reverse turn conformation, depending on its stereochemistry.
 <p>Chapter 2</p>	synthesis of β -Morpholino-amino acid This new β -amino acid can stabilize a very stable reverse γ -turn conformation when it is inserted in α,β -peptides
 <p>Chapter 3</p>	synthesis of $\beta^{2,3}$ -diaryl-amino acids and preparation of α/β -peptides. The secondary structure of each peptide was studied. Moreover, self-assembly of a $\alpha\beta$ -tripeptide composed by the $\beta^{2,3}$ -diaryl amino acid coupled with <i>L</i> -Ala- <i>L</i> -Arg was investigated.

In the second part of this thesis I will focus on two other subjects beyond the β -amino acids, that are:

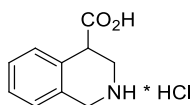
 <p>Chapter 4</p>	<p>synthesis of isoxazoline containing scaffold, as parallel β-sheet mimics. Also in this case model peptides were prepared and their secondary structure were studied.</p>
 <p>Chapter 5</p>	<p>synthesis and study on Double Functionalized Collagen Model Peptides. This part of my thesis was performed during my internship at ETH (Eidgenössische Technische Hochschule, Zürich, Switzerland) in Wennemers Group.</p>

All hybrid α/β -peptides were studied using NMR Spectroscopy (^1H , ^{13}C , HMBC, HMQC, NOESY; ROESY). Molecular modelling was also performed in collaboration with Dr. Contini, from DISFARM, Università degli Studi di Milano.

***Tetrahydroisoquinoline-4-carboxylic Acid/ β -Alanine as
flexible reverse turn mimic***

Aim of the project

This part of my PhD thesis is focused on tetrahydroisoquinoline-4-carboxylic acid **1** named β -TIC (Figure 1), a constrained cyclic β -amino acid that was for the first time prepared in enantiopure form.



1 β -TIC

Figure 1: β -TIC

To the best of our knowledge, β -TIC was never studied for its ability to induce well defined structure when inserted in a peptide sequence. For this reason, we first study the enantioselective synthesis of β -TIC. Then we focused on the use of both enantiomers for the preparation of peptide models.

This work was published on *Chemistry- a European Journal*⁶⁰.

β -TIC is a benzo-condensed analogue of nipecotic acid (Nip). As already explained in the General introduction, *Gellman et al.* used Nip as a turn inducer when inserted into β -peptide sequences as a homo-dipeptide^{42,16,39}. Curiously, the (*R*)-Nip-(*S*)-Nip dipeptide segment, or the (*S*)-(*R*) counterpart, gives β -peptide reverse turns that promote hairpin formation. On the other hand, dipeptides containing Nip in the same stereochemistries are ineffective, similar to when a single Nip unit is matched with an acyclic β -aminoacid⁴².

Even if it is reported in the literature that segments composed by β -acyclic AA combined with cycloalkane β -amino acids did not display reverse turn propensity¹⁶, our challenge has been to use compound **1** β -TIC to generate this motif.

Turn regions are often involved in the protein interaction interface, making this motif an important tool for the modulation of PPIs. An important feature to be taken into account for the design of PPI modulators is the flexibility of the proteins. So, their adaptability in the formation of a complex with the protein is of relevance^{50,51}. The

use of flexible turn tools, that can accommodate themselves to the target in a better way with respect to the rigid turn mimics, can represent an effective strategy. For this reason, we envisaged that the combination of β -TIC with flexible β -Ala could be interesting for the modulation of PPI.

Our hypothesis was that the aromatic part of β -TIC could induce a further constraint in the dipeptide architecture able to better orient the groups involved in hydrogen bonding. On the other hand, the insertion of flexible β -alanine might constitute a molecular trick to modulate rigidity and adaptability^{50,51}. Another important feature to favour PPI interaction is the type of functional group of the turn region. An aromatic residue could be considered a key element in stabilising the complex through non-covalent bonds⁶¹. This construct could thus provide a simple model system to be used in the development of peptidomimetics targeting PPIs. As a result, β -TIC represents the ideal amino acid to reach this target. Finally, the use of β -TIC/achiral β -alanine, instead of two chiral amino acids of opposite conformation, as reported for nipecotic acid, makes the synthetic approach of the corresponding turn easier.

β -TIC is a very expensive commercially available compound, and its preparation, in racemic form, has already been reported in literature⁶². Herein, we revisited the synthetic protocol reducing the synthetic steps, which allows us to obtain ethyl ester of **1** on a gram scale and in excellent yield.

The obtainment of enantiopure β -TIC was not trivial because the H- α proton at benzylic position is very acidic, which favours a potential racemization under non-mild conditions.

For this reason, we envisaged in an enzymatic resolution as best protocol to avoid the racemization.

To the best of our knowledge, in contrast with their β^3 -homologs, few enzymatic resolutions of β^2 -amino acids have been described in the literature. Furthermore, the reported one gave poor results in terms of enantioselectivity and efficiency⁶³⁻⁶⁵.

More recently, oxazinones were used as suitable precursors for the enzymatic dynamic kinetic resolution of non-cyclic β^2 amino-acids⁶⁴. The most similar analogues on which kinetic resolution have been carried out, although with scarce success, have been reported by *Kanerva et al.*⁶⁵ Despite these not so encouraging results, we considered it would be worth attempting an enzymatic resolution, firstly for its simplicity, but also for its potential success.

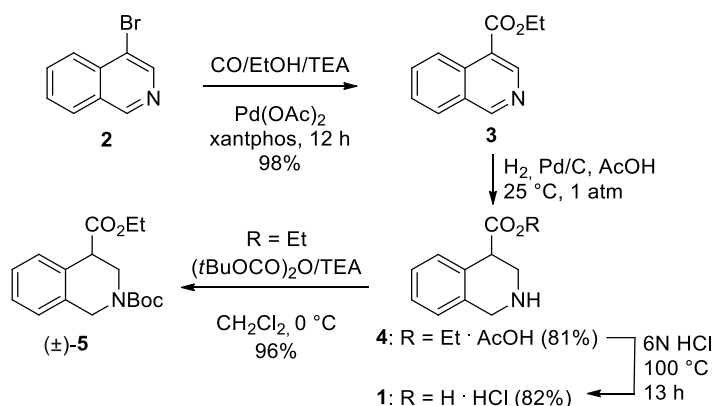
After succeeding in the obtainment of β -TIC in enantiopure form, in the second part of my research, as it said above, I focused on the use of β -TIC to prepare short model peptide sequences containing both *L*- α - and β -Aas, namely, tetrapeptides Fmoc-*L*-Ala- β -TIC- β -Ala-*L*-Val-OBn (Fmoc=fluorenylmethyloxycarbonyl, Bn=benzyl). To prove the correlation between the conformation of the peptides and β -TIC stereochemistry, both β -TIC enantiomers were tested. Both computational and spectroscopic studies were performed to prove the ability of the β -TIC- β -Ala construct to generate a turn structure.

Synthesis

β -TIC synthesis

As reported in literature, amino acid **1** is prepared from 3-bromoisoquinoline in four steps and an overall yield of 45% (Scheme 1). Herein, we revisited the synthetic procedure to decrease the synthetic steps, and focus on the synthesis of the ethyl ester of β -TIC, which is the starting material for enzymatic resolution. Ester **3** (98%) was directly prepared from 4-bromoisoquinoline **2** by using a procedure recently reported for the preparation of the corresponding methyl ester⁶⁶, which consisted of a carbonylation reaction in the presence of EtOH/TEA, Pd(OAc)₂ and xantphos as a ligand. The reduction of the pyridine ring⁶⁷ with H₂ in the presence of Pt₂O in AcOH gave the expected compound **4** (85%; Scheme 1). Amino-acid **1** (as HCl salt,

quantitative yield) was obtained by hydrolysis of compound **4** with 6N HCl (100 °C, 13 h; Scheme 1).



Scheme 1: Synthetic pathway to synthesize β -TIC 1

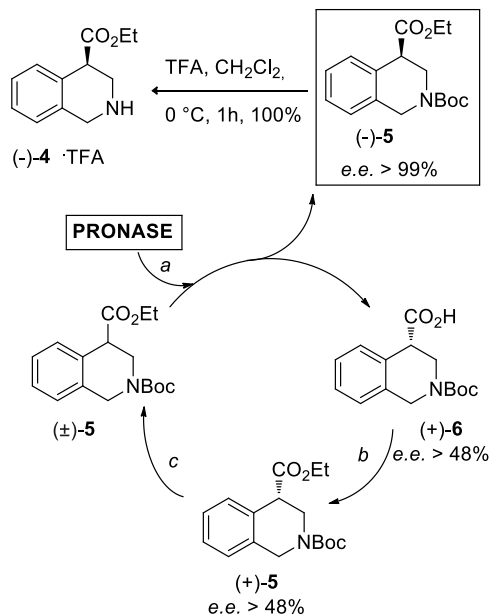
It has to be underlined that, starting from the cheap, commercially available **2**, amino acid **1** was prepared on the gram scale (10 g) in three steps and an overall yield of 83%. The preparation of Boc-derivative **5** (60%) was achieved starting from **4** through a reaction with Boc-anhydride (dioxane/H₂O/NaHCO₃, 80 °C). The yield of **5** was dramatically increased (96%) upon using TEA (2.2 equiv.) as the base in CH₂Cl₂ (25 °C, 26 h; Scheme 1).

Enzymatic resolution of N-Boc derivative 5

The *N*-Boc-protected ethyl ester **5** was chosen as the substrate for enzymatic resolution. This ester was more stable, with respect to the corresponding methyl derivative, to the spontaneous hydrolysis under enzymatic resolution conditions (buffer at pH 8, 37 °C). Moreover, the hydrogen at C-4 is sufficiently acidic to permit the continuous racemization of the substrate⁶⁸. This would give a basis for trying to work under dynamic kinetic resolution conditions⁶⁹.

The enzyme screening and all the work to find the right conditions for enzymatic resolution was performed in collaboration with by Dr. Davide Tessaro, from ‘Politecnico di Milano’.

After the intensive screening that involved about 40 commercial hydrolases of various subclasses (esterases, lipases, proteases, peptidases), Pronase (a mixture of proteases extracted from the extracellular fluid of *Streptomyces griseus*) proved to be the most convenient catalyst in terms of activity and specificity, being able to mediate the stereoselective hydrolysis of the precursor with although a not outstanding, but significative, enantioselectivity ($E=17$). The hydrolysis was carried out in a water/DMSO mixture kept at pH 8. When the conversion reached about 65-70%, we were able to isolate the starting ester with a very high enantiopurity (e.e.> 99%), together with the enantioenriched acid (e.e. 48%, for more details see ref. 60). Thus, the enzymatic kinetic resolution was able to provide an enantiopure material which could be further employed in the synthesis of the target oligopeptide. The reaction was scaled up (1.5 g). Moreover, ester (+)-**5** was finally recycled as a starting material for the successive batch to take advantage of the easy racemization of C-4 under basic conditions (DBU/CH₂Cl₂; Scheme 2). Finally, amino ester (-)-**4**·TFA was obtained in quantitative yield under standard conditions (TFA, CH₂Cl₂, 0 °C, 1h; Scheme 2).



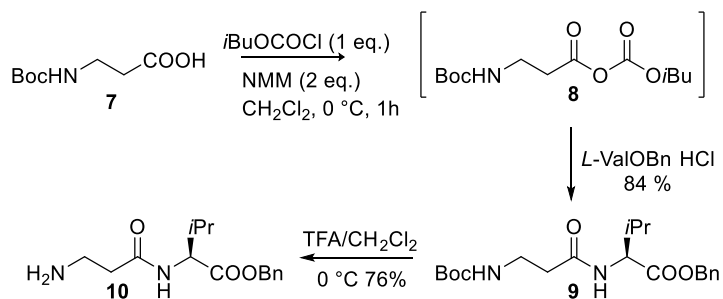
Scheme 2: Enzymatic resolution of β -TIC. a) 40 °C, pH 8, 10% DMSO; b) 4-dimethylaminopyridine (DMAP), CH_2Cl_2 , EtOH, 0 °C, then *N,N'*-dicyclohexylcarbodiimide (DCC); c) 1,8-diazabicyclo[5.4.0]undec-7-ene (DBU), CH_2Cl_2 , trifluoroacetic acid (TFA).

Peptide synthesis

To assess the ability of TIC to induce a turn and to evaluate the effect of the configuration at β^2 carbon, two model tetrapeptides, *i.e.* *Fmoc-N-(L)Ala-TIC- β -Ala-(L)Val-OBn*, containing both the *R*- and *S*- stereoisomer, were prepared.

The synthesis of dipeptide Boc-*N*- β -Ala-(*L*)-Val-OBn **9** (Scheme 3) is not reported in the literature. Its preparation from Boc- β -alanine **7** and the benzyl ester of *L*-Val hydrochloride using the standard protocol [HOBT (1.2 equiv.)/EDC (1.2 equiv.), DIPEA (3 equiv.), CH_2Cl_2 , 0.1 M] gave poor yields since a 2,6-dioxotetrahydropyrimidine by-product was formed. An increase of the yields for compound **9** was achieved by transforming first Boc-*N*- β -Ala-OH into its corresponding anhydride [*i*BuOCOC₂Cl (1 equiv.), *N*-methylmorpholine (NMM, 2 equiv.), CH_2Cl_2 , 0 °C, 1h)] that was directly condensated with NH-*L*-Val-OBn·HCl affording dipeptide **9** in 84% yield. After nitrogen deprotection [$\text{CF}_3\text{CO}_2\text{H}$, CH_2Cl_2 ,

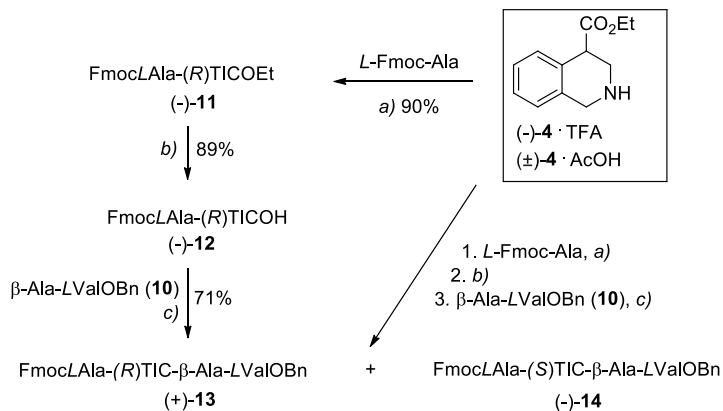
0 °C, 1h], dipeptide **10** was obtained in 76% yields after purification by flash chromatography.



Scheme 3: Synthesis of dipeptide β -Ala-(L)-Val-COOBn

β -TIC ester (-)-**4**·TFA was left to react with Fmoc-L-Ala using the standard coupling conditions (HOBT/ EDC/CH₂Cl₂, 25 °C, 8h). Product (-)-**11** was obtained with 90% yield.

To avoid the racemization of β -TIC during hydrolysis of the ester function, different conditions were tested. Acid (-)-**12** (89%) was successfully obtained without racemization from (-)-**11** using Me₃SnOH⁷⁰ (CH₂Cl₂, 80 °C, 10 h). The reaction of (-)-**12** with **10** (HOBT/EDC, DMF, 25 °C, 2h) gave (+)-**13** (71%). Peptide (+)-**13** was obtained in a very good overall yield (57%) starting from (-) **4**. The whole protocol could be performed from racemic compound **4**, without separation of any intermediate. Tetrapeptides (+)-**13** and (-)-**14** were obtained in 43% overall yield and were separated by column chromatography.



Scheme 4: Synthesis of diastereoisomeric peptides (+)-**10** and (-)-**11**. a) 1Hydroxybenzotriazole (HOBT)/1-ethyl-3-(3-dimethylaminopropyl)carbodiimide (EDC), CH₂Cl₂/DMF, 0 °C, then *N,N*-diisopropylethylamine (DIPEA), 25 °C, 8h; b) Me₃SnOH, CH₂Cl₂, 80 °C, 10 h; c) HOBT/EDC, DMF, 25 °C, 2h.

NMR study and computational analysis of (+)-**13** and (-)-**14** model peptides

NMR characterization of tetrapeptides

Both peptides (+)-**13** and (-)-**14** were fully characterized by NMR (^1H , ^{13}C , HMQC, HMBC, TOCSY and ROESY experiments in CDCl_3 , 20 Mm, 500 MHz). In the Experimental part section all resonances are reported.

^1H NMR spectrum of peptides (+)-**13** showed the presence of two rotamers (**13** and **13'**, 1:1) at TIC tertiary amide bond.

All NH signals in both rotamers are well dispersed, indicating defined conformations. Furthermore, NH resonances of the same amino acid in the two rotamers fall in the same region. Valine NHs resonate at lower fields (δ 7.88 and 7.16, respectively) with respect to NHs of β -alanine (δ 6.62 and 6.10) and alanine (δ 5.70 and 5.96). Interestingly, $\text{NH}_{\beta\text{Ala}}$ is characterized by different multiplicity in the two conformers **13** and **13'** (t and dd, respectively). Our hypothesis is that the backbone of β -Ala is present in different conformations due to the different H-bond network in the two rotamers.

The solvent titration of the NH chemical shifts was performed (Figure 3). The polar solvent DMSO added to the CDCl_3 solution induces similar chemical shift changes in both rotamers. A pronounced downfield shift with increasing concentrations of DMSO was observed for $\text{NH}_{\beta\text{Ala}}$ ($\Delta\delta_{\text{NH}}$: 0.66 and 1.02, respectively) indicating its solvent exposure. The intermediate value for NH_{Ala} ($\Delta\delta_{\text{NH}}$: 0.47 and 0.69, respectively) suggests that this NH is partially solvated, being at the *N*-terminus. The chemical shift of NH_{Val} is insensitive to the solvent ($\Delta\delta_{\text{NH}}$: 0.14 and 0.19, respectively), confirming its shielding from the solvent. This datum, together with its resonance at low field, confirms that NH of valine is involved in a strong intramolecular hydrogen bond. Comparing the stability of the H-bond network of the two rotamers, it is evident that rotamer **13** is less sensitive to DMSO with respect to **13'**, indicating a stronger H-bond stability.

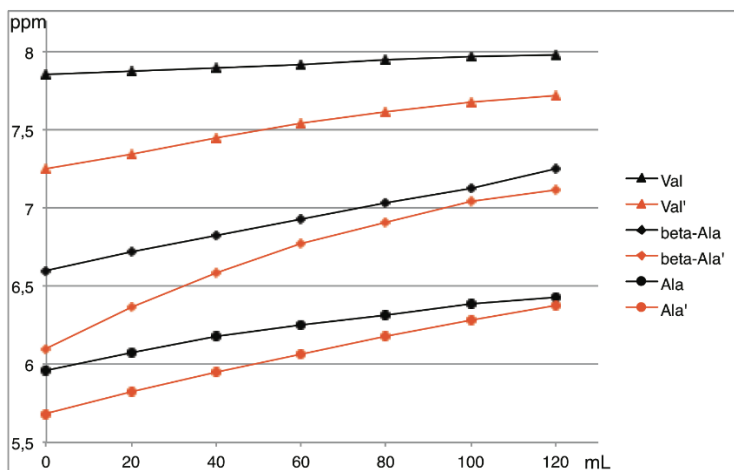


Figure 2: Plots of the δ_{NH} s in the ^1H NMR spectra of (+)-**13** as a function of the increasing amount of DMSO added to the CDCl_3 solution (v/v) (peptide concentration: 20 mM). Black: **13**; Red: **13'**.

Noesy/Roesy experiments at different mixing times (from 100, 200, 300 ms) gave interesting information on the secondary structure of peptide (+)-**13** and, together with J values of the TIC protons, allowed to assign the R -stereochemistry to TIC.

A significant pattern signals for **13** (Figure 3), proves the formation of a turn. In the Figure 3A/B spatial proximities between $\text{H}_{\text{TIC-3}}$ and both NH_{Val} and $\text{H-3}_{\beta\text{-ALA}}$ are highlighted.

Me_{Ala} showed, also, proximity with H-1_{TIC} (Figure 3C) confirming that the carbonyl function of Ala is oriented inside the turn (E rotamer). Furthermore, a complete set of $\text{CH/NH}(i, i+1)$ is present. (See the table in the Experimental Part).

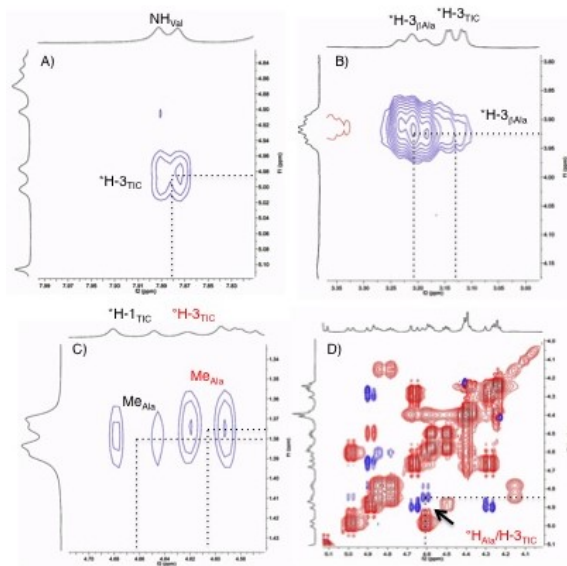


Figure 3: Zoom of significant ROEs to define turn structures of peptide (+)-**13** (CDCl_3 , 20 mM): *black: **13**; °red: **13'**. A), B), D: 200 ms, C) 100 ms.

Taking all these data together, we can conclude that (+)-**13**, containing (*R*)-TIC enantiomer, gave two turn conformations that are in equilibrium in solution (Figure 4).

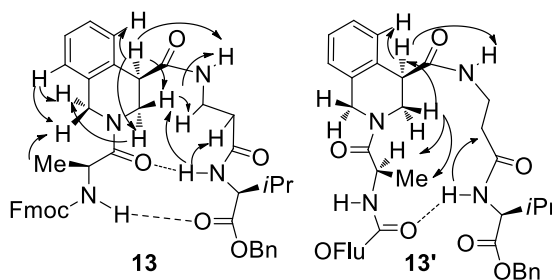


Figure 4: Two turn conformations hypothesized for compound **13**

The formation of a strong H-bond between C=O of alanine with NH_{Val} (12-membered ring) is proposed for the *E*-rotamer **13**. The stability of the turn is reinforced by a further H-bond between the NH_{Ala} and C=O of Valine. On the other hand, the *Z*-rotamer **13'** forms a strong H-bond between NH_{Val} with C=O of the Fmoc group. In this case a bigger turn (15-membered ring) was formed (Figure 4).

Peptide (-)-**14**, containing *S*-TIC, is present as a mixture of three conformers in a 1:0.6:0.1 ratio. Only the two main isomers, named **14** and **14'**, were fully

characterized (See the Experimental part). A complete set of CH/NH ($i, i+1$) ROEs were detected exclusively at C-termini arm for **14'** (Figure 5). Me_{Ala} shows spatial proximity with H-1_{TIC} in both conformers (**14**, m; **14'**, w). In both cases, intrastrand ROEs are absent. Differently from (+)-**13**, NH signals are not dispersed, and the DMSO titration gave $\Delta\delta_{\text{NH}}$ values larger than 0.7, except for NH_{Val} ($\Delta\delta_{\text{NH}}$ 0.5) (Figure 6). These data indicate that all the isomers of peptide (-)-**14** did not assume a preferred conformation.

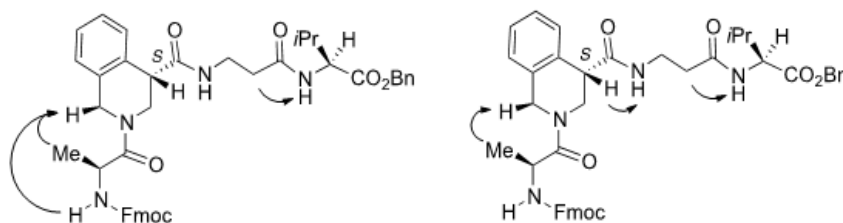


Figure 5: Conformations hypothesized for **14** and **14'**

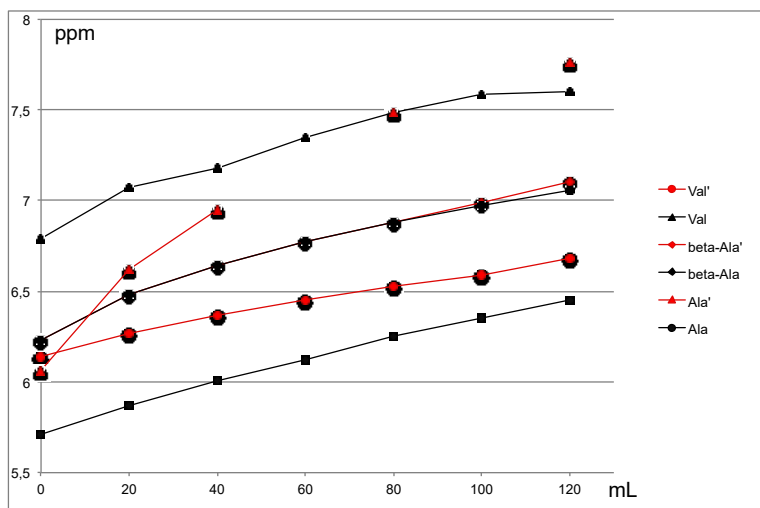


Figure 6: Plots of the δ_{NH} s in the ^1H NMR spectra of (-)-**14** as a function of the increasing amount of DMSO added to the CDCl_3 solution (v/v) (peptide concentration: 20 mM). Black: **14**; Red: **14'**.

Computational analysis for conformers **13** and **13'**

All the computational studies were performed by Dr. Alessandro Contini, from DISFARM, Università degli Studi di Milano.

Based on NOE data, a computational refinement of structures of **13** and **13'** was attempted by means of molecular dynamics (MD) simulations. Distance restraints derived from NMR spectroscopy experiments were used to drive simulated annealing (SA) experiments, which consisted of a quick heating phase followed by a slow cooling phase.

The simulation was repeated three times, starting from randomly chosen conformations, and full convergence was observed. The structures of both **13** and **13'** fit well with the geometries proposed in Figure 7 and can be considered as models of peptide turns.

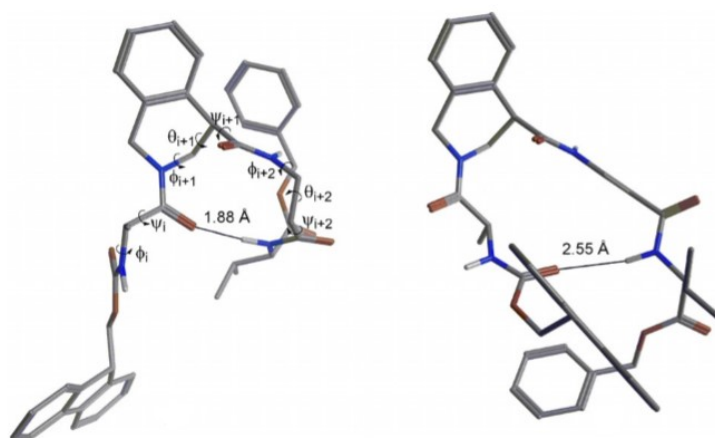


Figure 7: Structures of **13** and **13'** obtained by restrained MD SA.

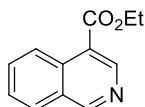
Conformation **13** is characterized by a peptide bond between Ala-1 and β -TIC in pseudo-*cis* configuration. Indeed, the Ala-1 C=O points “inward” with respect to the turn curvature and is involved in a rather strong hydrogen bond with Val-4 NH (O \cdots H distance=1.88 Å), which makes this turn rather similar to a type II β turn. Conversely, in conformation **13'**, the Ala-1- β -TIC peptide bond is in a pseudo-*trans* configuration and a hydrogen bond can be observed between the Fmoc carbonyl group and Val-4 NH. Selected torsional angles, show that the β -TIC geometry is similar in both conformations. Principal differences in the turn core, in addition to the configuration of the Ala-1- β -TIC peptide bond, are found in the β -Ala dihedral angles (ϕ_{i+2} , θ_{i+2} and ψ_{i+2}). Indeed, a *gauche* conformation is observed for the

two β -Ala methylene groups in **13**, in accordance with experimental data, whereas a staggered conformation (corresponding to a fully extended backbone) is found for **13'**. Another important difference between the two conformations is observed for the benzyloxy-protected valine that terminates the turn core. Indeed, in conformer **13**, the benzyl group is oriented toward the β -TIC scaffold, whereas in **13'** it points toward the Fmoc group (fluorine moiety). It is possible that turn conformations are stabilized by the hydrophobic collapse of aromatic rings in polar solvents. Computational data indicate that peptide **14** exists in a mixture of three isomers, but none of them can assume a preferred conformation.

In conclusion, changing the already known procedure, I synthesized β -TIC compound shortening the synthetic steps and reaching higher yield. The synthesis was performed in gram scale, as well as the enzymatic kinetic resolution of compound **4**. The two obtained enantiomers of β -TIC were used to prepare model hybrid α/β -peptides. It was found that (*R*)- β -TIC is able to provide a peptide reverse turn when linked to β -alanine, as demonstrated by computational and NMR spectroscopy studies on tetrapeptide model Fmoc-*L*-Ala-(*R*)- β -TIC- β -Ala-*L*-Val-OBn.

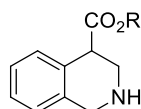
Experimental part

Synthesis of ethyl isoquinoline-4-carboxylate (3)



Compound **3** was prepared according to the know procedure, used for the methyl ester (RIF), starting from 4-bromo-isoquinoline (**2**) (10 g, 48 mmol) in the presence of EtOH (70 mL), TEA (70 mL), Pd(OAc)₂ (430 mg, 1.96 mmol) and xantphos (555 mg, 0.96 mmol) under CO atmosphere. Pure ethyl ester **3b** (9.5 g, 98%) was obtained after column chromatography on silica gel (*n*hexane/AcOEt, 1:0 to 0:1). M.p. 48 °C (MeOH/Et₂O). MS (ESI): *m/z* (%): 202.1 [M+1]⁺. ¹H NMR (CDCl₃, 200 MHz): δ = 9.37 (s, 1H), 9.18 (s, 1H), 8.34 (d, *J* 8.4 Hz, 1H), 8.03 (d, *J* = 8.1 Hz, 1H), 7.84 (t, *J* 7.0 Hz, 1H), 7.67 (t, *J* 7.0 Hz, 1H) 4.50 (q, *J* 7.3, 2H), 1.48 (t, *J* 7.3, 3H). ¹³C NMR (CDCl₃, 300 MHz): δ = 14.5, 61.5, 120.9, 125.3, 127.8, 128.4, 128.7, 132.4, 134.1, 147.0, 157.0, 166.7. Elemental analysis calcd (%) for C₁₂H₁₁NO₂: C, 71.63; H, 5.51; N, 6.96; found C, 71.47; H, 5.63; N, 6.67.

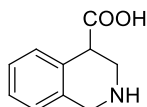
Synthesis of ethyl 1,2,3,4-tetrahydroisoquinolin-4-carboxylate AcOH (4).



In a round bottomed flask Pt₂O (1 g, 4.41 mmol) was suspended in acetic acid (45 mL). The solution was stirred under H₂ atmosphere for 15 min. and then the isoquinoline-4-carboxylate **3** (8.8 g, 44 mmol) was added. The mixture was stirred under H₂ atmosphere at 25 °C for 24 h. After filtration over a celite plug, the solvent was removed under reduce pressure. The crude mixture was purified by column chromatography (CH₂Cl₂/MeOH, from 80:1 to 40:1) giving pure compound **4** as a

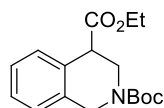
pale yellow oil (9.9 g, 85%). IR (NaCl) ν_{\max} = 3400, 1728 cm^{-1} . MS (ESI): m/z (%): 206.2 $[\text{M}+1]^+$. ^1H NMR (CDCl_3 , 200 MHz): δ = 7.64 (s, 2H, exch.), 7.33-7.04 (m, 4H), 4.16 (q, J 7.3 Hz, 2H), 4.07 (s, 2H), 3.73, 3.55, 3.15 (ABX system, J 13.6, 4.8, 2.9 Hz, 3H), 1.97 (s, 3H), 1.24 (t, J 7.3 Hz, 3H); ^{13}C NMR (CDCl_3 , 500 MHz): δ = 14.3, 22.2, 42.1, 44.6, 46.2, 61.6, 126.8, 127.0, 127.9, 129.8, 130.6, 134.2, 173.6, 176.1. elemental analysis calcd (%) for $\text{C}_{14}\text{H}_{19}\text{NO}_4$: C, 63.38; H, 7.22; N, 5.28; found C, 62.02; H, 7.56; N, 4.87.

Synthesis of 1,2,3,4-Tetrahydroisoquinoline-2-carboxylic Acid ·HCl (1).



Operating in a sealed tube, compound **4** (11 g, 41 mmol) was suspended in HCl (6 N, 25 mL) and the mixture was heated at 120°C for 9 h. The solvent was removed under reduced pressure and the residue was crystallized affording pure **1** (8.8 g, quantitative yield). Mp 237 °C (MeOH/Et₂O). IR (KBr) ν_{\max} 3030, 1725, 1609 cm^{-1} . MS (ESI): m/z (%): 178.1 $[\text{M}+1]^+$. ^1H NMR (DMSO- d_6 , 200 MHz) δ = 11.0-8.5 (brs, 3H), 7.21-7.45 (m, 4H), 4.23 (s, 2H), 4.10 (t, J 5.5 Hz, 1H), 3.14-3.61 (m, 2H). ^{13}C NMR (DMSO- d_6 , 50 MHz) δ = 41.1, 42.7, 44.2, 127.7, 128.2, 128.3, 129.6, 129.8, 130.3, 173.2. Elemental analysis calcd (%) for $\text{C}_{10}\text{H}_{12}\text{ClNO}_2$: C, 56.21; H, 5.66; N 6.56; found C, 55.83; H, 5.85, N, 6.02.

Synthesis of Ethyl N-Boc-1,2,3,4-tetrahydroisoquinolin-4-carboxylate (5)



In a three necked round bottom flask equipped with a magnetic stirrer, nitrogen inlet, and thermometer, compound **4** (3 g, 11.3 mmol) was dissolved in dry CH₂Cl₂ (15 mL) and the solution was cooled to 0 °C. Triethylamine (5.1 mL, 32.2 mmol) was added. After 10 min., di-*tert*-butyl dicarbonate (3.8 g, 17.5 mmol) was slowly added and the stirring was continued for 2 h at 25 °C. The reaction mixture was washed with KHSO₄ (pH = 3, 0.5 N, 5 mL) and then dried over Na₂SO₄. The solvent was removed under reduced pressure and product **5** was obtained as a colorless oil (4.5 g, 96%). IR (NaCl) ν_{\max} = 1736, 1699 cm⁻¹. MS (ESI): *m/z* (%): 328.2 [M+Na]⁺. ¹H NMR (CDCl₃, 200 MHz): δ = 7.27-7.12 (m, 4H), 4.73, 4.48 (AB system, *J* 17.2 Hz, 2H), 4.24, 3.81, 3.59 (ABX system, *J* 13.2, 5.1, 4.4 Hz, 3H), 4.17 (q, *J* 7.0 Hz, 2H), 1.48 (s, 9H), 1.25 (t, *J* 7.0, 3H). ¹³C NMR (CDCl₃, 200 MHz): δ = 14.4, 28.6 (x3), 44.1, 45.1, 46.0, 61.3, 80.3, 126.7 (x2), 127.7, 129.1, 131.9, 133.9, 154.9, 172.2. Elemental analysis calcd (%) for C₁₇H₂₃NO₄: C, 66.86; H, 7.59; N, 4.59; found C, 66.58; H, 7.80; N, 4.43.

Enzymatic resolution of compound 5 with Pronase

A 250 mL three necked round-bottomed flask was immersed in a thermostatic oil bath, equipped with a magnetic stirrer and connected to an automatic titration device through the necks (burette, electrode and temperature probe, respectively). The bath temperature was set to 40°C and the titrator reservoir was filled with 0.5 M NaOH. In the flask, TRIS base (75 mg, 0.6 mmol) was dissolved in water (120 mL) together with *Pronase* (1.00 g), and the pH was adjusted to 8 with 1M NaOH. Compound **5** (1.50 g; 5.2 mmol) was dissolved in DMSO (12 mL) and added dropwise to the solution under stirring. The titrator was regulated for keeping the reaction mixture at pH = 8, and the data collection was started. At fixed intervals, aliquots were taken from the solution and analyzed by HPLC [Chiralcel[®] OD column (250 x 4.6 mm), 25 °C, *n*hexane/2-propanol, 9:1, flow 1 mL/min; 210 nm.]. When *e.e.* of substrate **5** was found to be over 99% (usually around 65-70% of conversion, after 6-8 days),

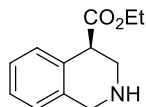
the titration was switched off and the stirring was interrupted. The reaction mixture was poured in a separatory funnel and extracted twice with Et₂O. The organic layers were brought together and dried on anhydrous Na₂SO₄. The solvent was removed leaving an oily residue corresponding to ester (-)-**5** (432 mg, *e.e.* 99%): [α]_D²⁵ = -36.4 (*c* = 1 in CHCl₃).

The aqueous phase was acidified to pH 3 with 6M HCl and extracted twice with Et₂O. The organic layers were brought together, dried on anhydrous sodium sulfate and the solvent was removed, leaving an oily residue corresponding to acid (+)-**6** (432 mg, *e.e.* 48%). NMR data of compound **6** are in agreement with those reported in the literature⁷¹.

Recycle of the enantio-enriched acid (+) 6 to racemic 5

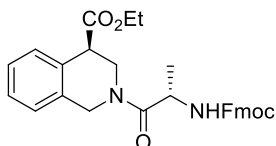
Acid (+)-**6** (*e.e.* 48%; 1 g, 3.6 mmol) was dissolved in dry CH₂Cl₂ (33 mL) and the solution was cooled to 0 °C. DIMAP (44 mg, 0.36 mmol), EtOH (1.5 mL) were added and then DCC (819 mg, 4 mmol) dissolved in CH₂Cl₂ (5 mL) was slowly dropped. The reaction was stirred at 25 °C for 1 h. The solvent was removed. The crude reaction mixture was taken up with Et₂O. The solid was filtered and the crude was purified by column chromatography affording pure ester (+)-**5** (618 mg, 56%). The enantioenriched ester (+)-**5** (600 mg, 2.08 mmol) was dissolved in CH₂Cl₂ (3 mL) and DBU (300 μ L, 2.01 mmol) was added. The solution was stirred at 25 °C for 3 h. The reaction was monitored by HPLC [Chiracel OD; *n*hexane/2-PrOH, 9:1; 1 mL/min; 210 nm]. The organic layer was washed with 0.1 N HCl solution (3 mL). The aqueous layer was extracted with Et₂O (3 x 3 mL). The organic layers were brought together and dried over Na₂SO₄ affording racemic ester **5** in quantitative yield.

Synthesis of Ethyl (R)-1,2,3,4-tetrahydroisoquinolin-4-carboxylates CF₃CO₂H (-)4.



Enantiopure ester (-)-**5** (140 mg, 0.46 mmol) was dissolved in dry CH₂Cl₂ (5 mL) and the solution was cooled at 0 °C. CF₃CO₂H (0.5 mL) was added and the solution was stirred for 1.5 h at 25 °C. After solvent evaporation, (-)-**4** · CF₃CO₂H (147.3 mg, quantitative yield) was isolated: $[\alpha]_D^{25} = -42.3$ ($c = 1$ in MeOH). ¹H NMR (MeOD, 200 MHz) $\delta = 7.55$ - 7.24 (m, 4H), 4.38 (s, 2H), 4.23 (q, J 7.2 Hz, 2H), 4.19, 3.90, 3.52 (ABX system, J 13.1, 5.2, 3.6 Hz, 3H), 1.27 (t, J 7.2 Hz, 3H). Elemental analysis calcd (%) for C₁₄H₁₆F₃NO₄: C, 52.67; H, 5.05; N, 4.39; found C, 52.19; H, 5.48; N, 3.91.

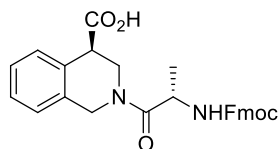
Synthesis of Fmoc-(L)-Ala-(R)-TICOEt (-)-**11**



Fmoc-*L*-Ala (88.7 mg, 0.28 mmol) was dissolved in CH₂Cl₂ (3 mL) and DMF (0.5 mL), the solution was cooled to 0 °C and HOBT (42.3 mg, 0.31 mmol) and EDC (60.1 mg, 0.31 mmol) were added. The mixture was stirred at 0°C for 1h. Then compound (-)-**4** (100 mg, 0.31 mmol), dissolved in CH₂Cl₂ (0.5 mL) and DIPEA (97.5 μ L 0.56 mmol) were added. The reaction mixture was stirred at room temperature for 8h. A saturated solution of NaHCO₃ (4 mL) was added. The aqueous layer was separated and the organic layer was washed first with a saturated solution of NH₄Cl (4 mL) and then with a saturated solution of NaCl (4 mL). The organic layer was dried over Na₂SO₄. The solvent was removed under reduced pressure and the crude mixture was purified by column chromatography (*n*hexane/AcOEt, 7:3). Pure compound (-)-**8** was obtained as a colorless oil (130 mg, 90%). $[\alpha]_D^{25} = -11$ ($c = 1$ in CDCl₃); ¹H NMR (CDCl₃, 300 MHz): δ (mixture of rotamers: 1:1) = 7.76 (d, J 7.7, 2H), 7.63-7.60 (m, 2H), 7.42-7.15 (m, 8H), 6.06 (d, J 7.1 Hz, 0.5H), 5.95 (d, J

7.7 Hz, 0.5H), 5.19, 4.49 (AX system, J 17.6 Hz, 1H), 4.96-4.92 (m, 0.5H), 4.78, 4.67 (AB system, J 17.7 Hz, 1H), 4.79-4.62 (m, 0.5H), 4.38-4.09 (m, 6H), 3.89-3.85 (m, 1H), 3.65-3.53 (m, 1H), 1.42+1.37 (d, J 6.7 Hz, 1.5+1.5H), 1.27+1.20 (t, J 7.2, 1.5+1.5H); ^{13}C NMR (CDCl_3 , 300 MHz): δ = 14.4 (14.3), 19.6 (19.5), 42.2, 44.5, 44.7, 47.2, 47.5 (47.4), 61.9 (61.5), 67.2 (67.1), 120.2, 129.5-125.4 (x12), 132.0 (130.8), 132.7 (132.1), 141.5, 144.2 (144.1), 144.3 (144.2), 155.8 (155.6), 171.1, 171.9; MS (ESI): m/z (%): 499.2 [$\text{M} + 1$] $^+$; elemental analysis calcd (%) for $\text{C}_{30}\text{H}_{30}\text{N}_2\text{O}_5$: C, 72.27; H, 6.06; N, 5.62; found C, 71.96; H, 6.39; N, 5.39.

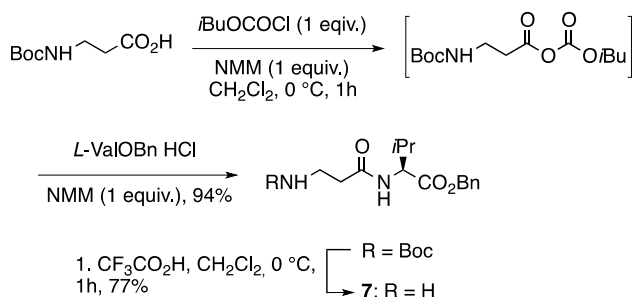
Synthesis of Fmoc(L)Ala-(R)TIC-OH (-)-12



Dipeptide (-)-**11** (110 mg, 0.22 mmol) was dissolved in DCE (7 mL). Me_3SnOH (320 mg, 1.8 mmol) was added and the mixture was stirred under reflux at 80°C for 24 h. The solution was then cooled at room temperature, diluted with CH_2Cl_2 (25 mL) and washed twice with a solution of KHSO_4 (40 mL, 0.05 M) and then with a saturated solution of NaCl (40 mL). After the separation of the aqueous layer, the organic layer was dried over Na_2SO_4 . The solvent was removed under reduced pressure and the crude mixture was purified by column chromatography ($\text{CH}_2\text{Cl}_2/\text{MeOH}$ 20:1). Pure compound (-)-**12** was isolated as a colorless oil (92 mg, 89%). $[\alpha]_{\text{D}}^{25} = -15.4$ ($c = 1$ in CDCl_3). MS (ESI): m/z (%): 471.2 [$\text{M}+1$] $^+$, 493.3 [$\text{M} + \text{Na}$] $^+$. ^1H NMR (CDCl_3 , 300 MHz): δ (mixture of rotamers: 1:1) = 7.80-7.76 (m, 2H), 7.63-7.57 (m, 2H), 7.44-7.17 (m, 8H), 6.31 (d, J 8.1 Hz, 0.5H), 6.00 (d, J 7.4 Hz, 0.5H), 5.27, 5.11 (AB system, J 17.6 Hz, 1H), 5.07-4.97 (m, 0.5H), 4.84, 4.70 (AB system, J 16.6 Hz, 1H), 4.82-4.76 (m, 0.5H), 4.48-4.17 (m, 4H), 3.95-3.88 (m, 1H), 3.60-3.58 (m, 0.5H), 3.36 (dd, J 13.3, 3.8, 0.5H), 3.10-2.10 (brs, 1H), 1.42+1.37 (d, J 6.7 Hz, 1.5+1.5H). ^{13}C

NMR (CDCl₃, 300 MHz): δ = 19.5, 42.6, 44.0 (44.4), 44.6 (44.8), 47.1, 44.4, 67.1 (67.2), 120.2, 125.2-129.9 (x13), 131.4, 132.6, 141.2, 144.0 (m), 156.1, 173.3, 174.4. Elemental analysis calcd (%) for C₂₈H₂₆N₂O₅: C, 71.47; H, 5.57; N, 5.95; found C, 71.02; H, 5.89; N, 5.54.

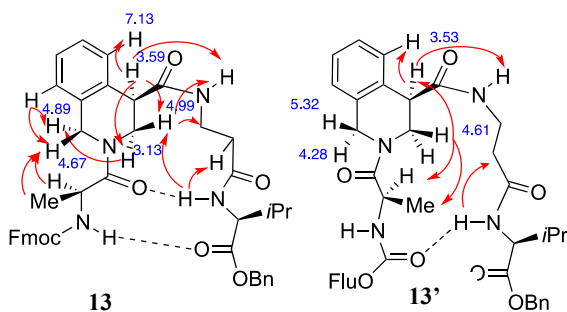
Synthesis of β -Ala-(L)ValOBn (10)



Boc- β -Alanine (500 mg, 2.64 mmol) was dissolved in CH₂Cl₂ (20 mL). The solution was cooled to 0 °C and then NMM (1 equiv.) and *i*BuOCOC*l* (1 equiv.) were added. The reaction was stirred at 0 °C for 1h. A saturated solution of NaHCO₃ (30 mL) was added. The aqueous layer was separated, and extracted twice with CH₂Cl₂ (20 mL). The organic layer was dried over Na₂SO₄. The solvent was removed under reduced pressure and the anhydride intermediate Boc- β -AlaOCO₂*i*Bu was obtained as a colorless oil (52%). The anhydride was dissolved in CH₂Cl₂ (15 mL) at 0°C and ValineOBn derivative (1 equiv.) was added. After 5 min., NMM (1 equiv.) was added dropwise. The reaction was stirred at room temperature for 12 h. A saturated solution of NH₄Cl (30 mL) was then added. The aqueous layer was separated, and extracted with CH₂Cl₂ (2 x 20 mL). The organic layer was washed with a saturated solution of NaCl (2 x 30 mL) and dried over Na₂SO₄. The solvent was removed under reduced pressure affording Boc- β -Ala-(L)-ValOBn (84%) as a colorless oil that was used without further purification. The nitrogen deprotection was achieved dissolving dissolved Boc- β -Ala-(L)-ValOBn in CH₂Cl₂ (20 mL) and keeping the solution

at 0°C. TFA (5 mL) was added and the reaction was stirred at 0 °C for 1h. After removing of the solvent under reduced pressure, the crude mixture was purified by column chromatography (CH₂Cl₂/MeOH, 30 : 1 + 0.3% TEA) affording pure **7** (76%). $[\alpha]_D^{25} = +11.3$ (*c* 1, CHCl₃). ¹H NMR (CDCl₃, 200 MHz) $\delta = 7.8$ (d, *J* 8.4 Hz, 1H, exch.), 7.10-7.40 (m, 5H), 5.21, 5.15 (AB system, *J* 12.4 Hz, 2H), 4.58 (dd, *J* 9.0, 5.0 Hz, 1H), 3.76-3.39 (m, 2H), 2.98 (t, *J* 6.1 Hz, 2H), 2.23-2.18 (m, 1H), 1.95 (s, 2H, exch.), 0.98-0.76 (m, 6H); IR (NaCl) $\nu_{\max} = 2755, 1731, 1678$ cm⁻¹; MS (ESI): *m/z*: 278.1 [M]⁺. Elemental analysis calcd (%) for C₁₅H₂₂N₂O₃: C, 64.73; H, 7.97; N, 10.06; found C, 64.43; H, 8.19; N, 9.88.

Synthesis of Fmoc(L)Ala-TIC-βAla-(L)Val-OBn (+)-13.



Dipeptide (-)-**11** (80 mg, 0.17 mmol) was dissolved in CH₂Cl₂ (2 mL). The solution was cooled to 0 °C and HOBT (27.6 mg, 0.20 mmol) and EDC (39.1 mg, 0.20 mmol) were added. The mixture was stirred at 0°C for 1h. Boc-β-Ala-(L)-ValOBn (**10**) (51.8 mg, 0.18 mmol) was dissolved in CH₂Cl₂ (0.5 mL) and DIPEA (59 μL, 0.34 mmol) was added. The reaction mixture was stirred at 25 °C for 8 h. The organic layer was washed with a saturated solution of NaHCO₃ (4 mL), saturated solutions of NH₄Cl (4 mL), and NaCl (4mL) and then dried over Na₂SO₄. The solvent was removed under reduced pressure. The crude mixture was purified by column chromatography (*n*hexane/AcOEt, 1:0 to 0:1) affording pure (+)-**13** (94.4 mg, 76%). $[\alpha]_D^{25} = +31.6$ (*c* = 1 in CDCl₃). MS (ESI): *m/z* (%): 731.3 [M+1]⁺. Elemental

analysis calcd (%) for $C_{43}H_{46}N_4O_7$: C, 70.67; H, 6.34; N, 7.67; found C, 70.41; H, 6.59; N, 7.50.

AA	atom	¹ H δ	Multiplicity <i>J</i> (Hz)	¹³ C δ	NOEs/ROEs
Ala	CO			172.3	
	CH	4.78		47.1	Me _{Ala} (s), NH _{Ala} (w)
	Me	1.385	d, <i>J</i> 6.4	19.6	H-1 _{TIC} (4.67, w), CH _{Ala} (s)
	NH	5.70	d, <i>J</i> 8.2		CH _{Ala} (w), Me _{Ala} (w)
	Fmoc	4.24 (CH) 4.44-4.36 (CH ₂) Arom: 7.78, 7.61, 7.41, 7.32		47.2, 66.9, 155.6 Arom: 120.2, 125.3, 127.3, 144.4, 143.8	CH: 7.61 (s)
TIC	CO			170.9	
	4	3.59	br	45.7	H-5 _{TIC} (s), NH _{βAla} (m), H-3 _{TIC} (4.99, m)
	3	4.99, 3.13	d <i>J</i> 15 dd <i>J</i> 3.2, 13.3	43.5	4.99: NH _{Val} (w), NH _{βAla} (w), H-3 _{βAla} (3.92, vw), H-4 TIC(m) 3.13: H-4 _{TIC} (vw), H-1 _{TIC} (4.89, w)
	1	4.89, 4.67	d, <i>J</i> 16.3	47.2	H-8 _{TIC} (s), 4.89: H- 3 _{TIC} (3.13, w), 4.67: Me _{Ala} (w)
	Arom	H-5: 7.13 H-8: 7.19 H-6: 7.24 H-7: 7.31		129.3 126.1 127.9 127.2 C: 132.8, 132.1	H-4 _{TIC} (s) H-1 _{TIC} (s)
β-Ala	CO			173.5	
	2	2.45 2.27	m m	36.1	NH _{Val} (m), H- 3 _{βAla} (3.92, vw)

	3	3.92 3.21	m t J 12.3	37.0	H-3 _{TIC} (4.99, vw), H-2 _{βAla} (2.27, vw), NH _{βAla} (vw)
	NH	6.62	dd, J 8.4, 3.0		H-4 _{TIC} (m), H-3 _{βAla} (vw), H-3 _{TIC} (4.99, w)
Val	CO			172.4	
	CH	4.58	Overl.	58.6	Me _{Val} (1.02, s), CH _{Val} (m)
	CH	2.38-2.25	m	29.8	
	Me	1.02	d, J 6.8	19.3	NH _{Val} (m), CH _{Val} (s)
		0.98	d, J 6.8	18.2	
	OCH ₂ Ph	5.31, 5.17 7.41, 7.33	d, J 12.3	67.2 Arom: 135.4, 128.4	
NH	7.88	d, J 8.4		H-3 _{TIC} (4.99, w), H-2 _{βAla} (m), Me _{Val} (s), Me ₂ CH _{Val} (s), CH _{Val} (m)	

Table 1: NMR for Rotamer **13** (CDCl₃, 20 Mm, 500 MHz)

AA	atom	¹ H δ	Multiplicity <i>J</i> (Hz)	¹³ C δ	NOEs/ROEs
Ala	CO			171.8	
	CH	4.86		47.2	H-3 _{TIC} (4.61,m), Me _{Ala} (m)
	Me	1.38	d, <i>J</i> 6.9	19.6	H-3 _{TIC} (4.61,m), CH _{Ala} (vs), NH _{Ala} (s)
	NH	5.96	d, <i>J</i> 7.3		CH _{Ala} (m), Me _{Ala} (m),
	Fmoc	CH: 4.24 CH ₂ : 4.44- 4.36 Arom: 7.78, 7.41, 7.32, 7.61		47.2, 67.0, 155.6 Arom: 120.2, 125.3, 127.3, 143.9, 141.2	Arom: 7.61(s)
TIC	CO			170.9	
	4	3.53	br	46.1	H-5 _{TIC} (s), NH _{βAla} (w), H-3 _{TIC} (4.61,w)
	3	4.61, 3.47	d, <i>J</i> 13.9, dd, <i>J</i> 13.9, 3.6	45.0	4.61: CH _{Ala} (m), Me _{Ala} (m), H-4 _{TIC} (w)
	1	5.32, 4.28	d, <i>J</i> 12.0	44.6	4.28: H-8 _{TIC} (m)
	Arom	H-5: 7.15 H-8: 7.22 H-6: 7.25 H-7: 7.31		129.1 127.1 128.1 127.1 C: 133.4, 131.4	H-4 _{TIC} (s) H-1 _{TIC} (m)
β-Ala	CO			172.4	
	2	2.46, 2.33	m	34.9	NH _{Val} (w), H3 _{βAla} (m)

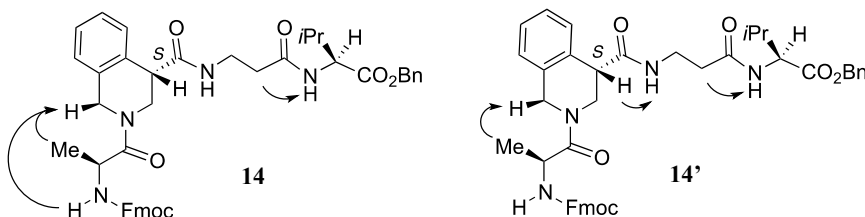
	3	3.56, 3.43	m	36.1	NH $_{\beta}$ Ala (vw)
	NH	6.10	t, <i>J</i> 5.3		H-4 $_{TIC}$ (w), H-3 $_{\beta}$ Ala(vw)
Val	CO			173.5	
	CH	4.51	dd, <i>J</i> 8.4, 5.5	57.8	Me $_{val}$ (s), CH-3 $_{val}$ (m)
	CH	2.21- 2.13	m	30.3	
	Me	0.88, 0.85	d, <i>J</i> 6.9 d, <i>J</i> 6.9	19.1 17.9	
	OCH $_2$ Ph	5.19, 5.12 7.31	d, <i>J</i> 12.2	66.9 Arom: 135.6, 128.2	
	NH	7.16	Overl.		CH $_{val}$ (w), H-2 $_{\beta}$ Ala(w)

Table 2: NMR data for Rotamer **13'** (CDCl $_3$, 20 Mm, 500 MHz)

Synthesis of Fmoc(L)Ala-TIC- β Ala-(L)Val-OBn (+)-**13** and (-)-**14**.

Starting from racemic **4**:AcOH (500 mg, 1.88 mmol), the mixture of (+)-**13** and (-)-**14** was obtained using the same reaction conditions described for the transformation of (-)-**4** into (+)-**13**, without separation of intermediates of the *R* and *S* series. A crude mixture of diastereoisomeric peptides were obtained in 43% overall yield (170 mg). It was possible to partially separated compounds (+)-**13** and (-)-**14** by column chromatography (*n*hexane/AcOEt, 1:0 to 0:1).

(-)-**14**: $[\alpha]_D^{25} = -38.0$ ($c = 1$ in CDCl $_3$). MS (ESI): m/z (%): 731.3 $[M+1]^+$. Elemental analysis calcd (%) for C $_{43}$ H $_{46}$ N $_4$ O $_7$: C, 70.67; H, 6.34; N, 7.67; found C, 70.35; H, 6.63; N, 7.47.



AA	atom	¹ H δ	Multiplicity <i>J</i> (Hz)	¹³ C δ	NOEs/ROEs
Ala	CO			172.6	
	CH	4.86		47.3	Me _{Ala} (s)
	Me	1.45	d, <i>J</i> 6.7	18.2	H-1 _{TIC} (4.84,m), NH _{Ala} (vw)
	NH	5.76	d, <i>J</i> 8.0		H-1 _{TIC} (4.84,w), Me _{Ala} (vw)
	Fmoc	4.36- 4.33(CH ₂) 4.22 (CH) Arom: 7.78, 7.41, 7.33, 7.60	m m	67.1 47.1 CO: 155.8 Arom: 120.0, 125.0, 127.7, 144.0, 141.2	CH ₂ /CH (7.61 vs)
TIC	CO			170.9	
	4	3.73	m	46.2	H-5 _{TIC} (w)
	3	4.88, 3.40	overl	42.9	
	1	4.84, 4.63	d, <i>J</i> 19.8	44.9	NH _{Ala} (w), Me _{Ala} (m), H-8 _{TIC} (s)
	Arom	7.23 (H-8), 7.19 (H- 5) ^a , 7.26, 7.32 (H- 6/H-7)	Overl m	127.5, 128.5, 127.2, 125.2 C 131.3, 133.2	H-8: H-1 _{TIC} (s) H-5: H-4 _{TIC} (w)
β-Ala	CO			171.3	
	2	2.36	overl.	35.3	H-3 _{βAla} (vw), NH _{Val} (w)
	3	3.35, 3.67	overl.	35.8	H-2 _{βAla} (vw)
	NH	6.28	overl.		
Val	CO			171.8	
	CH	4.52	overl.	57.3	Me _{Val} (m), CH- 3 _{Val} (s)
	CH	2.17	m (overl.)	31.9	CH _{Val} (s)
	Me	0.85 0.88	d, <i>J</i> 5.8 d, <i>J</i> 7.5	17.7 18.9	NH _{Val} (m), CH _{Val} (w)
	OCH ₂ Ph	5.21, 5.14	d, <i>J</i> 12.2	66.9	

		Arom: 7.37		Arom: 128.4, C 135.2	
	NH	6.86	d, <i>J</i> 7.0		CH _{val} (m), H- 2 _{βAla} (m)

^aTentatively assigned

Table 3: NMR for Rotamer **14** (CDCl₃, 20 Mm, 500 MHz)

AA	atom	$^1\text{H } \delta$	Multiplicity <i>J</i> (Hz)	$^{13}\text{C } \delta$	NOEs/ROEs
Ala	CO			171.6	
	CH	4.93		47.1	Me _{Ala} (s)
	Me	1.42	d, <i>J</i> 6.2	19.0	H-1 _{TIC} (4.52,w)
	NH	6.18	d, <i>J</i> 8.3		
	Fmoc	4.40-4.36 (CH ₂) 4.23 (CH) Arom: 7.78, 7.41, 7.33, 7.60	m m	66.9 47.2 CO: 155.6 Arom: 120.0, 125.0, 127.7, 144.0, 141.2	CH/CH ₂ : (7.61,s)
TIC	CO			170.1	
	4	3.76	m	45.7	NH _{βAla} (m), H-3 _{TIC} (4.52,m), H-5 _{TIC} (m)
	3	4.52, 3.63	m	45.4	
	1	5.02, 4.54	m	46.9	5.02: H-8 _{TIC} (m)
	Arom	7.07 (H-8) 7.23 (H-5) ^a , 7.30- 7.20 (H-6/H-7)	d m	126.5, 127.9 C 132.0, 131.1	H-8: H-1 _{TIC} (m) H-5: H-4 _{TIC} (m)
β-Ala ok	CO			171.0	
	2	2.46, 2.40	overl.	35.4	H-3 _{βAla} (s), NH _{Val} (m),
	3	3.52, 3.47	overl.	35.5	H-2 _{βAla} (s),
	NH	6.29	overl		H-4 _{TIC} (m), H- 3 _{βAla} (m),
Val	CO			171.7	
	CH	4.57		57.1	Me _{Val} (m), CH- 3 _{Val} (s), NH _{Val} (w)
	CH	2.19	m	31.0	CH _{Val} (s)
	Me	0.88 0.92	d, <i>J</i> 6.9 d, <i>J</i> 7.7	17.0 18.9	CH _{Val} (m)

	OCH ₂ Ph	5.22, 5.16 Arom 7.37	d, <i>J</i> 11.8	67.1 Arom: 128.4, C 135.2	
	NH	6.14	d, <i>J</i> 8.6		Me _{Val} (0.88, w), CH _{Val} (w), H- 3 _{βAla} (m)

^aTentatively assigned

Table 4: NMR for Rotamer 14' (CDCl₃, 20 Mm, 500 MHz)

Morpholine β -amino acid as γ -turn inducer

Aim of the project

In this part of my project, we developed a new cyclic β -Aa, containing morpholino ring, (**Morph β -AA 1**, Figure 1.)

Considering the molecular features of **Morph β -AA**, its use for the peptide/peptidomimetics preparation is of great interest.

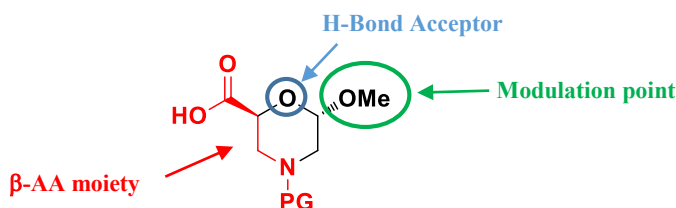


Figure 1: General formula of **Morph β -AA 1**

First, as a β -Aa, it could confer an elevated stability in proteolytic environment. Furthermore, the presence of the acetal function could be of general interest in case of a possible functionalization of C-6 with different nucleophiles such as nucleobases, fluorescent probes and chimeric AAs. Finally, the acetal moiety could be of relevance in a peptide sequence considering its ability as H-bond acceptor. Before going through our research results, a literature overview of peptides including scaffolds containing specific features of our **Morph β -AA 1** (Figure 2) is here reported.

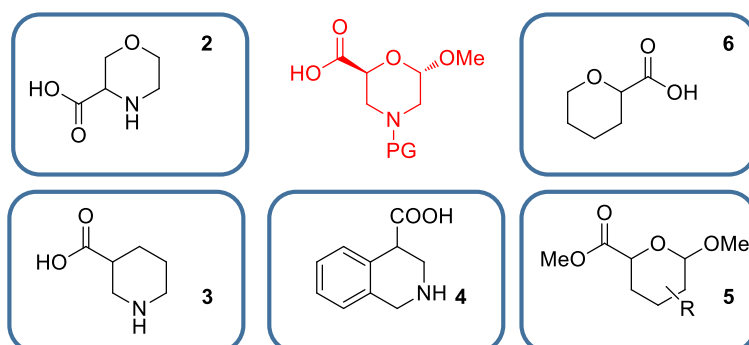


Figure 2: Scaffolds similar to our **Morph β -AA 1** used for the preparation of foldamers

The preparation and use of the parent **Morph α -AA 2** (Figure 3) and its analogues **7-9** is reported in the literature.

Trabocchi *et al.*⁷² claimed the formation of β -turn structures when amino acids **2,5-9** are inserted in model peptides of general formula *N*-Boc-(*D*)-Ala-(*D*)-Val-Morph α -AA-Gly-(*D*)-Leu-(*D*)-Val-OMe.

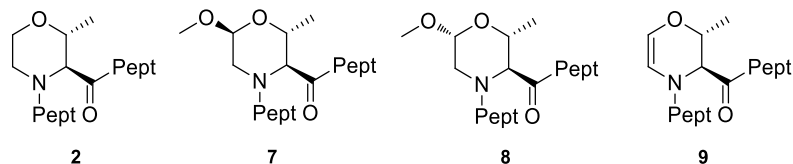


Figura 3: Different **Morph α -AAs** used by Trabocchi *et al.* as β -turn inducers

All this scaffolds act as proline surrogates, forming stable reverse turn stabilized by intramolecular hydrogen bonds, despite on the conformational changes of the heterocyclic structure imposed by the different hybridization of the atoms or the stereochemical arrangements of the substituents in the secondary structure (Figure 4). Thus, this study suggested also the possibility of the functionalization of the morpholine ring without significant loss of the β -turn secondary framework. In fact, the 3,4-dihydro-2H-[1,4]oxazine-containing peptide **9** showed a more compact structure stabilized by an additional γ -turn (Figure 4)

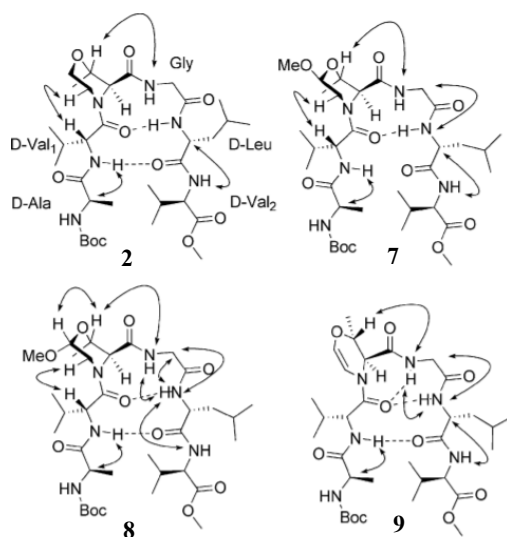


Figure 4⁷²: Reverse turn conformations for peptides **2-5**: the arrows indicate significant ROEs cross peaks

Gellman group used Nip (**3**, Figure 2), as a homo-dipeptide and turn inducer when inserted in α - or β - sequences. Segment composed by *R*-Nip-*S*-Nip or its enantiomer gives β -peptide reverse turns that promote the hairpin formation^{39,42}. (See Chapter 1)

One of the main feature of **Morph β -AA 1** is the presence of the acetal function near the carboxylic function. This could also give rise a specific orientation to the carbonyl group at C-2, due to a possible repulsive effect between the oxygens.

For this reason, I explored the literature aiming to find α -peptides containing the simple 6-alkoxy-pyran-2-carboxylic acid **5** or sugar like moieties.

No examples of functionalized peptides with moiety **6** are reported.

On the other hand, conformational studies on sugar amino acids (SAAs) has been reported⁷³. *Kessler* group designed and synthesized several new peptidomimetics containing amino-carbohydrates as building blocks. These scaffolds (Figure 5) represent sugar-like ring structures carrying an amino and a carboxylic function. They have a specific conformational influence on the backbone of peptides due to the distinct substitution patterns of the pyranose sugar ring. Different SAAs (**SAA1 α** , **SAA1 β** , **SAA2**, **SAA3**, and **SAA4**) were found able to induce different secondary structures when inserted in α -peptides depending on substitution patterns and stereochemistries of the functional groups on the ring (Figure 5).

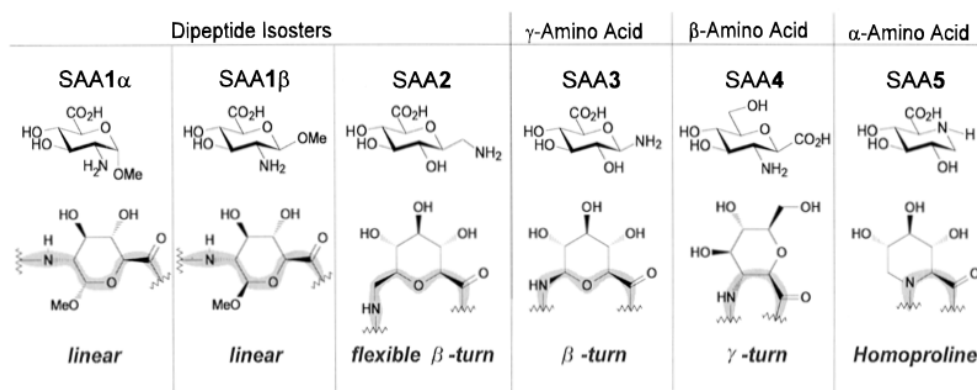


Figure 5⁷³: Structures of peptidomimetics with SAAs discussed in the *Kessler's* work

In particular, **SAA1 α** and its regioisomer **SAA1 β** are very similar to our **Morph β -AA** in the carboxy/acetal region. It was described that **SSA1 α** , when inserted in a short sequence, i.e. compound **10** (Figure 6), maintains the extended conformation of Phe-Leu sequence, according to the specific feature of this dipeptide.

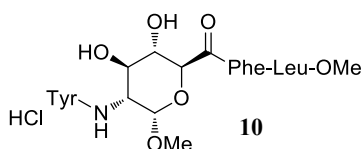


Figure 6: SSA1 α -containing peptide

To summarize the literature data, scaffolds like Nip and β -TIC are β -turn inducers when inserted in specific amino acid sequences. On the contrary, SSA1 α does not influence the extended dipeptide conformation. Furthermore, considering all the prepared peptides containing the **SAA** scaffolds, it seems that the oxygen atom of the ring does not influence the secondary structure of the peptide through H-bonds or dipole interactions.

Taken together this information and considering the features of our amino acid, we expected that our amino acid is a potential turn-inducer. As a result, in the second part of this chapter, we used the Morph β -AA for the preparation of peptide models that were studied by molecular modelling and NMR.

Inaspected results were found concerning the peptides conformation containing **Morph β -AA 1**. In fact, our amino acid is a γ -turn inducer.

γ -turn

In this paragraph an overview of the γ -turn was reported due to its implication on the hybrid α/β -peptides described in this chapter.

Every type of turn secondary structure has an important role in protein structure because of their capability to provide a direction change of a polypeptide.

Single and multiple γ -turns have been much less commonly studied in comparison with the extensively investigated β -turn conformation⁷⁴.

γ -Turns have been reviewed for the first time by Smith & Pease⁷⁵ (1980), Toniolo (1980)⁷⁶ and Rose et al. (1985)⁷⁷. Later on, different review articles on this fundamental 3D-structural motif were published^{78,79}.

A γ -turn is defined by the existence of a hydrogen bond between the CO group of one residue (i) and the NH of the ($i+2$) residue. In this respect it is like a β -turn but with one less residue. γ -Turns are pseudo-cyclic structures formed by seven terms that are stabilized by an intramolecular H-bond. The *trans* amide groups lie in two planes, which make an angle of about 115° .

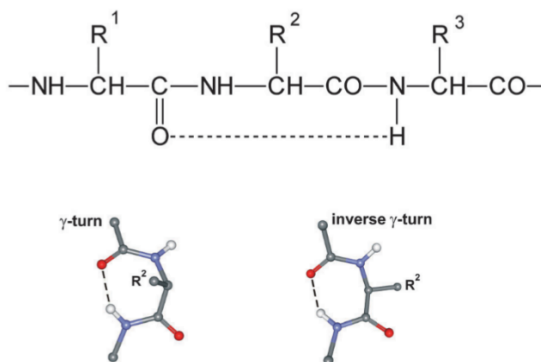


Figure 7: Two different representations of a peptide main chain folded into an axial/classical γ - or equatorial/inverse γ -turn. The intramolecular H-bonds, which generate seven-membered pseudo-ring structures, are marked as dashed lines.

As it is depicted in the Figure 7, if R^2 is not an H atom, two types of γ -turn could exist, depending on the equatorial or axial side-chain dispositions of R^2 : axial/classical γ - or equatorial/inverse γ -turn. As the main difference, the dihedral angles of classical γ -turn are $\phi_{i+1}(75^\circ)$ and $\psi_{i+1}(-65^\circ)$ and for the inverse one $\phi_{i+1}(-75^\circ)$ and $\psi_{i+1}(65^\circ)$. Some deviations from the usual *trans*-planarity of the two ω amide torsion angles are often found. However, the small energy penalty associated with these torsions is more than compensated for by the energy of the H-bond⁷⁴.

Classical γ -turns are less common than the inverse type and quite rare in proteins. However, their presence in a sample of proteins of known three-dimensional

structure was found, yet in 1988⁸⁰. In fact, it was found it occurs at the edge of the second hypervariable region of the light chain in some immunoglobulins.

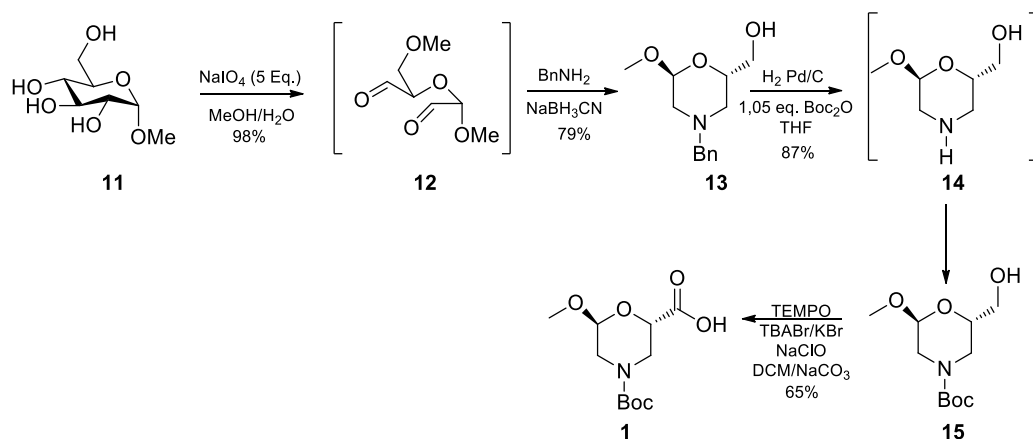
Almost all the classical γ -turns are associated with a reversal in the main chain direction. In most cases, the turn lies at the loop end of a β -hairpin.

On the other hand, inverse γ -turns, although giving rise to a kink in the chain, rarely occur within β -hairpins and are seldom situated at a position of reversal, by 180°, in chain direction⁸⁰.

Synthesis

Morph β -AA synthesis

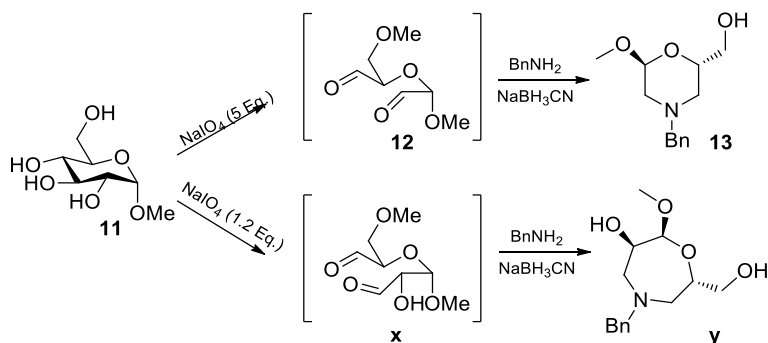
The enantiopure **Morph β -AA 1** was synthesized in five steps starting from the cheap commercially available α -D-glucopyranose **11**.



Scheme 1: Synthesis of Morph β -AA 1

The first two synthetic steps, an oxidation followed by a reductive amination, are reported in the literature⁸¹. In particular, the first reaction is critical for the overall yield of the entire synthetic pathway because of the formation of the by-product **x**, the precursor of *N*-benzyl-oxazepane ring **y** (Scheme 2). For this reason, compound **11** was oxidized with a large excess of sodium periodate (5 eq.) in a solution of

MeOH/H₂O at room temperature for 12 h affording compound **12** in quantitative yield.



Scheme 2: Synthesis of Compound 13

The crude compound **12** was used without further purification for the reductive amination step. The reaction was first performed according to the synthetic protocol reported in the literature⁸¹ by reaction of aldehyde **2** (3 equiv.) with benzylamine (1 eq.) in the presence of NaBH₃CN (5 eq., pH 7, MeOH, 25 °C, 24h). It was claimed that morpholino-derivative **13** was isolated in 84% yield. On the other hand, only 50% of **13** was obtained when I used this protocol.

For this reason, the reductive amination of aldehyde **12** was optimized. In detail, to avoid the double amination on the two-aldehyde moieties, starting from 1 equiv. of **12** and operating in MeOH at 25 °C (pH 7) in the presence of NaBH₃CN (5 equiv.), one equivalent of benzylamine was firstly added. After 12 h, a further crop of benzylamine (2 eq.) was added, affording product **13** (after 12 h) in very good yield (79%).

A one-pot reaction consisting in the nitrogen deprotection and Boc-protection of amine intermediate **14** was then performed [H₂ (1 atm), Pd/C (10% loading), Boc₂O (1.2 eq.), 25 °C, 2 h] affording compound **15** (87 %, Scheme 1).

Finally, the oxidation of the alcohol function affording the final **Morphβ-AA 1** was studied. Due to the presence of amino function, very sensitive to the oxidant, different procedures were tested. Both TEMPO [0.1 equiv., in the presence of BIAB

(2.2 equiv.), MeCN] and KMnO₄ [5 equiv. in the presence of CuSO₄·5H₂O (2 equiv.), MeCN] failed. A successful protocol consisted in a phase-transfer oxidation procedure [TEMPO (0.22 equiv.), NaClO (0.02 equiv.), TBABr (0.14 equiv.), KBr (0.02 equiv.),] operating in NaHCO₃ solution (1 M) and CH₂Cl₂ at 25 °C, that allow us to obtain **Morphβ-AA 1** in very good yield (83%).

It has to be underlined that, even if this synthetic protocol consists of 5 steps., a couple of intermediates were not isolated (compounds **12** and **14**), decreasing the purification steps. Finally, starting from the α-D-glucopiranoside **11**, the optimized synthetic protocol was scaled-up (5 g) and the enantiopure new **Morphβ-AA 1** was obtained in 56 % overall yield.

Peptide synthesis

In order to study the ability of the new **Morphβ-AA 6** to induce a stable secondary structure when inserted in peptides, the model compounds reported in the Table 1 were prepared.

Compound	Sequence	PM
17	<i>N</i> -Boc-Morphβ- <i>L</i> -Leu- <i>L</i> -Val-NH ₂	472.3
17a	<i>N</i> -Boc-Morphβ- <i>L</i> -Leu- <i>L</i> -Val-OBn	563.3
19	<i>N</i> -Boc- <i>L</i> -Val-Gly-Morphβ- <i>L</i> -Leu- <i>L</i> -Val-NH ₂	628.4
22	<i>N</i> -Boc-Morphβ- <i>L</i> -Leu- <i>L</i> -Val-Morphβ- <i>L</i> -Leu- <i>L</i> -Val-OBn	918.5

Table 1: Synthesized model peptides

It's well known that the dipeptide Leu-Val has intrinsic property to adopt an extended conformation. For this reason, this dipeptide was selected to evaluate the role of **Morphβ-AA** in peptide folding.

Considering the importance of the C-terminus in stabilizing the secondary structure of a peptide, tripeptide **17** and **17a** were synthesized.

Since the **Morph β -AA** is an analogue of the turn inducers NIP or TIC, as explained in the introduction, pentapeptide model **19** and hexa-peptide **22**, containing two β -morpholino moieties, were prepared.

The peptide synthesis was performed in liquid phase and the following general procedure were used:

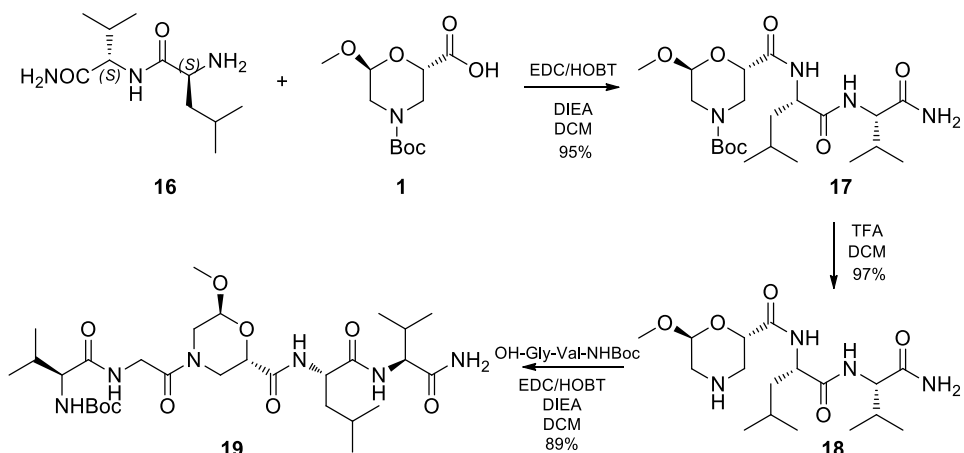
a) peptide coupling (compounds 17, 17a, 19, 22): after the activation of the carboxylic acid with HOBT (1.1 eq.) and EDC (1.1 eq.) in CH₂Cl₂ (0 °C, 1 h), the unprotected *N*-terminus amino acid or peptide (1 eq.) and DIEA (2 eq. in CH₂Cl₂), were added and the stirring was continued overnight at 25 °C;

b) deprotection of nitrogen atom (compounds 18 and 21): the deprotection of *N*-terminus was performed in a solution of TFA/DCM (1:1; 2h, 25 °C).

Preparation of pentapeptide model *N*-Boc-Val-Gly- β -Morph-Leu-Val-CONH₂ (**19**)

The dipeptide NH₂-Leu-Val-CONH₂ **16** was condensed with Morph β -AA **1** affording tripeptide *N*-Boc-Morph β -Leu-Val-CONH₂ (**17**; 95 %). *N*-Boc-Val-Gly-Morph β -Leu-Val-CONH₂ (**19**, 89%) was obtained after Boc-deprotection of **17** and its condensation with *N*-Boc-Val-Gly-OH. Each peptide was purified by flash chromatography.

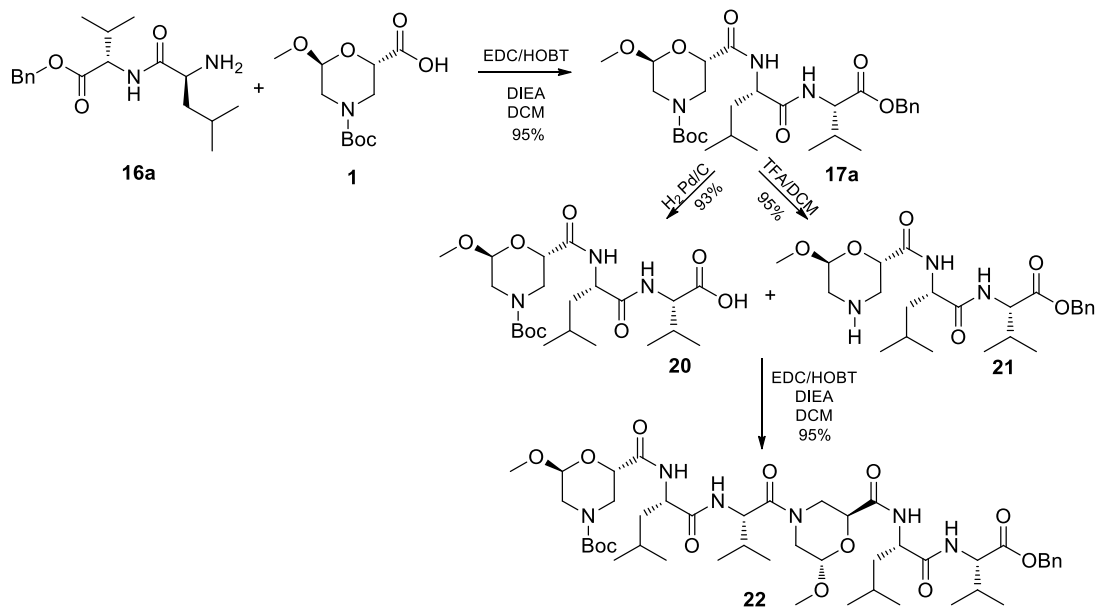
The synthesis is very efficient and pentapeptide **19** was obtained with a very good overall yield (82%) from **1** (Scheme 3).



Scheme 3: Synthesis of compound **19**

Preparation of hexapeptide model Boc-N-Morph β -Leu-Val-Morph β -Leu-Val-OBn (**22**)

The dipeptide $\text{NH}_2\text{-Leu-Val-OBn}$ **16** was made to react with compound **1**, affording tripeptide $\text{N-Boc-Morph}\beta\text{-Leu-Val-OBn}$ (**17a**; 69%). After N-termini deprotection, compound **21** was isolated in 95%. The $\text{N-Boc-Morph}\beta\text{-Leu-Val-OH}$ **20** (93%) was synthesized by reduction of compound **17a** under H_2 atmosphere, using Pd/C (10% loading, THF, 2h). The condensation of **20** with **21**, gave $\text{N-Boc-Morph}\beta\text{-Leu-Val-Morph}\beta\text{-Leu-Val-OBn}$ (**22**) in 50 % yield. Each peptide was purified by flash chromatography. Compound **22** was obtained from **1** in 4 steps and 31% overall yield (Scheme 4).



Scheme 4: Synthesis of compound 22

Computational analysis and NMR study of compounds 17, 17a, 19, 22

Computational analysis of compound *N*-Ac-Morph β -Leu-Val-NH₂

Computational analysis (conformational source) of tripeptide *N*-Ac-Morph β -Leu-Val-NH₂ were performed. It shows the presence of three main conformations with the same energy (0.5 kcal/mol), in which the morpholine ring is present as a boat (Figure 8A) and a chair (Figures 8B and 8C), these last differing from the *E* and *Z* tertiary amide conformation, respectively.

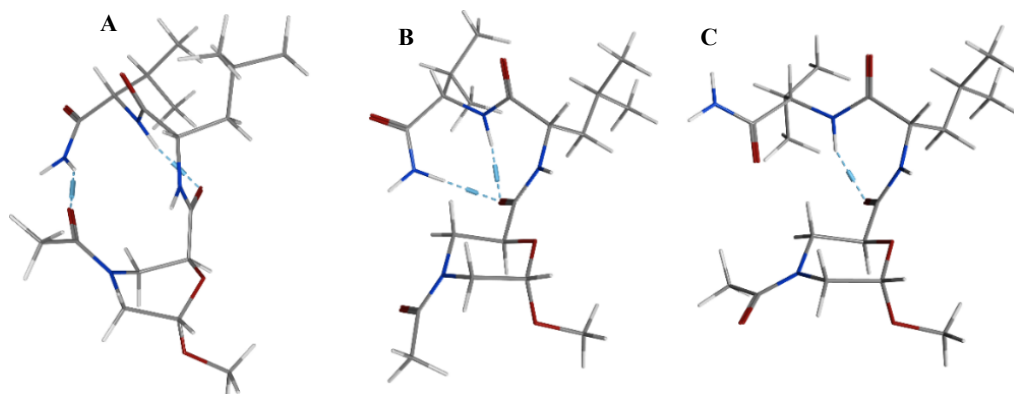


Figure 8: A-C main conformations (E: (0.5 kcal/mol) of peptide 17 obtained by computational analysis

Interestingly, as it is shown in the figure, in all the structures a H-bond is present between NH_{Val} and CO_{Morph} corresponding to the presence of a γ -turn, a motif less commonly investigated so far, in comparison with β turn conformation⁷⁴. Moreover, the boat conformation (Figure 8A) favours a H-bond between NH_2 and CO_{Boc} .

An additional γ -turn is observed in the conformer B, formed thanks to the H-bond between NH_2 and CO_{Morph} in conformer (Figure 8B).

γ -Turn conformations are classified in the less stable classical γ -turn and in the inverse turn⁷⁴. In both cases the *trans* amide group lies in two planes (angle of about 115°). As main difference, the position of R^2 of the second amino acid: its axial position gives a classical γ -turn [$\phi_{i+1}(75^\circ)$ and $\psi_{i+1}(-65^\circ)$] and the equatorial one an inverse γ -turn [$\phi_{i+1}(75^\circ)$ and $\psi_{i+1}(-65^\circ)$]. In our case, $\phi_{i+1}(+60^\circ)$ and $\psi_{i+1}(-47^\circ)$ angles were detected, that fit with an inverse γ -turn.

NMR analysis of tripeptide 17

The peptide 17 was characterized by NMR (^1H , ^{13}C , HMBC, HMQC, NOESY; MeCN, 0.01, 500 MHz) that allowed to assign unequivocally the chemical shift to each proton of morpholino ring (Figure 9B), characterized by *S,S* absolute configuration at C-2 and C-6 (Figure 9A).

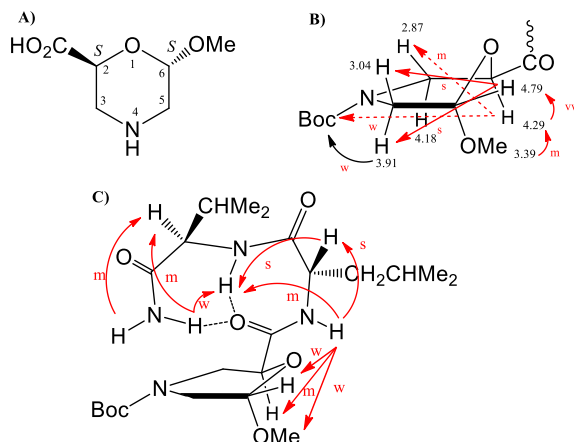


Figure 9: NOEs (red lines) and H-bond (dotted lines) for peptide 17. A) Stereochemistry of morpholino ring. B) NOEs of morpholino ring protons. C) NOEs between the different amino acids of peptide 17..

Well dispersed amide protons are present, suggesting that the peptide chain could assume an ordered conformation. $J_{\text{NH/CH}}$ values larger than 8 Hz are consistent with the classic γ -turn (dihedral angles: Leucine -4.3° , J 8.5 Hz; Valine 156.2° , J 8.5 Hz; data in agreement with conformation B of Figure 8B). Of relevance, the Noesy experiment (900 ms) showed spatial proximity between H-2 and Boc (w) and between this last and H-5 (δ 3.91, w).

The observed spatial proximity between H-2 and the Boc allow us to conclude that the *Z* conformation characterizes the tertiary amide, corresponding to conformation B of Figure 8. In the same time the absence of NOE between the H-3 and H-5 in axial position excludes a pure chair conformation of the morpholino ring, suggesting an equilibrium between a chair and a boat conformation (Figure 9B).

NOEs between this proton and both OMe (w) and H-6 (w) proved NH_{Leu} orientation toward the oxygen region of the ring.

Furthermore, a complete set of CH/NH ($i, i+1$) as well as NH/NH ($i, i+1$) NOEs are present. The medium NOE between NH_{Leu} and NH_{Val} is consistent only with the conformation of Figure 8A.

The temperature variation experiment (273-323 K) in an ulterior confirmation of our hypothesis: it showed low variation of $\Delta\delta/\Delta T$ values for all NHs (NH_{Leu} -1.8; NH_{Val} -1.9; NH_2 -2.7, -3.3 ppb/K; Table 2). According to the molecular modelling studies,

we can conclude that NH_{Val} and NH_2 are indeed involved in a strong and medium H-bond, respectively. A γ -turn, with the formation of the seven-member ring due to the formation of the H-bond between NH_{Val} and CO_{Leu} , is here proposed.

As underlined before, NH_{Leu} is not involved in a H-bond, even if it possesses a very low $\Delta\delta/\Delta T$ value. This founding confirms that a very stable conformation, induced by the two other H-bonds, was present and it avoid the vibration of the NH_{Leu} .

In conclusion, considering that the NOEs between NH_{Leu} and the morpholino ring are not compatible with the conformation reported in Figure 8A, as well as that NH_2 is not involved in H-bond in the conformation of Figure 8C, our hypothesis is that conformation of Figure 8B is the most representative in solution.

NMR analysis of tripeptide 17a

All the proton chemical shifts of tripeptide **17a** were assigned. Furthermore, the dispersed amide signals predicted a well-defined conformation of the peptide chain also in this case. Compound **17a**, that differs from **17** only for the ester function on C-terminus instead of the amide one, showed a similar behavior of the analogue **17**. As shown in Figure 10A, the NOEs signals between H-3 and H-5 in axial position with Boc-moiety indicate the *Z* configuration of the tertiary amide.

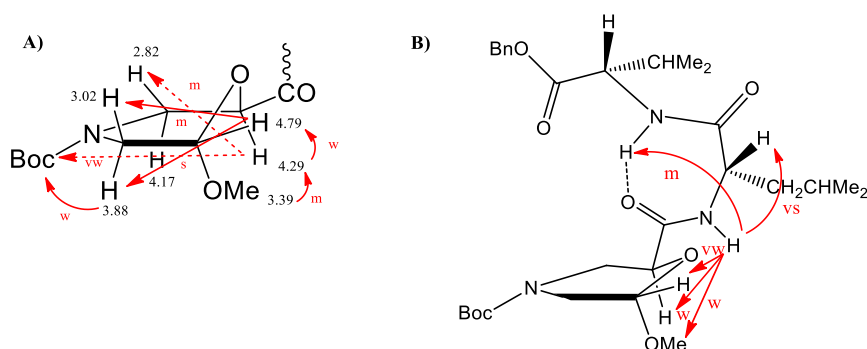


Figure 10: NOEs (red lines) and H-bond (dotted lines) for peptide **17a**. A) NOEs of morpholino ring protons. B) NOEs between the different amino acids of peptide **17a**

As shown in Figure 10B, NH_{Leu} is well oriented toward the oxygen region of morpholino ring. As for compound **17**, the same NOEs between this proton and both OMe (w) and H-6 (w) were detected. (Figure 10B).

The same patterns of signals, although with different intensities, between the NH_{*i*}/NH_{*i*+1} and CH_{*i*}/NH_{*i*+1} are present in **17a**, suggesting the same conformation of peptide **17**.

The temperature variation experiment (273-323 K) showed low variation of $\Delta\delta/\Delta T$ values for the two NHs (NH_{Leu} -1.8; NH_{Val} -3.3 ppb/K, Table 2) and it confirms the presence of a very stable secondary structure of tripeptide **17a**.

However, a higher $\Delta\delta/\Delta T$ value of NH_{Val} in **17a** was found in comparison with NH_{Val} that tripeptide **17** (-1.9 ppb/K, Table 2), meaning that the γ -turn, characterized by the H-bond between NH_{Val}- CO_{Morph β} , is less stable. Our idea is that the CONH₂ contribution in the formation of a further H-bond (see conformations A and B, Figure 8) in peptide **17** plays a big role in the stability of the γ -turn.

Surprisingly, the same $\Delta\delta/\Delta T$ value of NH_{Leu}, is observed, proving that the oxygen morpholino region is strongly determinant in orienting the NH of the second AA, or with an H-bond or determining a constrained environment that gives a well-defined orientation to this proton.

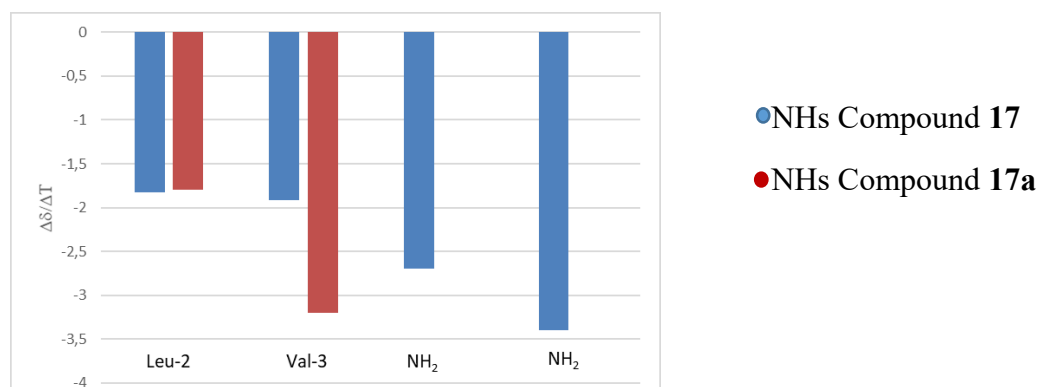


Table2: $\Delta\delta/\Delta T$ NH values for both peptides **17** and **17a** (273-323 K)

NMR analysis of pentapeptide **19**

NMR analysis of pentapeptide **19** showed the presence of a mixture of two isomers (60:40 ratio). The morpholino ring is present in two different conformations. H-chemical shifts of the major isomer are similar to that of tripeptides **17**, as well as the H-2/H-3 J values (J 11.0, 3.3 Hz). The minor isomer **19'** differs both for the chemical shifts and J values of H-2 (J 10.6, 6.4 Hz). Analogous NOEs were detected for the protons of morpholino ring in the major (Figure 11A) and minor isomers (Figure 11B). Furthermore, the protons of an isomer show spatial proximities with the corresponding protons of the second isomer. These data confirmed that a morpholino ring equilibrium occurs between the two isomers.

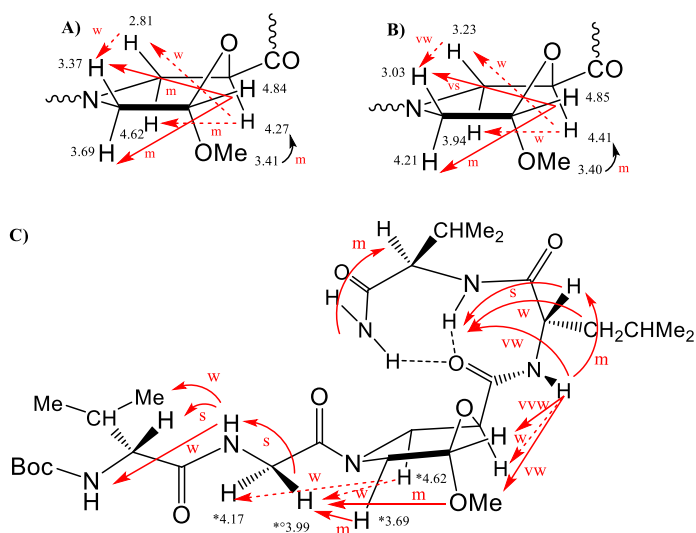


Figure 11: NOEs (red lines) and H-bond (dotted lines) for peptide **19**. A) NOEs of morpholino ring protons for the major isomer. B) NOEs of morpholino ring protons for the minor isomer. C) NOEs between the different amino acids of peptide **19**.

The NOE signals between the different AAs are reported in Figure 11C only for the major isomer **19**, because, due to the overlapped signals or similar NOEs between the two isomers, we were not able to identify the difference between the two conformers **19** and **19'**.

Our hypothesis, supported also by the previous results for tripeptides **17**, is that a γ -turn is present in both isomers at *C*-termini.

Comparing tripeptide **17** with pentapeptide **19**, as main difference, a spatial proximity (*w*) was detected between axial H-3 and H-5 of morpholino ring, not present in **17**, indicating that the equilibrium is shifted toward the morpholino-chair conformation. Analogous Noes, with different intensity, were observed at *C*-termini region between the protons of acetal region and NH_{Leu} , as well as between Leu/Val_1 , except for $\text{NH}_2/\text{CH}_{\text{Val}}$.

The experiment at variable temperature (273-323 K) also showed similar $\Delta\delta/\Delta T$ values with respect to **17** (NHVal_5 -2; NH_2 -2.5 ppb), being $\Delta\delta/\Delta T$ of NH_{Leu} the lowest one (-1.5 ppb; Table 3). As a result, the γ -turn is confirmed in this case too, independently from the elongation of the chain at *N*-termini.

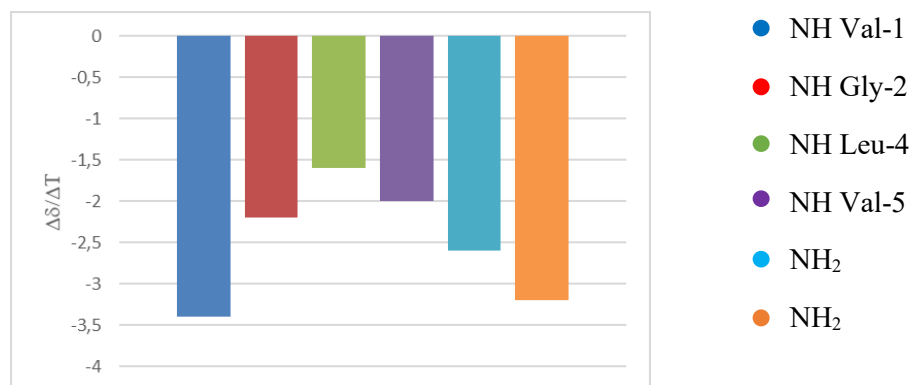


Table 3: NH $\Delta\delta/\Delta T$ values for peptide **19** (273-323 K).

Surprisingly, focusing to *N*-termini region, the α -protons of the glycine are diastereotopic: H at higher field showed spatial proximity with Heq-5 (*s*), Heq-3 (*vw*) and OMe (*w*), and with its NH (*m*), suggesting the orientation of the *N-terminus* chair upper the ring. On the other hand, the proton at lower field does not show any NOE with the ring, suggesting a defined orientation of the chain.

Furthermore, both CH/NH ($i, i+1, s$) and NH/NH ($i, i+1, m$) NOEs were detected. Finally, the low $\Delta\delta/\Delta T$ of NH_{Gly} (-2.2 ppb, Table 3) suggests the formation of a H-bond between this proton and C=OVal₁ (seven member ring) with the consequently formation of a second γ -turn⁸².

NMR analysis of hexapeptide 22

NMR experiments of hexapeptide **22** showed the presence of as mixture of two isomers (60:40 ratio). It was found that the protons of an isomer show spatial proximities also with the protons of the second isomer in the NOESY experiment, meaning that an equilibrium occurred between the two conformers.

Except for Me groups and Morph-1 that are overlapped in both conformers, the proton signal patterns were completely assigned for each isomers. Moreover, as we expected, the γ -turns are present at *C*- and *N-termini* in both conformers, in the same region observed for the previous peptides.

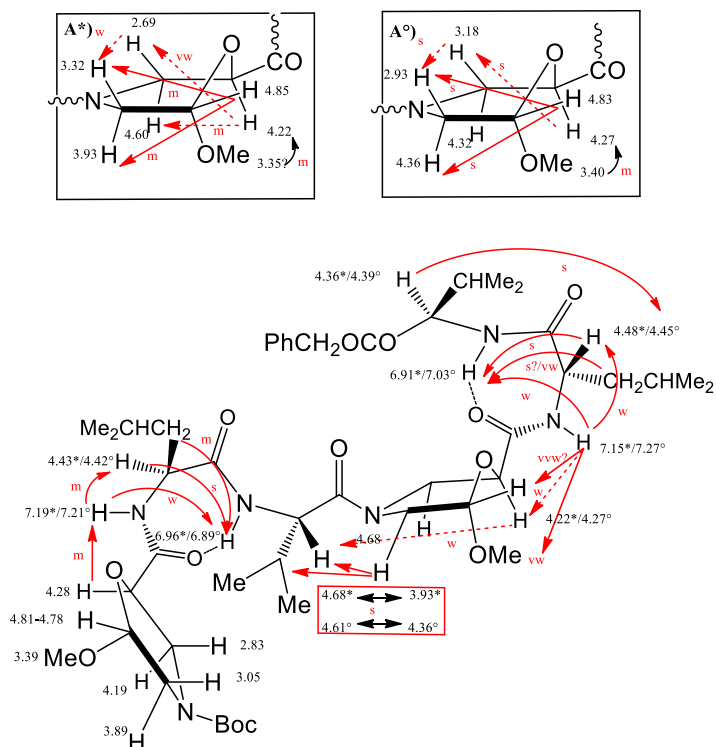


Figure 12: NOEs (red lines) and H-bond (dotted lines) for peptide **22**. A) NOEs of morpholino ring protons for the major isomer. B) NOEs of morpholino ring protons for the minor isomer. C) NOEs between the different amino acids of peptide **22**

The main difference between the two conformers is the spatial proximity between the protons of Morf β -4 and CH_{Val3}. In fact, this last proton shows proximity with both protons at C-3 in conformer **22**. On the other hand, proximities between CH_{Val3} and H-5 were detected in conformer **22'**. This suggested the presence of the two rotamers at tertiary amide bond involving CO_{Val3} and the tertiary amide of Morf β -4, being **22** the *E* rotamer and **22'** the *Z* one.

The temperature variation experiment (273-323 K) showed low variation of $\Delta\delta/\Delta T$ values for all NHs (NH_{Leu2} -1.8; NH_{Val3} -2.4; NH_{Leu5} -1.2; NH_{Val6} -1.8 ppb/K Table 4) for isomer **22** indicating that all hydrogens are involved in a very strong H-bond or are inserted in a very constrained situation.

Based on the data of NOEs experiments and $\Delta\delta/\Delta T$ values, our hypothesis is that two γ -turns are present in hexapeptide **22**.

$\Delta\delta/\Delta T$ NH values for isomer **22'** are a little bit higher ($\text{NH}_{\text{Leu}2}$ -1.8; $\text{NH}_{\text{Val}3}$ -3; $\text{NH}_{\text{Leu}5}$ -2; $\text{NH}_{\text{Val}6}$ -3.4 ppb/K, Table 4), mostly those of valines, indicating a lower propensity to give the γ -turn of Z rotamer.

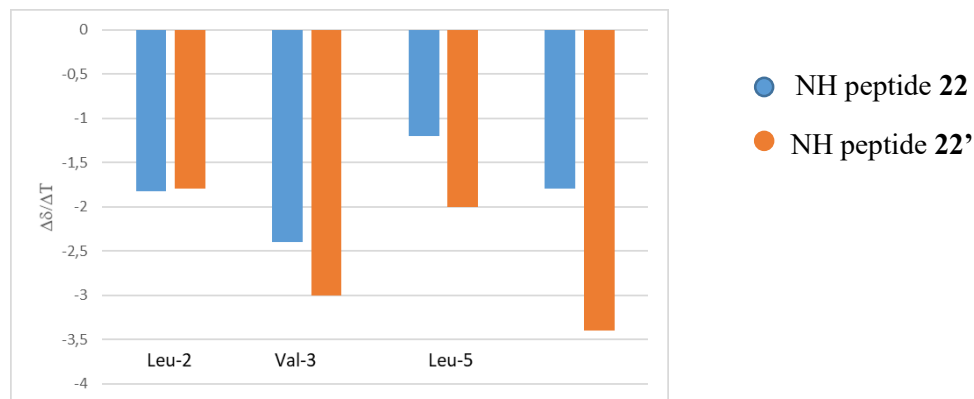
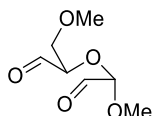


Table 4: $\Delta\delta/\Delta T$ NH values for both conformers **22** and **22'** (273-323 K)

In conclusion, considering the explained data, it must be underlined that our new enantiopure **Morph β -AA 1** has the strong ability to induce a γ -turn formation. This is probably due to the propensity of the acetal region of the morpholino ring to specifically orient the NH_{Leu} , favoring the formation of a strong H-bond between the morpholino carbonyl group and NH_{Val} ($i+2$ H-bond), independently from the substitution pattern at *N-terminus*. Furthermore, even if cyclic β -amino acids are able to induce turn conformation to be used to build hairpins, the constrained situation, presumably created by the presence of the oxygen of the morpholino, orients the β -turn in a well-defined manner preventing intrastrand interactions, as demonstrated for penta- and hexa-peptides **19** and **22**, respectively.

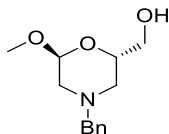
Experimental part

Synthesis of '3-hydroxy-2-(1-methoxy-2-oxoethoxy)propanal' (12)



Operating under nitrogen atmosphere, a solution of NaIO₄ (5.5 g, 25.7 mmol) dissolved in distilled water was added dropwise to a stirred solution of methyl α -D-glucopyranose **11** (1 g, 5.2 mmol) in MeOH (48 mL) at 0° C. The reaction mixture was stirred overnight and then concentrated in vacuo. The resulting colourless solid was suspended in AcOEt, filtered through a Celite pad and concentrated under reduced pressure to yield the crude dialdehyde (5.1 mmol., 0.8 g, 98%). Compound **12** was immediately used without further purification for the preparation of compound **13**. T.L.C.: R_f (CH₂Cl₂/MeOH = 20/1) = 0.26 (Detected with p-anisaldehyde). For further characterization see reference⁸¹.

Synthesis of '2S,6S-(4-benzyl-6-methoxymorpholin-2-yl)methanol' (13)



In a two-neck round-bottom flask, equipped with magnetic stirrer and nitrogen inlet, compound **12** (0.9 g, 5.3 mmol) was dissolved in MeOH (53 mL). NaBH₃CN (0.6 g, 8.8 mmol) and benzylamine (0.2 mL, 1.8 mmol) were added and the pH was adjusted to 7 with AcOH.

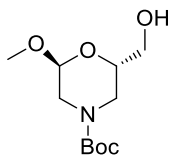
The solution was stirred overnight and then benzylamine (0.4 mL, 3.5 mmol) was added and the pH was newly adjusted to 7.

After 16 h the reaction was concentrated in vacuo and the crude was dissolved in AcOEt (30 mL). The organic layer was washed with water (5x30 mL), dried over Na₂SO₄, filtered and the solvent was removed under reduced pressure.

The residue was purified by flash chromatography (CH₂Cl₂/MeOH = 20/1) affording

product **13** (996 mg, 4.2 mmol, 79%)¹ as a colourless oil. For further characterization see reference⁸¹.

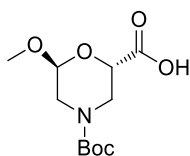
Synthesis of 2S,6S-(4-Boc-6-methoxymorpholin-2-yl)methanol' (15)



Operating in a round-bottom flask equipped with magnetic stirrer, compound **13** (558 mg, 2.4 mmol) was dissolved in THF (47 mL). Boc₂O (539 mg, 2.5 mmol) and Pd/C (635 mg, 10% loading) were added to the solution.

The suspension was stirred under H₂ (1 atmosphere) at 25 °C. After 2 h, the mixture was filtered on Celite pad. The solution was concentrated in reduced pressure and the yellow oil was dissolved in DCM, washed with a 5% solution of KHSO₄ (mL) and a saturated solution of NaCl (mL). The organic layer was dried over Na₂SO₄, filtered and concentrated in vacuum. Purification of the crude by flash chromatography (CH₂Cl₂/MeOH = 20/1) afforded product **15** (505 mg, 2 mmol, 87%) as colorless oil. TLC: R_f (CH₂Cl₂/MeOH = 20/1) = 0.31 (Detected with phosphomolibdic acid). IR (NaCl) ν_{max}: 3437; 1680 cm⁻¹. [α]_D²⁰ = +2.17. MS (ESI): *m/z* calcd for [C₁₁H₂₁NO₅]: 247.14; found: *m/z* 270.13 [M+Na]⁺. ¹H NMR (300 MHz, CDCl₃): δ 4.72 (m, 1H), 3.90-4.01 (m, 3H), 3.71 (dd, *J* = 11.8, 3.6 Hz, 2H), 3.60 (dd, *J* = 11.8, 3.6 Hz, 1H), 3.37 (s, 3H), 2.03 (m, 1H), 2.83 (m, 1H), 2.08 (brs, 1H), 1.46 (s, 9H) ppm. ¹³C NMR (75 MHz, CDCl₃): δ 155.6, 96.6, 80.5, 67.9, 63.8, 55.1, 46.9, 44.1, 28.74 ppm.

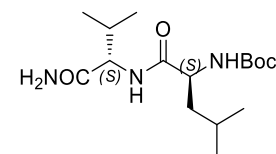
Synthesis of '2S,6S-(4-Boc-6-methoxymorpholin-2-yl)carboxylic Acid (1)



Operating in a round-bottom flask equipped with magnetic stirrer, compound **15** (1.2 g, 4.7 mmol) was dissolved in CH₂Cl₂ (17 mL) and the solution was cooled to 0 °C. TBABr (105 mg, 0.33 mmol), KBr (56 mg, 0.5 mmol), TEMPO (161 mg, 1.03 mmol), a solution of NaHCO₃ in water (1 M, 7.6 mL), NaClO (8.6 mL, 0.02 mmol), and brine (1 mL) were added. After 20 min., a saturated solution of NaHCO₃ (5.6 mL) was finally added and the mixture was stirred at 25 °C overnight.

The layers were separated. The aqueous phase was acidified with HCl (20 mL, 30%) and extracted with AcOEt (2 x 20 mL). The combined organic layers were dried over Na₂SO₄, filtered and concentrated under reduced pressure. The crude mixture was purified by flash chromatography (CH₂Cl₂/MeOH = 30/1) affording pure product **1** as colourless oil (1.0 g, 3.88 mmol, 83%). TLC: R_f(CH₂Cl₂/MeOH = 20/1) = 0.4 (Detected by phosphomolibdic acid). [α]_D²⁰ = +103.16 (c 1, MeOH). IR (NaCl) ν_{max}: 2976.9, 1750.1 1651.6 cm⁻¹. MS (ESI): *m/z* calcd for [C₁₁H₁₉NO₆]: 261.12; found: *m/z* 284.0 [M+Na]⁺. ¹H NMR (300 MHz, CDCl₃): δ 5.55 (brs, 1H), 4.81 (brs, 1H), 4.58 (dd, *J* = 10.4 - 3.3 Hz, 1H), 4.30 (brs, 1H), 3.93 (brs, 1H), 3.44 (s, 3H), 3.14 (m, 1H), 3.08 (m, 1H), 1.49 (s, 9H) ppm. ¹³C NMR (75 MHz, CDCl₃): δ 172.7, 155.2, 96.6, 81.2, 67.1, 55.7, 46.4, 44.6, 30.0 ppm.

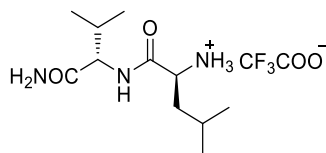
Synthesis of 'N-Boc-Leu-Val-CONH₂'



In a round-bottom flask equipped with a magnetic stirrer and thermometer, *N*-Boc-(*L*)-Leucine (500 mg, 2.2 mmol) was dissolved in CH₂Cl₂ (22 mL) and the solution was cooled to 0 °C. HOBt (351 mg, 2.6 mmol) and EDC (514 mg, 2.6 mmol) were added. After 1 h, (*L*)-valinamide (329.7 mg, 2.2 mmol) dissolved in CH₂Cl₂ was dropped, followed by the addition of DIEA (0.56 mL, 3.25 mmol). The reaction mixture was stirred for 24 h and then it was washed with 5% KHSO₄ (10 mL), a

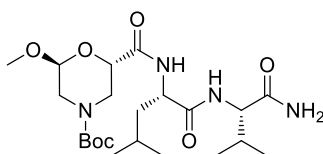
saturated solution of NaHCO₃ (10 mL), brine (10 mL). After drying over Na₂SO₄, the solvent was removed under reduced pressure. Purification of the crude product by crystallization from Et₂O (10 mL) afforded '*N*-Boc-Leu-Val-CONH₂' (668 mg, 2.0 mmol, 94%) as a white solid. TLC: R_f (CH₂Cl₂/MeOH = 30/1): 0.28 (Detected by ninhydrin). For further characterization see reference ⁸³.

Synthesis of '*NH*₂-Leu-Val-CONH₂' (**16**)



In a round-bottom flask equipped with magnetic stirrer, '*N*-Boc-Leu-Val-CONH₂' (960 mg, 3 mmol) was dissolved in CH₂Cl₂ (4 mL). The solution was cooled to 0 °C and then 99% TFA (4 mL) was added. The solution was stirred at r.t. for 2 h and concentrated under reduced pressure. Product **16** was isolated as a white solid (650 mg, 2.8 mmol, 97%). TLC: R_f (AcOEt/*n*Hex,=1/1): 0.20 (Detected by ninhydrin). For further characterization see reference ⁸³.

Synthesis of '*N*-Boc-Morphβ-Leu-Val-CONH₂' (**17**)



In a round-bottom flask equipped with magnetic stirrer, compound **1** (160 mg, 0.6 mmol) was dissolved in CH₂Cl₂ (7 mL). The solution was cooled to 0 °C. After that, HOBT (99 mg, 0.7 mmol) and EDC (150 mg, 0.7 mmol) were added and the solution was left to 0 °C for 1 h. Finally, compound **16** (205 mg, 0.6 mmol) was added and pH 8 was adjusted with DIEA (100 μL, 0.61 mmol). The solution was left at room temperature for 24 h. The crude was washed first with a solution of KHSO₄ (5%, 10

mL) then with a saturated solution of NaHCO₃ (10 mL) and finally with brine (10 mL).

After the separation of the aqueous layer, the organic one was dried over Na₂SO₄ and the solvent was removed under reduced pressure. After purification by crystallization with AcOEt/nhexane, pure product **17** was isolated as white solid (274 mg, 0.58 mmol, 95%). TLC: R_f (AcOEt/nHex = 1/1) = 0.25 (Detected by phosphomolibdic acid). [α]_D²⁰ = +52.56 (c 1, MeOH). IR (NaCl) ν max: 1644.18; 1678.56 cm⁻¹. MS (ESI): m/z calcd for [C₂₂H₄₀N₄O₇]: 472.29; found: m/z 496.58 [M+Na]⁺.

AA	atom	¹ H NMR δ	Multiplicity <i>J</i> (Hz)	¹³ C NMR δ	Noesy
Morph- 1	CO			169.1	
	H-2	H _{ax} 4.29	dd, <i>J</i> 10.8 <i>J</i> 3.2	67.6	NH _{Leu} (m) H-6 (vw) H-3 _{ax} (m) OMe (m) Boc (w)
	H-3	H _{ax} 2.87	br	45.1	H-2 (m)
		H _{eq} 4.18	overl		
	H-5	H _{ax} 3.04	br	46.3	H-6 (s) ----- H-6 (s) Boc (w)
H _{eq} 3.91		d, <i>J</i> 13.7			
	H-6	H _{eq} 4.79	br	96.7	H-5 _{ax} (s) H-5 _{eq} (s) OMe (s)

					NH _{Leu} (w)
	OMe	3.39		54.4	H-6 (s) H-2 (m) NH _{Leu} (w)
	Boc	1.46	s	27.3, 79.2	H-5 _{eq} (w) H-2 (w)
	CO			^a	
Leu-2	CO			171.7	
	CH	4.44	m	51.2	NH _{Leu} (s) NH _{Val} (s)
	CH ₂	1.62	m	40.6	CH _{Leu} (s)
	CH			24.8	
	Me	0.94	overl	21.0	
		0.97		22.3	
	NH	7.20	d, <i>J</i> 8.1		OMe (w) H-2 (m) H _{Leu} (s) H-6 (w) NH _{Val} (m)
Val-3	CO			172.8	
	CH	4.18	overl	57.7	NH ₂ (m)
	CH _{isopr}	2.09		30.6	H _{Val} (m)
	Me	0.90	d, <i>J</i> 9.9	17.1	NH _{Val} (s) CH _{Val} (4.18, s)
		0.94	overl		

	NH	6.83	d, <i>J</i> 8.5		Me _{Val} (0.90, vs) CH/CH ₂ Leu (s) CH _{Val} (m) CH _{Leu} (s) NH ₂ (5.78, w; 6.29, vw) NH _{Leu} (m)
	NH ₂	5.78	s		CH _{Val} (4.18, m) CH _{Val} (2.09, w) NH _{Val} (w) ----- CH _{Val} (m) CH _{isoprVal} (w) NH _{Val} (vw)
		6.29			

Table 5: ¹H, ¹³C NMR (CD₃CN, 10 mM, 500 MHz) and NOE (900 ms) data for tripeptide **8**

^a Not assigned

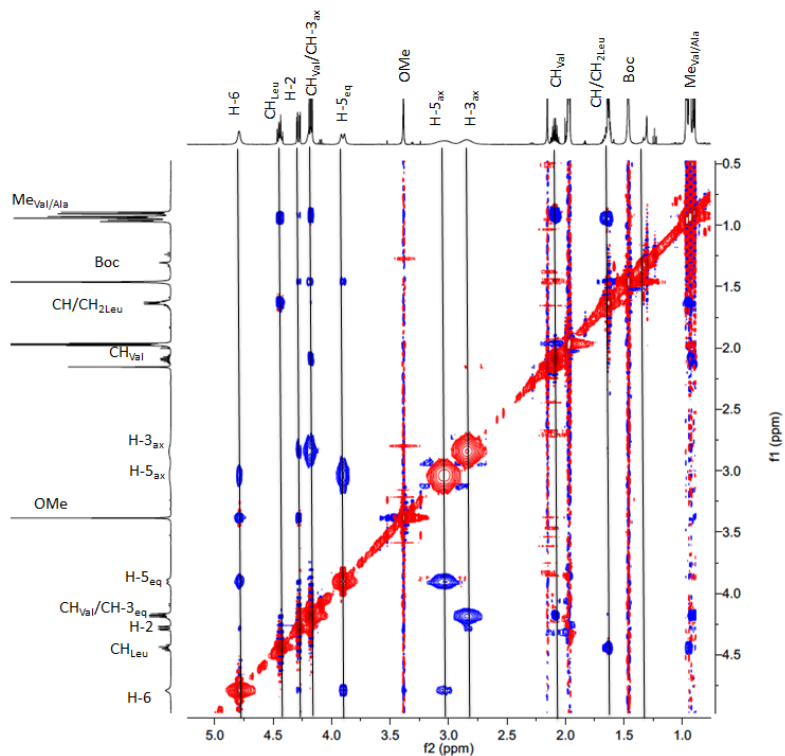


Figure 13: Magnification of CH/CH region of the NOESY experiment

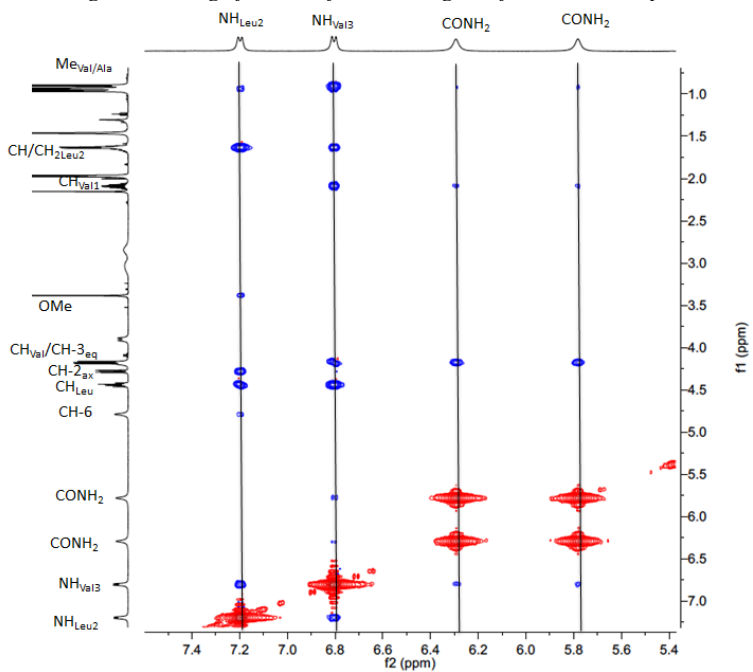
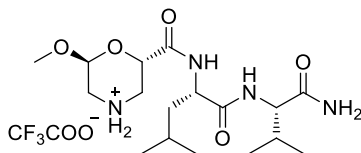


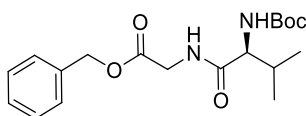
Figure 14: Magnification of CH/NH region of the NOESY experiment

Synthesis of 'CF₃COO⁻(NH₃-Morphβ-Leu-Val-CONH₂)' (**18**)



In a round-bottom flask equipped with magnetic stirrer, compound **17** (60 mg, 0.18 mmol) was dissolved in CH₂Cl₂ (4 mL). The solution was cooled to 0 °C and TFA was slowly dropped (4 mL). The solution was stirred at room temperature for 2 h. Afterwards the solvent was removed under reduced pressure, affording product **18** as a white solid (58 mg, 0.12 mmol, 97%). TLC: R_f (CH₂Cl₂/MeOH = 20/1) = 0.1 (Detected by phosphomolibdic acid). IR (NaCl) ν max: 1673.83; 1543.76 cm⁻¹. MS (ESI): m/z calcd for [C₁₇H₃₂N₄O₅]: 372.32; found: m/z 373.29 [M+H]⁺. ¹H NMR (CD₃OD, 300 MHz): δ 5.1 (s, 1H), 4.7 (dd, $J = 11.7, J = 2,71$), 4.25 (m, 1H), 4.1 (m, 1H), 3.45-3.6 (m, 4H), 3.05 (m, 1 H), 2.03 (m, 1H), 1.55 (m, 2H), 0.97-1.10 (m, 12 H) ppm. ¹³C NMR (75 MHz, CD₃OD): δ 174.4, 172.7, 167.9, 94.3, 64.6, 58.2, 54.6, 51.6, 43.73, 40.25, 30.7, 29.3, 24.5, 21.9, 20.5, 18.3, 17.1 ppm.

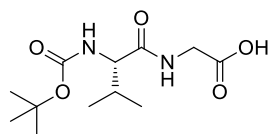
Synthesis of 'N-Boc-Val-Gly-OBn'



N-Boc-Val-COOH (9.0 mmol), Gly-OBzl tosylate (9.0 mmol), and TEA (22 mmol) were dissolved in anhydrous MeCN (72 mL). HBTU (9.0 mmol) was added and the mixture was stirred for 30 h at room temperature. A saturated NaCl solution (210 mL) was added, and the crude compounds were extracted with AcOEt. The organic phase was washed with a 10% aqueous citric acid solution (100 mL), H₂O (100 mL), 4% NaHCO₃ solution (100 mL), and then H₂O (100 mL). The '*N*-Boc-Val-Gly-OBn' was purified by a silica gel column chromatography (EtOAc/hexane = 51/2). Yield

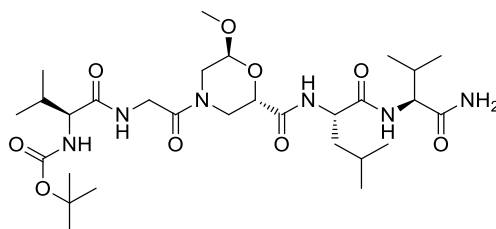
83%. ^1H NMR (DMSO, 400 MHz): δ 7.36 (s, 5H), 5.12 (s, 2H), 3.83-3.98 (m, 2H), 1.92 (brs, 1H), 1.38 (s, 9H), 0.82-0.85 (m, 6H) ppm. ^{13}C NMR (100 MHz, DMSO): δ 171.9, 169.6, 155.3, 135.8, 128.3, 128.0, 127.9, 77.9, 65.8, 59.4, 40.6, 30.4, 28.1, 19, 18 ppm. For further characterization see reference ⁸³.

Synthesis of 'N-Boc-Val-Gly-OH'



Boc-Val-Gly-OBzl (5 g, 13.72 mmol) in glacial acetic acid (50 ml) was hydrogenated at 40 psi in the presence of 10% palladium-carbon catalyst (0.5 g) for 6 h. The catalyst was filtered and the filtrate concentrated under reduced pressure. The residue was taken in 4% NaHCO_3 solution (20 mL) and extracted with EtOAc (3 x 20 mL). The aqueous solution was cooled, acidified to pH 2 and extracted into CHCl_3 (3 x 20 mL). The combined organic layers were washed with saturated NaCl solution (20 mL), dried over anhydrous MgSO_4 and the solvent removed under reduced pressure. The peptide was precipitated from EtOAc/Pet ether, 3.83 g (Yield: 100%). M.p.: 109-113 °C. The analysis calculated for $\text{C}_{12}\text{H}_{22}\text{N}_2\text{O}_4$ was C, 52.54%; H, 8.08%; N, 10.21%. The observed composition was C, 52.34%; H, 8.22%; N, 10.28%. For further characterization see reference ⁸³.

Synthesis of 'N-Boc-Val-Gly-Morph β -Leu-Val-CONH₂' (19)



In a round-bottom flask equipped with a magnetic stirrer and thermometer, dipeptide N-Boc-Val-Gly-OH (46.6 mg, 0.2 mmol) was dissolved in CH_2Cl_2 (3 mL) and the

solution was cooled to 0 °C. HOBt (28 mg, 0.2 mmol) and EDC (41 mg, 0.2 mmol) were added. After 1 h, compound **18** (75 mg, 0.17 mmol) in CH₂Cl₂ (15 mL) was dropped, followed by the addition of DIEA (30 μL, 0.17 mmol). The reaction mixture was stirred for 24 h and then it was washed with KHSO₄ (5%, 10 mL), a saturated solution of NaHCO₃ (10 mL) and brine (10 mL). After drying over Na₂SO₄, the solvent was removed under reduced pressure. Purification of the crude product by crystallization from AcOEt/nhexane afforded compound **19** (97 mg, 0.2 mmol, 89%) as a white solid. TLC: R_f (CH₂Cl₂/MeOH = 20/1): 0.30 (Detected by phosphomolibdic acid). M.p.: 145.2 °C. [α]_D²⁵ = +40.12 (c 1, MeOH). IR (NaCl) ν_{max}: 1677.5; 1647.96 cm⁻¹. MS (ESI): *m/z* calcd for [C₂₉H₅₂N₆O₉]: 628.38; found: *m/z* 629 [M + H]⁺; 651 [M + Na]⁺.

AA	atom	¹ H δ	Multiplicity <i>J</i> (Hz)	¹³ C δ	Noesy
Val-1	CO			171.6	
	CH	3.96	overl.	59.7	NH _{Gly} (s) NH _{Val} (m)
	CH _{isopr}	2.13-2.05		30.6	
	Me	0.95	d, <i>J</i> 6.0	18.6	NH _{Gly} (s)
		0.90		16.9	
	NH	5.53	br		NH _{Gly} (w) CH _{Val} (m)
	CO			^a 162.7	
Boc	1.44		27.6	CH _{Val} (w)	
Gly-2	CO			167.4	
	CH ₂	3.99	overl.	40.6	NH _{Gly} (s) H _{eq-3} (w)

		4.17			H _{eq} -5 (m) OMe (3.41, m) ----- H _{eq} -3 (w)
	NH	6.98	br		CH _{Gly} (s) NH _{Val1} (w) CH _{Val1} (s) Me (0.95, w) CH _{isoprVal1} (w)
Morf	CO			168.7	
	CH-2	4.27	dd, <i>J</i> 11.0, 3.3	67.8	NH _{Leu4} (w) H-3 (4.62 m, 2.81 w) OMe (m)
	CH ₂ -3	H _{ax} 2.81 H _{eq} 4.62	dd, <i>J</i> 13.3, 11.0 d, <i>J</i> 13.3	43.7	H-5 _{ax} (w) H-2 (w) H-3 (s) ----- H-2 (m) CH _{2Gly} (w) H-3 _{ax} (s)
	CH ₂ -5	H _{ax} 3.37 H _{eq} 3.69	overl d, <i>J</i> 14.0	47.5	H-3 _{ax} (w) H-5 _{eq} (s) H-6 (m) ----- CH _{Gly} (3.99, m) H-6 (m) H-5 _{ax} (s)

	CH-6	4.84	br	95.3	OMe (m) H-5 (3.69 m, 3.37 m)
	OMe	3.41		54.6	H-2 (m) H-6 (s) CH _{Gly} (3.99, m)
Leu-4	CO			171.7	
	CH	4.44		51.4	NH _{Val5} (s)
	CH ₂ CH	1.68-1.62	m	40.4 24.6	NH _{Val5} (w) NH _{Leu} (m)
	Me	0.96 0.94	overl.	22.3 21.0	
	NH	7.20	d, <i>J</i> 8.1		CH _{Leu} (m) H-2 (w) H-6 (vww) OMe (vw) NH _{Val5} (vw)
Val-5	CO			172.9	
	CH	4.18	m	57.7	NH ₂ (w) NH _{Val5} (m)
	CH	2.13-2.05	m	30.6	
	Me	0.93 0.90	d, <i>J</i> 7.3	21.0 16.8	
	NH	6.83	d, <i>J</i> 8.6		CH/CH ₂ Leu (w)

					CH _{Leu} (s) CH _{Val5} (m) NH _{Leu4} (vw)
	NH ₂	5.79 6.31	s s		CH _{Val5} (w)

Table 6: ¹H, ¹³C NMR (CD₃CN, 9 mM, 500 MHz) and NOE (500 ms) data for peptapeptide **19**

^aTentatively assigned

Minor isomer **19'**

AA	atom	¹ H δ	Multiplicity <i>J</i> (Hz)	¹³ C δ	Noesy	
Val-1	CO			171.5		
	CH	3.96	overl	59.7	NH _{Gly} (vs) NH _{Val1} (m)	
	CH	2.13-2.05		30.61		
	Me		0.95	d, <i>J</i> 6.0	18.7	
			0.90		16.9	
	NH	5.53	overl		NH _{Gly} (m) CH _{Val1} (m)	
		CO			162.7 ^a	
	Boc	1.44	overl	27.6		
Gly-2	CO			167.9		
	CH ₂	4.02	overl	40.5		
	NH	6.95	overl			
Morf	CO			^b		
	H-2	4.41	dd, <i>J</i> 10.6, 6.4	67.9	H-3 (3.23,w; 3.94,m)	

					MeO (m) NH _{Leu} (vw)
	H-3	H _{ax} 3.23 H _{eq} 3.94	m overl	45.5	H-2 (w) H-5 _{ax} (vw) H-3 _{eq} (s) ----- H-2 (w) H-3 _{ax} (s)
	H-5	H _{ax} 3.03 H _{eq} 4.21	dd <i>J</i> 13.7, 2.6 overl	44.1	H-6 (m) H-3 _{ax} (vw) H-5 _{eq} (s) ----- H-5 _{ax} (s) H-6 (4.85, m)
	H-6	4.85	brs	96.4	OMe (m) H-5 (3.03 m, 4.21 m)
	OMe	3.40		54.5	H-2 (m)
Leu-4	CO			171.6	
	CH	4.45		51.6	NH _{Val5} (s) NH _{Leu4} (s)
	CH/CH ₂	1.68-1.62	m	40.5 24.6	
	Me	0.96 0.94	overl	22.3 21.0	
	NH	7.29	d, <i>J</i> 8.2		CH _{Leu4} (m) NH _{Val5} (vw)

Val-5	CO			172.9	
	CH	4.19	m	57.6	NH ₂ (w) NH _{Val5} (m)
	CH _{isopr}	2.13-2.05	m	30.7	
	Me	0.94 0.91		^a 21.0 19.9	
	NH	6.88	d, <i>J</i> 7.9		CH/CH ₂ Leu (w) CH _{Leu} (s) CH _{Val5} (m) NH _{Leu4} (vw)
	NH ₂	5.87 6.35	s		CH _{Val5} (w)

Table 7: ¹H, ¹³C NMR (CD₃CN, 9 mM, 500 MHz) and NOE (500 ms) data for peptide **19'**

^aTentatively assigned; ^b Not assigned

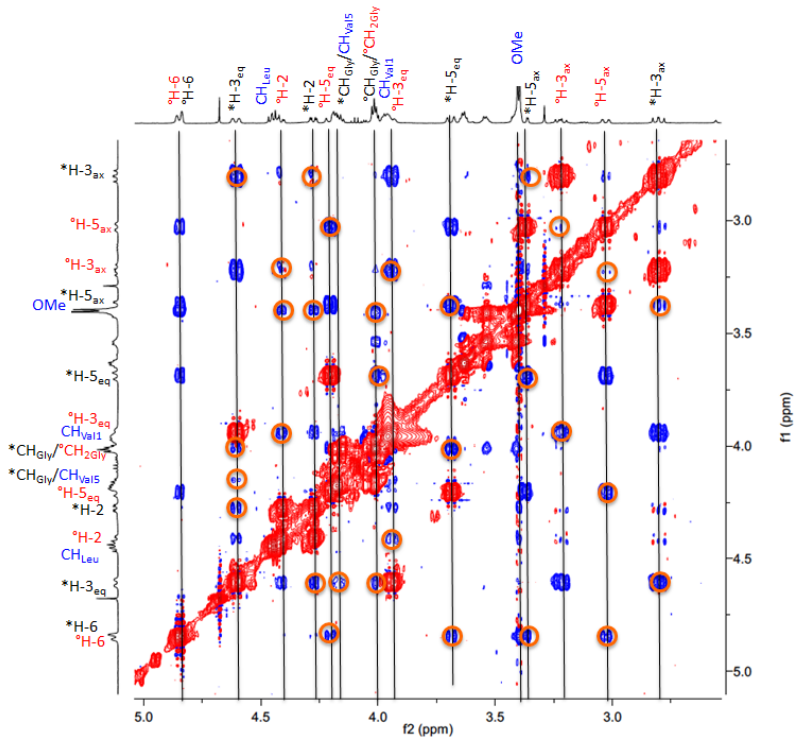


Figure 15: Magnification of CH/CH region of NOESY experiment

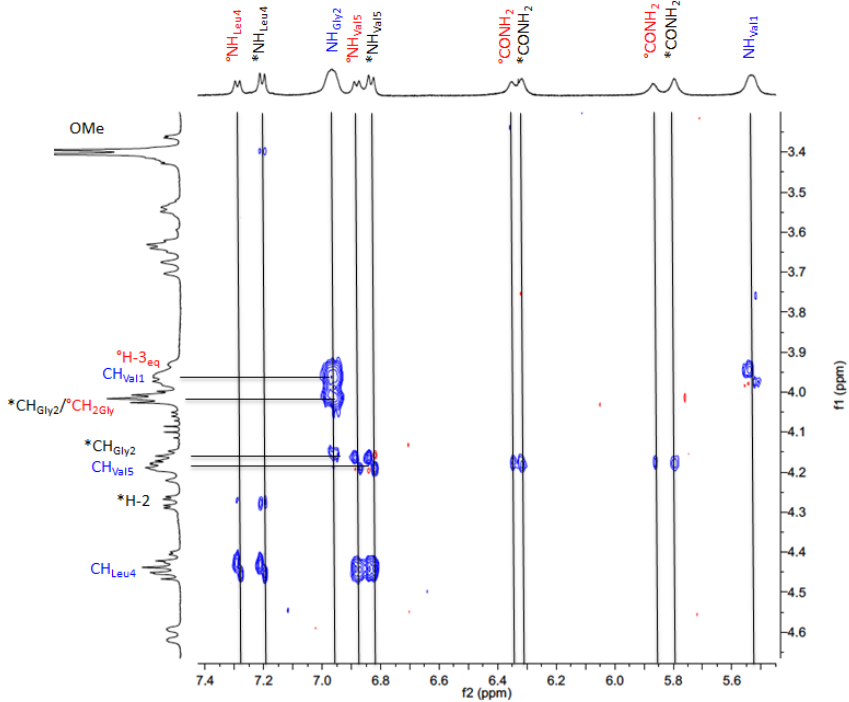


Figure 16: Magnification of CH/NH region of NOESY experiment

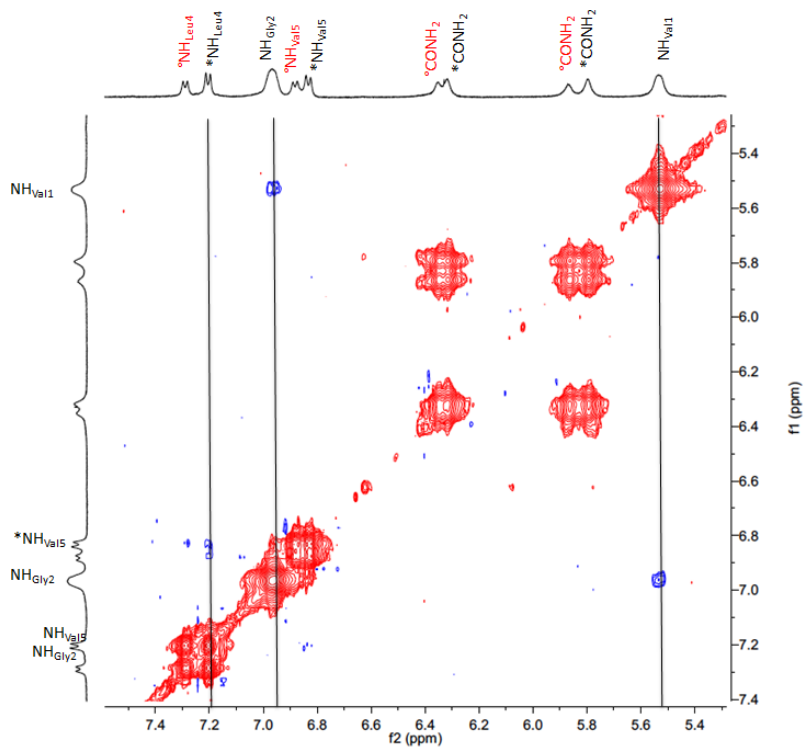
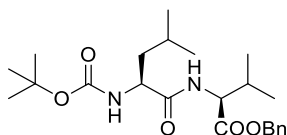


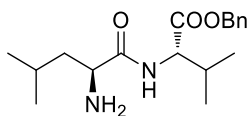
Figure 17: Magnification of NH/NH region of NOESY experiment

Synthesis of 'N-Boc-Leu-Val-OBn'



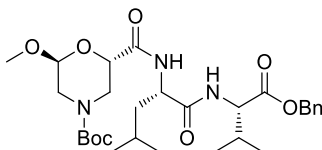
A solution of *L*-valine benzyl ester (6.0 g, 28.9 mmol) and *N*-Boc-leucine (6.7 g, 29.1 mmol) in anhydrous THF (150 mL) at 0° C was treated with *N*-methyl morpholine (15.5 mL, 14.3 g, 141 mmol) and HOBT (4.5 g, 33.6 mmol), followed by addition of EDC (6.5 g, 34.1 mmol). The mixture was stirred at r.t. for 12 h, then treated with a saturated solution of NaHCO₃ (100 mL) and extracted with CH₂Cl₂ (5 × 30 mL). The combined organic layers were dried (Na₂SO₄) and concentrated in vacuo. Flash column chromatography (*n*hexane/AcOEt = 7/3) afforded *N*-Boc-Leu-Val-OBn (11.3 g, 27.0 mmol, 93%) as a white solid. For further characterization see reference

Synthesis of 'NH₂-Leu-Val-OBn' (16a)



A solution of *N*-Boc-Leu-Val-OBn (5.7 g, 13.5 mmol) in anhydrous CH₂Cl₂ (19.0 mL) at 0° C was treated dropwise with trifluoroacetic acid (12.0 mL, 18.4 g, 162 mmol). The resulting mixture was stirred at r.t. for 1 h, then concentrated in vacuo. The residue was dissolved in CH₂Cl₂ (100 mL) and basified with 2M NaOH (80 mL). The layers were separated, and the aqueous layer was extracted with CH₂Cl₂ (3 × 30 mL). The combined organic layers were dried (Na₂SO₄) and concentrated to afford compound **16a** (4.3 g, 13.5 mmol, 100%) as a yellow oil⁸⁴.

Synthesis of 'N-Boc-Morphβ-Leu-Val-OBn' (17a)



In a round-bottom flask equipped with magnetic stirrer, compound **1** (311 mg, 1.2 mmol) was dissolved in CH₂Cl₂ (15 mL). The solution was cooled to 0 °C. After that, HOBT (178 mg, 1.3 mmol) and EDC (259 mg, 1.3 mmol) were added and the solution was left to 0 °C for 1 h. Finally, compound **16a** (500 mg, 1.2 mmol) was added and pH 8 was adjusted with DIEA (0.2 mL, 1.3 mmol). The solution was left at room temperature for 24 h. The crude mixture was washed first with a solution of a 5% solution (20 mL) KHSO₄, then with a saturated solution of NaHCO₃ (20 mL) and finally with brine (20 mL).

The organic layer was dried over Na₂SO₄ and the solvent was removed under reduced pressure. Purification by silica gel flash chromatography (AcOEt/nhexane = 2/1) afforded compound **17a** as white foam (460 mg, 0.82 mmol, 69%). TLC: R_f

(CH₂Cl₂/MeOH = 20/1) (Detected by phosphomolibdic acid) = 0.27. M.p.: 50 °C.
 [α]_D²⁰ = +5 (c 0.3, MeOH). IR (NaCl) *v max*: 3319; 2964; 2934; 1703; 1656 cm⁻¹.
 MS (ESI): *m/z* calcd for [C₂₉H₄₅N₃O₈]: 563.32; found: *m/z* 586.56 [M+Na]⁺.

AA	atom	¹ H NMR <i>δ</i>	Multiplicity <i>J</i> (Hz)	¹³ C NMR <i>δ</i>	Noesy
Morph- 1	CO			^a 168.8	
	H-2	4.25	dd, <i>J</i> 10.9 <i>J</i> 3.2	67.5	NH _{Leu} (w) H-3 _{ax} (m) OMe (w)
	H-3	H _{ax} 2.82	br	45.59	H-2 (m) H-3 _{eq} (s) ----- H-3 _{ax} (s) Boc (vw)
		H _{eq} 4.17	d, <i>J</i> 13.1		
	H-5	H _{ax} 3.03	br	45.95	H-6 (m) H-5 _{eq} (vs) ----- H-6 (m) H-5 _{ax} (vs) Boc (vw)
		H _{eq} 3.88	d, <i>J</i> 14.4		
H-6	4.78	br	96.25	H-5 _{ax} (m) H-5 _{eq} (m) OMe (m) NH _{Leu} (vw)	
OMe	3.36	s	54.4	H-6 (m) NH _{Leu} (w)	

	Boc	1.46	s	27.48,79.67	H-5 _{eq} (w) H-3 _{eq} (w)
	CO			^a 154.2	
Leu-2	CO			^a 171.2	
	CH	4.47	m	50.9	NH _{Leu} (s) CH/CH ₂ (s) NH _{Val} (s) Me (m)
	CH/CH ₂	1.57	overl	40.9 24.50	CH _{Leu} (s) Me (vs) NH _{Leu} (s)
	Me	0.90 0.91	overl	21.1 22.3	
	NH	7.14	d, <i>J</i> 8.4		OMe (w) CH/CH _{2Leu} (s) H-2 (m) H-6 (vw) CH _{Leu} (s) NH _{Val} (w)
Val-3	CO			^a 171.9	
	CH	4.36	dd, <i>J</i> 5.7 <i>J</i> 8.3	57.6	Me (s) CH _{isoprVal} (m) NH _{Val} (m)
	CH _{isopr}	2.15	m	30.4	Me (s) CH _{Val} (m)
	Me	0.89	overlapped	17.2	NH _{Val} (s) CH _{Val} (s)

		0.93		18.3	
	NH	6.89	d, <i>J</i> 7.9		Me (0.91, s) CH ₂ Leu (w) CH _{Val} (m) CH _{isoprVal} (w) CH _{Leu} (s) NH _{Leu} (w)
	OCH ₂	5.14	dd, <i>J</i> 12.4 <i>J</i> 17.5	66.5	CH _{Val} (vw) Bn (m)
	Bn	7.41-7.36	m	128.24 128.50 129.56 136.04	CH ₂ isprLeu (vw) OCH ₂ (m)

Table 8: ¹H, ¹³C NMR (CD₃CN, 20 mM, 500 MHz) and NOE (1.1 s) data for tripeptide 17a

^a Tentatively assigned

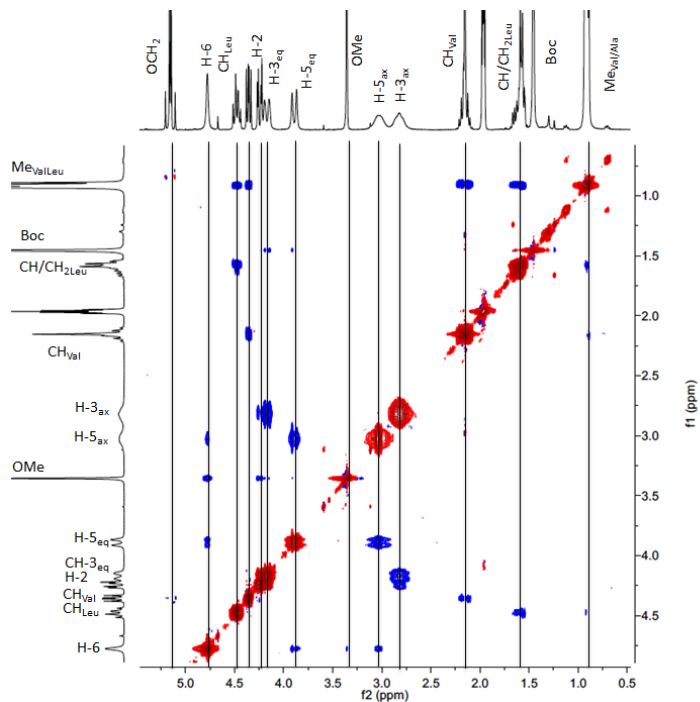


Figure 18: Magnification of CH/CH region of NOESY experiment

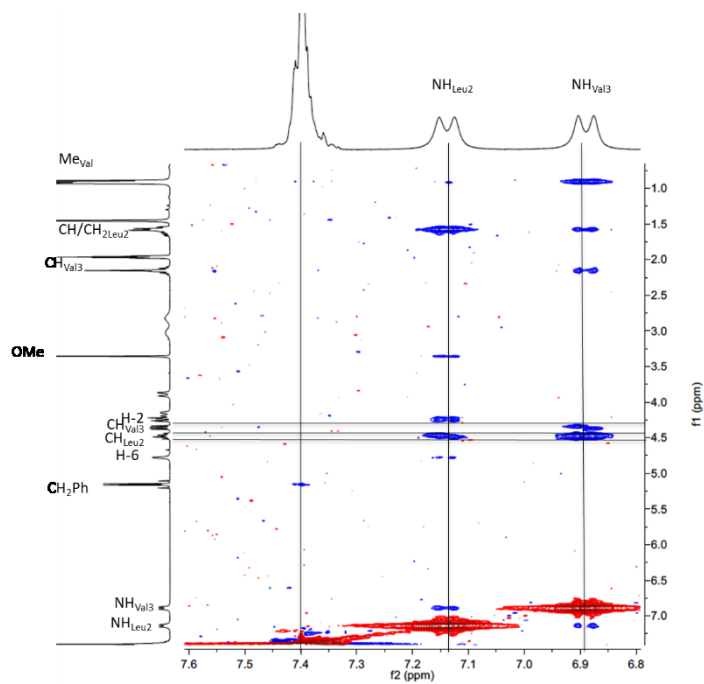
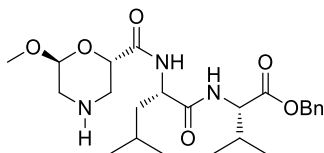


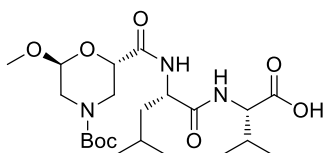
Figure 19: Magnification of CH/NH region of NOESY experiment

Synthesis of 'NH-Morph β -Leu-Val-OBn' (21)



In a round-bottom flask equipped with magnetic stirrer, compound **17a** (100 mg, 0.2 mmol) was dissolved in CH₂Cl₂ (4 mL). TFA was slowly dropped (4 mL) at 0 °C. After 2h the solvent was removed and the crude mixture was dissolved in CH₂Cl₂ (mL), washed with a saturated solution of NaHCO₃ (5 mL) and dried over Na₂SO₄. The organic solution was concentrated under reduced pressure and after flash chromatography on silica gel (CH₂Cl₂/MeOH = 40/1) compound **21** was recovered as yellow oil. (97.6 mg, 0.169 mmol, 95%). TLC: R_f (CH₂Cl₂/MeOH = 40/1) (Detected by phosphomolibdic acid) = 0.27. [α]_D²⁰ = -43 (c 0.6, MeOH), IR (NaCl) *v* max: 1536.42; 1658.23; 1739.9; 3307.07 cm⁻¹. MS (ESI): *m/z* calcd for [C₂₉H₄₅N₃O₈]: 463.27; found: *m/z* 464.33 [M+H]⁺. ¹H NMR (300 MHz, CDCl₃): δ 7.25-7.3 (m, 5H), 6.97-6.89 (m, 2H), 5.12 (dd, *J* = 27.49-12.23 Hz), 4.58-4.47 (m, 3H), 4.24 (dd, *J* = 10.92-2.57 Hz, 1H), 3.33 (s, 3H), 3.27 (d, *J* = 2.34 Hz, 1H), 2.84 (m, 2H), 2.61 (dd, *J* = 13.19-11.35 Hz, 1H), 2.33 (s, 2H), 2.10-2.16 (m, 1H), 1.46-1.67 (m, 3H) 0.82-0.89 (m, 12H) ppm. ¹³C NMR (75 MHz, CDCl₃): δ 171.7, 171.4, 170.0, 135.3, 128.5, 128.4, 128.3, 96.6, 68.6, 66.9, 57.2, 55.0, 50.9, 48.1, 47.8, 40.8, 31.0, 24.7, 22.8, 22.1, 18.9, 17.6 ppm.

Synthesis of 'N-Boc-Morph β -Leu-Val-OH' (20)



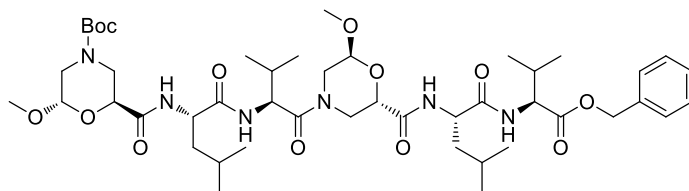
In a round-bottom flask equipped with magnetic stirrer, compound **17a** (99 mg, 0.2 mmol) was dissolved in THF (3.5 mL) and Pd/C (100 mg, 10% loading) was added

to the solution.

The suspension was stirred under H₂ (1 atmosphere) at 25 °C and, after 2 h, the catalyst was filtered on Celite pad.

The solvent was removed under reduced pressure and the obtained clear oil was dissolved in CH₂Cl₂ (20 mL) and washed with a saturated solution of NaHCO₃ (20 mL). The aqueous layer was then acidified with HCl 37% until pH 2 and the product was extracted with CH₂Cl₂ (20 mL). The organic layer was concentrated under vacuum, affording compound **20** (77.6 mg, 0.164 mmol, 93%) as colourless oil. TLC: R_f(CH₂Cl₂/MeOH = 40/1) (Detected by phosphomolibdic acid) = 0.32. [α]_D²⁰ = +24 (c 1, CHCl₃). IR (NaCl) *v max*: 1530.93; 1631.62; 1685.21; 1702.51; 2917.50, 3271.65 cm⁻¹. MS (ESI): *m/z* calcd for [C₂₉H₄₅N₃O₈]: 473.27; found: *m/z* 496.42 [M+Na]⁺. ¹H NMR (300 MHz, CDCl₃): δ 7.25 (brs, 1H), 7.12 (d, *J* = 8.4 Hz, 1H), 4.71 (m, brs, 2H), 4.48 (m, 1H), 4.31 (m, 2H), 4.31 (m, 2H), 3.97 (brs, 1H), 3.33 (s, 3H), 3.09 (dd, *J* = 14.50-7.40 Hz, 1H), 2.93 (brs, 1H), 2.75 (brs, 1H), 2.17 (m, 1H), 1.55 (m, 3H), 1.44 (s, 9H), 0.89 (m, 12H) ppm. ¹³C NMR (75 MHz, CDCl₃): δ 174.10, 171.61, 169.12, 155.06, 96.34, 80.75, 67.46, 57.42, 55.10, 51.11, 47.05, 45.64, 45.34, 41.02, 31.23, 29.66, 28.30, 24.73, 22.78, 22.27, 18.97, 17.59 ppm.

Synthesis of 'N-Boc-Morphβ-Leu-Val-Morphβ-Leu-Val-OBn' (22)



In a round-bottom flask equipped with a magnetic stirrer and thermometer, compound **20** (99.6 mg, 0.2 mmol) was dissolved in CH₂Cl₂ (3 mL) and the solution was cooled to 0 °C. HOBt (30 mg, 0.22 mmol) and EDC (43 mg, 0.22 mmol) were added. After 1 h, compound **21** (100 mg, 0.2 mmol) in CH₂Cl₂ (1 mL) was dropped, followed by the addition of DIEA (38 μL, 0.31 mmol). The reaction mixture was

stirred for 24 h and then it was washed with a solution of KHSO_4 (5%, 5 mL), a saturated solution of NaHCO_3 (5 mL), brine (5 mL). After drying over Na_2SO_4 , the solvent was removed under reduced pressure. Purification of the crude product by silica gel flash chromatography ($\text{AcOEt}/n\text{hexane} = 2:1$) afforded compound **22** (92 mg, 0.1 mmol, 50%) as a white solid. TLC: $R_f(\text{AcOEt}/n\text{hexane} = 2/1)$ (Detected by phosphomolibdic acid) = 0.3. M.p.: 96 °C. $[\alpha]_{\text{D}}^{20} = +18$ (c 0.3, MeOH). IR (NaCl) ν_{max} : 3414.11; 2960.79; 1740.35 cm^{-1} . MS (ESI): m/z calcd for $[\text{C}_{46}\text{H}_{74}\text{N}_6\text{O}_{13}]$: 918.53; found: m/z 942.60 $[\text{M}+\text{Na}]^+$.

AA	atom	$^1\text{H} \delta$	Multiplicity J (Hz)	$^{13}\text{C} \delta$	Noesy
Morf-1	CO			^a	
	H-2	4.28	overl	^b overl	OMe (s) NH _{Leu2} (m)
	H-3	H _{ax} 2.83	br	43.5	H-3 _{eqMorph4} (vvs)
		H _{eq} 4.19			H-3 _{axMorph4} (vvs) Boc (w)
	H-5	H _{ax} 3.05	br	48.4	H-5 _{eqMorph4} (vvs) H-6 _{Morph4} (w)
		H _{eq} 3.89	br		H-5 _{axMorph4} (vvs) H-6 _{Morph4} (s) Boc (w)
	CH-6	4.79	br	96.3	OMe (s) H-5 _{Morph4} (3.89,s; 3.05,w)
OMe	3.39		54.5	H-2 _{Morph4} (s)	

					H-6 _{Morph4} (s)
	BOC	1.46		27.5, 79.7	H-3 _{eqMorph4} (w) H-5 _{eqMorph4} (w)
Leu-2	CO			<i>e</i>	
	CH	4.43	m	51.6	NH _{Val3} (m) NH _{Leu2} (m) Me _{Leu2} (vs) CH _{2Leu2} (vs)
	CH/CH ₂	1.64-1.56	m	40.9 <i>c</i>	
	Me	<i>f</i> 0.96 0.94	overl.	<i>d</i>	
	NH	7.21	d <i>J</i> 8.1		NH _{Val3} (w) CH _{Leu2} (m) H-2 _{Morph1} (m)
Val-3	CO			<i>f</i> 170.4	
	CH	4.61	m	53.2	H-5 _{eqMorph4} (m) Me _{Val3} (s)
	CH	2.23	overl	30.4	NH _{Val3} (m)
	Me	0.87		<i>e</i>	NH _{Val3} (vs)
	NH	6.89	br		CH _{Leu2} (4.43,m) NH _{Leu2} (w) CH _{Val3} (m) Me _{Val3} (vs)
	CO			168.4	

Morf-4	H-2	4.22	dd, <i>J</i> 11.0, 3.3	67.9	NH _{Leu5} (w) H-3 _{Morph4} (4.59 s, 2.69 w) OMe (m)
	H ₂ -3	H _{ax} 2.69 H _{eq} 4.59	dd, <i>J</i> 13.3, 11.0 d <i>J</i> 13.3	43.5	H-5 _{axMorph4} (w)
	H ₂ -5	H _{ax} 3.32 H _{eq} 3.93	overl d <i>J</i> 14.0	48.0	H-3 _{axMorph4} (w) H-6 _{Morph4} (m) H-5 _{eqMorph4} (s) ----- H-5 _{axMorph4} (s) H-6 _{Morph4} (m) CH _{Val3} (m)
	H-6	4.85	br	95.8	OMe (s) H-5 _{Morph4} (m)
	OMe	3.37	overl	54.5	H-6 _{Morph4} (s) H-2 _{Morph4} (m)
Leu-5	CO			171.9	
	CH	4.49	m	51.9	NH _{Val6} (m) CH _{2Leu5} (s) Me _{Leu5} (0.93, s) NH _{Leu5} (m)
	CH/CH ₂	1.68-1.62	m	40.9 <i>b</i>	NH _{Val6} (m) NH _{Leu5} (s) CH _{Leu5} (s)
	Me	0.96	overl.	<i>d</i>	NH _{Leu5} (vw)

		0.93			
	NH	7.14	d <i>J</i> 8.1		Me _{Leu5} (0.93, vw) CH _{2Leu5} (1.59,s) CH _{Leu5} (4.49,m) H-2 _{Morph4} (w) NH _{Val6} (w)
Val-6	CO			^f 171.25	
	CH	4.37	m	57.66	CH _{isoprVal6} (vs) Me _{Val6} (0.93,vs) NH _{Val6} (m)
	CH	2.18	m	30.3	CH _{Val6} (vs)
	Me	0.93	d, <i>J</i> 7.3	^e	NH _{Val6} (vs)
		0.90			
	NH	6.91	d, <i>J</i> 8.6		CH/CH _{2Leu5} (m) CH _{Leu5} (m) NH _{Leu5} (w) CH _{isoprVal6} (w) CH _{Val6} (m) Me (0.93, vs)
	OBn	CH ₂ 5.16 Ph: 742- 7.40	dd <i>J</i> 12.5 m	66.5	CH _{Val5} (4.28, m) OCH ₂ (m) Me (0.92m) Me (0.87,w)

Table 9: ¹H, ¹³C NMR (CD₃CN, 9 mM, 500 MHz,) and NOEs (500 ms) data for 22.

^a169.1 or 168.9; ^b67.6-67.3 region; ^cCH: 27.5 or 24.5; ^d24.5-21.1; ^e19.1-16.4, ^fNot

assigned, °Tentatively assigned

Minor isomer 22'

AA	atom	¹ H δ	Multiplicity <i>J</i> (Hz)	¹³ C δ	Noesy
Morf-1	CO			^a	
	H-2	4.28	overl	68.0 (overl)	OMe (s) NH _{Leu2} (m)
	H ₂ -3	H _{ax} 2.83 H _{eq} 4.19	br	45.1	H-3 _{eqMorph4} (vvs) ----- H-3 _{axMorph4} (vvs) Boc(w)
	H ₂ -5	H _{ax} 3.05 H _{eq} 3.89	br br	Not detected	H-5 _{eqMorph4} (vvs) H-6 _{Morph4} (w) ----- H-5 _{axMorph4} (vvs) H-6 _{Morph4} (s) Boc (w)
	H-6	4.79	br	96.3	OMe(s), NH _{Leu2} (w) H-5 _{Morph4} (3.89,s; 3.05,w)
	OMe	3.39	s	54.5	H-2 _{Morph4} (s) H-6 _{Morph4} (s)
	BOC	1.46			H _{eq} -3 _{Morph4} (w) H _{eq} -5 _{Morph4} (w)
	Leu-2	CO			171.6

	CH	4.43	m	51.9	NH _{Val3} (m) NH _{Leu2} (m) Me _{Leu2} (vs) CH _{2Leu2} (vs)
	CH/CH ₂	1.64-1.56	m	40.9 <i>b</i>	NH _{Val3} (w) CH _{Leu2} (vs)
	Me	0.96 0.93	overl.	<i>c</i>	CH _{Leu2} (s)
	NH	7.19	d, <i>J</i> 8.1		CH _{Leu2} (m) CH _{2Leu2} (s) H-2 _{Morph1} (m) H-6 _{Morph1} (w) NH _{Val3} (w)
Val-3	CO			169.9	
	CH	4.68	m	53.4	Me (0.87,s) H-3 _{Morph4} (4.32,s) NH _{Leu2} (m)
	CH	2.07	overl	30.5	NH _{Val3} (m)
	Me	0.87		<i>d</i>	NH _{Val3} (w)
	NH	6.96	br		CH _{Leu2} (m) CH _{2Leu2} (1.62,w) NH _{Leu2} (w) CH _{Val3} (m) Me _{Val3} (vs) CH _{Val3} (2.07,w)
	CO			168.35	
	CH-2	4.27	dd, <i>J</i> 10.6	68.0	MeO (s)

Morf-4			6.4		NH _{Leu5} (m)
	CH-3	H _{ax} 3.18	m	47.2	H-3 _{eqMorph4} (s) H-5 _{axMorph4} (s) ----- H-3 _{axMorph4} (s) CH _{Val3} (s)
		H _{eq} 4.32	overl		
	CH-5	H _{ax} 2.93	dd <i>J</i> 13.7, 2.6	43.8	H-6 _{Morph4} (m) H _{eq} -5 _{Morph4} (s) H _{ax} -3 _{Morph4} (s) ----- H _{ax} -5 _{Morph4} (s) H-6 _{Morph4} (m) OMe(s)
		H _{eq} 4.36	Overl		
	CH-6	4.83	br	96.5	OMe (s) H-5 _{Morph4} (2.93m, 4.36 s) NH _{Leu5} (vw)
	OMe	3.34		54.5	H-2 _{Morph4} (s) H _{eq} -5 _{Morph4} (s) H-6 _{Morph4} (s)
Leu-5	CO			172.0	
	CH	4.45		51.4	NH _{Val6} (m) NH _{Leu5} (m) Me _{Leu5} (s) CH ₂ _{Leu5} (vs)
	CH/CH ₂	1.68-1.62	m	40.9 <i>b</i>	NH _{Val6} (w)
	Me	0.96	overl.	<i>c</i>	

		0.93			
	NH	7.27	d, <i>J</i> 8.2		NH _{Val6} (w) CH/CH ₂ Leu5 (s) CH _{Leu5} (m) H-2 _{Morph4} (m) H-6 _{Morph4} (vw)
Val-6	CO			171.3	
	CH	4.39	m	57.6	NH _{Val6} (m) Me _{Val6} (s)
	CH _{isopr}	2.13-2.05	m	30.3	NH _{Val6} (m)
	Me	0.94 0.92		^d	NH _{Val6} (vs)
	NH	7.03	d, <i>J</i> 7.9		CH _{Val6} (m) CH _{isoprVal6} (m) Me _{Val6} (0.92, vs) NH _{Leu5} (w) CH _{Leu5} (m) CH ₂ Leu5 (1.60, w)
	OBn	CH ₂ 5.16 Ph: 742- 7.40	dd <i>J</i> 12.5 m	66.5	Ph (m) Me (0.92, w) ----- OCH ₂ (m)

Table 10: ¹H, ¹³C NMR (CD₃CN, 9 mM, 500 MHz,) and NOEs (500 ms) data for isomer 22'.

^a169.1 or 168.9; ^bCH: 27.5 or 24.5; ^c24.5-21.1; ^d19.1-16.4;

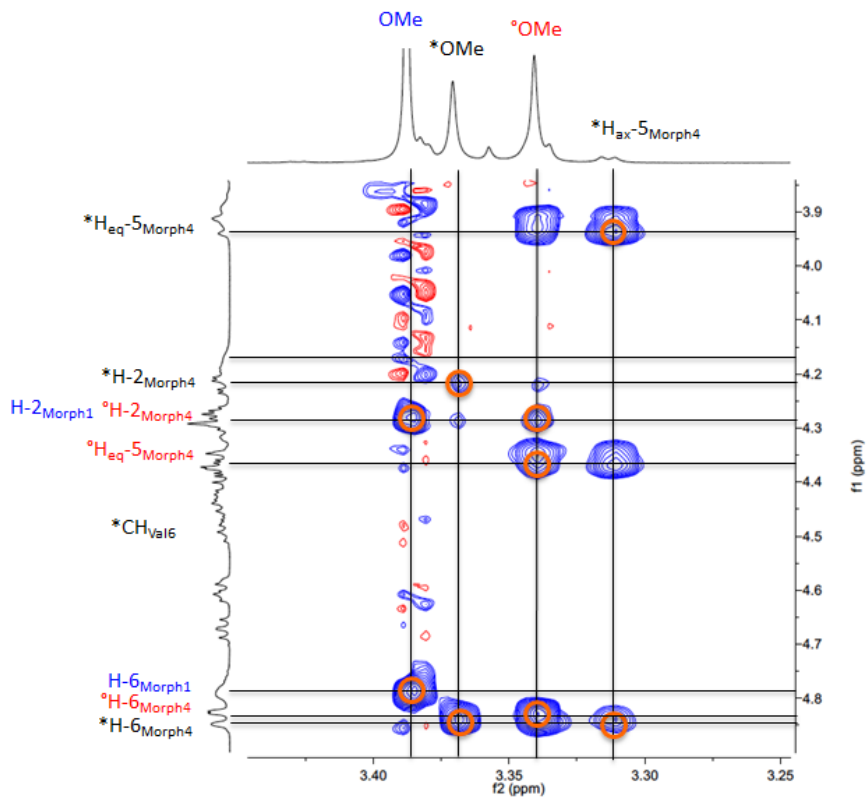


Figure 20: Magnification of CH/CH region of NOESY experiment

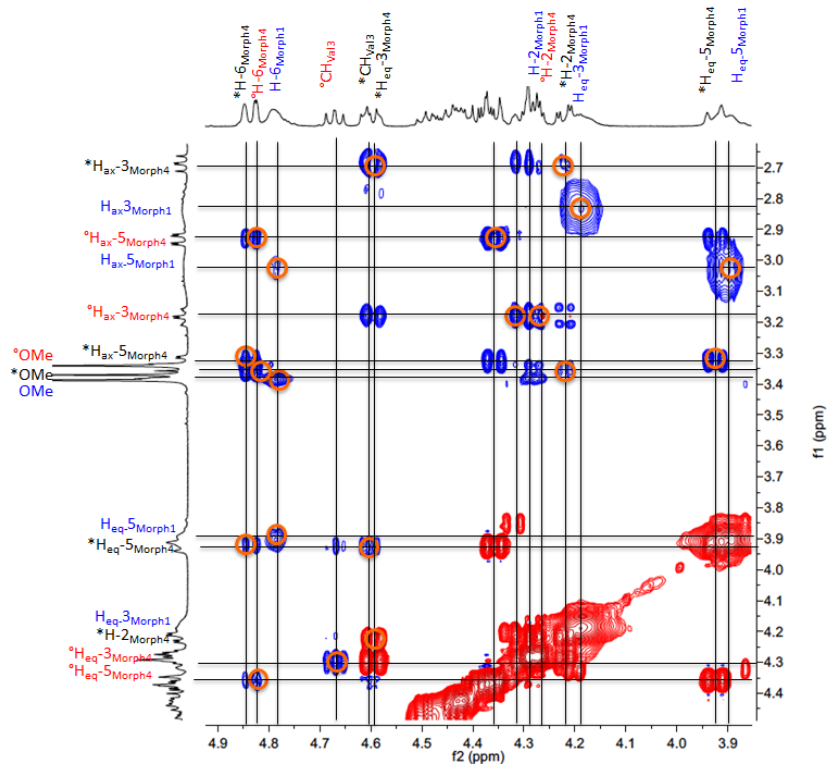


Figure 21: Magnification of CH/CH region of NOESY experiment

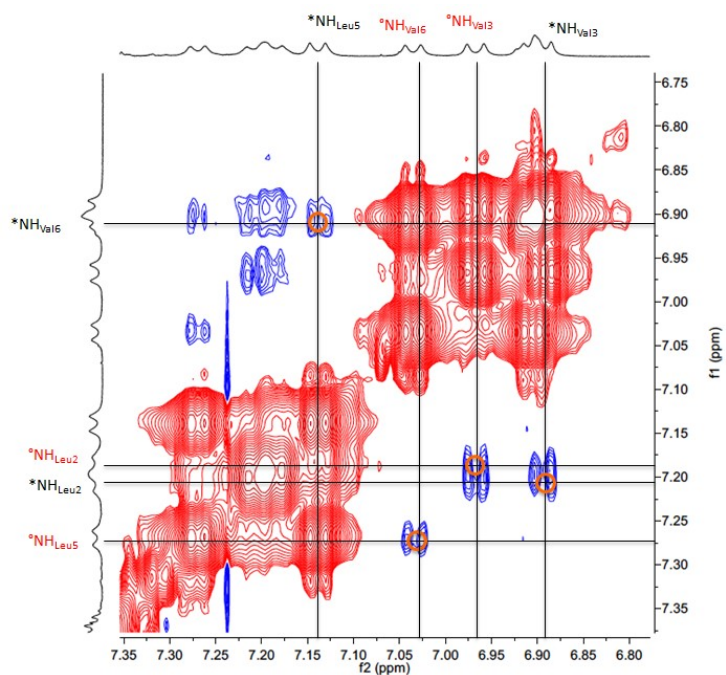


Figure 22: Magnification of NH/NH region of NOESY experiment

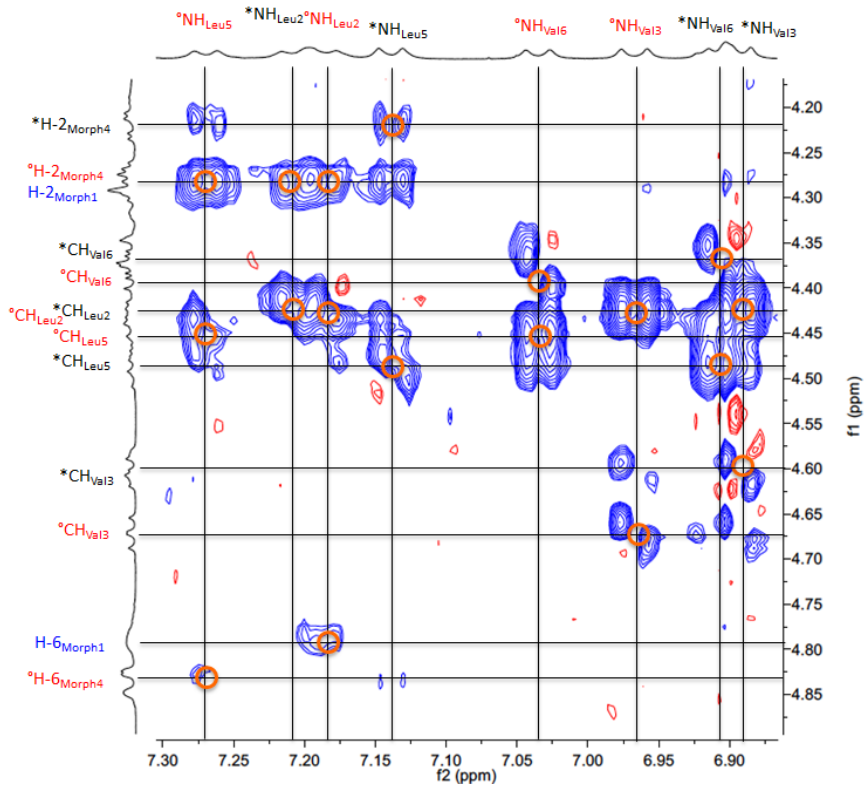


Figure 23: Magnification of CH/NH region of NOESY experiment

***2,3-Diaryl- β -amino acid for the preparation of α,β Foldamers
and its use for nanomaterial application***

Aim of the project

The β -amino acid motif is recurrent in biologically active compounds such as β -lactam antibiotics⁸⁵⁻⁸⁷, Taxol derivatives and β -peptides^{2,17,85-92} (Figure 1). Moreover, the synthesis of new non-proteinogenic β -amino acids for the preparation of peptidomimetics, is getting interest in nanomedicine field^{3,4,6}.

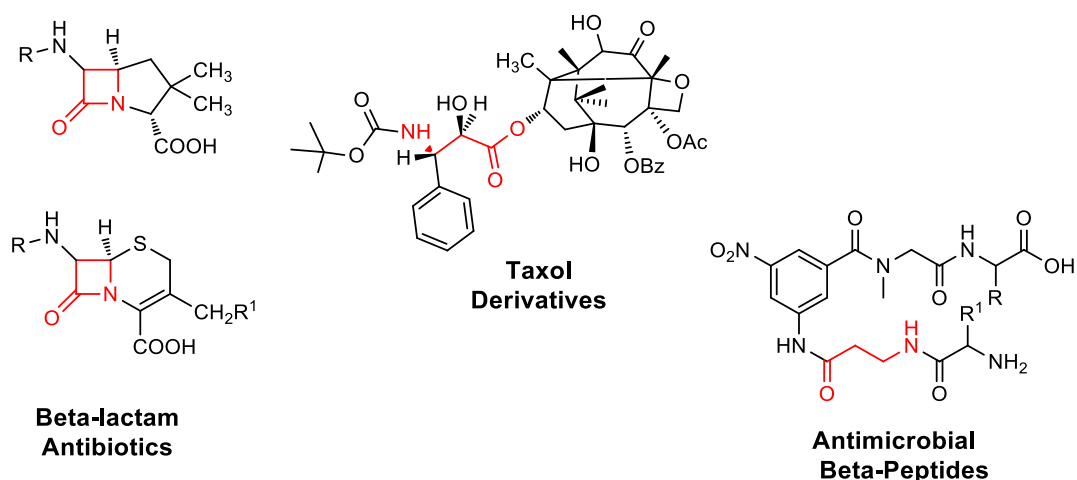


Figure 1: Biologically active compounds containing β -AAs motif

As explained in the General Introduction Chapter, the conformation of the $\beta^{2,3}$ -oligomeric peptides is connected with the stereochemistry of the amino acid. The *syn*- $\beta^{2,3}$ -amino acid, preferring a *trans* conformation, favors extended conformations and the *anti*- $\beta^{2,3}$ amino acid, preferring a *gauche* conformation, favors helix contents. α/β -Peptides have enlarged the scope of foldamers, leading to new molecular architectures, depending mainly on the substitution on C2 and C3 atoms of the β -residue^{93,94,95}.

Recently, our research group reported on a diastereoselective synthesis of a series of *syn*- S^*,S^* - $\beta^{2,3}$ -diaryl amino acids that represent a new class of amino acids. This synthesis was performed through a very efficient TiCl_4/TEA -catalyzed Mannich-like reaction⁹⁶.

The aim of this project is the preparation of $\alpha,\beta^{2,3}$ -peptides, using amino acid **1** (Figure 2) both for the presence of the aryl groups, that could favour π - π stacking, and of a fluorine that could increase lipophilicity.

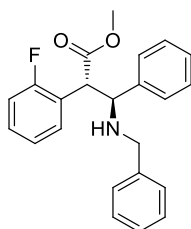
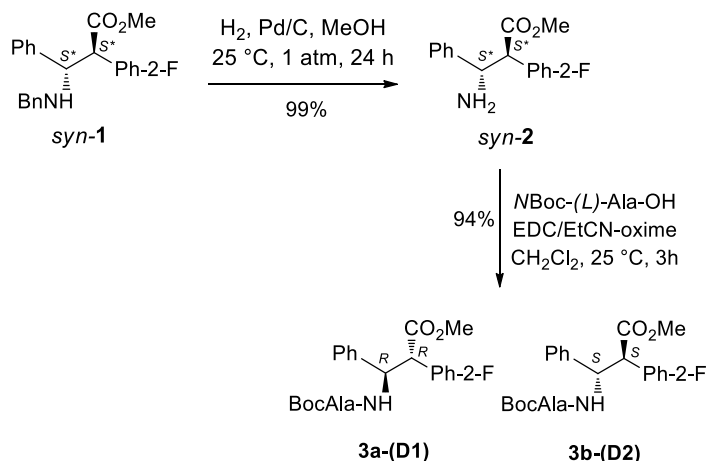


Figure 2: Biaryl β -AA *syn-1*

Since it is not possible to predict which is the stereochemistry of compound **1** that could give a stable secondary structure if it is combined with an *L*- α -amino acid, we prepared $\alpha,\beta^{2,3}$ -peptide sequences containing *L*-Ala alternated with both *R,R*- $\beta^{2,3}$ - and *S,S*- $\beta^{2,3}$ -diarylamino acid **1**. Di- tetra and hexa- $\alpha,\beta^{2,3}$ -peptides were prepared for both series and their conformation was studied by using NMR, CD and UV analyses.

Peptide synthesis

Dipeptides **3a-D1** and **3b-D2** were efficiently synthesized in gram scale from racemic *syn-1* (Scheme 1)⁹⁶. Amino acid **1** was firstly deprotected at nitrogen atom by catalytic reduction (H_2 , Pd/C, MeOH, 25 °C, 1 atm, 24 h) affording *S*,S**- $\beta^{2,3}$ -diarylamino acids **2** in quantitative yield. The condensation reaction of **2** with *N*Boc-(*L*)-AlaOH [HOBT (1.1 equiv.); EDC (1.1 equiv.) in CH_2Cl_2 25 °C, overnight] gave diastereoisomers **3a-(D1)** and **3b-(D2)** in 66% overall yield. The yield increased to 80% using [HOAT (1.1 equiv.); EDC (1.1 equiv.) CH_2Cl_2 , 25 °C, 8h]. The best result (94%) was achieved using EDC (1.1 equiv.)/EtCN-oxime (1.1 equiv.) in CH_2Cl_2 (25 °C, 3h). The couple of diastereoisomers **3a-(D1)** and **3b-(D2)** were easily separated by column chromatography on silica gel (Scheme 1).



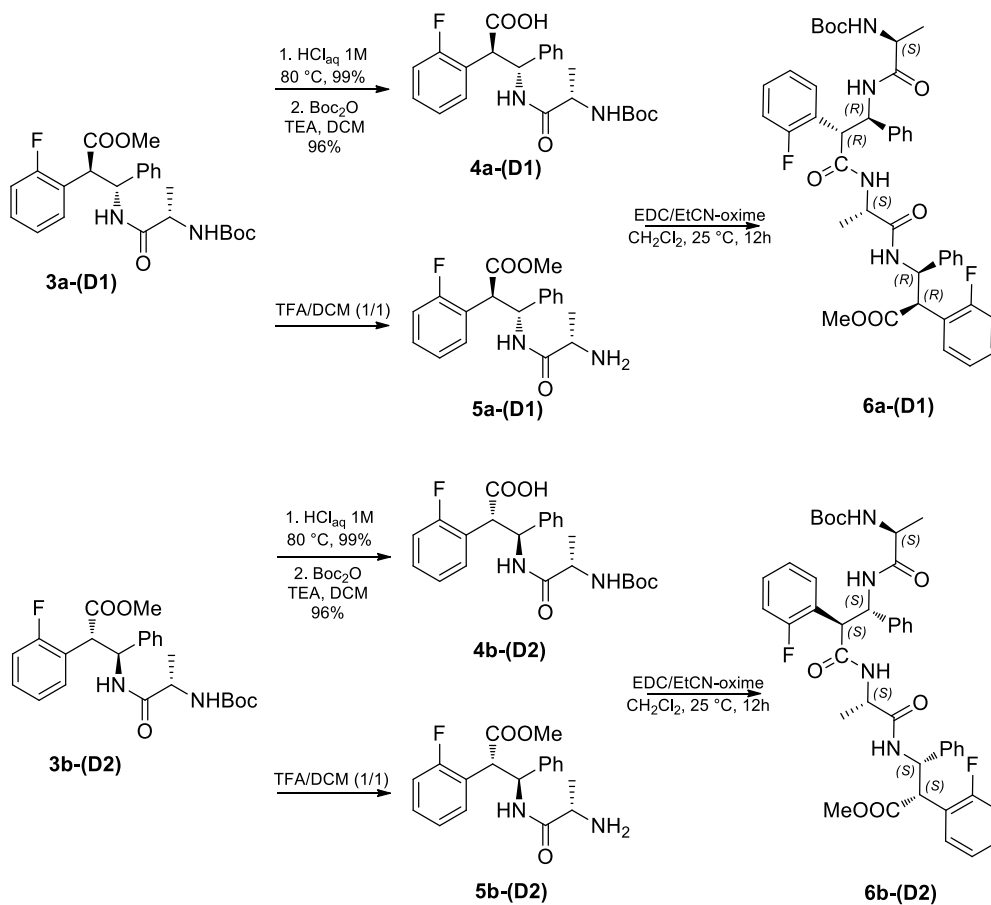
Scheme 1: Synthesis of Dipeptide **3a-(D1)** and **3b-(D2)**

The deprotection at *C-terminus* of dipeptides **3a-(D1)** and **3b-(D2)** with LiOH or KOH gave some problems since a partial epimerization of the alanine stereocenter was observed even at low temperatures.

For this reason, an additional step was added, deprotection both at *C-* and *N-termini* operating in aq. solution of HCl 1M (80 °C, 12 h, 99%). Starting from the deprotected NH₂-**D1**-COOH and NH₂-**D2**-COOH, nitrogen was protected (BOC₂O in DCM, TEA, 25 °C, 12 h, 96%), affording **4a-(D1)** and **4b-(D2)** without epimerization.

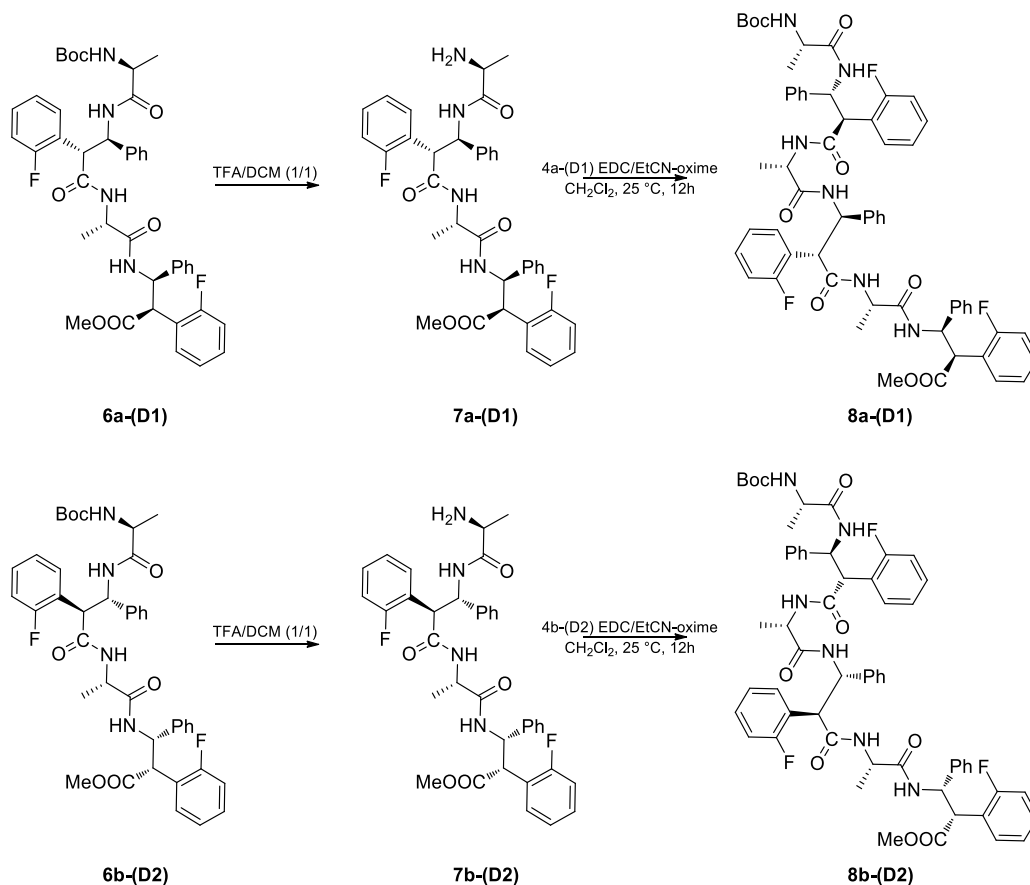
The deprotection of nitrogen atom on dipeptides **3a-(D1)** and **3b-(D2)** was easily performed using TFA in CH₂Cl₂ at room temperature for 1h, affording **5a-(D1)** and **5b-(D2)** in quantitative yields.

Tetrapeptide **6a-(D1)** was obtained from a coupling between **4a-(D1)** and **5a-(D1)** in CH₂Cl₂/DMF (10:1) as solvent, using EDC (1.1 equiv.)/EtCN-oxime(1.1 equiv.) as condensing agents (25°C, 24h). Compound **6a-(D1)** was isolated in 74% yield after purification on silica gel. Tetrapeptide **6b-(D2)** (76%) was obtained in an analogue way starting from **4b-(D2)** and **5b-(D2)** (Scheme 2).



Scheme 2: Synthesis of tetrapeptides **6a-(D1)** and **6b-(D2)**

Using the same protocols hexapeptide models **8a-(D1)** and **8b-(D2)** were synthesized (Scheme 3) and purified by column chromatography *via* deprotected compounds at *C-terminus* **4a-(D1)** and **4b-(D2)** and *N-terminus* **7a-(D1)** and **7b-(D2)**.



Scheme 3: Synthesis of hexapeptide **8a-(D1)** and **8b-(D2)**

All the model peptides present in the Schemes 2 and 3 were synthesized, but I'm still working on the characterization of compounds **6b-(D2)** and **8b-(D2)** for the study of their secondary structure.

Model peptide characterization

Solid state (X-ray analysis) of 3b-D2

The characterization of the two dipeptides **3a-(D1)** and **3b-(D2)** were reported on an article published on *Organic Letters*⁴⁷.

It has to be highlighted that only **3b-(D2)** gave crystals suitable for X-ray analysis while, despite numerous attempts, we were unable to grow any good single crystal from dipeptide **3a-(D1)** solutions.

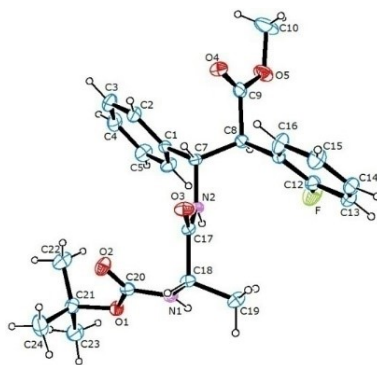


Figure 3: ORTEP view of the compound **3b-(D2)** showing atom-labeling scheme. Displacement are at the 40% probability level

NMR Characterization

All peptides were fully characterized by NMR 500 MHz (^1H , ^{13}C , HMBC, HMQC, NOESY) to study their secondary structures.

Characterization of **3a-(D1)** and **3b-(D2)**

Even if the NMR characterization (CDCl_3 , 500 MHz) of dipeptides **3a-(D1)** and **3b-(D2)** has been already reported⁴⁷, to better understand the spectroscopic characteristics of tetra- and hexapeptides, a summary is here given.

Only slight differences on the chemical shifts as well as on the NOE signals were observed for the two peptides (Figure 7). It is well known that the substituent effect is of relevance on the local conformation of a β -amino acid. Concerning $\beta^{2,3}$ amino acids, it is reported that the *syn* stereoisomer strongly favours the *trans* conformation¹⁶. As expected, and according to $^3J_{\text{C}\beta\text{H}-\text{C}\alpha\text{H}}$ values (10 Hz), the β -amino acid in both dipeptides is characterized by a *trans* conformation. This datum is consistent with the conformation of the β -amino acid shown in the crystal structure

of **3b-D2** (see Figure 3). Noesy signals between CH_{Ala1} and NH-2 (vs) as well as between NH-1/NH-2 (vw) are observed in both compounds **3b-D2** and **3a-D1**.

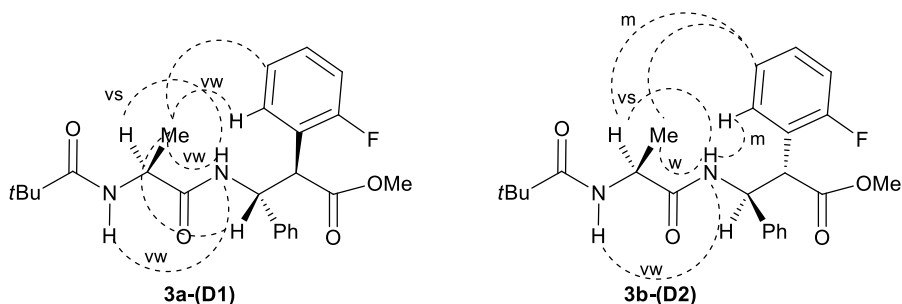


Figure 4: Significant Noesy (500 MHz, 10mM in CD_3CN , 300 ms) for dipeptides **3a-(D1)** and **3b-(D2)**

The experiment at variable temperature showed $\Delta\delta/\Delta T$ values more negative than -5 ppb/K for both NH of **3b-(D2)** dipeptide. The same experiments were performed on **3a-(D1)**. Lower $\Delta\delta/\Delta T$ values were detected in comparison with **3b-D2** dipeptide (Ala-1: -4 ppb K^{-1} ; beta-2: -3.8 ppb K^{-1} , Table 1).

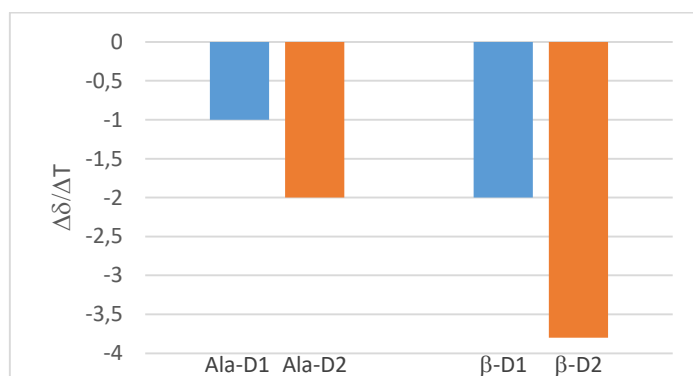


Table 1: $\Delta\delta/\Delta T$ values for dipeptides **3a-(D1)** and **3b-(D2)**

The DMSO titration experiment on **3b-(D2)** and **3a-(D1)** gave us similar results: the DMSO, added to the CDCl_3 solution, induced a strong downfield shift in the resonances of both NHs ($\Delta\delta > 1$) for **3b-(D2)**, and $\Delta\delta$ NH larger than 0.7 (Ala-1: 0.74; beta-2: 1.1) for **3a-(D1)**, indicating their solvent exposure (Figure 5). These data suggest that hydrogen bond are absent for **3b-D2** and **3a-D1** in solution.

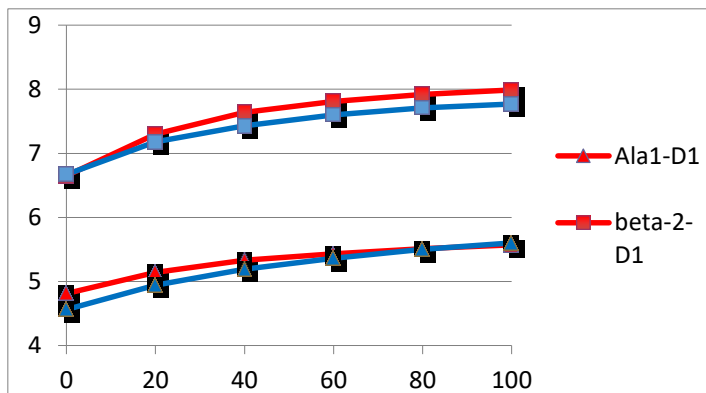


Figure 5: DMSO Titrations of peptides **3a-(D1)** and **3b-(D2)** in $CDCl_3$

All these NMR data suggest that both **3a-(D1)** and **3b-(D2)** do not possess a preferred conformation in solution.

Moreover, NMR analysis of **3b-(D2)** does not match with its X-Ray information, indicating a different behaviour of this dipeptide in solution and in solid state. In fact, the alanine moiety possesses a different orientation. An intermolecular H-bond between NH of alanine of a dipeptide sequence with the carbonyl group of β -AA of a second sequence occurred in the solid state. On the other hand, NH involvement in hydrogen bond was not confirmed in NMR solution studies.

NMR Characterization of tetrapeptide 6a-(D1)

NMR experiment ($CDCl_3$, 10 mM, 400 MHz) allowed to assign unequivocally the chemical shift to each proton (See Experimental part, Figure 6).

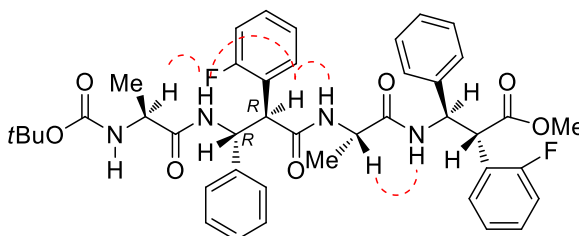


Figure 6: Proposed structure for isomer **6a-(D1)**. Dotted lines indicated non-sequential NOEs in the Noesy spectrum.

An extended conformation for **6a-(D1)** is proposed, because large NH/C β -H and C α -H/C β -H J values are observed, indicating the antiperiplanar orientation between these hydrogens (See Table 4 in the experimental part). Moreover, no Noesy signals between NH/NH ($i, i+1$) were detected, while Noesy pattern signals CH/NH ($i, i+1$) are present with high intensity. This finding highlights the extended propensity in solution of this tetrapeptide.

To evaluate the exposition of the NHs to the solvent, proper characteristic for an extended conformation, NMR analysis at different temperatures were performed.

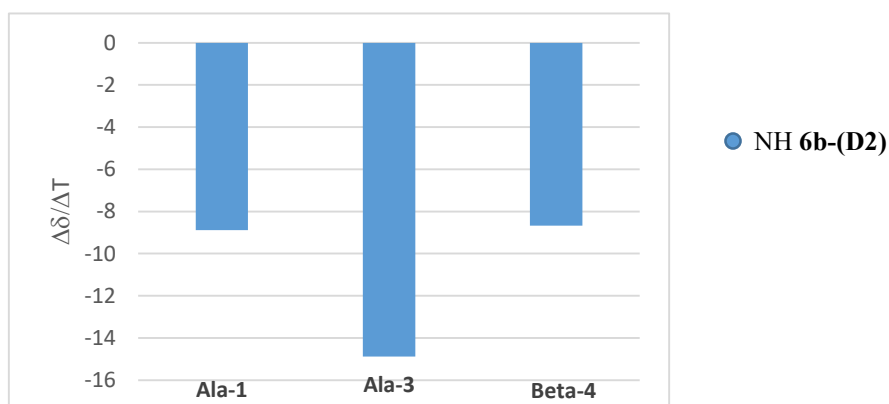


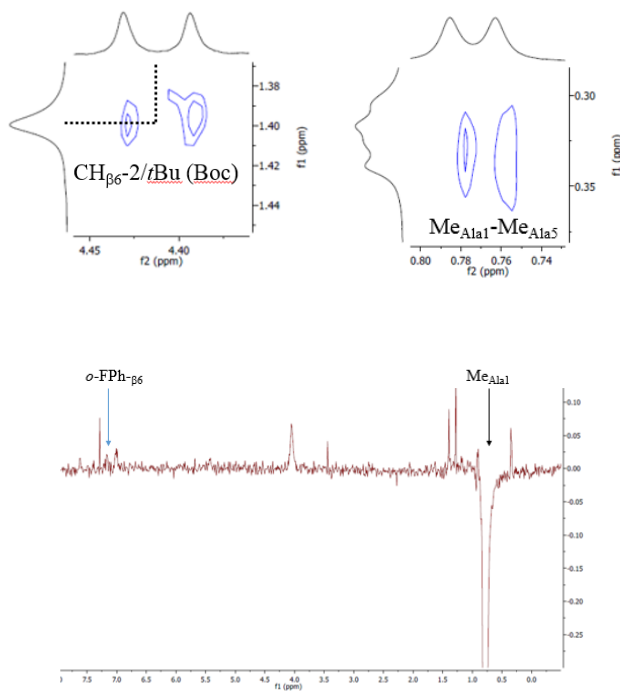
Table 2: Temperature dependence of the NH proton chemical shifts (273-333 K) for 6a-D1 tetrapeptide

As we can see from the Table 2, the temperature variation experiment (283-328 K) showed high $\Delta\delta/\Delta T$ variation (more negative than -8 ppb/K) values for all NHs (NH_{Ala-1} -8.8 ppb/K, NH_{Ala-3} -14.8 ppb/K, NH_{Beta-4} -8.6 ppb/K), confirming the exposition of all NHs to the solvent. This is another confirmation of proposed extended conformation. Since the NH of Beta-2 is an overlapped signal (See the Table 4 in the Experimental Part) it was impossible to evaluate the shift of this NH at variable temperature.

NMR Characterization of hexapeptide 8a-(D1)

A fully extended conformation is also proposed for hexapeptide **8a-(D1)**, proved by the large NH/C β -H and C α -H/C β -H J values, indicating the antiperiplanar orientation between these hydrogens. This finding is also confirmed by the NHs of alanines (J values of 6.5-9 Hz and present as a doublet)⁹⁷.

Interestingly, spatial proximities between CH β_6 -2/Boc group, *o*-FPh of β -amino acid $_6$ with both Me $_{Ala1}$ and Boc, and Me $_{Ala1}$ /Me $_{Ala5}$ (s) were detected in Noesy/Roesy experiments (Figure 7).



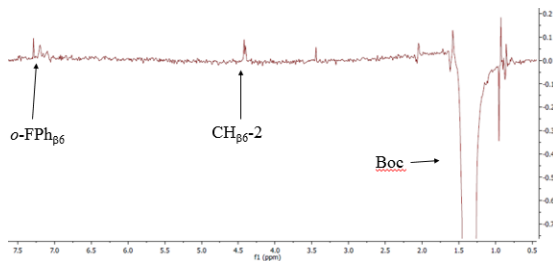


Figure 7: Significant Noes (CDCl_3 , 10mM, 450ms) demonstrating the spatial proximity between interstrand *C*-terminus and *N*-terminus. A) Zoom of $\text{CH}\beta_6\text{-2/Boc}$ Noe B) Zoom of MeAla1/MeAla5 Noe C) Row for *o*-FPh of β -6 amino acid/ MeAla1 Noe D) Row for *o*-FPh of β -6 amino acid/ Boc Noe

Due to the low resolution of the β -amino acids protons in position 2 and 4, only weak NOE signals were detected. Anyway, these Noesy signals support the formation of an antiparallel pleated sheet arrangement in which the *C*-terminus of one strand is faced on the *N*-terminus of a second strand (Figure 8).

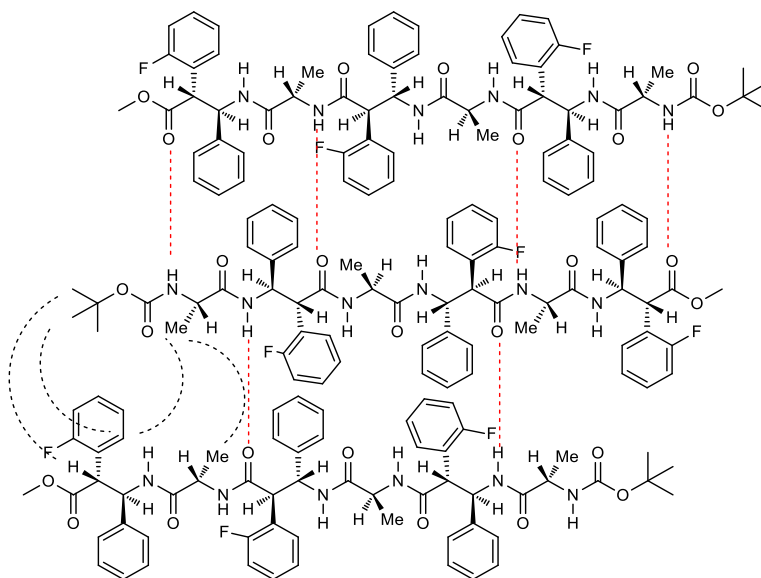


Figure 8: Black-Dotted lines indicated non-sequential NOEs in the Noesy spectrum. Red-Dotted lines indicate sequential NOEs in the Noesy spectrum. Black-Dotted lines indicated non-sequential NOEs in the Noesy spectrum. Red-Dotted lines indicate sequential NOEs in the Noesy spectrum.

To envisage the secondary structure of compound **8a-(D1)**, both solvent titration studies and temperature dependence of the NH proton chemical shifts were performed. For the overlapping of some NH protons in the aromatic region, the study

of the conformation of this peptide was not trivial.

The temperature variation experiment (273-333 K) showed NH proton chemical shifts about 3.1-3.5 ppb/K for β -2 and Ala-5. On the other hand, NH of β -4 seems to be not involved in a H-bond situation. We have not significant information about Ala-1 and Ala-3 amide bond, due to the overlapped signals.

Solvent titration studies were matched with TOCSY experiments [**8a-(D1)** (10 mM); 0%, 9% and 20% v/v of DMSO] to ensure the correct correlation between NH proton with the corresponding amino acid and to detect the correct chemical shift. Figure 9 shows the results related the NH mobility.

The polar solvent dimethylsulfoxide (DMSO) added to the CDCl_3 solution induces a strong downfield shift in the resonances of NH-6 ($\Delta\delta > 1$), NH-3 (0.54) and NH-4 (0.89) indicating their solvent exposure. Instead, the analysis showed that NH-1 and NH-5 are strongly involved in a H-bond ($\Delta\delta \text{ NH} < 0.05$) indicating that these protons are solvent shielded. Finally, NH-2 is involved in a medium-weak H-Bond ($\Delta\delta = 0.35$). The obtained results are in agreement with the proposed H-Bond Network shown in Figure 8.

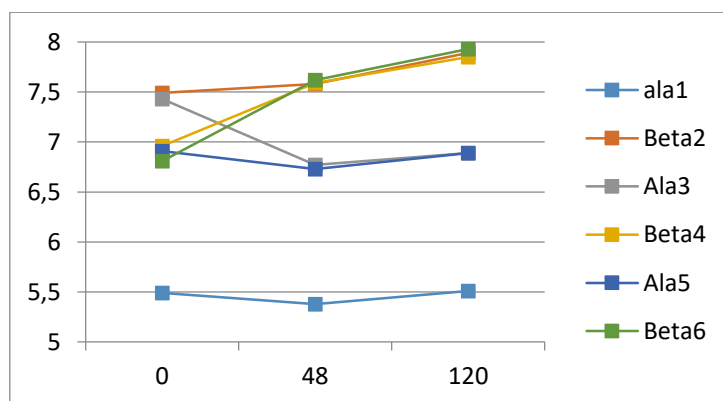


Figure 9: DMSO Titrations of peptide **8a-(D1)** in CDCl_3 . NH chemical shift were evaluated by TOCSY analysis

As a result, three H-bonds are predictable as shown in Figure 8.

In conclusion, all the $\alpha,\beta^{2,3}$ -sequences, explained in this chapter, represent to the best of our knowledge, the first examples of combination of chiral α -amino acids and $\beta^{2,3}$ -amino acids.

The peptides of **D1** series were characterized by NMR spectroscopy to understand the secondary structure that they can assume in solution. Our results confirm the literature data: *syn* $\beta^{2,3}$ -amino acids favor a *trans* conformation. Its combination with a α -amino acid generates fully extended conformations. In particular, an antiparallel β -sheet was detected for **8a-(D1)** suggesting that our *syn* $\beta^{2,3}$ -amino could drive interesting conformations.

Nanomaterial application

As we recently reported⁴⁷, the self-assembly behaviour of dipeptides **3a-(D1)** and **3b-(D2)** in water was investigated using solvent displacement procedure. We found that depending on the stereochemistry of the β amino acid (in fact, only **3b-(D2)** gave ordered supramolecular structure), these dipeptides are able to self-assemble into proteolytic stable nanotubes due to the presence of intermolecular hydrogen bonds, and Van der Waals interactions leading mainly to hydrophobic constructs. These architectures were also able to enter in the cell locating in the cytoplasmic/perinuclear region, representing interesting candidates for biomedical applications. For this reason, I investigated the self-assembly behaviour of an ultra-short tripeptide containing **3b-(D2)** dipeptide.

Self-assembly of an amphipathic $\alpha\alpha\beta$ -tripeptide into cationic spherical particles for intracellular delivery

In this work, I studied the self-assembly of an ultra-short $\alpha\alpha\beta$ -tripeptide (Figure 10) containing an *L*-Arg–*L*-Ala sequence and the unnatural fluorine substituted $\beta^{2,3}$ -diaryl-amino acid **1**.

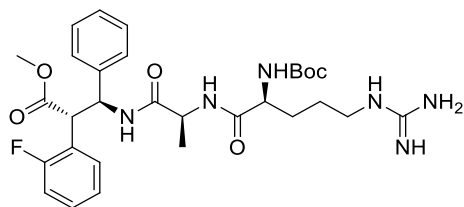


Figure 10: General formula of **T2R**

This tripeptide, simply called **T2R**, contains an unnatural β -amino acid moiety, that could confer protease stability to the peptide and a guanidinium group, a trigger for the formation of spherical supramolecular structure.

The balance between hydrophobicity and charges is crucial for both colloidal stability and membrane penetration.

For this reason, I introduced an *L*-Arg residue in the hydrophobic **D2** structure. In this way, a polar interaction could drive the self-assembly. The cationic guanidinium group on the side chain of *L*-Arg, could influence the shape as well as the overall superficial charge of the aggregates. As a result, in the second part of this chapter, I reported the development of cell penetrating cationic submicron-aggregates composed by the ultra-short **T2R** tripeptide (Figure 11) that are able to deliver small molecules into the cell.

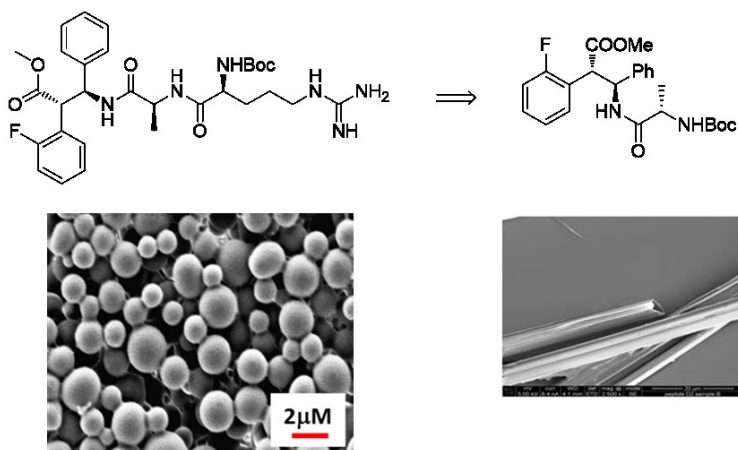


Figure 11: **T2R** and its self-assembly in spherical aggregates (Left). **D2** and its self-assembly in nanotube (Right)

Literature overview of Cationic Nanoparticles

In this paragraph an overview of the Cationic Nanoparticles was reported due to its implication on the self-assembly behavior of **T2R**.

The use of nanoparticles appeals to scientists across many disciplines due the opportunity to engineer many properties that might otherwise be incompatible on a single device.

Furthermore, the study of new approaches to carry exogenous entities (e.g. drugs, proteins, oligonucleotide siRNA) directly into cells is a very active research field.

Nowadays, nanoparticles are considered efficient devices that could introduce exogenous entities into cells⁹⁸. Lately, also exosomes, biological microvesicles released from cells, are considered new potential carriers⁹⁹.

In particular, cationic nanoparticles (NP⁺) are positively charged nanoaggregates that are widely employed in biomedicine¹⁰⁰, pharmaceutical technology¹⁰¹ and antimicrobial science materials¹⁰².

The reason why NP⁺ are getting attention in these fields is their ability to penetrate the cells in a non-endocytotic way¹⁰³, featuring fast and large uptake, without toxic effects to the cell if introduced at low concentration¹⁰⁴. These properties make NP⁺ promising candidates for drug delivery¹⁰⁵.

A wide variety of cationic polymers self-assemble into NP⁺, and most of them are characterized by the presence of basic functions on the surface. This includes amines or guanidines^{100,101,106}. NP⁺ can be also obtained by the functionalization of anionic or neutral polymers with cell penetrating peptides, such as positively charged oligopeptides composed mainly of arginine and/or lysine residues^{106,107}. In all cases, the polymer is the molecular tool that directs the process of self-assembly while the cationic charge decorates the NP⁺. As it is said above, the positive charge on the surface of NP⁺ imparts several advantages and one of them is the delivering of active macromolecules with a negative charge such as DNA or proteins^{108,109}.

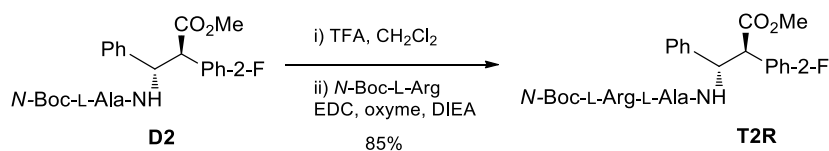
On the other hand, it has to be underlined that polymeric NP⁺ suffer several drawbacks such as aggregation, instability and cytotoxicity, related to not only the positive surface charge but also the size and geometry of the constructs^{100,110}. In the past decade, natural biopolymers, such as oligosaccharides, oligonucleotides, and proteins have been widely exploited for the development of new smart materials¹¹¹. For this reason, peptides are nowadays considered, due to their modular nature, structural diversity, biocompatibility, relative chemical and physical stability, and synthetic accessibility^{12,112}. Furthermore, peptides can hierarchically self-assemble in a reproducible way through free-energy driven processes, e.g. van der Waals, electrostatic, hydrogen bonding, hydrophobic and π - π stacking interactions¹¹². The balance of these forces affects their arrangement that depends on their molecular composition, assembly and environment (pH, solvent, temperature, and ionic strength). An added value of peptides is the possibility of introducing unnatural amino acids into them thus expanding the scope of the resulting nano-architectures together with obtaining more proteolitically stable materials⁵³. In particular, short peptides and peptide mimics are themselves profitable delivery systems as they could bring both features, *i.e.* self-assembly and cell penetration, into a single molecule, and because of their biocompatibility and low toxicity.

Result

Synthesis and self-assembly studies

Compound **T2R** was synthesized starting from dipeptide **D2**, already described in the previous chapter (Scheme 1). First, **D2** was deprotected on the *N*-termini with TFA in CH₂Cl₂.

The coupling of **5b-(D2)** with *N*-Boc-*L*-Arg was performed using EDC and Oxyme as coupling reagents and DIEA as base (24 h, rt) affording **T2R** in 85% overall yield (Scheme 4).



Scheme 4: Synthesis of T2R

Compound **T2R** was characterized by $^1\text{H-NMR}$ (17 mM solution, CD_3CN , 293 K, 300 MHz). **T2R** was present in solution as a single extended conformer, in which the $\beta^{2,3}$ -diarylamino acid is characterized by a trans configuration according to $^3J_{\text{C}\beta\text{H}-\text{C}\alpha\text{H}}$ values (11.3 Hz).

A complete set of $\text{NH}, \text{C}\alpha\text{H}$ ($i, i + 1$) was detected by NOESY experiments ($t_{\text{mix}} = 300$ ms), but no NH, NH ($i, i + 1$) NOEs were observed. Moreover, the $^1\text{H-NMR}$ experiments at variable temperature were performed, proving the absence of any intramolecular hydrogen bonds.

Nanoparticles characterization

The self-assembly tendency of **T2R** was then investigated. The ‘Solvent displacement procedure’ was used, as in the case of compound **D2**⁴⁷: a stock solution of **T2R** in hexafluoroisopropanol, HFP (100 mg/mL), was diluted with water to a final concentration of 2 mg/mL. After an incubation of 24 h, the sample was characterized.

Using Dynamic Light Scattering (DLS), we observed the formation of assemblies having an average diameter of 675 ± 30 nm (Figure 12).

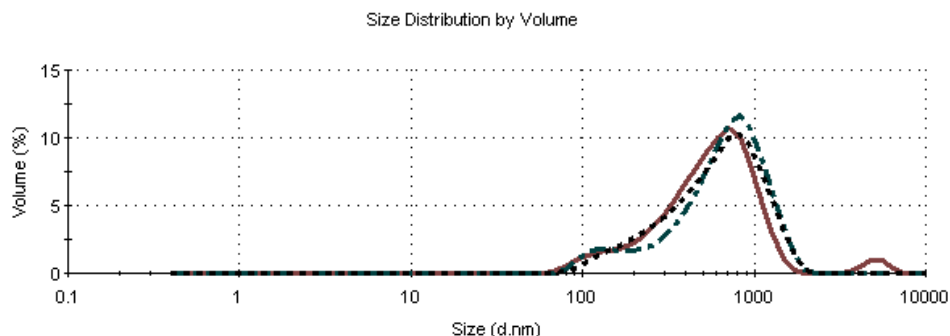


Figure 12⁴⁸: DLS of **T2R** supramolecular architecture

Scanning electron microscopy (SEM) and transmission electron microscopy (TEM) showed that **T2R** self-assembled in the aqueous medium into highly ordered spherical particles with sub-micrometric dimensions (Figure 13). Moreover, high-resolution SEM revealed that **T2R** could form spherical assemblies. The low magnification SEM images demonstrated, also, that these spherical assemblies are abundant. In addition, some of the spheres seemed connected, while others stood as distinct entities.

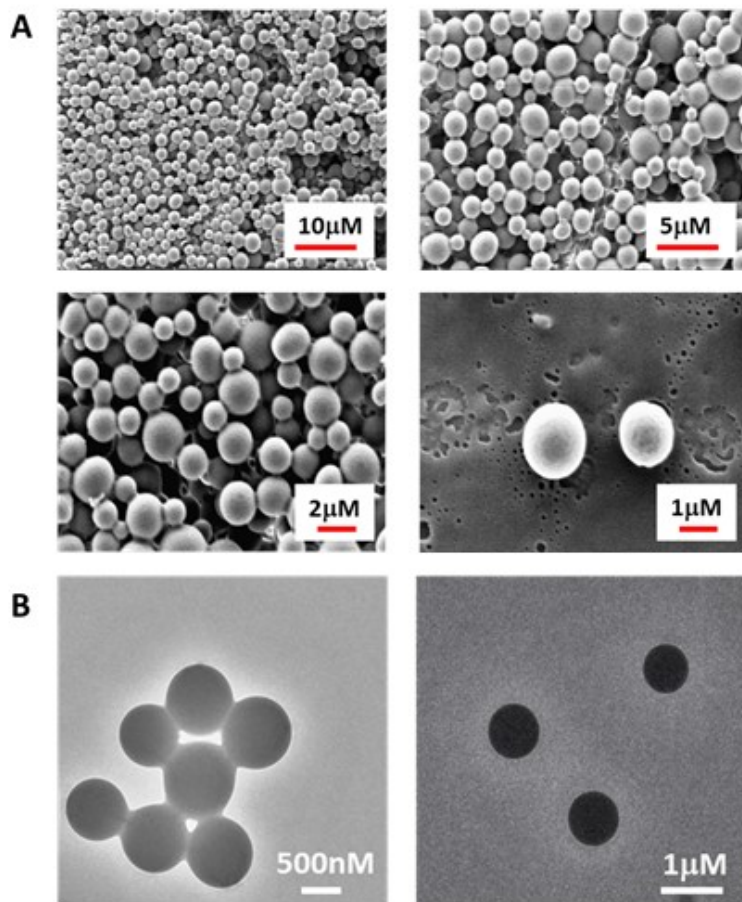


Figure 1348: Electron microscopy micrographs of the self-assembled structures formed by **T2R** A) HR-SEM and B) TEM micrographs of **T2R** self-assembled structures.

To deeply study the secondary conformation of these spherical entities we used Fourier transform infrared (FT-IR) analysis with the deconvolution of each spectrum (Figure 14).

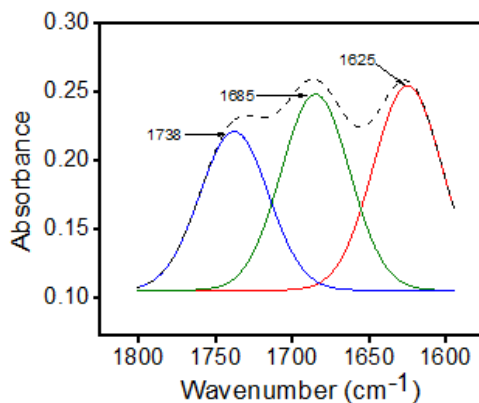
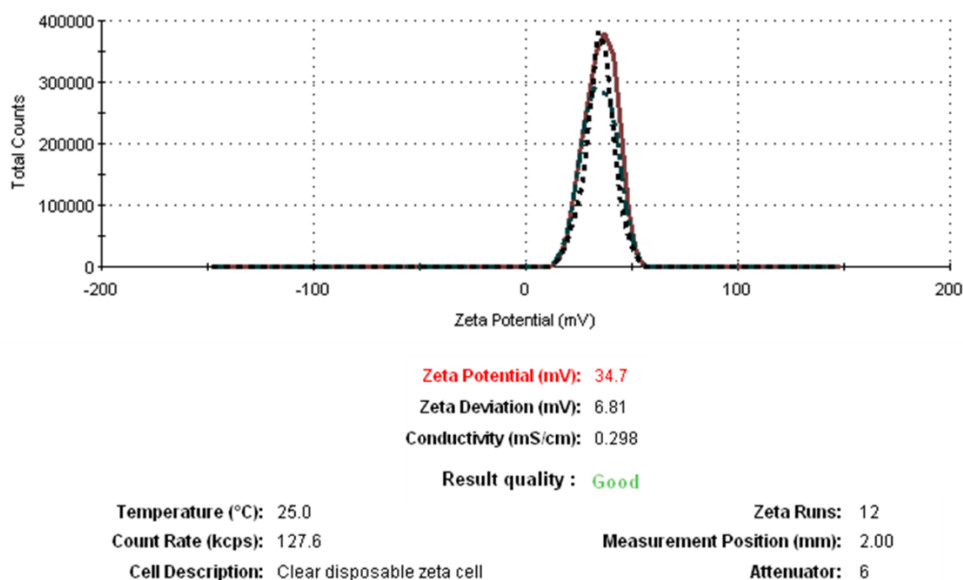


Figure 14⁴⁸: Deconvoluted FT-IR spectra of the self-assembled structures formed by **T2R**. The dashed-line indicates the original FT-IR spectra and the solid line represents the deconvoluted curves with a Gaussian function.

The FT-IR spectra of the spherical structures exhibited major peaks at 1625 cm^{-1} , 1685 cm^{-1} and 1738 cm^{-1} (Figure 14). The peak at 1738 cm^{-1} corresponds to the ester function. The appearance of two major peaks in the amide I region at 1625 cm^{-1} and 1685 cm^{-1} may suggest an anti-parallel β -sheet conformation of **T2R** in the aggregates¹¹³.

The zeta potential of **T2R** assemblies was +34.7 mV \pm 0.4 (Figure 15) confirming that the protonated guanidinium group is present on the outer sphere surface.



*Figure 15*⁴⁸: Zeta potential analysis of **T2R** aggregates

To demonstrate the effective advantage to use a tripeptide containing a β -amino acid as drug delivery system, the proteolytic stability was studied.

The protease stability of **T2R** was investigated, using Pronase from *Streptomyces griseus*, *i. e.* a mixture of endo- and esopeptidase able to hydrolyze standard peptide bonds. In our previous work, we found that Pronase is ineffective in cleaving the amide bond of the unnatural **D2** dipeptide⁴⁷. Solutions of **T2R** (PBS buffer with CaCl_2 , pH 7) in the presence or absence of Pronase were incubated at 25°C and monitored by RP-HPLC. Different Pronase concentrations were tested (0,5-1-10 mg/ml) maintaining the same **T2R** concentration (5 mg/mL). The complete hydrolysis of *L*-Arg-*L*-Ala- amide bond was observed only in the presence of high concentration of the enzyme (10 mg/mL) and after 3h (Figure 16). On the contrary, with 1 mg/mL of Pronase, the complete hydrolysis was obtained only after 24 h. Using 0.5 mg/mL of enzyme the total conversion did not occur (Figure 16).

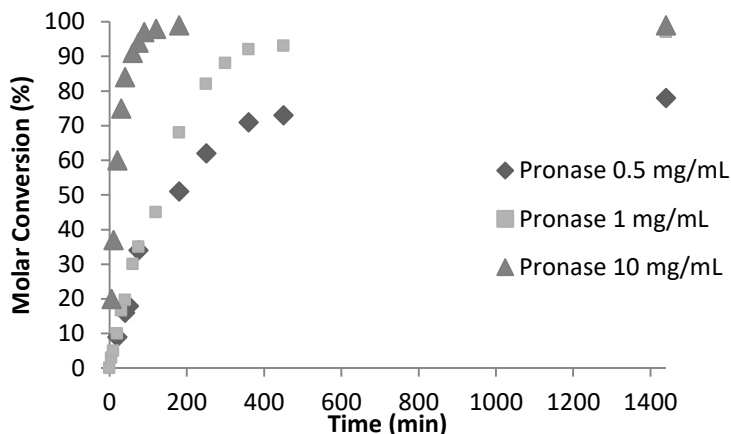


Figure 16⁴⁸. Protease stability analysis of **T2R** (5 mg/mL) using different concentrations of Pronase from *Styreptomycetes griseus*

To evaluate the potential of the spherical assembly formed by **T2R** to serve as a drug-delivery system, we self-assembled **T2R** in the presence of the dye rhodamine B (RhB). The incorporation of RhB was conducted during the **T2R** self-assembly, affording **RhB-T2R** in which the luminescent dye is incorporated within the aggregates. The fluorescence microscopic images of **RhB-T2R** are shown in Figure 17, indicating the loading of the RhB dye into the spherical structures. **T2R** calculated encapsulation efficiency (EE) was of 56.5%, while loading capacity (LC) was of 13.5%.

Dye Encapsulation Efficiency (EE) and Loading Capacity (LC)

RhB-T2R spheres were prepared as reported above, and left to precipitate overnight. The aqueous medium was decanted and the emission intensity at desired wavelength was measured. The dye encapsulation efficiency (EE), which is correlated with the concentration of the dye not incorporated or free untrapped dye, can be expressed by the equation¹¹⁴:

$$EE = \frac{\text{Actual concentration of the dye incorporated in nanoparticles}}{\text{Concentration of the theory amount of dye loaded in nanoparticles}} \times 100\%$$

As the concentration of the dye is directly proportional to emission intensity

$$EE = \frac{\text{Emission intensity of the dye incorporated in nanoparticles}}{\text{Emission intensity of the theory amount of dye loaded in nanoparticles}} \times 100\%$$

As the emission of the dye incorporated in nanoparticles is equal to the total emission subtracted the emission intensity of the not incorporated dye, EE can be calculated by:

$$EE = \frac{\text{Emission intensity of the theory amount of dye loaded} - \text{Emission intensity of the dye not incorporated}}{\text{Emission intensity of the theory amount of dye loaded}} \times 100\%$$

The loading capacity (w/w %LC) can be calculated by the following expression

$$LC = \frac{\text{Amount of the Entrapped drug/dye}}{\text{Nanoparticle weight}} \times 100\%$$

The molecular weight of the RhB = 479.02, the total volume of the resultant solution used for the dye incorporation study is 1mL and the Final effective concentration of the T2R is 2mg/mL. The concentration of RhB actually loaded is of 10^{-3} mol L⁻¹. Then the amount of the dye present in 1 ml is 0.48 mg. The amount of the entrapped dye by the nanoparticles is $0.48 \times EE = 0.48 \times 56.4\% = 0.2702$ mg.

$$LC = (0.2702/2) \times 100\% = 13.5\%$$

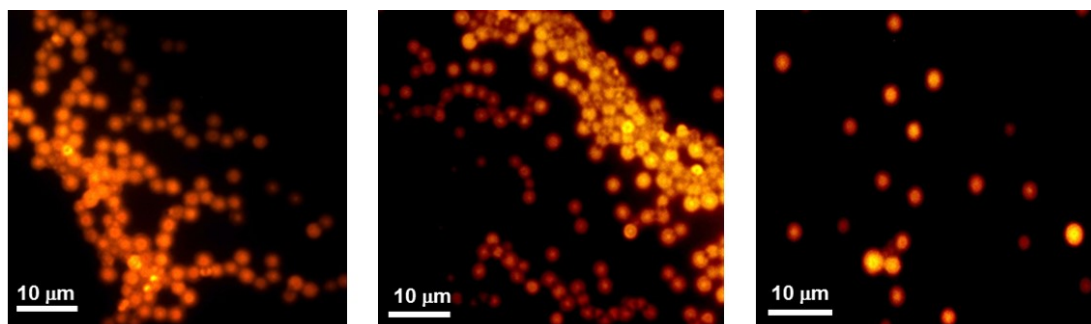


Figure 17⁴⁸: Fluorescence microscopy images of *RhB-T2R*

The release profile of the dye from **T2R** was then assessed using fluorescence measurement analyses. **RhB-T2R** was dispersed in PBS and transferred into a dialysis bag (MWCO 3kDa), immersed in PBS buffer at room temperature. Aliquots were analyzed at different time intervals for 10 days. The fluorescence measurements revealed that there is a steady increase in the emission intensity with increasing time (Figure 18A). Indeed, the concentration of the dye in the buffer (outside the dialysis bag) slowly increased with time. This is due to the release of the dye molecules from the self-assembled nanostructures. In particular, up to 114 hours (4.75 days), there was a steady/gradual increase in the emission intensity (measurements every hour, then every 4 hours). After, by analyzing the fluorescence with a time-intervals of 8 and 12 hours, we did not observe any significant increase in the emission intensity, indicating that the release process was completed and reached equilibrium. To confirm this hypothesis, we followed the dialysis system for a longer time (36 hours) and observed a significant increase in the emission intensity. The emission reached a plateau after 190 hours (7.9 days) (Figure 18B).

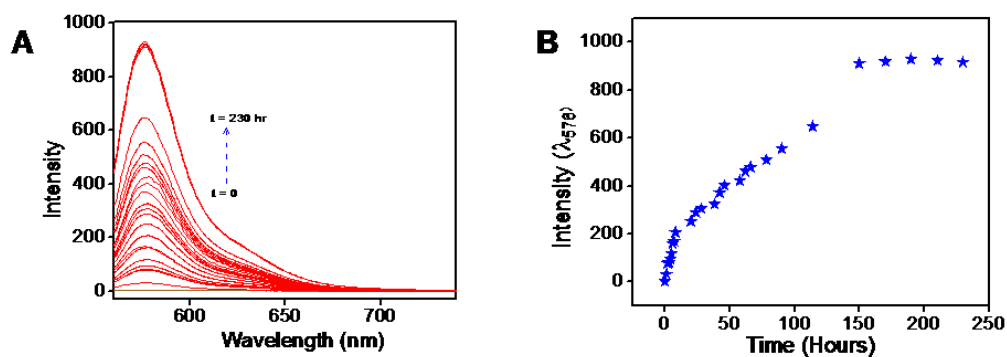


Figure 18⁴⁸: (A) Emission spectra of the PBS buffer solution outside the dialysis bag (contains the RhB-incorporated peptide self-assembled spheres) taken at different time intervals for 10 days. (B) The plot of measured emission intensity of the PBS buffer solution outside the dialysis bag (contain the RhB-incorporated peptide self-assembled spheres) with time; $\lambda_{Mon} = 576 \text{ nm}$, $\lambda_{Ext} = 542 \text{ nm}$.

Cell diffusion capability

Finally, the **T2R** aggregates were tested for their cells diffusion capability. HEK-293 cells¹¹⁵, a commonly used cell model for the biological research, were treated from 2h up to 16h with 150 μ M of **RhB-T2R**. Then, at confocal analyses the nanoparticles were clearly able to reach the intracellular compartments within the first 2h (Figure 19) as shown by the bright field image but the Rhodamine fluorescence was poorly detected probably because it was already released from the particles. Rhodamine fluorescence was instead well visible after 16h, timing that probably allowed a particles enrichment within the cells (Figure 19B). In accordance, the accumulated nanoparticles in the cell after 16h seemed to be in a larger amount (Figure 19E) compared to the detected Rhodamine fluorescence, probably because most of the nanoparticles had already released the fluorescent dye. Moreover, nanoparticles were distributed broadly into intracellular compartments (Figure 19B-C). Interestingly, the nanoparticles could not reach the nucleus as shown by the co-localization between the DAPI and the Rhodamine in which the presence of red dots is not detectable (Figure 19B-C).

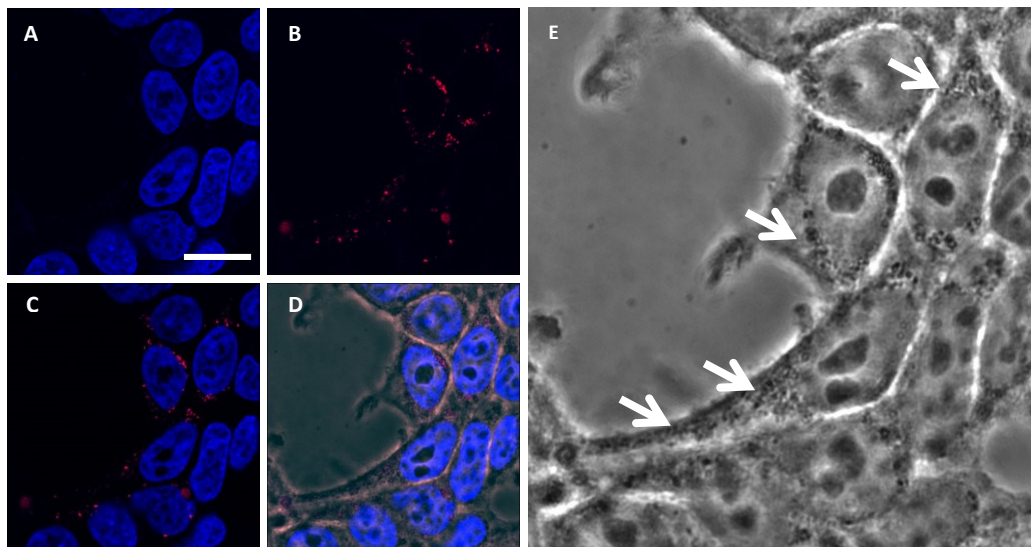
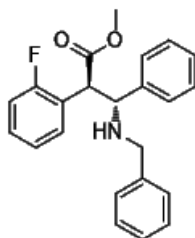


Figure 19⁴⁸: Confocal microscopy images of HEK cells treated for 16 h with RhB-T2R culture. A) Representative image of HEK cell culture nuclei stained with DAPI. B) Representative image of RhB-T2R in the HEK cells. C) Merged image of DAPI and RhB-T2R images. D) Merged image of DAPI, RhB-T2R and bright field images. E) Representative bright field image of HEK cells treated with RhB-T2R. Particles in the intracellular compartments are indicated by white arrows. Scale bar = 10 μ m

In conclusion, the self-assembly of ultra-short $\alpha\beta$ -tripeptide **T2R**, containing *L*-Arg-*L*-Ala sequence and an unnatural fluorine substituted $\beta^{2,3}$ -diaryl-amino acid, have been studied. The presence of Arg guanidinium group on the outer surface triggers the formation of spherical assemblies that are able to load small molecules and enter the cells. Due to the presence of unnatural $\beta^{2,3}$ -diaryl-amino, **T2R** positive charged spherical aggregates are proteolitically stable representing thus interesting candidates for the delivery of exogenous entities directly into the cells.

Experimental part

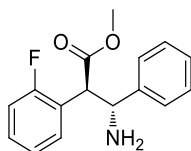
Synthesis of amino acid syn-1



Operating under N₂ atmosphere, methyl (2-F-phenyl)-acetate (315 mg, 1.9 mmol) and N-benzylidene-1-phenylmethanamine (353 mg, 1.8 mmol) were dissolved in CH₂Cl₂ (17 mL) and the mixture was cooled at -78°C. TiCl₄ (820 mg, 0.47 mL, 4.3 mmol), dissolved in CH₂Cl₂ (4 mL), was added in 15 minutes and the mixture was stirred for 30 minutes. Then, triethylamine (280 μL, 2 mmol) was added and stirring was continued for a further 15 minutes. A saturated solution of K₂CO₃ was dropped and the temperature was raised at 25 °C.

The white solid was filtered, the organic layers were separated and the aqueous layer was extracted with CH₂Cl₂. The combined organic layers were washed with brine, dried over anhydrous Na₂SO₄, filtered and concentrated. The crude residue was purified by flash chromatography using Hexane/EtOAc (9:1) as eluent, affording the amino acid *syn-1* (597 mg, 1.6 mmol, 86%). M.p.: 78.3 °C. IR (KBr) ν_{\max} = 1738.0, 1490.5, 1155.1 cm⁻¹. MS (ESI): *m/z* calcd for [C₂₃H₂₂FNO₂]: 363.16; found: *m/z* 364.1 [M+H]⁺. ¹H NMR (300 MHz, CDCl₃): δ 7.48-7.00 (m, 9H), 4.30 (AB system, *J* = 9.5, 2H), 3.55 (AB system, *J* = 13.9, 2H), 3.38 (s, 3H), 1.65 (br, 1H). ¹³C NMR (50 MHz, CDCl₃): δ = 50.7, 50.9, 52.0, 63.6, 115.7 (d, *J* = 22.9), 123.5, 124.5, 124.6, 127.1, 127.9, 128.2, 128.4, 128.6, 129.4, 129.5, 129.7, 143.4, 161.5 (d, *J* = 246), 171.98. ¹⁹F NMR (282 MHz, CDCl₃): δ = -117.4

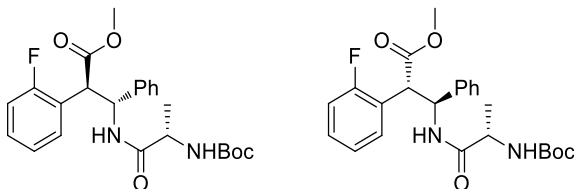
Synthesis of amino acid *syn-2*



Amino acid *syn-2* was obtained by deprotection of amino group on amino acid *syn-1*, by catalytic reduction. Amino acid *syn-1* (6.02 g, 16.6 mmol) was dissolved in MeOH (400 mL). Pd/C (3.7 g, 3.5 mmol) was added and the mixture was stirred under H₂ atmosphere at room temperature for 24 h.

The mixture was filtered on celite pad, the filtrated solution was concentrated under reduced pressure and the crude mixture was recrystallized (MeOH/*i*Pr₂O = 1/1), affording pure product *syn-2* (4.5 g, 16.4 mmol, 99%). Mp 81.2 °C. IR (KBr) ν_{max} : 1735.0, 1491.3, 1152.7, 757.8 cm⁻¹. MS (ESI): m/z calcd for [C₁₆H₁₆FNO₂]: 273.12; found m/z 274.1 [M+H]⁺. ¹H NMR (CDCl₃, 200 MHz) δ = 7.62-7.00 (m, 9H), 4.45 (AB system, J = 9.2 Hz, 2H), 3.46 (s, 3H); 1.50 (s, 2H). ¹³C NMR (CDCl₃, 50 MHz) δ = 52.0, 58.4, 115.7 (d, J = 22.9 Hz), 123.4, 123.7, 124.4, 127.3, 127.9, 128.7, 129.5, 143.2, 161.5 (d, J = 246.5 Hz), 172.3.

Synthesis of compounds *3a-(D1)* and *3b-(D2)*



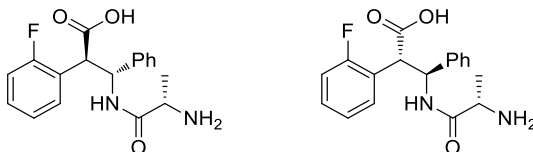
General procedure for the coupling: Boc-Alanine-OH (3.1 g, 16.3 mmol) was dissolved in CH₂Cl₂ (150 mL), the solution was cooled to 0°C and then EDC (3.1 g, 16.1 mmol) and EtCN-oxime (2.3 g, 16.1 mmol) were added. The mixture was stirred

at 0°C for 1h. After this time, racemic amino acid *syn*-**2** (4 g, 14.7 mmol), dissolved in DCM (100 mL), and DIEA (2.56 mL, 14.7 mmol) were added and the mixture was stirred at room temperature for 3 h. A saturated solution of NaHCO₃ (200 mL) was then added. The aqueous layer was separated and the organic one was washed first with a saturated solution of NH₄Cl (200 mL) and then with a saturated solution of NaCl (200 mL). The organic layer was dried over Na₂SO₄ and the solvent was removed under reduced pressure. Dipeptides **3a-D1** and **3b-D2** were obtained as a mixture of diastereoisomers (6.1 g, 94%) and were separated by column chromatography on silica gel using n-hexane/AcOEt (5:1) as eluent (**3a-D1**: 45%, **3a-D2**: 43%).

(2R,3R)-(D1): $[\alpha]_D^{25} = +34.5$ (CHCl₃, c 0.6). IR (KBr) ν_{\max} 3372.2, 1737.2, 1671.9, 1517.2 cm⁻¹. MS (ESI): m/z calcd for [C₂₄H₂₉FN₂O₅]: 444.21; found m/z 467.4 [M+Na]⁺. ¹H NMR (CDCl₃, 500 MHz) δ = 7.54 (ddd, J = 7.6, 1.5 Hz, 1H), 7.44-7.31 (m, 3H), 7.31 (ddd, J = 7.6, 1.3 Hz, 1H), 7.20 (ddd, J = 8.3, 1.3 Hz, 1H), 7.15-7.10 (m, 3H), 7.07 (d, J = 10.8 Hz, 1H), 5.69 (dd, J = 10.9, 10.7 Hz, 1H), 5.38 (brs, 1H), 4.50 (d, J = 10.9 Hz, 1H), 3.82-3.78 (m, 1H), 3.46 (s, 3H), 1.35 (s, 9H), 0.81 (d, J = 6.7 Hz, 3H). ¹³C NMR (CDCl₃, 125 MHz) δ = 17.8, 27.9 (x 3C), 49.6, 50.1, 52.2, 54.1, 79.1, 115.7, 117.7, 124.8, 124.9, 127.8, 128.2, 128.9, 129.8, 130.1, 130.2, 140.9, 155.5, 161.2, 171.3, 172.2.

(2S,3S)-(D2): $[\alpha]_D^{25} = +53.6$ (CHCl₃, c 0.6). MS (ESI): m/z calcd for [C₂₄H₂₉FN₂O₅]: 444.21; found m/z 467.4 [M+Na]⁺. ¹H NMR (CDCl₃, 500 MHz) δ = 7.54 (ddd, J = 7.6, 1.4 Hz, 1H), 7.58-7.30 (m, 3H), 7.30 (ddd, J = 7.6, 1.2 Hz, 1H), 7.19 (ddd, J = 9.6, 8.3 Hz, 1H), 7.15-7.10 (m, 3H), 7.07 (d, J = 9.9 Hz, 1H), 5.68 (dd, J = 10.5, 9.9 Hz, 1H), 5.38 (brs, 1H), 4.52 (d, J = 10.5 Hz, 1H), 3.80-3.74 (m, 1H), 3.46 (s, 3H), 1.37 (s, 9H), 0.92 (d, J = 6.7 Hz, 3H). ¹³C NMR (CDCl₃, 125 MHz) δ = 17.6, 27.9 (x 3C), 49.6, 51.1, 52.1, 53.9, 79.4, 115.7, 117.7, 124.8, 124.9, 127.7, 128.2, 128.6, 128.8, 130.1, 130.3, 140.9, 155.5, 161.2, 171.4, 172.5.

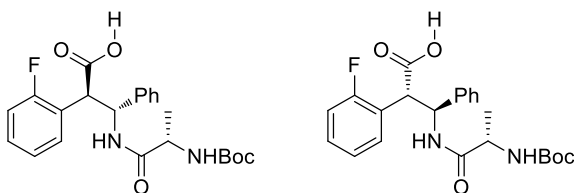
Synthesis of compound $\text{NH}_3^+\text{-D1-OH}$ and $\text{NH}_3^+\text{-D2-OH}$



Compound $\text{NH}_3^+\text{-D1-OH}$: y: (99 %). M.p.: 153.3 °C. IR (KBr) $\nu_{\text{max}} = 3429.6, 1963.9, 1713.5, 1672.7, 1492.5 \text{ cm}^{-1}$. MS (ESI): m/z calcd for $[\text{C}_{19}\text{H}_{21}\text{FN}_2\text{O}_3]$: 330.14; found: m/z 331.16 $[\text{M}+\text{H}]^+$. ^1H NMR (300 MHz, CD_3OD): 7.67-7.15 (m, 9H), 5.77 (d, $J = 11.8$, 1H), 4.53 (d, $J = 11.8$, 1H), 3.63 (m, 1H), 0.88 (d, $J = 7.15$, 3H). ^{13}C NMR (75 MHz, CDCl_3): $\delta = 16.2, 48.8$ (d, $J = 3.0$), 54.3, 115.2 (d, $J = 22.9$), 123.5 (d, $J = 14.6$), 124.4 (d, $J = 3.5$), 127.6, 127.9, 128.5, 129.5 (d, $J = 8.06$), 129.6, 140.1, 161.1 (d, $J = 245.6$), 168.6, 172.4.

Compound $\text{NH}_3^+\text{-D2-OH}$: y: (99 %). M.p.: 153.3 °C. IR (KBr) $\nu_{\text{max}} = 3219.9, 1954.4, 1719.5, 1688.6, 1492.3 \text{ cm}^{-1}$. MS (ESI): m/z calcd for $[\text{C}_{19}\text{H}_{21}\text{FN}_2\text{O}_3]$: 330.14; found: m/z 331.4 $[\text{M}+\text{H}]^+$. ^1H NMR (300 MHz, CD_3OD): 7.67-7.01 (m, 9H), 5.69 (d, $J = 11.7$, 1H), 4.64 (d, $J = 11.8$, 1H), 3.53 (m, 1H), 1.21 (d, $J = 7.0$, 3H). ^{13}C NMR (75 MHz, CDCl_3): $\delta = 16.3, 48.7$ (d, $J = 3.0$), 54.9, 115.2 (d, $J = 22.8$), 123.6 (d, $J = 14.5$), 124.5 (d, $J = 3.5$), 127.7, 128.0, 128.6, 129.5 (d, $J = 8.06$), 129.7, 140.5, 161.4 (d, $J = 246.1$), 168.8, 172.6.

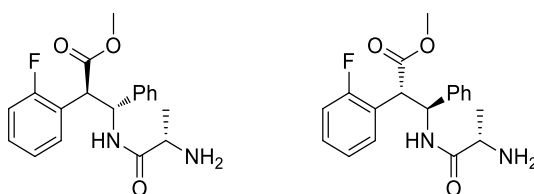
Synthesis of compound 4a-(D1) and 4b-(D2)



Compound 4a-(D1): y: (96%). IR (KBr) ν_{\max} = 3430.2, 1717.14, 1658.01, 1493.14 cm^{-1} . MS (ESI): m/z calcd for $[\text{C}_{19}\text{H}_{21}\text{FN}_2\text{O}_3]$: 430.19; found: m/z 353.3 $[\text{M}+\text{Na}]^+$. ^1H NMR (200 MHz, CDCl_3): δ 7.5-7.10 (m, 9H), 6.8 (m, 1H), 6.8 (m, 1H), 4.45 (d, J = 9.9, 1H), 3.9 (m, 1H), 1.2 (s, 9H), 1.0 (d, J = 6.3 Hz, 3H). ^{13}C NMR (50 MHz, CDCl_3): δ = 17.9, 22.9, 28.4, 29.2, 29.5, 29.9, 32.1, 48.8, 50.0, 54.5, 80.5, 114.3, 115.5 (d, J = 22.9 Hz), 122.4, 122.6, 124.7, 124.8, 127.6, 128.1, 128.8, 129.9, 130.2, 139.6, 155.8, 161.1 (d, J = 246.1 Hz), 171.9, 173.8

Compound 4b-(D2): y: (96%). IR (KBr) ν_{\max} = 2924.9, 1716.32 cm^{-1} . MS (ESI): m/z calcd for $[\text{C}_{19}\text{H}_{21}\text{FN}_2\text{O}_3]$: 430.19; found: m/z 453.1 $[\text{M}+\text{Na}]^+$. ^1H NMR (300 MHz, CDCl_3): δ 7.4-6.9 (m, 10 H), 5.6 (t, J = 8.80, 1H), 5.67 (m, 1H), 4.45 (d, J = 8.6, 1H), 3.82 (m, 1H), 1.2 (brs, 9H), 1.2 (d, J = 6.3, 3H). ^{13}C NMR (75 MHz, CDCl_3): δ = 14.2, 17.9, 23.2, 24.0, 28.3, 29.2, 29.6, 29.9, 30.6, 32.1, 39.0, 49.1, 52.4, 54.3, 68.4, 115.4 (d, J = 22.9 Hz), 122.6, 122.8, 124.6, 124.7, 127.5, 128.1, 128.8, 128.9, 129.0, 129.6, 129.8, 130.4, 130.5, 131.1, 139.8, 156.1, 161.1 (d, J = 246.1 Hz), 172.0, 173.9.

Synthesis of compound 5a-(D1) and 5b-(D2)



General procedure for deprotection on N termini: Boc-*N*-protected dipeptide (100 mg) was dissolved in CH_2Cl_2 (4 mL) and cooled to 0°C . After 5 minutes, TFA (4 mL) was slowly dropped to the solution. The mixture was stirred at room temperature for 1 h. The solvent was removed under reduced pressure affording dipeptide **3** as trifluoroacetic salt. The product was washed first with saturated solution of NaHCO_3 and then with saturated solution of NaCl . After the separation

of the aqueous layer, the organic layer was dried over Na₂SO₄ and the solvent was removed under reduced pressure, affording the desired product.

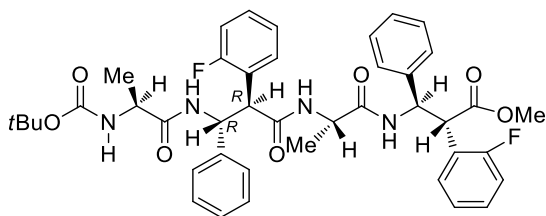
Compound 5a-(D1): y: (79.1 mg, 99%). M.p.: 87.2 °C. IR (KBr) ν_{\max} = 1732.64, 1660.85, 1493.60 cm⁻¹. MS (ESI): m/z calcd for [C₁₉H₂₁FN₂O₃]: 344.15; found: m/z 345.3 [M+H]⁺. ¹H NMR (200 MHz, CDCl₃): δ 7.77-6.97 (m, 10H), 5.69 (t, J = 10.2 Hz, 1H), 4.54 (d, J = 10.4, 1H), 3.53 (s, 3H), 3.26 (q, J = 7 Hz, 1H), 1.99 (s, 2H), 1.45 (d, J = 7 Hz, 3H). ¹³C NMR (50 MHz, CDCl₃): δ = 21.1, 49.2 (d, J = 3.0), 50.7, 52.5, 54.7, 110.0, 115.4 (d, J = 22.9), 123.1, 124.9, 127.7, 128.3, 129.4, 129.9, 130.2, 140.4, 161.2 (d, J = 245.5), 171.4, 174.0.

Compound 5b-(D2): y: (80 mg, 99%). M.p.: 87.7 °C. $[\alpha]_{\text{D}}^{25}$ = +76.8 (CHCl₃, c 1.0). IR (KBr) ν_{\max} = 1736.54, 1670.79, 1591.76, 1494.62 cm⁻¹. MS (ESI): m/z calcd for [C₁₉H₂₁FN₂O₃]: 344.15; found: m/z 345.3 [M+H]⁺. ¹H NMR (300 MHz, CDCl₃): δ 8.02 (d, J = 9.53, 1H), 7.57 (ddd, J = 1.47, J = 7.33, 1H), 7.41-6.98 (m, 9H), 5.67 (t, J = 10.11, 1H), 4.52 (d, J = 10.48, 1H), 3.49 (s, 3H), 3.40-3.80 (m, 2H), 0.84 (d, J = 6.88, 3H). ¹³C NMR (75 MHz, CDCl₃): δ = 19.6, 49.0 (d, J = 3.0), 50.0, 52.2, 54.3, 115.2 (d, J = 21.8), 122.5 (d, J = 13.82), 124.5 (d, J = 3.46), 127.4, 127.9, 128.6, 129.5 (d, J = 8.06), 129.8 (d, J = 3.45), 139.6, 161.1 (d, J = 245.3), 171.0, 172.1.

Synthesis of compound 6a-(D1) and 6b-(D2)

For the synthesis see the general procedure for the peptide coupling.

Complete NMR Characterization for Tetrapeptide **6a-(D1)** (CDCl₃, 10 mM, 293 K, 400MHz)



AA	atom	¹ H	<i>J</i> (Hz)	¹³ C	Noesy ^a	
Ala-1	CO			171.6		
	CH	3.92	brs	49.4	NH _{β2} (m), Me _{Ala1} (vs), Ar(6.98 m), NH _{Ala1} (w)	
	Me	0.86	<i>J</i> 6.9	18.4	NH _{Ala1} (m), CH _{Ala1} (vs), NH _{β2} (vw),	
	NH	5.08	<i>J</i> 4.8		Me _{Ala1} (m), CH _{Ala1} (w),	
	Boc	Me	1.39		28.4	Ar (7.39vw, 7.0vw), H _{β4-2} (vww)
		C			79.8	
		CO			155.5	
Beta-2	CO			169.2		
	2	4.19	d, <i>J</i> 11.0	50.3	NH _{β2} (w), H _{β2-3} (s), Ar(7.35vs, 7.61 vw, 6.98vw), NH _{Ala3} (vs), F(-118.16, vs)	

	3	5.76	brs	54.4	H β ₂ -2(s), Ar(7.35vs, 7.61vs), F (-118.16 vs)
	NH	6.99	Overl.		CH _{Ala1} (m), H β ₂ -2(w), Me _{Ala1} (w), Ar(7.19s, 7.35s),
	Arom	7.61 _{F-6} 7.23 _{F-4} 7.05 _{F-5} 6.98 _{F-3} - 7.37- 7.20		129.6 _{F-6} 128.5 _{F-4} 124.5 _{F-5} (<i>J</i> 9.8) 115.3 _{F-3} (<i>J</i> 17.0) 162.2 _{F2} (<i>J</i> 242.2) 123.0 _{F1} (<i>J</i> 13.6) 127.3 ^c 129.5 127.8 140.0 (q)	F ₆ : NH β ₂ (vs), Ar(7.05vs), H β ₂ -3(s), H β ₂ -2(w), Boc(w) F ₃ : H β ₂ -2(vw), CH _{Ala1} (m), F (-118.43vs) 7.35: H β ₂ -3(vs), H β ₂ -2(vs), NH β ₂ (s),
Ala-3	CO			170.5	
	CH	3.98	brs	48.4	Me _{Ala3} (m), NH β ₄ (vs), NH _{Ala3} (vw),
	Me	0.48	d, <i>J</i> 6.9	17.6	H _{Ala3} (m), NH _{Ala3} (s), NH β ₄ -3(vw), Ar(7.39m, 7.06vw)

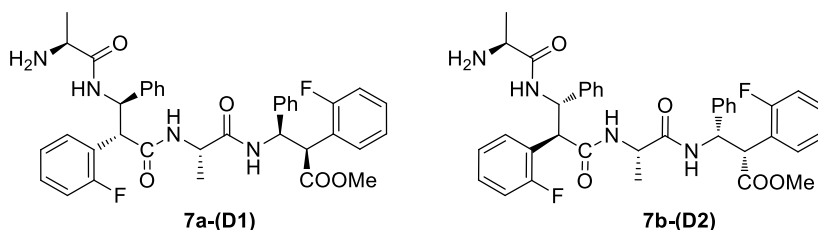
	NH	6.39	brs		H β ₂ -2(vs), Me _{Ala3} (s), CH _{Ala3} (w), F(-118.45w)
4	Beta- CO			170.9	
	2	4.38	d, <i>J</i> 10.7	48.7 (<i>J</i> _{CF} 1.9)	H β ₄ -3(s), NH β ₄ (s), Ar(7.18 vs; 7.49 m), F (s, -118.43vs) Boc (vww)
	3	5.62	t, <i>J</i> 10.3	55.3	NH β ₄ (m), H β ₄ -2(s), Ar(7.15s, 7.49vs), F (-118.45 vs)
	NH	6.52	d, <i>J</i> 10.7		H _{Ala3} (vs), H β ₄ -2(s), H β ₄ -3(m), Ar(7.16 m)
	Arom	7.49 _{F-6} 7.23 _{F-4} 7.06 _{F-5} 6.94 _{F-3} - - 7.30- 7.25			129.6 _{F-6} 128.5 _{F-4} 124.5 _{F-5} (<i>J</i> 9.8) 115.0 _{F-3} (<i>J</i> 16.5) 162.2 _{F2} (<i>J</i> 242.2) 122.4 _{F1} (<i>J</i> 14.4) 129.5 ^b 128.6 ^b 127.3 139.2(q)

	OMe	3.52	s	52.1	Ar (7.53s, 7.06w), H β ₄ -3(s), H β ₄ -2(vs)
--	-----	------	---	------	---

Table 3: ¹H, ¹³C NMR (CDCl₃, 10 mM, 400 MHz,) and NOEs (500 ms) data for isomer **6a-(D1)**.

^a450 ms at 300 K. ^bTentatively assigned.

Synthesis of **7a-(D1)** and **7b-(D2)**



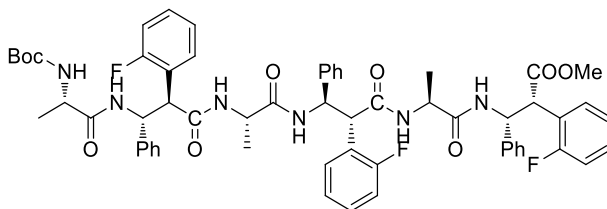
For the synthesis see the general procedure of the deprotection on *N termini*.

Compound 7a-(D1): (y: 96%) Mp: 90.2 °C. IR (KBr) ν_{\max} = 1739.06, 1651.28, 1492.24, 1232.45 cm⁻¹. MS (ESI): m/z calcd for [C₁₉H₂₁FN₂O₃]: 656.15; found: m/z 657.1 [M+H]⁺ ¹H NMR (CDCl₃, 200 MHz) δ = 7.80-7.70 (m, 1H), 7.70-7.57 (m, 1H), 7.55-7.45 (m, 1H), 7.40-6.90 (m, 16H), 6.48 (d, J = 9.27 Hz, 1H), 6.10 (d, J = 6.94 Hz, 1H), 5.62 (m, 2H), 4.39 (d, J = 10.5 Hz, 1H), 4.12 (d, J = 10.3 Hz, 1H), 3.97 (q, J = 5.88 Hz, 1H), 3.48 (s, 3H), 3.22 (m, 1H), 1.84 (brs, 2H), 1.03 (d, J = 6.54 Hz, 3H), 0.55 (d, J = 6.84 Hz, 3H). ¹³C NMR (CDCl₃, 50 MHz) δ = 17.9, 21.2, 30.1, 36.8, 49.2, 48.3, 48.8, 50.8, 52.6, 55.0, 55.0, 115.2 (d, J = 22.9 Hz), 115.7 (d, J = 22.8 Hz), 115.8, 122.7, 122.9, 123.3, 123.5, 124.9, 124.9, 125.0, 125.0, 127.5, 127.6, 128.1, 128.3, 128.9, 129.6, 129.7, 129.9, 129.9, 120.0, 130.2, 130.3, 139.7, 140.6, 161.0 (d, J = 241.3 Hz), 162.1 (d, J = 241.1 Hz), 169.7, 170.8, 171.2, 174.4.

Synthesis of compound **8a-(D1)** and **8b-(D2)**

For the synthesis see the general procedure for the peptide coupling.

Complete NMR Characterization for Hexapeptide **8a-(D1)** (CDCl₃, 10 mM, 293 K, 500 MHz)



AA	atom	¹ H	Multiplicity <i>J</i> (Hz)	¹³ C	Noesy CH	
Ala-1	CO			172.1		
	CH	4.05		49.7	Me _{Ala1} (vs)	
	Me	0.77	<i>J</i> 7.0	19.6	NH _{Ala1} (w), CH _{Ala1} (s), Ar(7.1m, 7.16m, 7.61m), Me _{Ala5} (s)	
	NH	5.49	<i>J</i> 6.8		Me _{Ala1} (vw)	
	Boc	Me	1.40		28.8	H _{β6-2} (s), Arom (7.17)
		C			79.8	
CO				155.8		
Beta-2	CO			171.0		
	2	4.55	<i>J</i> 9.4	50.7(<i>J</i> _{CF} 2.2)		
	3	5.97	<i>tJ</i> 11.1	53.9	NH _{Ala3} (vs), Arom(7.61 vs)	
	NH	7.49	overl.			
	Arom	7.61 _{F-6} 6 7.16, 6.97 Ph: 7.43, 7.19, 7.15, 7.00		129.5 _{F-6} (brs) 129.7 _{F-4} (<i>J</i> 8.5) 124.5 _{F-5} (<i>J</i> 3.5) 116.0 _{F-3} (<i>J</i> 22.2) 157.2 _{F2} (<i>J</i> 246.1) 122.7 _{F1} (<i>J</i> 14.1)	F ₆ : NH _{β2} (s), Ar(7.00vs), H _{β2-3} (s), H _{β2-3} (vs), Me _{Ala3} (w)	

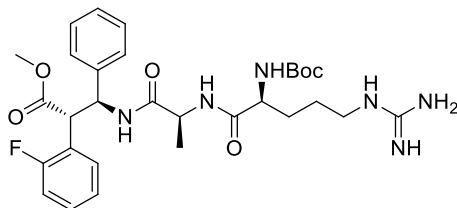
				127.8 ^b 128.8 ^b 126.8 140.4 (q)	
Ala-3	CO			171.4	
	CH	4.19		48.9	Me _{Ala3} (m),
	Me	0.32	<i>J</i> 6.9	18.8	H _{Ala3} (m), 6.96(vw), 7.17(vs), NH _{Ala3} (w), 7.49(m)
	NH	7.43	overl.		
Beta-4	CO			171.1	
	2	4.27	<i>d</i> , <i>J</i> 10.7	51.3	
	3	5.92	<i>t</i> <i>J</i> 11.4	53.6	H _{β4-2} (w), H _{β2-3} (w), 7.48(vs), 7.16(vs)
	NH	6.88	overl.		H _{Ala3} (vs), H _{β4-2} (m), H _{β4-3} (m), Ar(7.32 m)
	Arom	7.48 _{F-6} 7.25 _{F-4} 7.13 _{F-5} 7.06 _{F-3} 7.00, 6.94 - 7.16- 7.25m		129.9 _{F-6} (<i>J</i> 2.0) 130.1 _{F-4} (<i>J</i> 7.4) 125.0 _{F-5} (<i>J</i> 3.5) 115.7 _{F-3} (<i>J</i> 22.9) 161.1 _{F2} (<i>J</i> 245.0) 124.3 _{F1} (<i>J</i> 13.9) 129.2 ^b 128.6 ^b 127.6 139.7(q)	F ₆ : Ar(7.13s), H _{β4-3} (s), H _{β4-2} (vw), OMe(w) F ₅ : Ar(7.50s) F ₃ : OMe(w), F(-118.45)
Ala-5	CO			171.0	
	CH	4.09		48.7	Me _{Ala5} (vs)
	Me	0.35	<i>J</i> 6.5	18.8	H _{Ala5} (vs), 6.92(vw), 7.02(s), 7.15 (vs), 7.50(w). 6.93(w), Me _{Ala1} (s)

	NH	6.91	overl.		
Beta-6	CO			171.0	
	2	4.41	<i>J</i> 11.2	48.9	Boc(s), 7.19(vs), 7.50(s), H _{β6} -3(s),6.77(vwNH). OMe(m)
	3	5.69	<i>tJ</i> 10.6	54.1	H _{β6} -2(s),7.22(s), (7.50w, 7.19 vs)
	NH	6.76	overl.		
	Arom	Ph _{6F} 7.50, 7.17, 7.01 Ph: 7.22		Ph _F : 122.9 (<i>Jq</i>), 129.6, 161.1 Ph:126,9, 139.6q	H _{β6} - 3(vs),H _{β6} 2(m),H _{Ala5} (w),
	OMe	3.44		52.4	

Table 4: ¹H, ¹³C NMR (CDCl₃, 10 mM, 400 MHz,) and NOEs (500 ms) data for isomer **8a-(D1)**.

^aNOESY at 293 K. ^cTentatively assigned

Synthesis of compound T2R



Boc-NH-Arginine (82 mg, 0.25 mmol) was dissolved in CH_2Cl_2 (3 mL), the solution was cooled to 0°C and then EDC (52 mg, 0.27 mmol) and EtCN-oxime (40 mg, 0.27 mmol) were added. The mixture was stirred at 0°C for 1 h. Then dipeptide $\text{NH}_2\text{-D2}$ (85 mg, 0.25 mmol), dissolved in DCM (1 mL), and DIEA (1 eq., 43 μL , 0.247 mmol) were added and the mixture was stirred at room temperature overnight. A saturated solution of NH_4Cl was added. The aqueous layer was separated and organic layer was washed first with a saturated solution of NaHCO_3 and then with saturated solution of NaCl .

The organic layer was dried over Na_2SO_4 and the solvent was removed under reduced pressure. The crude mixture was recrystallized from DCM/ Et_2O (1:5), affording pure compound **T2R** (127.5 mg, 0.21 mmol, 86%). $[\alpha]_{\text{D}}^{25} = +35.0$ (CH_3OH , c 0.4). M.p.: 141.7°C . IR (KBr) $\nu_{\text{max}} = 3401.72, 1737.96, 1660.48, 1529.72, 1455.85\text{ cm}^{-1}$ MS (ESI): m/z calcd for $[\text{C}_{30}\text{H}_{41}\text{FN}_6\text{O}_6]$: 600.31; found: m/z 601.2 $[\text{M}+\text{H}]^+$. ^1H NMR (300 MHz, CD_3CN): $\delta = 8.31$ (br, 1H), 7.74 (d, $J = 8.8$, 1H), 7.61 (ddd, $J = 1.59, J = 7.56$), 7.50-7.12 (m, 9H), 6.62 (br, 3H), 5.66-5.69 (m, 2H), 4.58 (d, $J = 11.34$, 1H), 4.02-3.98 (m, 2H), 3.42 (s, 3H), 3.12 (m, 2H), 1.71 (br, 1H), 1.51 (m, 2H), 1.41 (s, 9H), 1.33 (m, 1H), 0.91 (d, $J = 7.3$, 3H). ^{13}C NMR (75 MHz, CD_3CN): $\delta = 16.9, 23.8, 27.5, 28.6, 39.9, 49.5, 50.1, 51.7, 53.1, 53.3, 79.1, 115.3$ (d, $J = 14.7$), 122.9 (d, $J = 14.4$), 124.2 (d, $J = 3.2$), 127.6, 127.7, 128.4, 129.6 (d, $J = 8.42$), 130.0 (d, $J = 2.88$), 140.7, 156.0, 157.5, 161.0 (d, $J = 245.8$), 171.0, 171.6, 171.9.

AA	atom		¹ H NMR δ (CD ₃ CN, 300 MHz)	Multiplicity <i>J</i> (Hz)	¹³ C NMR δ (CD ₃ CN, 75 MHz)	Noesy tmix=300ms	
Arg- 1	CO				171.88		
	CH		3.98	overlapped	53.07	NH _{Ala} (s); CH ₂ α (s); CH ₂ β (s); CH ₂ γ (m); NH _{Arg} (m); Boc (s)	
	CH ₂ α		1.71 1.33		39.91	CH _{Arg} (s); CH ₂ γ (w)	
	CH ₂ β		1.51	overlapped	23.85	CH ₂ γ (s); CH _{Arg} (s); NH _{Arg} (m)	
	CH ₂ γ		3.13		28.60	CH _{Arg} (m); CH ₂ α (w);	
	NH Guanidinium		8.31	br		CNH _{Guanidinium} (s); NH ₂ Guanidinium (s)	
	CNH Guanidinium		6.62	br	155.88	NH ₂ Guanidinium (s); NH Guanidinium (s)	
	NH ₂ Guanidinium		6.62	br			
	NH		5.66	overlapped		CH _{Arg} (m); CH ₂ β (m)	
	Boc	CO				157.5	
		C				79.07	
		CH ₃		1.41	s	27.56	CH ₂ α (s)
	CO				171.66		

Ala-2	CH	4.02	overlapped	50.06	CH _{3Ala} (s); NH _{Ala} (s); NH _{Beta3} (s)
	Me	0.91	d, $J = 7.3$	16.93	NH _{Beta3} (s); NH _{Ala} (s); CH _{Ala} (s)
	NH	7.53	overlapped	7.53	CH _{3Ala} (s); CH _{Ala} (s);
Beta-3	CO			170.98	
	2	4.58	d, $J = 11.34$	49.45	CH _{3Beta} (s); NH _{Beta} (s); CH _{F-6} (m); Ph (m); OMe (vw)
	3	5.69	overlapped	53.96	CH _{2Beta} (s); NH _{Beta} (m); CH _{F-6} (m); Ph (m); OMe (vw)
	Arom	7.61 _{F-6} 7.50-7.30 7.33 _{F-4} 7.19 _{F-5} 7.12 _{F-3}	ddd, $J = 1.59, J = 7.56$ overlapped overlapped overlapped overlapped	C _{F-6} 130.0 (d, $J = 2.88$) 140-128.4-127.7-127.6 C _{F-4} 129.6 (d, $J = 8.42$) C _{F-5} 124.2 (d, $J = 3.2$) C _{F-3} 115.3 (d, $J = 14.7$) C _{F-1} 122.9 (d, $J = 14.4$) C _{F-2} 161.0 (d, $J = 245.8$)	CH _{3Beta} (s); CH _{2Beta} (s); NH _{Beta} (s)
	NH	7.74	d, $J = 8.8$		CH _{Ala} (w); CH _{3Beta} (m); CH _{2Beta} (s); Ph (s)
	OMe	3.42	s	51.68	CH _{3Beta} (vw); CH _{2Beta} (vw)

Table 5: ¹H, ¹³C NMR (CD₃CN, 17 mM, 300 MHz) and NOE (300 ms) data for tripeptide **TR2**

Pronase stability of T2R

Enzymatic degradation studies were carried out in PBS buffer (0.01M, pH 7) in presence of CaCl₂ (10 mM). **T2R** (5 mg/ml) was incubated at 25°C under magnetic stirring in absence or in presence of Pronase from *Streptomyces griseus* (0-0.5-1-10 mg/ml). Aliquots (50 µl) of the sample were analyzed at different times from 0 h to 24 h. The reaction was quenched adding 10 µl of acetic acid (25% v/v) and 150 µl of a mixture H₂O: MeCN (60:40). The degradation of **T2R** was monitored by RP-HPLC (Phenomenex LUNA 5µ C18 250 x 4,60 mm) using as eluents 60% water with 0,1% TFA and 40% MeCN (flow rate of 0.8 ml/min). Detection was performed by UV measurement at 220 nm. To evaluate the stability of the enzyme, 1mg/ml of protease was stirred at 25°C. After 24 h, 5 mg/ml of **T2R** was added and aliquots were analyzed as previously described. The partial thermal inactivation of Pronase (1mg/ml) was observed after 24 h at 25°C, in fact adding **T2R** to the reaction system, the degradation carried out with a lower rate (t= 3h molar conversion= 46%).

Time (h)	Molar Conversion (%)
0	0
2	39
4	46
7	65
24	76

Table 6: Hydrolysis of **T2R** (5 mg/mL) with Pronase (1 mg/mL) at 25°C

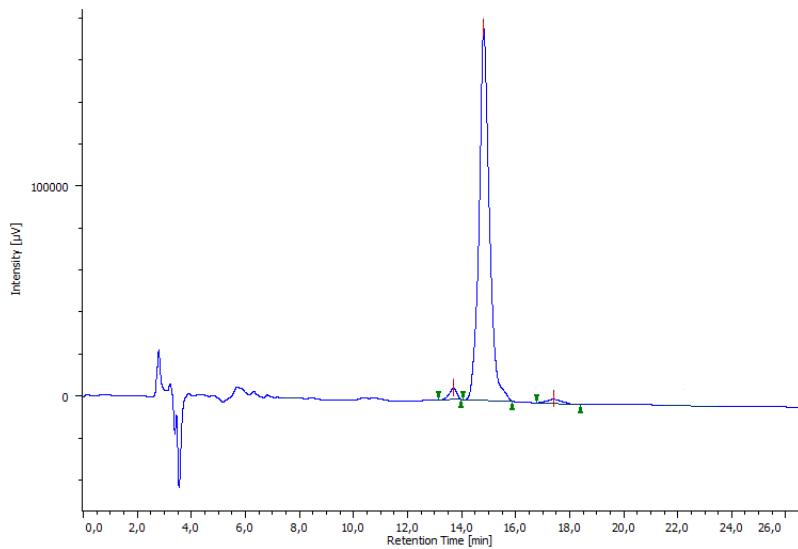


Figure 20: HPLC chromatogram of T2R

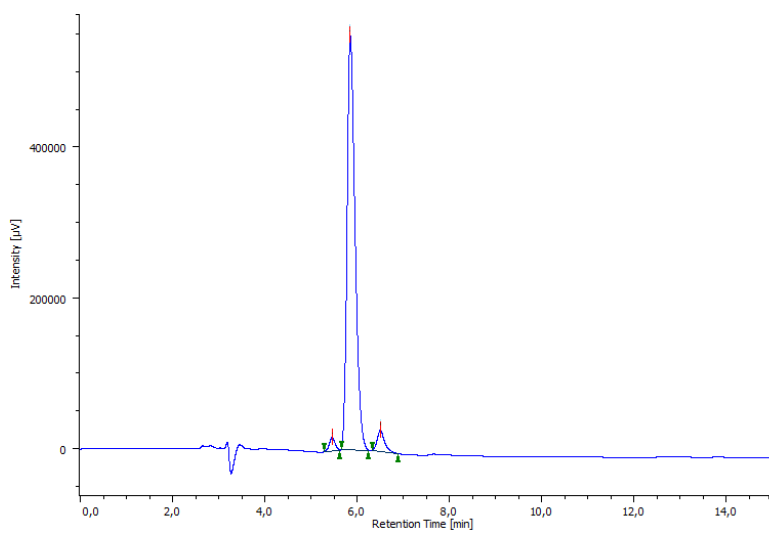


Figure 21: HPLC chromatogram of product NH₂-D2

Novel bicyclic Δ^2 -isoxazoline derivatives as potential turn inducers in peptidomimetic syntheses

Aim of the project

The aim of this project is the use of diastereoisomeric Δ^2 -isoxazoline compounds fused with a nitrogen containing ring in the preparation of hybrid peptide models.

As explained, non-natural molecular scaffold could mimic secondary structure elements, such as turn mimics, that are of great interest in different applications, ranging from catalysis to electrochemistry, biology and nanomedicine^{116,117}.

The appealing feature of this scaffold is the presence of two amino groups, making it a good candidate as potential turn inducers for parallel β -sheet mimics.



Figure 1: Left: Our isoxazoline-based scaffold; Right: general representation of parallel β -sheet mimic.

As explained in the Introduction, β -Sheets consist of extended polypeptide strands (β -strands) connected by a network of hydrogen bonds and occur widely in proteins. Parallel hairpins require a reverse-turn unit that can link together two strand segments via their C or N termini; segments constructed from only α -, β -, or other amino acids cannot fulfill this need because they have only one N and one C terminus. A variety of unnatural segments have been used to link peptide strands, N-terminus to N-terminus or C-terminus to C-terminus, in a manner that promotes parallel sheet formation¹¹⁸⁻¹²⁶.

Although the importance of both antiparallel and parallel β -sheets in the folded structures of proteins has long been recognized, there is a growing recognition of the importance of intermolecular interactions among β -sheets. Intermolecular interactions between the hydrogen-bonding edges of β -sheets constitute a

fundamental form of bio-molecular recognition and are involved in protein quaternary structure, protein-protein interactions, and peptide-protein aggregation. The importance of β -sheet interactions in biological processes makes them potential targets for intervention in diseases such as AIDS, cancer, and Alzheimer's disease^{127,128}.

The connection of a β -sheet with a scaffold able to induce a turn generates a more stable hairpin¹²⁹. Our interest in the isoxazoline scaffold derives from the large presence of isoxazole ring in a lot of pharmaceutical compounds and natural products, such as selective modulators of the multidrug resistance protein¹³⁰, anticoronavirus agents¹³¹ and anticancer agents^{132,133}. On the other hand, a turn formed by non-natural amino acids makes the peptidomimetic more stable to metabolic degradation. Furthermore, the oxazoline ring makes possible H-bond increasing possible interactions with protein.

The key step to obtain the Δ^2 -isoxazoline compounds is a [1,3]-dipolar cycloaddition reaction.

For this reason, a short overview of this reaction is given below.

Overview on [1,3]-cycloaddition reaction

The use of [1,3]-dipolar cycloaddition reactions to produce heterocycles is well known¹³⁴ and in particular, the synthetic and mechanistic aspects in the application of nitrile oxides as precursors of isoxazolines and isoxazoles have been extensively studied¹³⁵.

Despite the large number of methods for the preparation of nitrile oxides, the precursor of the isoxazoline ring, one of the most used method is the obsolete Mukaiyama' strategy¹³⁶, *via* dehydration of primary nitroalkanes. The limitations due to the intrinsic instability of nitrile oxide were partially overcome with the Huisgen's in situ method, that has been frequently employed as effective procedure^{137,138}. In fact, Huisgen explains the advantages of dehydrogenation of

aldoximes, *via* the halogenated derivatives such as hydroximoyl chlorides and bromides.

However, the main drawback in using nitrileoxides is their instability that affects the yield of the cycloaddition reaction, resulting in the isolation and purification problems of the reaction products.

According to several studies concerning nitrile oxides reactivity¹³⁴, it is known that nitrile oxides often rearrange to form an isocyanate. This transformation is favored when they are left alone at high temperature (110–140°C). On the other hand, the nitrile oxide tends to dimerize to produce furoxan at room or lower temperatures.

In general, [1,3]-cycloadditions give rings containing several contiguous stereocenters in one synthetic step. The configurations of these new stereocenters arise from the geometry of the dipole and dipolarophile as well as the topography (*endo* or *exo*) of the cycloaddition. As a result, different isomers could be expected, depending on the regio- and stereoselectivity of the reaction.

Being motivated by the wide utility of [1,3]-cycloaddition in synthesis of our scaffold (Figure 1), we focused on the development of an efficient synthetic strategy. Since we were interested in the functionalization of the isoxazole ring with a nitrogen containing chain (Figure 1), we selected as dipole a nitrile oxide generated *in situ* from a chloro-oxime, synthesized in a very good overall yield from a readily available chiral material., *i.e.* (*L*)-Phe. As dipolarophile we selected Benzyl-*N*-pyrroline, that contain a nitrogen atom and, being symmetric, avoid the formation of mixture of regioisomers.

Compound **9** was obtained in enantiopure form and satisfying yields as a mixture of two diastereoisomers. Studies concerning the control of the diastereoselection of the reaction were performed and they are still on going.

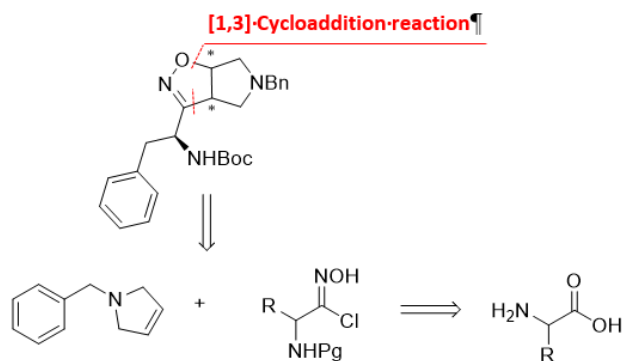


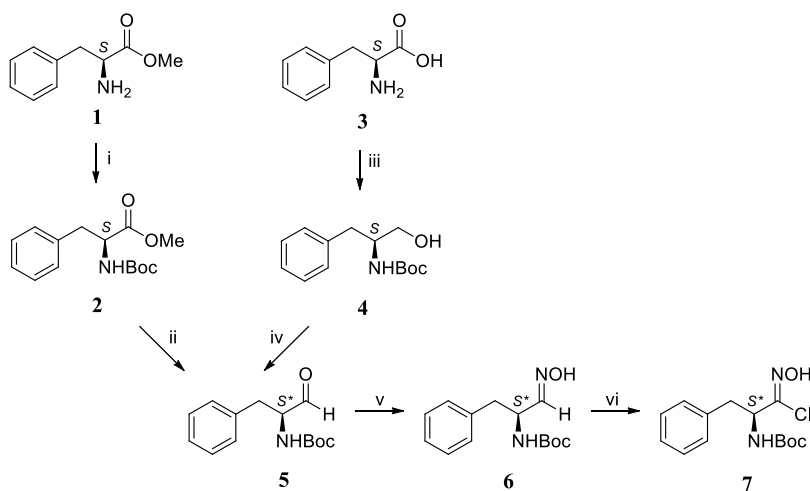
Figure 2: Retrosynthetic pathway to obtain our isoxazoline containing scaffold

Synthesis

Synthesis of isoxazoline containing scaffold

As said above, the key step to obtain the Δ^2 -isoxazoline compounds is a [1,3]-dipolar cycloaddition reaction.

The nitril-oxide, acting as a dipole, was synthesized starting from the readily available (*L*)-Phe **3** or the corresponding ester **1**.



Scheme 1: Synthesis of chloro-oxime **7**. Reagents and conditions. i) TEA, (Boc)₂O in CH₂Cl₂, 0°C to r.t.; ii) DIBAL-H, dry toluene, -78°C; iii) NaBH₄, I₂, TEA, (Boc)₂O in THF; iv) (COCl)₂, dry DMSO, in dry CH₂Cl₂, -78°C, TEA; v) H₂NOH·HCl, NaHCO₃ in THF, 0°C to reflux.

The key reagent for the formation of **7** is the aldehyde **5** that could be obtained in two different ways (Scheme 1).

In a first approach, we focused on the direct reduction of ester function to aldehyde. After protection of nitrogen atom of ester **1** with Boc (compound **2**), the reduction with DIBAL-H was performed giving aldehyde **5** that was obtained in very low overall yield (5%).

For this reason, we moved on to the “one-pot” synthesis of alcohol **4** (98%) using a procedure in which (*L*)-Phe was reduced and protected using first NaBH₄ and I₂ in MeOH for the reduction and then Boc₂O for nitrogen protection. Compound **4** was oxidized to the aldehyde **5**, obtained in 99% yield.

Starting from compound **5**, we succeeded in achieving oxime **6** (NaHCO₃, H₂NOH·HCl, THF, 0°C, then r.t. overnight, 73%) which was then transformed into the corresponding chloro-oxime **7** (NCS, CCl₄, 0 °C, then r.t., overnight, 97%).

This synthetic route is quite efficient, affording chloro-oxime **7** in four steps and 70% overall yield. However, this procedure has, as drawback, the racemization of compound **5**, during the oxidation from alcohol to aldehyde. Consequently, compounds **6** (HPLC analysis, Figure 3A), and consequently **7**, are obtained as a racemic mixture.

In order to avoid aldehyde racemization, we performed several studies. Swern oxidation was first performed at -78° C. Nevertheless, it resulted in a decrease of yields (40% instead of 99%) and moreover, the enantiopure aldehyde, and consequently oxime, was not obtained (HPLC analysis, Figure 3B). Very low yields were also detected using TEMPO as oxidant¹³⁹.

Finally, the oxidation in presence of Dess-Martin reagent was then investigated. This strategy, working in mild conditions (neutral pH, room temperature), avoids racemization, since it prevents keto-enol tautomerization, as reported in literature¹⁴⁰. Indeed, aldehyde **5** was obtained from **4** (Dess-Martin periodinane, DCM, r.t.) in high yields (93%) and with an enantiomeric excess of 100% (HPLC analysis, Figure 3C).

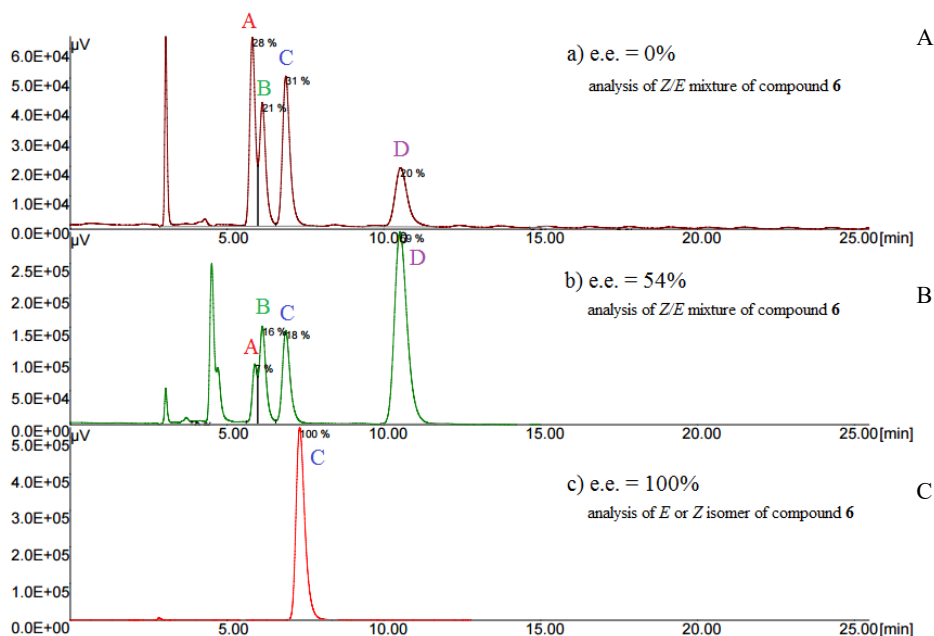


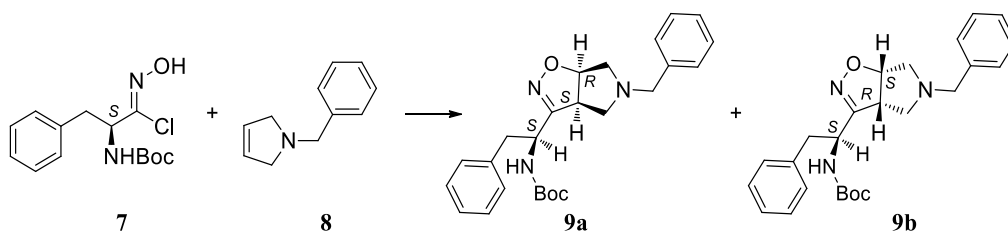
Figure 3: HPLC chromatograms of oxime **6** obtained using chiral stationary phase (tris-(3,5-dimethyl-phenyl)carbamoyl amylose), eluent: 8:2 *n*-hexane/*i*PrOH, flow rate: 1 mL min⁻¹. A and B: *E/Z* isomers of **6** with *R*-configuration C and D: *E/Z* isomers of **6** with *S*-configuration; Peaks with a retention time less than five minutes are impurities. a) Chromatogram of compound **6** derived from Swern oxidation performed in standard condition (-78°C to r.t.) (purple); b) chromatogram of compound **6** derived from Swern oxidation performed at -78°C (green); c) chromatogram of compound **6** derived from Dess-Martin oxidation (red).

[1,3] Cycloaddition studies: synthesis of Δ^2 -isoxazoline-fused pyrroline derivatives

Aiming to obtain Δ^2 -isoxazoline ring we used freshly distilled *N*-benzyl-pyrroline as dipolarophile.

According to the known procedure in which **7** was used as starting reagent for the preparation of nitrile-oxide¹⁴¹, the cycloaddition was firstly performed in CHCl₃ both at reflux and at 0°C and using TEA as base (Table 1, entries 1,2). In any case, the reaction did not work or gave very poor yield, probably due to the poor reactivity of nitrile oxide¹³⁴. DABCO was also selected as base, but the reaction was unsuccessful (Table 1, entry 3).

Determining *a priori* the optimal solvent for a dipolar cycloaddition is usually not possible, because the constant rate may be influenced by solvent features, such as the polarity or its ability to give hydrophobic interactions or hydrogen bonds with substrates. As a result, the reaction conditions were changed (Table 1), performing the reaction at room temperature and in other solvents. In our case, the use of a more polar aprotic solvent, such as acetonitrile (dielectric constant: $\epsilon = 37$) (Table 1, entry 4), rather than CHCl_3 ($\epsilon = 4.8$), allowed to obtain a couple of diastereoisomers **9a** and **9b** in 1:3 ratio and 38% yields (Table 1, entries 4). Interestingly, when the reaction was performed using an inorganic base, i.e. NaHCO_3 , the reaction was successful too. Better results in terms of yield, and mostly with a decrease of the reaction time, were found using MeCN (Table 1, entry 6) with respect to AcOEt ($\epsilon = 6$), (Table 1, entry 5). This could be due to the low solubility of the inorganic bases in organic solvent, allowing to generate the nitriloxide gradually avoiding decomposition of the chloroxime. Furthermore, using the inorganic base, we observed a decreasing of the diastereomeric ratio of **9a**, **9b** from 1:3 to 1:2. This behaviour is further reinforced by the use of Li_2CO_3 (Table 1, entry 7), where two diastereoisomers were formed in 1:1 ratio. This behavior could be probably ascribed to the smaller atomic radius of the Li in comparison with Na or to the different solubility of the LiCO_3 , that makes the cation more accessible to a possible coordination with coordinating moieties in the reagents.



Entry	Solvent	T (°C)	Base	Reaction time (h)	Diastereoisomeric ratio (9A/9B) ^e	9A + 9B % ^f

1	CHCl ₃ ^a	60	TEA (1.2 eq.)	18	-	6%
2	CHCl ₃ ^b	0-25	TEA (2 eq.)	48	-	traces
3	CHCl ₃ ^b	25	DABCO (2 eq.)	48	-	traces
4	CH ₃ CN ^c	25	TEA (2 eq.)	16	1:3	38%
5	EtOAc ^c	25	NaHCO ₃ (2.2 eq.)	17	1:2	32%
6	CH ₃ CN ^d	25	NaHCO ₃ (2 eq.)	5	1:2	51%
7	CH ₃ CN ^d	25	LiCO ₃ (0.5 eq)	4	1:1	48%

Table 1: a) The reaction was performed in CHCl₃ at reflux starting from **7** and **8** in 1:1 ratio; b) The reaction was performed in CHCl₃ at 0°C to r.t., starting from **7** and **8** in 1:1 ratio; c) The reaction was performed at r.t., starting from **7** and **8** in 2.2:1 ratio; compound **7** was added slowly over a period of an hour to the reaction mixture; d) The reaction was performed at r.t., starting from **7** and **8** in 2:1 ratio; compound **7** was added slowly over a period of 2 hours to the reaction mixture; e) Calculated by NMR; f) Isolated product

Even if diastereomers **9a** and **9b** were collected as a quite inseparable mixture, their purification on silica gel column chromatography, followed by a crystallization (AcOEt/*n*-hex), allowed the isolation and characterization of the main diastereoisomer **9b**. The purification of the other diastereoisomer was not possible under classical conditions.

Preliminary studies on mechanism of the key step [1,3]- cycloaddition reaction: NMR and computational study

¹H NOESY analysis in CD₃CN of the major diastereoisomer **9b** shows different significant spatial proximities, allowing us to assign the 3a*R*,6a*S*-configuration to the new generated stereocenters with respect to the *S* configuration of the side chain.

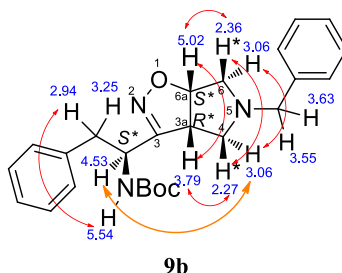


Figure 4: NOE signals of compound **9b**

Moreover, the absolute configuration of the isoxazoline scaffold was confirmed by the single-crystal X-ray analysis. Suitable needle-shape crystals of **11b**, debenzylated **9b** obtained as explained below, were obtained from slow evaporation, at 25 °C, of a CDCl₃/Et₂O (1:10) solution.

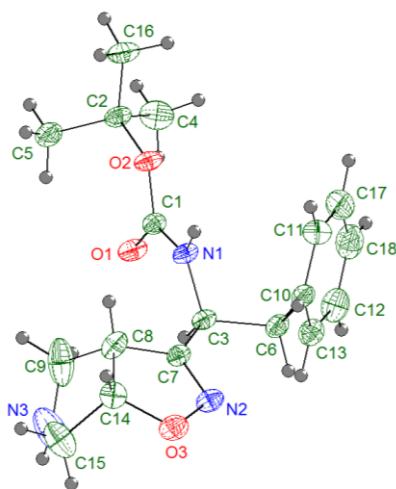


Figure 5: Single crystal structure of compound **11b**

The crystallographic analysis proved also the stereochemistry of the major isomer **9b** (3a*R*,6a*S*-configuration at the new generated stereocenters), already hypothesized with the computational calculations, displayed below.

In our conditions, the cycloaddition reaction can give a couple of diastereoisomeric isoxazolines owing to the presence of a stereocenter in the nitrile oxide, considering that the dipolarophile is symmetric.

It is known that the use of a nitrile oxide containing a stereocenter and an achiral dipolarophile generally produce a 1:1 mixture of diastereomeric isoxazolines. On the other hand, the diastereoselectivity control is usually induced by a dipolarophile containing a stereocenter or when chiral centers are contained in both reagents¹³⁴.

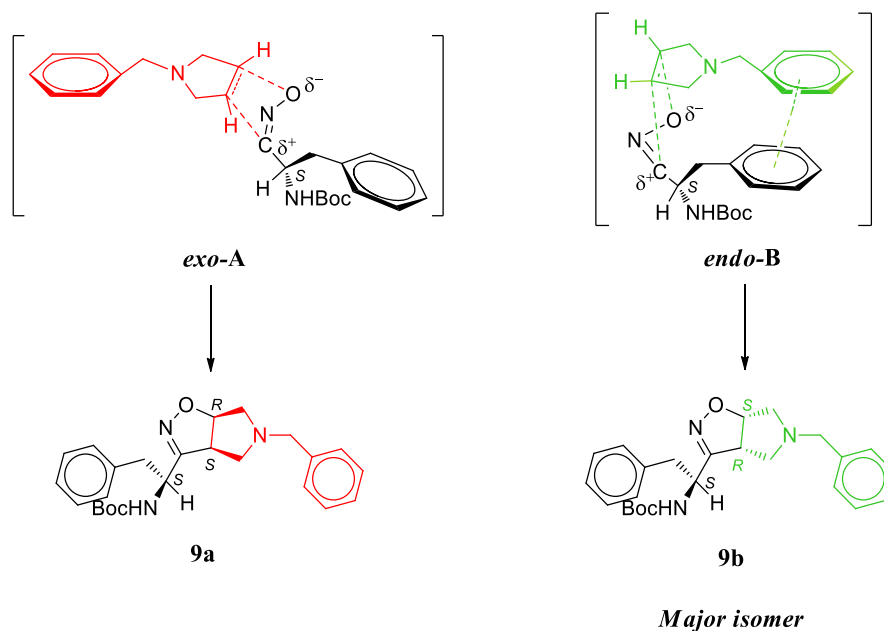
The above general behavior of our cycloaddition reaction disagrees with our achievements. As reported, the cycloaddition reaction can give a couple of

diastereoisomeric isoxazolines with a partial control of the diastereoselectivity, even with the presence of a stereocenter in the nitrile oxide.

Our results concerning the diastereoselectivity are quite interesting and buck the trend, because it seems to be also connected with the choice of the base. In fact, their distribution is dependent on the presence or absence of a cation.

Two main possible mechanisms of this cycloaddition reaction have been postulated depending on the reaction conditions. In our opinion two main forces could influence the diastereoselectivity, i.e. the π -interactions^{142,143,144} and a coordination of the inorganic base cation.

Considering the reaction in the presence of the organic base, our hypothesis is that π -interactions between the phenyl group of the dienophile and that of the dipole stabilize the *endo*-transition state **B** with respect to the *exo*-transition state **A**, giving compound **9b** as major isomer. Another possible hypothesis is that this stereoisomer is more stable than **9a** (Scheme 2).



Scheme 2: Proposed transition states in the cycloaddition reaction of **7** with **8** in the absence of a metal cation.

The above hypotheses have been supported by computational studies, which will predict transition states with lowest energy as well as the stability of the products.

Therefore, in collaboration with professor Alessandro Contini of University of Milan, we succeeded in obtaining preliminary computational information. The relative stability of the two diastereomers **9a** and **9b** was studied by molecular mechanics and quantum mechanical calculations. After designing the molecular structures using MOE software, compounds **9a** and **9b** were subjected to conformational search *via* "Low Mode MD" simulation, implemented in MOE.

MMFF94x was used as force field coupled with born solvent model, specifying a dielectric constant of 37.5, (equal to the acetonitrile). It was set a "Rejection Limit" of 100, an "Iteration Limit" of 100000 and "MM Iteration Limit" of 1000. Concerning compound **9a**, 203 different conformations were obtained in an energy range of 7 kcal/mol. 240 conformations were obtained for the compound **9b** in the same range. The most stable conformations for each compound (20 conformations for **9a**, 25 for **9b**) have been subjected to geometry optimization and vibrational frequencies calculation at a maximum interval of 2 kcal/mol from the more stable conformation.

DFT level of theory HCTH/6-31+g(d) was used, followed by the calculation of the energy in HCTH/6-311+g(d,p) level, using CPCM solvent model for acetonitrile. The most stable conformation for each compound is shown in Figure 6.

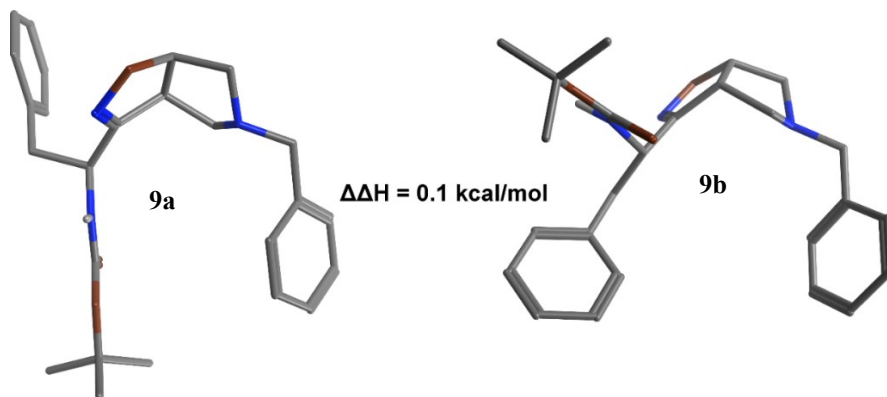


Figure 6: Most stable conformations obtained for the compounds **9a** and **9b**

From a thermodynamic point of view, the energy of the two diastereoisomers is almost equivalent, with a value of $\Delta\Delta H = 0.1$ kcal/mol in favor of the derivative **9b**. Therefore, the experimentally observed diastereoselectivity should be determined by the transition state, suggesting that the reaction is under kinetic control.

The structures of the corresponding transition states were generated starting from the optimized geometries of the most stable conformations of **9a** and **9b**, and successively optimized using the same level of theory. Energies were then calculated in the HCTH/6-311+g(d,p) level, using the CPCM solvent model for acetonitrile.

The optimized structures of **TS-9a** and **TS-9b** are shown in Figure 7.

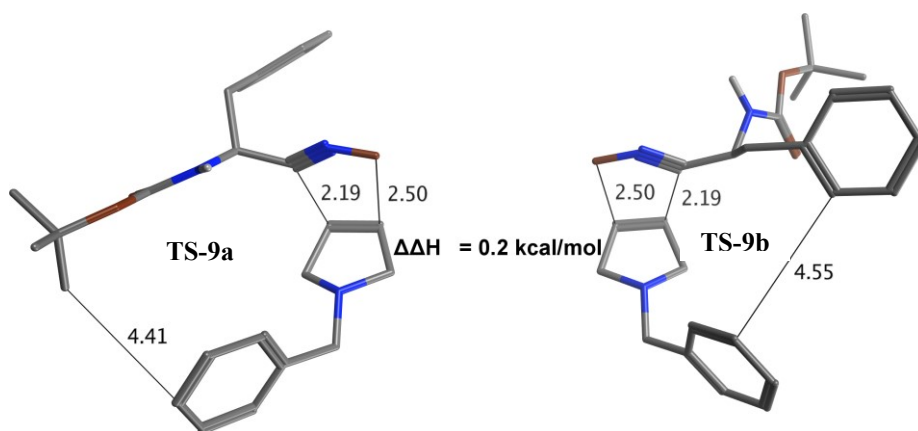


Figure 7: Optimized structures of **TS-9a** and **TS-9b**.

Although the enthalpy difference $\Delta\Delta H$ between the two geometries is still very low (0.2 kcal/mol), **TS-9b**, leading to **9b**, is favored. If the reaction is under kinetic control, the ratio between **9a** and **9b** can be calculated accordingly to the Arrhenius equation (1):

$$\frac{[15a]}{[15b]} = e^{\frac{H_{15b} - H_{15a}}{RT}} \quad (1)$$

With $R = 0.00198588$ (universal gas constant, expressed in kcal/mol \cdot K⁻¹) and $T = 298.15$ K.

Thus, with an enthalpy difference of 0.2 kcal/mol, the predicted ratio for **9a** and **9b** is 28:72, respectively, more or less corresponding to a ratio of 1:3. Since this is the ratio experimentally obtained, we can conclude that the reaction is under kinetic control.

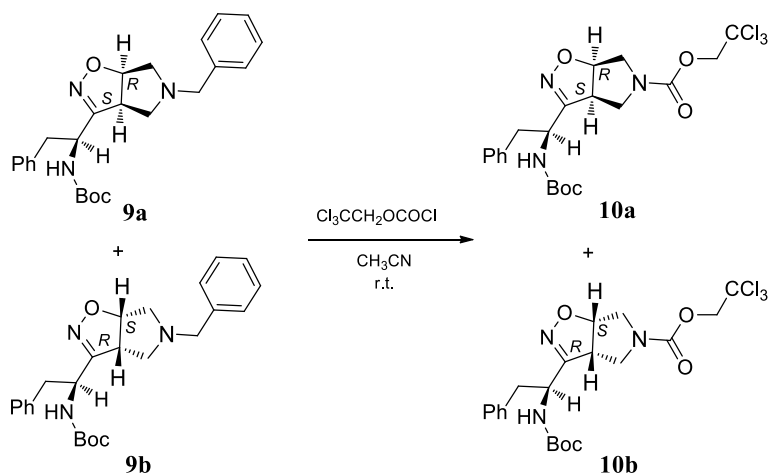
As reported, when the reaction was performed in the presence of a coordinating metal cation, such as Na⁺ and Li⁺, we observed a decreasing of the diastereoselectivity. This finding could be explained if a complementary mechanism, involving the coordination of the cation.

Peptide synthesis

In order to use diastereoisomers **9a** and **9b** for peptide synthesis, it was necessary the orthogonal deprotection of the nitrogen of the pyrrolidine ring with respect to Boc-protected amine. Due to the instability of isoxazoline nucleus to the catalytic reduction with H₂, a different procedure was adopted, consisting in a debenzoylation/acetylation reaction according to known procedures¹⁴⁵.

The use of 2,2,2-trichloroethyl chloroformate allowed us to efficiently replace, using a “one pot” reaction, the benzyl function with Troc-group (Troc-Cl, MeCN, 2 h;

97%). This group is very labile in different mild conditions, as reported in the literature^{146–148}.

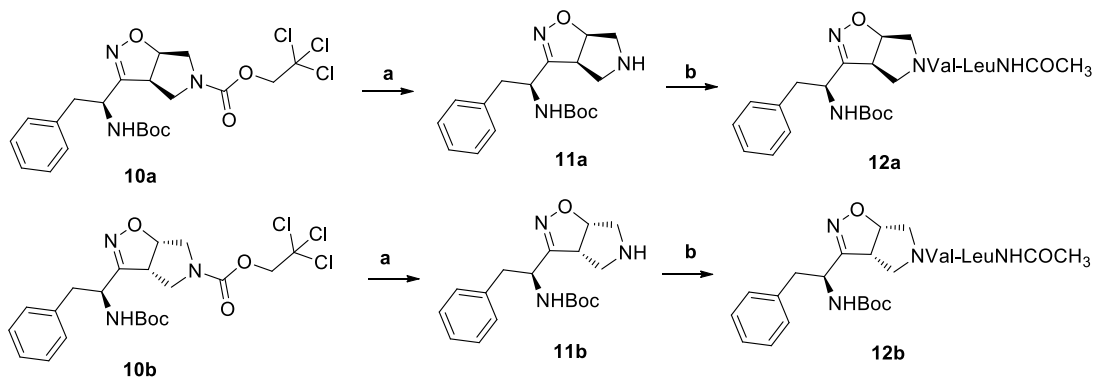


Scheme 3: Reaction of compounds 9a and 9b in the presence of 2,2,2-trichloroethyl chloroformate (1 eq.), in CH₃CN at r.t.

After the obtainment of the mixture **10a** and **10b**, the two diastereoisomers were easily separated by flash chromatography (See the Experimental Part).

The orthogonal deprotection of the nitrogen of the pyrrolidine ring was not trivial because it's known that Troc-group is labile in acidic condition as well as the Boc protecting-group. However, we found a procedure¹⁴⁹ that gave us the desired result. Dissolving compound **10** in AcOH (90%) and adding powder Zn (Scheme 4) compound **11** was obtained with 90% yield.

In order to evaluate the ability of our scaffolds, **9a** and **9b**, to induce a turn or a different stable secondary structure when inserted in a natural sequence, two small peptides models, i.e. **12a** and **12b** were prepared. The dipeptide *N*-Ac-Leu-Val-OH was chosen for its attitude of having an extended conformation. We obtained compound **12a** and **12b** in very good yield (83% overall yield starting from compound 10) using liquid phase protocol and the classic coupling agents as shown in Scheme 4



Scheme 4: Synthesis of peptides **12a** and **12b**. Conditions: a) Zn, AcOH, rt, 90 %; b) EDC, HOBT, DCM, DIEA, 92%.

Characterization by NMR spectroscopy of tripeptides compound **12b** and **12a**

The peptide **12b** was characterized by NMR (^1H , ^{13}C , HMBC, HSQC, NOESY; MeCN, 20 mM, 300 MHz) that allowed to confirm the stereochemistry of the stereocenters of the oxazoline scaffold (Figure 4). Furthermore, the NMR analysis of compound **12b** showed the presence of at least two isomers (60:40 ratio). It was found that a proton of an isomer shows spatial proximities also with the protons of the second isomer in the NOESY experiment. These data confirmed that an equilibrium occurs between the two isomers.

Well dispersed amide protons are present, suggesting that the peptide chain could assume an ordered conformation.

Moreover, H_α of all AAs are at lower field with respect to random coil residues. As further confirmation, $^3J_{\text{HN/CH}}$ are higher than 8Hz both for *CHBn*, that could be considered the equivalent of Phe, and Valine. These data suggest the a β strand conformation could be taken in consideration^{150,151}. The $\delta\Delta/\delta T$ analysis indicates that NHBoc is involved in a H-bond (-4.5 ppb) for isomer **12b** and NHLeu (-4 ppb) for isomer **12b'** (Table 2). Since these isomers are in equilibrium, these values are consistent with a medium H-bond. Coalescence of NHBoc signal occurs at 313K. A completed coalescence for all NHs takes place at 323K.

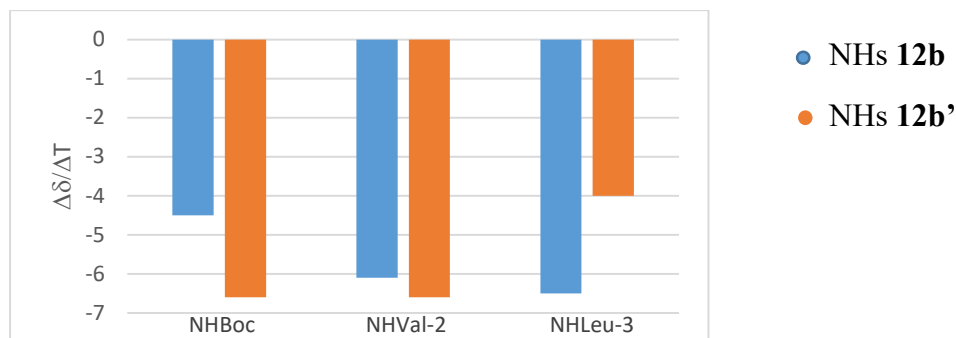


Table 2: $\Delta\delta/\Delta T$ NH values for both conformers **12b** and **12b'** (273-323 K)

According to the detected NOEs (Figure 8), our hypothesis is that NH_{Boc} forms a H-bond with $\text{C}=\text{O}_{\text{Leu}}$ in rotamer **12b**. In fact, a medium NOEs was detected between $\text{H}_{4\gamma}$ and CH_{Bn} . This spatial proximity is not consistent with the formation of a H-bond between NH_{Boc} and $\text{C}=\text{O}_{\text{Val}}$, giving a very constrain ring preventing spatial proximity between the two mentioned protons. On the other hand, NH_{Val} is involved in a H-bond with $\text{C}=\text{O}_{\text{Boc}}$ moiety in isomer **12b'**.

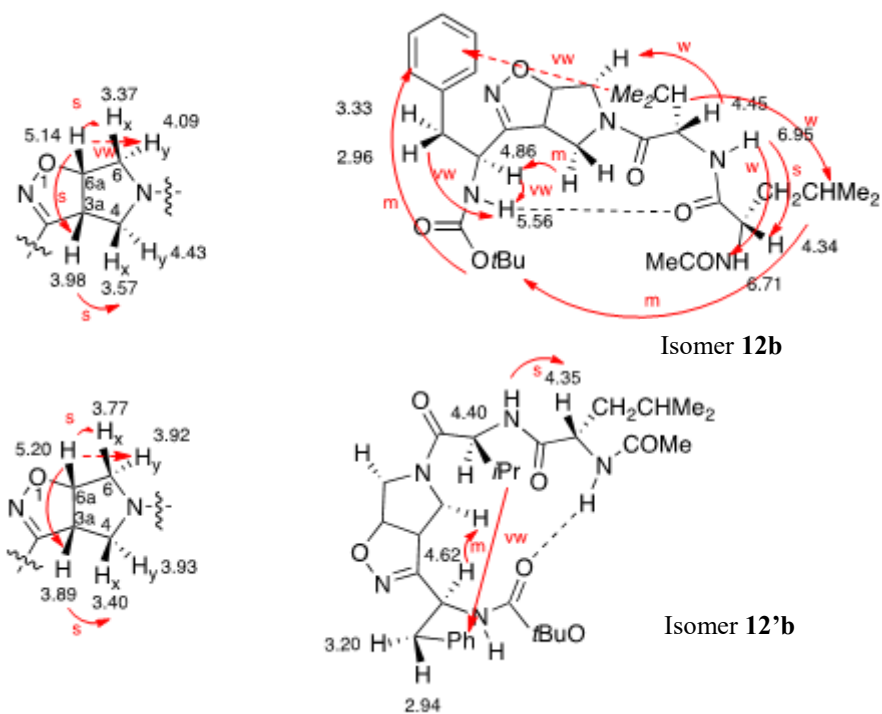


Figure 8: NOEs of isoxazoline scaffold protons of both isomers **12b** and **12'b** (Left). C) NOEs between the different amino acids of peptide **12b** and **12'b** (Right).

The typical strong NOE between $\text{CH}_{\text{Leu}} / \text{NH}_{\text{Val}}$ and the intrastrand proximity between the phenyl ring and the *i*Pr group in both isomers were found supporting the idea that a parallel sheet could be induced by our scaffold.

Focusing on the minor diastereoisomer **12a**, it is present as a mixture of two conformers (almost 1:1 ratio), with a third minor isomer. Several signals are overlapped avoiding a fine characterization of the main isomers.

Larger $\Delta\delta/\Delta T$ values with respect to **12b** were detected (Table 3). A completed coalescence for all NHs took place at 313K.

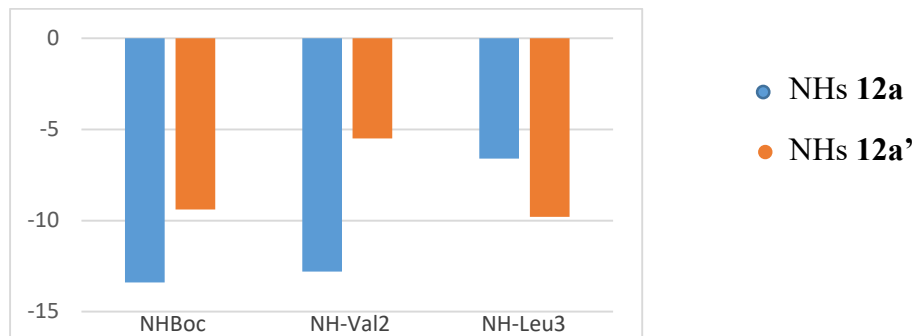


Table 3: $\Delta\delta/\Delta T$ NH values for both conformers 12a and 12a' (273-323 K)

Several NOEs are present between CH_{Val} with both protons of H-4 and H-6 as well as between CH_{Leu} with H-4x and H-6y. Taken together these data, a random conformation for this peptide is suggested (Figure 9).

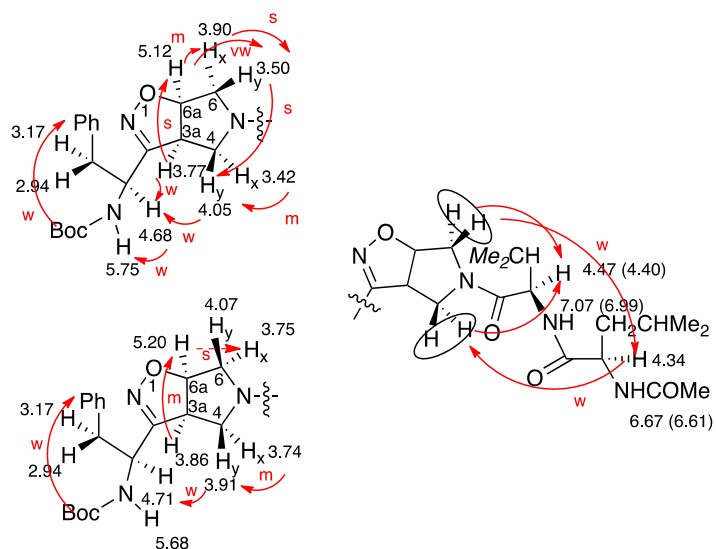


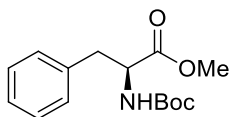
Figure 9: NOEs of isoxazoline scaffold protons of both isomers 12a and 12a' (Left). C) NOEs between the different amino acids of peptide 12a and 12a' (Right).

In conclusion, with [1,3]-dipolar cycloaddition, we performed the synthesis of two isoxazoline derivatives containing the Phe moiety. The study of model peptides, containing this new molecular scaffold, proved that one of these, **9b**, allows the formation of a parallel β -sheet conformation.

Compound **12b** is present in solution as mixture of two conformers, thus the next step is to elongate the two arms of the parallel β -sheet model to study the possibility to stabilize one of the two conformers.

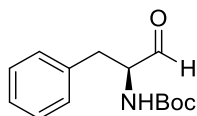
Experimental part

Synthesis of '(S)-(tert-butoxycarbonyl)-L-phenylalaninate' (2)



In a three-neck round-bottom flask equipped with a magnetic stirrer, nitrogen inlet, and thermometer, compound **1** (233 mg, 1.3 mmol) was dissolved in dry CH_2Cl_2 (13 mL) and the solution was cooled to 0 °C. Triethylamine (0.18 mL, 1.3 mmol) was added. After 10 min., di-*tert*-butyl dicarbonate (371 mg, 1.7 mmol) was slowly added and the stirring was continued overnight at 25 °C. The reaction mixture was washed with KHSO_4 (pH = 3, 0.5 N), brine and then dried over Na_2SO_4 . The solvent was removed under reduced pressure. Purification of the crude product by flash chromatography (hexane/AcOEt 9:1) afforded compound **2** (363 mg, 1.29 mmol, 99 %) as a white solid. TLC: R_f (hexane/AcOEt 9:1): 0.32. ^1H NMR (200 MHz, CDCl_3): δ 7.34 – 7.09 (m, 5H), 4.94 (br, 1H), 4.58 (dd, $J = 10.9, 7.3$ Hz, 1H); 3.71 (s, 3H), 3.12 – 3.00 (m, 2H), 1.41 (s, 9H) ppm.

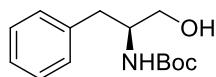
Synthesis of 'tert-butyl (1-oxo-3-phenylpropan-2-yl)carbamate' (5)



In a three-neck round-bottom flask, equipped with magnetic stirrer, thermometer and nitrogen inlet, compound **2** (363 mg, 1.29 mmol) was dissolved in dry toluene (10 mL) and the solution was cooled to -78 °C. A solution of diisobutylaluminum hydride (1M solution in toluene, 0.54 ml, 2.25 mmol) was slowly added. The reaction mixture was stirred at -78°C for 6 hours. At the end of reaction MeOH (0.13 mL) and s.s. Na_2SO_4 (0.49 mL) were added. The reaction mixture was stirred at r.t.

overnight and afterwards it was dried over Na₂SO₄ and filtered. The solvent was removed under reduced pressure, affording the product as yellow oil (17.4 mg, 0.07 mmol, 5%)-rif-. TLC: R_f (hexane/AcOEt 7:3): 0.35. MS (ESI): *m/z* calcd for [C₁₄H₁₉NO₃]: 249.14; found: *m/z* 250.20 [M+H]⁺. ¹H NMR (300 MHz, CDCl₃): δ 9.63 (s, 1H), 7.51 – 7.11 (m, 5H), 5.05 (br s, 1H), 4.42 (dd, 1H), 3.12 (d, *J* = 6.5 Hz, 2H), 1.41 (s, 9H) ppm.

Synthesis of 'tert-butyl (S)-(1-hydroxy-3-phenylpropan-2-yl)carbamate' (4)

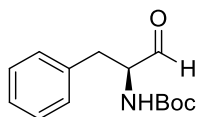


In a three-neck round-bottom flask, equipped with magnetic stirrer, thermometer and nitrogen inlet, compound **2** (1.27 g, 4.56 mmol) was suspended in toluene (15 mL). The suspension was cooled to -78° and diisobutylaluminum hydride (1M solution in toluene, 1.95 mL, 10.03 mmol) was added dropwise over 45 min. The reaction mixture was slowly heated for 2h and then was stirred at r.t. for 1h. The reaction mixture was subsequently quenched slowly with ice and 5% citric acid (1:1). The organic layer was separated and the aqueous was extracted with ethyl acetate. The combined organic layers were washed with brine, dried over Na₂SO₄, filtered and the solvent was removed under reduced pressure. Purification of the crude product by flash chromatography (hexane/AcOEt 8:2) afforded compound **4** (330 mg, 1.31 mmol, 29%) as a white solid¹⁴¹. TLC: R_f(hexane/AcOEt 7:3): 0.18. M.p.: 92°C. MS (ESI): *m/z* calcd for [C₁₄H₂₁NO₃]: 251.15; found: *m/z* 274.40 [M+Na]⁺. ¹H NMR (300 MHz, CDCl₃): δ 7.32 – 7.20 (m, 5H), 4.72 (d, 1H), 3.86 (br s, 1H), 3.66 (dd, 1H), 3.55 (dd, 1H), 2.83 (d, 2H), 2.08 (br s, 1H), 1.41 (s, 9H) ppm. [α]_D²⁰: -28,5° (c: 0.6 in CHCl₃).

Synthesis of 'tert-butyl (S)-(1-hydroxy-3-phenylpropan-2-yl)carbamate' (4)

In a three-neck round-bottom flask, equipped with magnetic stirrer, thermometer, nitrogen inlet and dropping funnel, NaBH₄ (400 mg, 15 mmol) was dissolved in THF (20 mL). The solution was cooled to 0°C and, stirring vigorously, a solution of I₂ (1530 mg, 6 mmol) in THF (5 mL) was added very slowly. L-phenylalanine **3** (1 g, 6 mmol) was afterwards added in one portion and the reaction mixture was stirred under reflux for 16 h. After cooling the solution to r.t., MeOH (13 mL) was added until discoloration. The reaction mixture was stirred for 30 min. The solution was re-cooled to 0°C and triethylamine (1.66 mL, 12 mmol) was added dropwise. After stirring for 10 min., a solution of di-*tert*-butyl dicarbonate (1400 mg, 6.4 mmol) in THF (4 mL) was dropped. The reaction mixture was stirred for additional 20 h. The solvent was removed under reduced pressure and the reaction crude was re-dissolved in ethyl acetate. The organic layer was washed with s.s. NH₄Cl and dried over Na₂SO₄. The solvent was removed under reduced pressure and the crude product was crystallized from hexane/ethyl acetate (12/1), affording compound **4** (1469 mg, 5.85 mmol, 97.5%) as a white solid.

Synthesis of 'tert-butyl (1-oxo-3-phenylpropan-2-yl)carbamate' (Parikh-Doering oxidation) (5)



In a three-neck round-bottom flask, equipped with magnetic stirrer, thermometer, nitrogen inlet and dropping funnel, a solution of **4** (95 mg 0.37 mmol) in triethylamine (0.16 mL, 1.16 mmol) were added in CH₂Cl₂:DMSO (1mL/1mL). The reaction mixture was cooled to 0°C and a dry solution of Py·SO₃ (390.90 mg, 0.37 mmol) in CH₂Cl₂:DMSO (2 mL/2mL) was dropped very slowly. The reaction mixture was stirred for 1 h at r.t. and it was quenched with ice/water:1/1 (10 mL). The aqueous layer was extracted with Et₂O (3x15 mL). Combined organic layers

were washed with 10% citric acid (2x10 mL), H₂O (2x10 mL), s.s. NaHCO₃ (10 mL), dried over Na₂SO₄, filtered and evaporated under reduced pressure. The crude product **5** (21.2 mg, 8.5 mmol, 23%) was immediately used without further purifications. For characterization see reference¹⁴¹.

Synthesis of 'tert-butyl (1-oxo-3-phenylpropan-2-yl)carbamate' (Swern Oxidation) (5)

In a three-neck round-bottom flask, equipped with magnetic stirrer, thermometer and nitrogen inlet, a solution of dry (COCl)₂ (0.25 mL, 3 mmol) in dry CH₂Cl₂ (2.5 mL) was added and cooled to -78°C. A solution of dry DMSO (0.24 mL, 3.4 mmol) in CH₂Cl₂ (1.0 mL) was dropped over 5 min, then the reaction was stirred for 15 min. A solution of **4** (500 mg, 2.0 mmol) in dry CH₂Cl₂ (2.5 mL) was afterwards dropped over 10 min. The reaction mixture was stirred for 30 min. and then a solution of dry triethylamine (1.12 mL, 8.0 mmol) was added dropwise over 10 min. The reaction was slowly heated to r.t. and was stirred for 1 hour. The reaction mixture was diluted with CH₂Cl₂ (16 mL) and washed with 10% citric acid (15 mL), H₂O (15 mL), s.s. of NaHCO₃ (15 mL) and dried over Na₂SO₄. The solvent was removed under reduced pressure. The crude compound (493 mg, 1.97 mmol, 99%) was immediately used without further purifications. For characterization see reference¹⁴¹.

Synthesis of 'tert-butyl (1-oxo-3-phenylpropan-2-yl)carbamate' (TEMPO Oxidation) (5)

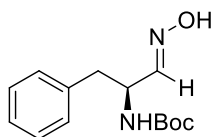
In a two-necked round-bottom flask, equipped with magnetic stirrer and thermometer, to a cold (0°C), rapidly stirred, biphasic mixture consisted of alcohol **4** (500 mg, 2.0 mmol), TEMPO free radical (6.25 mg, 0.04 mmol), sodium bromide (204.77 mg, 2.0 mmol), toluene (6 mL), ethyl acetate (6 mL) and water (1 mL), an

aqueous solution of 12.5% NaOCl (1.2 mL, 2.2 mmol) containing NaHCO₃ (487.25 mg, 5.8 mmol) was dropped over a period of 1-2 h. The aqueous layer was separated and washed with Et₂O (10 mL). The combined organic layers were washed with a solution of KI (10 mg) dissolved in 10% aqueous KHSO₄ (4 mL), then with 10% aqueous sodium thiosulfate (2 mL), brine (4 mL) and dried over Na₂SO₄. The solvent was removed under reduced pressure. The crude compound **5** (74.7 mg, 0.30 mmol, 15%) was immediately used for further reactions without purification.

Synthesis of 'tert-butyl (1-oxo-3-phenylpropan-2-yl)carbamate' (Dess-Martin Oxidation) (5)

In a round-bottom flask, equipped with magnetic stirrer, Dess-Martin oxidant (551 mg, 1.3 mmol) was suspended in CH₂Cl₂ (5mL) and dioxane (3mL). Afterwards a solution of alcohol **4** (300 mg, 1.19 mmol) in CH₂Cl₂ (1mL) was added dropwise over a period of 20 min. The reaction was stirred for 20 min at 25°C after the complete addition of **4**. When the reaction was complete, diethyl ether (2 mL) and sodium thiosulfate (0.5 g) in saturated sodium bicarbonate solution (2 mL) were added. The reaction was stirred for further 5 min before addition of ether (2 mL). The layers were separated and organic layer was washed with s.s. NaHCO₃ (2 x 4 mL), water (2 x 4 mL) and dried over Na₂SO₄. The solvent was removed under reduced pressure, affording **5** (300 mg, 1.2 mmol, 93%) as a pale-yellow oil.

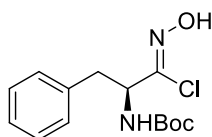
Synthesis of 'tert-butyl (1-(hydroxyimino)-3-phenylpropan-2-yl)carbamate' (6)



In a bottom flask, equipped with magnetic stirrer and thermometer, corresponding aldehydes **5** (500 mg, 2 mmol) was dissolved in THF (7.5 mL) at 0°C. NaHCO₃

(102.5 mg, 1.22 mmol) and $\text{H}_2\text{NOH}\cdot\text{HCl}$ (148.3 mg, 2.3 mmol) were subsequently added to the solution. The reaction mixture was heated slowly to r.t. and stirred overnight. The reaction mixture was concentrated under reduced pressure and the residue was extracted with ethyl acetate (4x4.5 mL). The combined organic layers were washed with brine (4.5 mL), dried over Na_2SO_4 and concentrated *in vacuo*. Purification of the crude product by flash chromatography (hexane/AcOEt 8:2) and crystallization from hexane/AcOEt (15/1) afforded compound **6** (385.4 mg, 1.46 mmol, 72.5 %) as a white solid¹⁴¹. **Cis/trans isomers of compound 6**: TLC: R_f (hexane/AcOEt 7:3): 0.45. M.p. = 118.5°C. MS (ESI): m/z calcd for $[\text{C}_{14}\text{H}_{20}\text{N}_2\text{O}_3]$: 264.15; found: m/z 286.9 $[\text{M}+\text{Na}]^+$. ^1H NMR (300 MHz, CD_3CN): δ 8.59 (s, 1H), 7.49 – 7.26 (m, 6H), 5.26 (br s, 1H), 4.40 (ddd, $J = 14.4, 8.4, 6.0$ Hz, 1H), 2.99 (dd, $J = 6.3, 13.7$ Hz, 1H), 2.86 (dd, $J = 8.24, 13.7$ Hz, 1H), 1.39 (s, 9H) ppm. TLC: R_f (hexane/AcOEt 7:3): 0.30. M.p. = 120.3°C. ^1H NMR (300 MHz, CD_3CN): δ 8.90 (s, 1H), 7.48 – 7.12 (m, 5H), 6.67 (d, $J = 6.1$ Hz, 1H), 5.44 (br s, 1H), 4.90 (m, 1H), 2.99 (dd, $J = 4.9, 13.7$ Hz, 1H), 2.81 (dd, $J = 9.3, 13.7$ Hz, 1H), 1.39 (s, 9H) ppm.

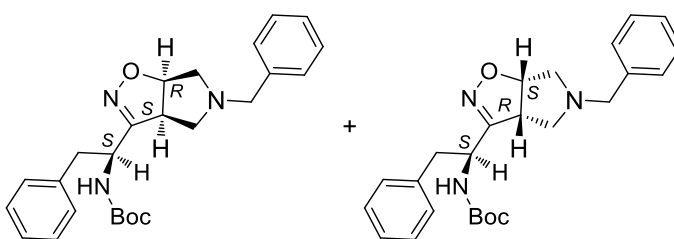
Synthesis of ‘tert-butyl (1-chloro-1-(hydroxyimino)-3-phenylpropan-2-yl)carbamate’ (7)



In a bottom flask, equipped with magnetic stirrer and thermometer, corresponding oxime **6** (550 mg, 2.08 mmol) was suspended in CCl_4 (20 mL) and *N*-chlorosuccinimide (277.74 mg, 2.08 mmol) was added portionwise over a period of 60 min at 0°C. Afterward, the reaction mixture was refluxed overnight. The solution was cooled to 0°C and filtered in order to remove the *N*-succinimide formed. The solvent was removed under reduced pressure, affording product **7** (601,2 mg, 2.01

mmol, 97 %) as yellow oil. TLC: Rf (hexane/AcOEt 7:3): 0.45. MS (ESI): m/z calcd for $[C_{14}H_{19}ClN_2O_3]$: 298.11; found: m/z 299.5 $[M+Na]^+$. 1H NMR (300 MHz, CD_3CN): δ 9.34 (s, 1H), 7.38 – 7.23 (m, 5H), 5.75 (br s, 1H), 4.63 (dd, $J = 15.1, 7.7$ Hz, 1H), 3.07 (dd, $J = 13.8, 7.7$ Hz, 1H), 2.94 (dd, $J = 13.7, 8.5$ Hz, 1H), 1.39 (s, 9H) ppm. For further characterization see reference¹⁵².

CYCLOADDITION - *Synthesis of Δ^2 -isoxazoline-fused pyrroline nuclei (9a + 9b)*



1,3- Dipolar Cycloaddition in $CHCl_3$, in presence of TEA

Chloro-oxime **7** (113 mg, 0.38 mmol) was dissolved in $CHCl_3$ (5 mL). N-benzyl-3-pyrroline (60.51 mg, 73 μ L, 0.38 mmol) was added in one portion and then triethylamine (64 μ L, 0.46 mmol) was dropped over 60 min at r.t. The reaction mixture was stirred under reflux for 18 h and H_2O (3 mL) was afterwards added. The organic layer was extracted and washed with 10% citric acid (2.5 mL), 5% $NaHCO_3$ (2.5 mL) and brine (2x2.5 mL). The organic layer was dried over Na_2SO_4 and the solvent was removed under reduced pressure. Purification of the crude product by flash chromatography (hexane/AcOEt 8:2) afforded the diastereoisomeric mixture **9a/9b** (9.6 mg, 0.023 mmol, 6 %) as a white solid.

1,3- Dipolar Cycloaddition in $CHCl_3$, in presence of DABCO

Chloro-oxime **7** (55 mg, 0.19 mmol) was dissolved in $CHCl_3$ (2.5 mL). N-benzyl-3-pyrroline (30.25 mg, 25 μ L, 0.19 mmol) was added in one portion at $0^\circ C$ and then DABCO (20.9 μ L, 0.19 mmol) was dropped over 60 min at $0^\circ C$. The reaction

mixture was stirred for 23 hours at r.t. and sonicated for other 24 hours. TLC showed just traces of diastereoisomeric mixture **9a/9b**.

1,3-Dipolar Cycloaddition in CHCl₃, in presence of NaHCO₃

Chloro-oxime **7** (55 mg, 0.19 mmol) was dissolved in CHCl₃ (2.5 mL). N-benzyl-3-pyrroline (30.25 mg, 25 μL, 0.19 mmol) was added in one portion at 0°C, followed by the addition of NaHCO₃ (15.9 mg, 0.19 mmol). The reaction mixture was stirred for 23 hours at r.t. and sonicated for other 24 hours. TLC showed just traces of diastereoisomeric mixture **9a/9b**.

1,3- Dipolar Cycloaddition in AcOEt, in presence of NaHCO₃

Chloro-oxime **7** (179 mg, 0.6 mmol) was dissolved in AcOEt (3 mL). Distilled N-benzyl-3-pyrroline (79.62 mg, 95 μL, 0.5 mmol) was added in one portion at r.t, followed by the addition of NaHCO₃ (100 mg 1.2 mmol). The reaction mixture was stirred for 2 hours and chloro-oxime **7** (149 mg, 0.5 mmol) and NaHCO₃ (63 mg, 0.75 mmol) were subsequently added portionwise. The reaction mixture was stirred for additional 14 h and then H₂O (8 mL) was poured into. The organic layer was extracted and washed with 5% KHSO₄ (6 mL), s.s. NaHCO₃ (6 mL) and brine (2x7mL). The organic layer was, then, dried over Na₂SO₄ and the solvent was removed under reduced pressure. Purification of the crude product by flash chromatography (hexane/AcOEt 9:1) afforded the diastereoisomeric mixture **9a/9b** (2:1, 67.40 mg, 0.16 mmol, 32 %) as a white solid.

1,3 Dipolar-Cycloaddition in CH₃CN, in presence of TEA

Chloro-oxime **7** (179 mg, 0.6 mmol) was dissolved in CH₃CN (3 mL). Distilled N-benzyl-3-pyrroline (79.62 mg, 95 μL, 0.5 mmol) was added in one portion at r.t, followed by triethylamine (83.6 μL, 0.6 mmol). The reaction mixture was stirred for 2 hours and chloro-oxime **7** (149 mg, 0.5 mmol) and triethylamine (70 μL, 0.5 mmol) were afterwards added portionwise. The reaction mixture was stirred for additional 14 h. The solvent was removed under reduced pressure and the residue was re-dissolved in CH₂Cl₂. The organic layer was extracted and washed with 5% KHSO₄ (6 mL), s.s. NaHCO₃ (6 mL) and brine (2x7mL). The organic layer was, then, dried

over Na₂SO₄, filtered and the solvent was removed under reduced pressure. Purification of the crude product by flash chromatography (hexane/AcOEt 9:1) afforded the diastereoisomeric mixture **9a/9b** (3:1, 80.04 mg, 0.19 mmol, 38 %) as a white solid.

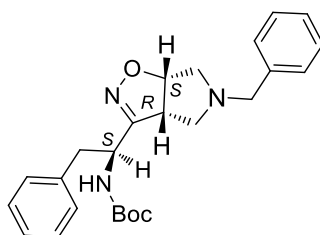
1,3 Dipolar-Cycloaddition in CH₃CN, in presence of NaHCO₃

Chloro-oxime **7** (100 mg, 0.33 mmol) was dissolved in CH₃CN (3 mL). Distilled N-benzyl-3-pyrroline (66.88 mg, 79.9 μL, 0.42 mmol) was added in one portion at r.t, followed by the addition of NaHCO₃ (26.9 mg, 0.32 mmol). The reaction mixture was stirred for 1 hours and chloro-oxime **7** (150 mg, 0.51 mmol) and NaHCO₃ (42.85 mg, 0.51 mmol) were subsequently added portionwise over 60 min. The reaction mixture was stirred for additional 4 h at r.t. The solvent was removed under reduced pressure. Purification of the crude product by flash chromatography (hexane/AcOEt 9:1) afforded the diastereoisomeric mixture **9a/9b** (2:1, 90 mg, 0.21 mmol, 51%) as a white solid.

1,3 Dipolar-Cycloaddition in CH₃CN, in presence of NaHCO₃

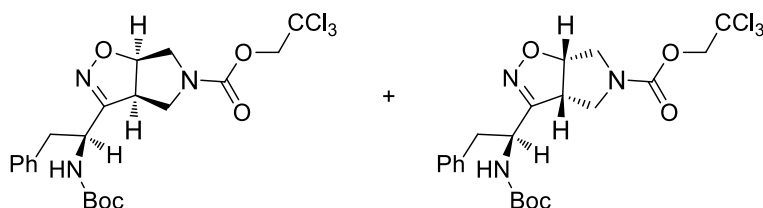
Chloro-oxime **7** (322 mg, 1.07 mmol) was dissolved in CH₃CN (6 mL). Distilled N-benzyl-3-pyrroline (172 mg, 1.07 mmol) was added in one portion at r.t, followed by the addition of Li₂CO₃ (40 mg, 0.53 mmol). The reaction mixture was stirred for 1 hours and chloro-oxime **7** (322 mg, 1.07 mmol) and Li₂CO₃ (40 mg, 0.53 mmol) were subsequently added portionwise over 60 min. The reaction mixture was stirred for additional 3 h at r.t. The solvent was removed under reduced pressure. Purification of the crude product by flash chromatography (hexane/AcOEt 9:1) afforded the diastereoisomeric mixture **9a/9b** (1:1, 216 mg, 0.51 mmol, 48%) as a white solid.

Characterization of tert-butyl (1-(5-benzyl-3a,5,6,6a-tetrahydro-4H-pyrrolo[3,4-d]isoxazol-3-yl)-2-phenylethyl)carbamate (9b)



R_f (hexane/AcOEt 1:1): 0.57. M.p.: 99.3°C. MS (ESI): m/z calcd for $[C_{25}H_{31}N_3O_3]$: 421.24; found: m/z 422.24 $[M+H]^+$; 444.26 $[M+Na]^+$. 1H NMR (300 MHz, CD_3CN): δ 7.42 – 7.13 (m, 10H), 5.53 (d, $J = 8.8$ Hz, 1H), 5.01 (dd, $J = 9.4, 4.6$ Hz, 1H), 4.53 (dd, $J = 14.1, 9.9$ Hz, 1H), 3.83 – 3.69 (m, 1H), 3.55 (dd, $J = 22.4, 13.3$ Hz, 2H); 3.25 (dd, $J = 14.2, 5.2$ Hz, 1H), 3.06 (d, $J = 9.6$ Hz, 2H), 2.94 (dd, $J = 13.9, 9.7$ Hz, 1H), 2.36 (dd, $J = 11.0, 4.8$ Hz, 1H), 2.27 (dd, $J = 10.0, 7.1$ Hz, 1H), 1.40 (s, 9H) ppm. ^{13}C NMR (75 MHz, CD_3CN): δ 159.41, 138.92, 132.42, 129.30, 128.47, 128.39, 128.28, 128.20, 126.99, 126.63, 126.32, 83.94, 61.86, 58.38, 55.95, 53.06, 48.78, 37.72 ppm.

Synthesis of '(3aR,6aS)-2,2,2-trichloroethyl 3-((S)-1-((tert-butoxycarbonyl)amino)-2-phenylethyl)-6,6a-dihydro-3aH-pyrrolo[3,4-d]isoxazole-5(4H)-carboxylate' (10a+10b)

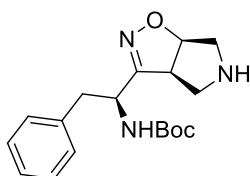


In a round-bottom flask, equipped with magnetic stirrer, diastereoisomeric mixture of **9a/9b** (50 mg, 0.12 mmol) was dissolved in CH_3CN (2 mL). 2,2,2-Trichloroethylchloroformate (16.5 μ L, 0.12 mmol) was added dropwise to the solution. The reaction mixture was stirred for 2 hours; the solvent was then removed

under reduced pressure. Purification of the crude product by flash chromatography (hexane/AcOEt 3:1) afforded the products **10a** (23.8 mg, 0.05 mmol) and **10b** (35.7 mg, 0.07 mmol) as white solids with 98% yield. **10a** TLC: R_f (hexane/AcOEt 7:3): 0.23. M.p. $[\alpha]_D^{20} = -68.5$ (c 1, MeOH) 125.5 °C. IR (NaCl) ν_{\max} : 3355.6, 3060.9, 2948.6, 1717.2, 1690.3 cm^{-1} . MS (ESI): m/z calcd for $[\text{C}_{21}\text{H}_{26}\text{Cl}_3\text{N}_3\text{O}_5]$: 505.9; found: m/z 528.62 $[\text{M}+\text{Na}]^+$. ^1H NMR (300 MHz, CDCl_3): δ 7.36 – 7.23 (m, 5H), 5.13 (brs, 2H), 4.76-4.66 (m, 3H), 3.98 (brs, 1H), 3.85 (brs, 1H), 3.64 (brs, 1H), 3.47-3.42 (m, 2H), 3.22 – 3.05 (m, 2H), 1.43 (s, 9H) ppm. ^{13}C NMR (75 MHz, CDCl_3): 159.7, 155.0, 152.5, 136.4, 129.2, 128.7, 127.1, 110.0, 85.0, 80.2, 75.0, 53.4, 52.9, 49.8, 49.2, 48.4, 40.1 ppm.

10b TLC: (hexane/AcOEt : 7/3): 0.19. M.p. 104.1. $[\alpha]_D^{20} = +31$ (c 1, MeOH). IR (NaCl) ν_{\max} : 3376.1, 3064.7, 2957.4, 1723.8, 1683.6 cm^{-1} . MS (ESI): m/z calcd for $[\text{C}_{21}\text{H}_{26}\text{Cl}_3\text{N}_3\text{O}_5]$: 505.9; found: m/z 528.48 $[\text{M}+\text{Na}]^+$. ^1H NMR (300 MHz, CDCl_3): δ 7.34 – 7.23 (m, 5H), 5.22 – 5.17 (m, 1H), 4.76 - 4.66 (m, 4H), 3.96 – 3.77 (m, 3 H), 3.67 – 3.54 (m, 2H), 3.44 – 3.32 (m, 1H), 3.04 – 3.11 (m, 1H), 1.38 (s, 1H) ppm. ^{13}C NMR (75 MHz, CDCl_3): 159.5, 155.2, 152.4, 136.8, 129.4, 128.6, 126.9, 95.4, 84.4, 80.3, 75.0, 53.7, 52.5, 48.6, 48.3, 38.5, 28.2 ppm.

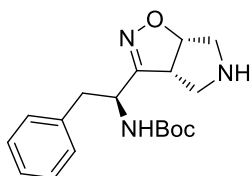
Synthesis of 'tert-butyl ((S)-2-phenyl-1-((3aS,6aR)-4,5,6,6a-tetrahydro-3aH-pyrrolo[3,4-d]isoxazol-3-yl)ethyl)carbamate' (11a)



In a round-bottom flask, equipped with magnetic stirrer, compound **10a** (40 mg, 0.08 mmol) was dissolved in a solution of AcOH 90% in water (0.4 mL). Then Zn (40 mg) was added and the reaction was left stirred for 2h.

After that, the zinc was filtered and the reaction was concentrated in vacuo to eliminate the acetic acid. The crude was re-dissolved in AcOEt (4 mL) and the byproduct (white solid) was filtered away. The crude was extracted with NaHCO₃ (2 x 4 mL) and purified by flash chromatography (DCM/MeOH 40:1) affording pure compound **11a** as white solid (63 mg, 80% yield). TLC: R_f (DCM/MeOH : 40/1): 0.12. [α]_D²⁰ = -4 (c 1, MeOH) MS (ESI): *m/z* calcd for [C₁₈H₂₅Cl₃N₃O₃]: 331.19; found: *m/z* 332.2 [M+H]⁺. ¹H NMR (300 MHz, CDCl₃): δ 7.35 – 7.22 (m, 5H), 5.27 – 5.24 (m, 1H), 5.11 – 5.09 (m, 1H), 4.70 – 4.63 (m, 1H), 3.43 – 3.30 (m, 3H), 3.31 – 3.09 (m, 3H), 3.07 – 2.82 (m, 2H), 1.42 (s, 9H) ppm. ¹³C NMR (75 MHz, CDCl₃): 159.4, 155.2, 136.4, 129.3, 128.7, 127.0, 86.7, 80.1, 56.2, 55.9, 51.3, 49.7, 40.2, 28.3 ppm.

Synthesis of 'tert-butyl ((S)-2-phenyl-1-((3aR,6aS)-4,5,6,6a-tetrahydro-3aH-pyrrolo[3,4-d]isoxazol-3-yl)ethyl)carbamate' (11b)

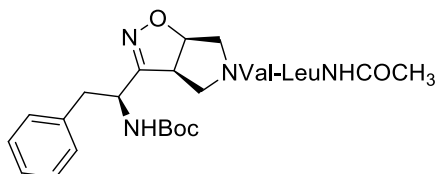


In a round-bottom flask, equipped with magnetic stirrer, compound **10b** (40 mg, 79 μmol) was dissolved in a solution of AcOH 90% in water (0.4 mL). Then Zn (40 mg) was added and the reaction was left stirred for 2h.

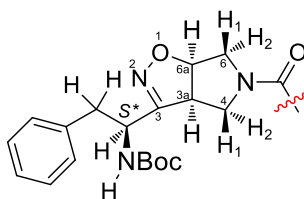
After that, the zinc was filtered and the reaction was concentrated in vacuo to eliminate the acetic acid. The crude was re-dissolved in AcOEt (4 mL) and the byproduct (white solid) was filtered away. The crude was extracted with NaHCO₃ (2 x 4 mL) and purified by flash chromatography (DCM/MeOH 40 : 1) affording pure compound **11b** as white solid (63 mg, 0.19 mmol, 80% yield). TLC: R_f (DCM/MeOH : 40/1): 0.12. [α]_D²⁰ = +12 (c 1, MeOH). MS (ESI): *m/z* calcd for [C₁₈H₂₅Cl₃N₃O₃]: 331.19; found: *m/z* 332.18 [M+Na]⁺. ¹H NMR (300 MHz, CDCl₃): δ

7.20 – 7.40 (m, 5H), 5.10 - 5.20 (m, 1H), 4.87 – 4.45 (m, 2H), 3.63 (m, 3H), 3.4 – 3.21 (m, 2H), 3.0 – 3.15 (m, 1H), 2.6 – 2.8 (m, 2H), 2.0 – 1.8 (m, 2H), 1.2 (s, 9H) ppm. ^{13}C NMR (75 MHz, CDCl_3): 158.9, 155.2, 137.1, 129.3, 127.0, 126.6, 87.1, 80.3, 56.7, 55.9, 51.5, 49.1, 39.3, 28.2 ppm.

Synthesis of 'tert-butyl ((S)-1-((3aS,6aR)-5-((S)-2-((S)-2-acetamido-4-methylpentanamido)-3-methylbutanoyl)-4,5,6,6a-tetrahydro-3aH-pyrrolo[3,4-d]isoxazol-3-yl)-2-phenylethyl) carbamate' (12a)



In a round-bottom flask equipped with a magnetic stirrer and thermometer, dipeptide Ac-*N*-Leu-Val-OH (46 mg, 0.17 mmol) was dissolved in CH_2Cl_2 (3 mL) and the solution was cooled to 0 °C. HOBt (25 mg, 0.22 mmol) and EDC (36 mg, 0.19 mmol) were added. After 1 h, compound **11a** (55 mg, 0.17 mmol) in CH_2Cl_2 (1 mL) was dropped, followed by the addition of DIEA (29 μL , 0.17 mmol). The reaction mixture was stirred for 24 h and then it was washed with KHSO_4 (5%, 5 mL), s.s. NaHCO_3 (5 mL), brine (5 mL). After drying over Na_2SO_4 , the solvent was removed under reduced pressure. Purification of the crude product by flash chromatography (DCM/MeOH 40:1) afforded compound **12a** (66,3 mg, 0.11 mmol, 65%) as a white solid. TLC: R_f (DCM/MeOH : 40/1): 0.20. $[\alpha]_{\text{D}}^{20} = -90$ (c 0.3, MeOH). MS (ESI): m/z calcd for $[\text{C}_{31}\text{H}_{48}\text{N}_6\text{O}_6]$: 585.36; found: m/z 586.36 $[\text{M}+\text{H}]^+$.



AA	atom	$^1\text{H NMR } \delta$	Multiplicity J (Hz)	$^{13}\text{C NMR } \delta$	Noesy
C2-1	Ph	7.48-7.17	m	129.3 128.1 126.4 138.7(q)	$\text{CH}_2\text{-Ph}$ (m) CHBn (vw) Boc (m) Verifica dopo aleMev _{Val} (vw) ^a
	CH_2Ph	3.33 2.96	m m	36.8	Ph (m) CHBn (w) NH_{Boc} (vw)
	CHBn	4.87	m	48.7	CH_2Ph (3.33,w) H-4 _y (m) NH_{Boc} (w) Ph (vw)
	NH_{Boc}	5.56	d J 8.8		CHBn (vw) CH_2Ph (2.96,vw)
	$t\text{BuOCO}$	1.34	s	27.6, 79.0 155.6	Ph (m) CHCH_2Leu (m)
	CH_{3a}	3.98	Overl.	53.7	CH-4 _x (s) CH _{6a} (s)
	C_3			159.7	
	CH-4 _x	3.57	m	48.7	CH _{3a} (s) CH-4 _y (s)
	CH-4 _y	4.43	Overl.	48.7	CHBn (m) CH-4 _x (s)
	CH-6 _x	3.37	Overl.	52.5	CH _{6a} (s) CH-6 _y (vs)
	CH-6 _y	4.09	Overl.		CH _{Val} (w) CH-6 _x (vs) CH _{6a} (vw)
CH _{6a}	5.14	Overl.	82.7	CH-6 _x (s) CH-6 _y (vw) CH _{3a} (s)	
Val-2	CO		169.7		
	CH	4.45	Overl.	55.3	Me_2CH (s) CH-6 _y (w) NH_{Val} (m)
	Me_2CH	2.07-1.92	m	30.67	CH _{Val} (m) Ph(vvw) NH_{Val} (w) CHCH_2Leu (w)

	Me	0.87, 0.93	Overl.		Ph (w) ^a CH _{Val} (s) NH _{Val} (s)
	NH	6.95	d <i>J</i> 8.5		Me ₂ CH (s) CH/CH ₂ Leu (w) NH _{Leu} (w) CH _{Leu} (s) CH _{Val} (m)
Leu-3	CO			172.1	
	CH	4.34		^a	NH _{Val} (s) Me (s) CHCH ₂ (m) NH _{Leu} (w)
	CHCH ₂	1.70-144	m	40.6, 24.4	CH _{Leu} (s) NH _{Leu} (m)
	Me	0.87, 0.93	m		
	NH	6.71	d <i>J</i> 8.0		CHCH ₂ (m) MeCO (m) CH _{Leu} (w) NH _{Val} (w)
	CO			170.0	
	MeCO	1.91		22.0	NH _{Leu} (m)

Table 4: ¹H, ¹³C NMR (CD₃CN, 20 mM, 300 MHz) and NOE (300 ms) data for **12b**

^aTentatively assigned; ^b51.6 or 51.8

Minor isomer

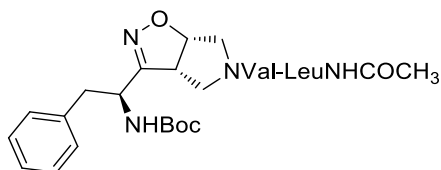
AA	atom	¹ H NMR δ	Multiplicity <i>J</i> (Hz)	¹³ C NMR δ	Noesy
C2-1	Ph	7.16-7.48	m	129.5, 128.1, 126.3, 138.0(q)	CH ₂ -Ph (m) CHBn(w) Boc (m) okMe _{Val} (vw) ^a
	CH ₂ Ph	3.20 2.94	dt <i>J</i> 12.8, 4.5 m	37.5	Ph (m) CHBn (w) NH _{Boc} (vw)
	CHBn	4.62	m	48.9	CH ₂ Ph (3.20,w) H-4 _y (m) NH _{Boc} (w) Ph (w)
	NH _{Boc}	5.65	d <i>J</i> 8.5		CHBn (vw) CH ₂ Ph (2.96,w)
	<i>t</i> Bu	1.34	s	27.56	Ph (m)
	CH _{3a}	3.89	Overl.	51.2	CH _{6a} (s)
	C ₃			160.3	
	CH-4 _x	3.40	m	48.1	CH-4 _y (vs)
	CH-4 _y	3.93	Overl.	48.7	CHBn (m)

					CH-4 _x (vs)
	CH-6 _x	3.77	dd <i>J</i> 11.8, 5.5	53.6 53.6	CH _{6a} (s) CH-6 _y (s)
	CH-6 _y	3.92	Overl.		CH-6 _x (s) CH _{6a} (s)
	CH _{6a}	5.20		84.8	CH-6 _x (s) CH-6 _y (s) CH _{3a} (s)
Val-2	CO			169.9	
	CH	4.40		55.9	Me(s) CH _{isopr} (m) NH _{Val} (s)
	Me ₂ CH	2.07-1.92		30.34	CH _{Val} (m) NH _{Val} (vw)
	Me	0.87, 0.93			CH _{Val} (s) NH _{Val} (s)
	NH	7.02	d <i>J</i> 8.5		Me(s) Me ₂ CH (s) CH _{Leu} (s)
Leu-3	CO			172.3	
	CH	4.35		^a	CHCH ₂ (s) MeCO(m) NH _{Leu} (w) NH _{Val} (s)
	CHCH ₂	1.71-1.46		26.69, 40.63	CH _{Leu} (s) NH _{Leu} (w)
	Me	0.87, 0.93			
	NH	6.63	d <i>J</i> 7.4		CH/CH ₂ (w) MeCO(m) CH _{Leu} (w)
	CO			170.0	
	Me	1.91		21.9	NH _{Leu} (m)

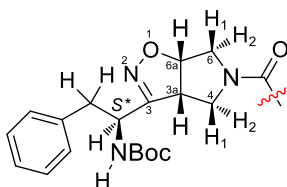
Table 5: ¹H, ¹³C NMR (CD₃CN, 20 mM, 300 MHz) and NOE (300 ms) data for **12b**^a

^a51.6 or 51.8

Synthesis of ‘tert-butyl ((S)-1-((3aR,6aS)-5-((S)-2-((S)-2-acetamido-4-methylpentanamido)-3-methylbutanoyl)-4,5,6,6a-tetrahydro-3aH-pyrrolo[3,4-d]isoxazol-3-yl)-2-phenylethyl) carbamate’ (12a)



In a round-bottom flask equipped with a magnetic stirrer and thermometer, dipeptide Ac-*N*-Leu-Val-OH (46 mg, 0.17 mmol) was dissolved in CH₂Cl₂ (3 mL) and the solution was cooled to 0 °C. HOBt (25 mg, 0.22 mmol) and EDC (36 mg, 0.19 mmol) were added. After 1 h, compound **11b** (55 mg, 0.19 mmol) in CH₂Cl₂ (1 mL) was dropped, followed by the addition of DIEA (29 μL, 0.17 mmol). The reaction mixture was stirred for 24 h and then it was washed with KHSO₄ (5%, 5 mL), s.s. NaHCO₃ (5 mL), brine (5 mL). After drying over Na₂SO₄, the solvent was removed under reduced pressure. Purification of the crude product by flash chromatography (DCM/MeOH 40:1) afforded compound **12b** (66,3 mg, 0.11 mmol, 65%) as a white solid. TLC: R_f (DCM/MeOH 40:1): 0.20. MS (ESI): *m/z* calcd for [C₃₁H₄₈N₆O₆]: 585.36; found: *m/z* 586.58 [M+H]⁺.



AA	atom	¹ H NMR δ	Multiplicity <i>J</i> (Hz)	¹³ C NMR δ	Noesy (700 ms)
C1-1	Ph	7.36-7.20	m	129.4, 128.3, 126.6, 137.8(<i>q</i>)	CH ₂ -Ph (m) CHBn(m) Boc (w)
	CH ₂ Ph	3.17 2.94	m	38.2	Ph (s) CHBn (m) NH _{Boc} (w)
	CHBn	4.68	m	49.7 ^a	CH ₂ Ph (m) NH _{Boc} (w) Ph (m) H _{3a} (w) H _{4y} (w) NHBoc(w)
	NH _{Boc}	5.75	d <i>J</i> 8.5		CHBn (w) CH ₂ Ph (2.92,w)
	<i>t</i> BuOCO	1.35	s	27.4, 79.1 155.2	Ph (w)
	CH _{3a}	3.77		51.4	CH _{6a} (s) CHBn(w)
	C ₃			160.8	

	CH-4 _x	3.42		48.4	CH-4 _y (m)
	CH-4 _y	4.05			CH-4 _y (m) CH-6 _y (s) CHBn(w) CH _{Val} (m)
	CH-6 _x	3.90	Overl.	52.2	
	CH-6 _y	3.50			CH _{6a} (vw) CH-4 _y (s) CH-6 _x (s)
	CH _{6a}	5.12	m	83.7	CH-6 _y (vw) CH-6 _x (m) CH _{3a} (s)
Val-2	CO			169.7	
	CH	4.47	Overl.	55.42 ^a	Me(s) CH(m) ^b
	Me ₂ CH	2.07-1.94		30.6	CH _{Val} (m)
	Me	0.93-0.83		^c	CH _{Val} (s) NH _{Val} (w)
	NH	7.01	d J 8.7		Me (s) Me ₂ CH (w) CH _{Val} (m) CH _{Leu} (s) NH _{Leu} (w)
Leu-3	CO			^d	
	CH	4.36	Overl.	51.8 ^a	NH _{Leu} (m) NH _{Val} (s) CHCH ₂ (m) Me(s)
	CHCH ₂	1.74-1.46		40.5, 24.5	Me(s) CH _{Leu} (m) NH _{Leu} (w)
	Me	0.96-0.85	Overl.	^c	
	NH	6.67	d J 7.7		CH/CH ₂ (m) MeCO(m) NH _{Val} (w)
	CO			169.9	
	Me	1.92	Overl.	21.9	NH _{Leu} (m) CH ₂ CH _{Leu} (m)

Table 6: ¹H, ¹³C NMR (CD₃CN, 20 mM, 300 MHz) and NOE (300 ms) data for **12a**

^aTentatively assigned; ^b several NOEs are present with H3 and H-6 but due to the overlapping of the CH_{Val} it is impossible to assign the corresponding spatial proximities; ^c30.5-16.9; ^d172.0 or 172.2

Minor isomer

AA	atom	¹ H NMR δ	Multiplicity J (Hz)	¹³ C NMR δ	Noesy
C1-1	Ph	7.36-7.20	m	129.4, 128.3, 126.5, 137.5(q) ^a	CH ₂ -Ph (m) CHBn(m) Boc (w)
	CH ₂ Ph	3.17 2.94	m	32.2	Ph (s) CHBn (m) NH _{Boc} (w)
	CHBn	4.71	m	48.8 ^a	CH ₂ Ph (m) Ph (m)
	NH _{Boc}	5.68	d J 8.4		CHBn (w) CH ₂ Ph (2.92,w)
	<i>t</i> BuOCO	1.35	s	27.4, 79.1 155.2	Ph (w)
	CH _{3a}	3.86		53.1	CH _{6a} (m) CH _{Val} (s)
	C ₃			160.5	
	CH-4 _x	3.74		49.2	CH-4 _y (s) CH _{3a} (m) CH _{Leu} (w)
	CH-4 _y	3.91			CH-4 _x (s)
	CH-6 _x	3.75		53.0	CH _{6a} (s)
	CH-6 _y	4.07			CH-6 _x (s) CH _{Val} (s) CH _{Leu} (w)
CH _{6a}	5.20		85.6	CH-6 _x (s) CH _{3a} (m)	
Val-2	CO			169.7 ^{app}	
	CH	4.46	Overl.	55.37 ^a	Me(s) CH(m) ^b
	Me ₂ CH	1.74-1.46	m	30.6	CH _{Val} (m)
	Me	0.96-0.85	Overl.	^c	CH _{Val} (s) NH _{Val} (w)
	NH	6.94	J 8.3		Me (s) Me ₂ CH (w) CHCH ₂ Leu(vw) CH _{Val} (m) CH _{Leu} (s) NH _{Leu} (w)
Leu-3	CO			^d	
	CH	4.34	Overl.	51.7 ^a	NH _{Leu} (m) NH _{Val} (s) CHCH ₂ (m) Me(s)

					CH-4 _x (w) CH-6 _y (w)
	CH/CH ₂	1.74-1.46	m	40.5, 24.5	Me(s) CH _{Leu} (m) NH _{Leu} (w)
	Me	0.96-0.85	Overl.	^c	
	NH	6.71	<i>J</i> 7.7		CH/CH ₂ (m) MeCO(m) NH _{Val} (w)
	CO			169.9	
	MeCO	1.92	Overl.	21.9	NH _{Leu} (m) CH ₂ CH _{Leu} (m)

Table 7: ¹H, ¹³C NMR (CD₃CN, 20 mM, 300 MHz) and NOE (300 ms) data for **12a**^a

^aTentatively assigned; ^bSeveral NOEs are present with H3 and H-6 but due to the overlapping of the CH_{Val} it is impossible to assign the corresponding spatial proximities; ^c30.5-16.9; ^d172.0 or 172.2

Effects of neighboring functionalized prolines on the stability of collagen triple helices

Introduction

Collagen is an abundant structural protein in mammals. In humans, it constitutes the one third of the whole protein domain and the 75% of the weight of the dry skin. It is also the most prevalent component of the extracellular matrix^{153–155} where it exists as a network of fibers and it is necessary for the structural integrity and malleability to accommodate both cellular growth and tissue development¹⁵⁶.

Collagen has different physical properties and biocompatibility, observed among the extracellular matrix, cartilage and bones. For this reason, synthetic collagen-based materials are attractive for biomedical applications, such as wound healing or tissue engineering^{157,158}. Moreover, stimuli-responsive collagen is also getting attention in drug discovery field for the controlled release of drugs in cancer therapy¹⁵⁹.

Collagen consists in three individual peptide strands that coil into each other, forming a right-handed triple helix^{153–155}. These triple helices can assembly into macroscopic fibrils and fibers. The single strands comprise about 300 tripeptides with Xaa-Yaa-Gly sequence and adopt polyproline II-like helix.

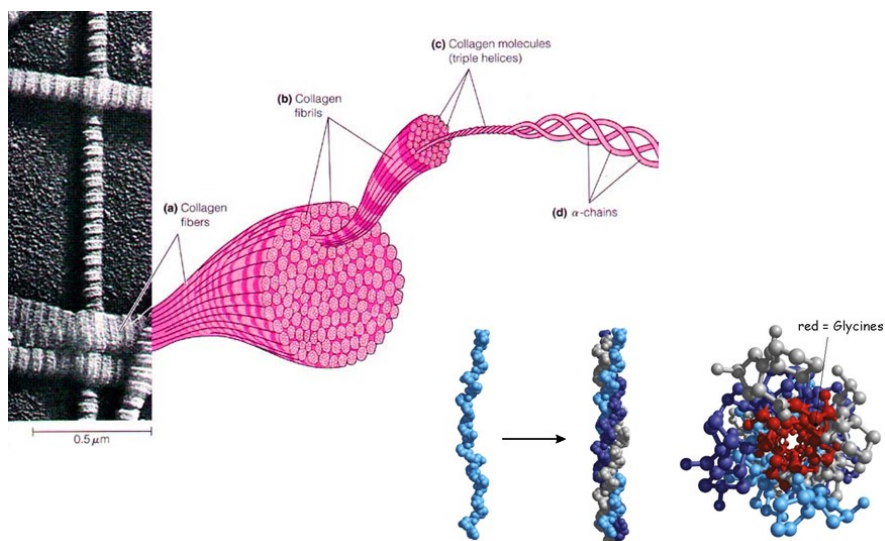


Figure 1: Collagen: from fibers to PPII helices

In nature almost all of the 20 proteinogenic amino-acids are in the Xaa and Yaa positions. It was found that (2*S*)-Proline (Pro) is most abundant in the Xaa position and (2*S*,4*R*)-hydroxyproline (Hyp) in the Yaa position, respectively^{153–158,160} and that all amide bonds are in *trans* conformation.

Crystal structure of short collagen model peptides (CMPs) revealed that Pro residues adopt mainly (C4)-*endo* ring pucker. Instead Hyp residues in Yaa position, possess a (C4)-*exo* ring pucker (Figure 2). On the other hand, Gly is crucial in every third position since it ensure a tight packing of the triple helix center¹⁶⁰. The triple helix is stabilized by interstrand hydrogen bonds (H-bonds) between the neighboring N-H of Gly and the C=O of Pro.

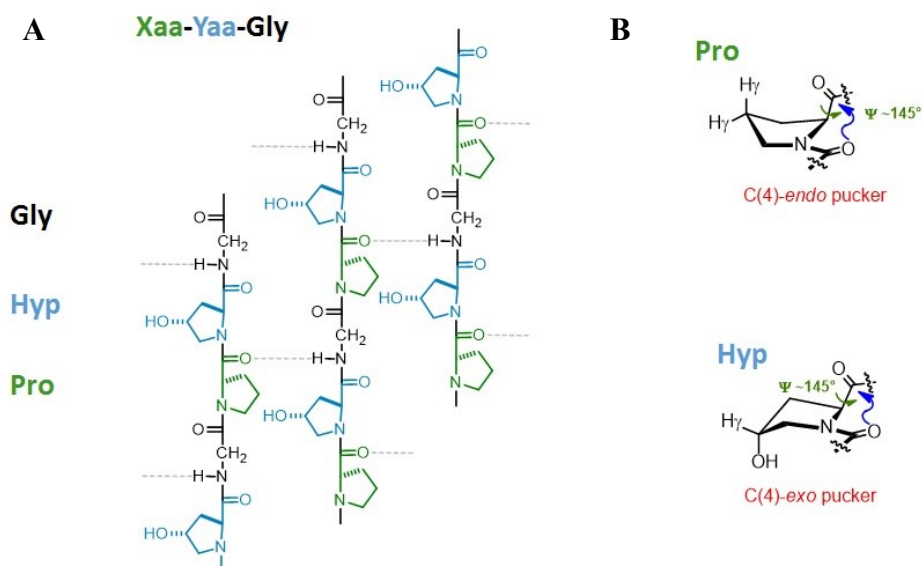


Figure 2¹⁶¹: A: General structure of Collagen. B: Right pucker of Pro and Hyp.

In the past decades, many studies have been done on synthetic short-chain collagen model peptides (CMPs), where Pro or Hyp residues are replaced by different substituted Pro. It has been demonstrated that interstrand H-bonds, the ring puckering and the avoidance of steric repulsions between strands are important features for the stability of the collagen triple helix^{162–164}.

In particular, short-chain CMPs have been studied in order to understand how the substituents at the C(4)-position of different proline derivatives affect the collagen triple helix stability and structure.

Studies on substituted *N*-acetylproline derivatives showed that electron-withdrawing groups (EWGs), such as F, N₃, NH₃⁺ or MeCONH, prefer conformation dictated by a gauche effect^{165–167}.

In fact, the EWG is in a pseudo-axial position and gauche to the *N*-acetyl group (Figure 3). By this way, the $\sigma^*_{\text{C-EWG}}$ and $\sigma^*_{\text{C-NAc}}$ orbitals are aligned in a near 180° angle with respect to the adjacent vicinal $\sigma_{\text{C-H}}$ orbital, promoting their interaction. This effect leads to a C(4)-*exo*-pucker for (*4R*)-configured proline. On the other hand, in the case of (*4S*)-configured proline derivatives, this stereoelectronic effect leads to a C(4)-*endo* pucker of the pyrrolidine ring.

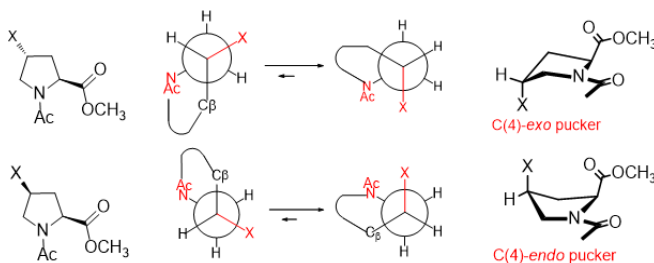


Figure 3: Preferred pyrrolidine pucker ring given by the type of C(4)-substituent

An additional feature to consider is the ‘preference for a *trans* amide bond’, measured by the *trans*:*cis* ratio of the substituted proline (Table 1).

Studying the crystal structure of C(4)-substituted proline, it was found that usually the *trans*:*cis* ratio is higher in the case of the (*4R*)-EWG-diastereoisomer than the (*4S*)-EWG-diastereoisomer.

On the other hand, in the case of 4-Methylprolines (Mep), the Ac-(*4S*)-Mep-OMe has higher *trans*:*cis* ratio than the Ac-(*4R*)-Mep-OMe (Table 1).

	X	(4 <i>R</i>)	(4 <i>S</i>)
Ac-Hyp-OMe	-OH	6.1	2.4
Ac-Azp-OMe	-N ₃	6.1	2.6
Ac-Flp-OMe	-F	6.7	2.6
Ac-Mep-OMe	-CH ₃	3.7	7.4

Table 1: $K_{trans:cis}$ measured by 1H -NMR

The higher *trans* fraction of the (4*R*)-substituted proline with an EWG is explained with an $n-\pi^*$ interaction between a lone pair of the acetyl oxygen and the π^* orbital of the methyl ester^{166,168} (as it is shown in Figure 4).

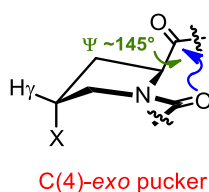


Figure 4: Exo pucker of (4*R*)-EWGPro

Raines group explained the importance of the *trans:cis* ratio in the stability of collagen triple helix. They synthesized CMP (ProYaaGly)₇, replacing the Hyp with different substituted prolines. They found that C γ substituent can enhance the conformational stability by favoring the *trans* isomer, thereby preorganizing the individual strands to resemble more closely the strands in a triple helix (Figure 5). The reason is that $K_{trans/cis}$ appears to be related to the main-chain dihedral angle, ψ . Thus, they proposed that a favorable $n-\pi^*$ interaction stabilizes both the *trans* prolyl peptide bond isomer and a ψ that is appropriate for triple helix formation¹⁶⁴.

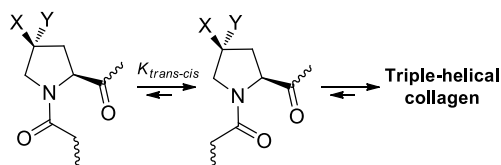


Figure 5: Relationship between cis-trans prolyl peptide bond isomerization and the formation of a collagen triple helix, which contains only trans peptide bonds. Pro: $X = H, Y = H$. Hyp: $X = H, Y = OH$. Flp: $X = H, Y = F$.

Wennemers group investigated the possibility to functionalize CMP triple helix replacing the Hyp in Yaa position with an azido-proline (Azp). They obtained a very stable CMP triple helix, having the Azp the same $K_{trans:cis}$ of the Hyp. Furthermore, starting from azido-CMP and different alkynes and using the click chemistry, they obtained new triazolyl-proline containing CMPs. With this work it was demonstrated that not only the ring pucker and the preference for a *trans* amide bond are responsible for the conformational stability of the collagen triple helix but also steric constraints play an important role^{169,170}.

More recently the same group designed a pH-responsive collagen triple helices that contain (C4)-aminoproline (Amp) residues¹⁷¹. They showed that the pH change affects not only the protonation state of the amino group but also trigger a flip of the ring pucker, inducing the formation or release of a transannular H-bond. As summarized in Figure 6, for (4*S*)-Amp containing CMP, pH could be the trigger for the stabilization/destabilization of CMP triple helix.

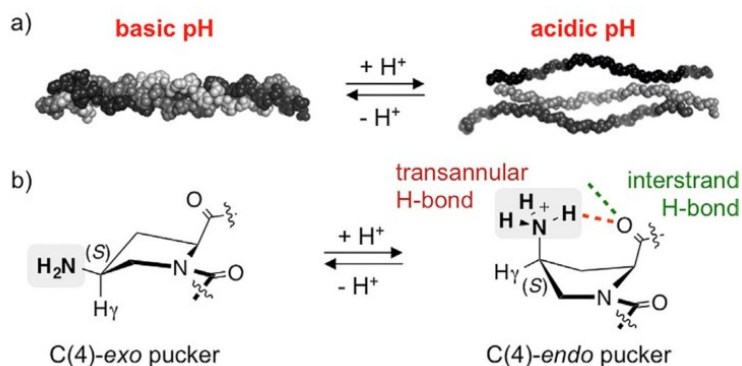


Figure 6¹⁷¹: Stability of Amp-containing CMP triggered by pH

These findings open possibilities for the development of pH-responsive collagen-based materials that are promising, for example, for the controlled release of drugs in an acidic environment¹⁵⁹.

Aim of the project

In the second semester of my second year of PhD I worked in the laboratories of Prof. Wennemers in ETH (Zurich, Switzerland) and I was involved in the synthesis of double functionalized CMP.

Taking in consideration the recent literature, we observed that most of the reported work was focused on triplet Xaa-Yaa-Gly CMPs, containing only one functionalized Pro. By the way, Raines group tested CMPs containing two neighbouring Flp. Firstly, they showed that CMPs Ac-((4*S*)-Flp-Pro-Gly)₇-NH₂ and Ac-(Pro-(4*R*)-Flp-Gly)₇-NH₂ form triple helices (Figure 7).

For this reason, they expected that a peptide containing both (4*S*)-Flp in Xaa position and (4*R*)-Flp in Yaa position could form a triple helix of unprecedented stability¹⁷². However, this peptide does not even fold into a triple helix. They reasoned that interstrand fluoro-fluoro interactions are adverse to triple helix stability.

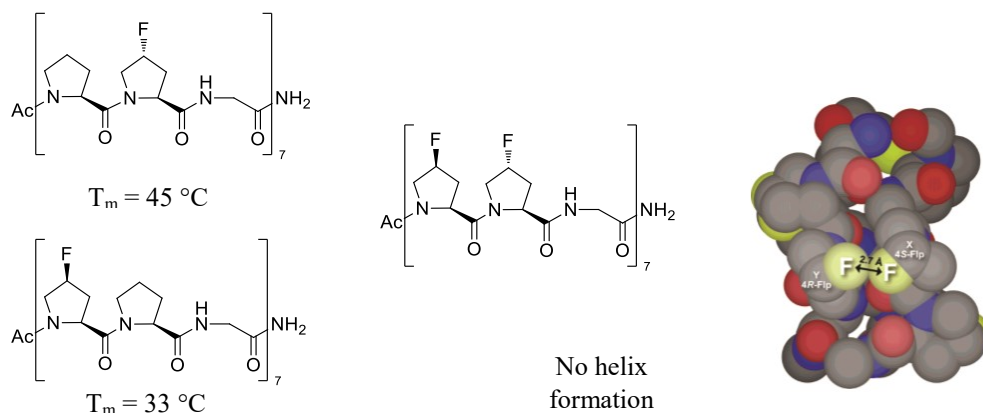


Figure 7: Flp-containing CMP studied by Raines group

An earlier experiment by Moroder, using a similar strategy, failed to produce a stable triple helix. They observed that the replacement of Pro in the Xaa position with (4*S*)-Flp prevented triple helix formation if (4*R*)-Hyp was in the Yaa position¹⁷³. They explained this result with a possible interstrand steric repulsion between the hydroxyl and fluoro groups.

These studies of Raines and Moroder groups are the only ones reported in the literature concerning CMPs containing two neighboring EWG substituted prolines. A systematic investigation of potential effects on triple helix stability due to neighboring substituted prolines on CMP is thus lacking.

In this work, we designed and synthesized the collagen triple helix of the type Ac-(Pro-Hyp-Gly)₃-XaaYaa-Gly-(Pro-Hyp-Gly)₃-NH₂.

In the Xaa position, azidoproline (Azp), aminoproline (Amp), or acetamidoproline (Acp) were inserted with both stereochemistries at C(4), while in the Yaa position, we placed the (4*R*)-Hyp. These peptides are then compared to the reference peptides with Pro in the Yaa position.

Furthermore, the influence of interactions between the neighboring strands on the thermal stability of collagen triple helices was examined using thermal denaturation experiments monitored by circular dichroism (CD) spectroscopy.

It was shown that neighboring functionalized CMPs of the type Ac-(Pro-Hyp-Gly)₃-(Xaa-Hyp-Gly)-(Pro-Hyp-Gly)₃-NH₂ form in general more stable triple helices,

whereas CMPs of the type Ac-((4*S*)-EWG-Hyp-Gly)₇-NH₂ do not form any triple helices at all, which is in agreement with the previous studies.

All these results show that no huge sterically or electronically destabilizing effects are present in our target compounds, on the contrary double functionalization on the middle repeat provide very stable triple helix.

Design and Peptide Synthesis

Synthesized References (CMP 2, 2', 4, 4', 6, 6') and Target (CMP 1, 1', 3, 3', 5, 5') compounds are showed in the Table 2.

CMP	Ac-(Pro-Hyp-Gly) ₃ -Xaa-Yaa-Gly-(Pro-Hyp-Gly) ₃ -NH ₂
CMP 1	Ac-(Pro-Hyp-Gly) ₃ -(4 <i>R</i>)Azp-Hyp-Gly-(Pro-Hyp-Gly) ₃ -NH ₂
CMP 1'	Ac-(Pro-Hyp-Gly) ₃ -(4 <i>S</i>)Azp-Hyp-Gly-(Pro-Hyp-Gly) ₃ -NH ₂
CMP 2	Ac-(Pro-Hyp-Gly) ₃ -(4 <i>R</i>)Azp-Pro-Gly-(Pro-Hyp-Gly) ₃ -NH ₂
CMP 2'	Ac-(Pro-Hyp-Gly) ₃ -(4 <i>S</i>)Azp-Pro-Gly-(Pro-Hyp-Gly) ₃ -NH ₂
CMP 3	Ac-(Pro-Hyp-Gly) ₃ -(4 <i>R</i>)Amp-Hyp-Gly-(Pro-Hyp-Gly) ₃ -NH ₂
CMP 3'	Ac-(Pro-Hyp-Gly) ₃ -(4 <i>S</i>)Amp-Hyp-Gly-(Pro-Hyp-Gly) ₃ -NH ₂
CMP 4	Ac-(Pro-Hyp-Gly) ₃ -(4 <i>R</i>)Amp-Pro-Gly-(Pro-Hyp-Gly) ₃ -NH ₂
CMP 4'	Ac-(Pro-Hyp-Gly) ₃ -(4 <i>S</i>)Amp-Pro-Gly-(Pro-Hyp-Gly) ₃ -NH ₂
CMP 5	Ac-(Pro-Hyp-Gly) ₃ -(4 <i>R</i>)Acp-Hyp-Gly-(Pro-Hyp-Gly) ₃ -NH ₂
CMP 5'	Ac-(Pro-Hyp-Gly) ₃ -(4 <i>S</i>)Acp-Hyp-Gly-(Pro-Hyp-Gly) ₃ -NH ₂
CMP 6	Ac-(Pro-Hyp-Gly) ₃ -(4 <i>R</i>)Acp-Pro-Gly-(Pro-Hyp-Gly) ₃ -NH ₂
CMP 6'	Ac-(Pro-Hyp-Gly) ₃ -(4 <i>S</i>)Acp-Pro-Gly-(Pro-Hyp-Gly) ₃ -NH ₂

Table 2: Target and Control compounds

All peptides were prepared on a 0.03 mmol scale by standard microwave-assisted solid phase synthesis, using Fmoc chemistry. We used Rink Amide resin to obtain an amidated *C-terminus* after the final cleavage of the peptides [Fmoc-amino acid/Fmoc-tripeptide (4 equiv., 0.2 M in DMF); *i*-Pr₂NEt (8 equiv. 2 M in 1-

methylpyrrolidine-2-one (NMP), HATU (4 equiv., 0.5 M in DMF)]. The acetylation to the *N-terminus* of each peptide was performed on resin [Acetic acid (3.0 equiv.), HATU (2.95 equiv.) and *i*-Pr₂Net (6 equiv.)].

For the peptides containing the Amp in Xaa position, on resin Staudinger reduction protocol [H₂O (0.65 mL/g resin) and P(CH₃)₃ (5.0 equiv./azide, 1 M in THF)] was applied and for Acp-containing CMP, acetylation of the primary amine was performed before the cleavage of the resin.

All the peptides were purified by reverse-phase HPLC on a Phenomenex Jupiter semipreparative C-18 column and eluted with acetonitrile/ H₂O gradients containing 0.1% TFA and 1% acetonitrile.

The concentration of the peptides was 0.2 mM. Thermal denaturation experiments were conducted by monitoring the molar ellipticity at 224 nm with a heating rate of 1°C/100 s. Before measurement, all samples were incubated at 5 °C for at least 24 hrs. The recorded data obtained from the thermal denaturation experiments were fitted to an ‘all or none’ transition in which three single strands combine to a triple helix as described by Engel *et al*¹⁷⁴.

Result and discussion

The designed CMPs allow us to examine the impact of neighboring functionalized CMPs on the collagen triple helix. As showed above, the natural most abundant (*4R*)-Hyp was inserted in the Yaa position and firstly, EWG groups, such as N₃, MeCONH, were inserted in Xaa position. Moreover, CMP containing Amp in Xaa position allowed us to study also the collagen behavior depending on the pH (NH₂/NH₃⁺). All the EWGs (N₃, MeCONH NH₃⁺) are expected to exhibit a prevalent gauche effect, instead the amino group should behave as a methyl group.

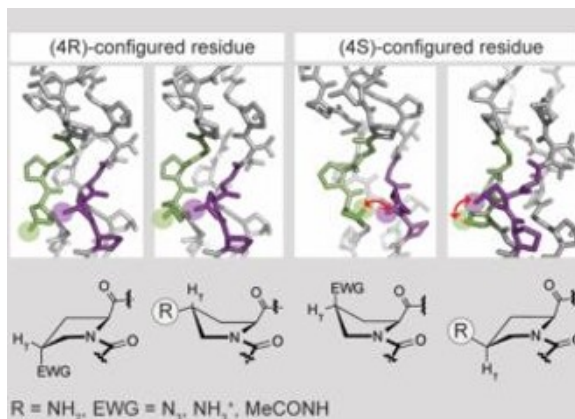


Figure 8: Ring pucker of different substituted prolines and stereochemistry at C(4)-proline position have different stereo-electronic effects on stability of triple helices

On the basis of molecular models (showed in the Figure 8), the **CMP 1**, **CMP 3**, and **CMP 5** triple helices should not have steric or electronic destabilizing effect. In fact, the substituents of the proline in Xaa position, independently from the electronic properties of the C(4)-substituent, should point outside the triple helix.

On the other hand, the triple helices of the (4*S*)-configured proline-containing CMPs should be affected by destabilizing effects, since the two substituent on the neighboring prolines points one towards each other.

Comparing the reference and the target compounds, we expected an increase of the triple helices stability of the target compounds in comparison with the control compounds: indeed, for the gauche effect, the $K_{trans:cis}$ and the right pucker of the ring, the Hyp in Yaa position should increase the thermal stability of the triple helix. To prove our hypothesis, the stability of the triple helices was evaluated analyzing the T_m with the CD. The T_m is the temperature in which half of the population is in an unfolded situation (SS) and half is as a triple helix (TH). Before analyzing T_m , CD spectra at 7 °C were recorded to verify the presence of a PPII secondary structure, corresponding to the conformation of the polyproline-single strand. After that, the triple helix/single strand equilibrium was analyzed by gel permeation chromatography (GPC).

Entry	CMP	GPC Analysis	T _m (° C)
1	CMP 1	Mainly TH	50
2	CMP 1'	TH and SS	38
3	CMP 2	-	42
4	CMP 2'	TH and SS	39
5	CMP 3 –pH 7-	Mainly TH	48
6	CMP 3 –pH 3-		49
7	CMP 3 –pH 9-		48
8	CMP 3' –pH 7.4-	TH and SS	38
9	CMP 3' –pH 3-		33
10	CMP 3' –pH 10.7-		43
11	CMP 4 –pH 7.4-	Mainly SS	42
12	CMP 4 –pH 3-		40
13	CMP 4 –pH 10.7-		44
14	CMP 4' –pH 7.4-	Mainly SS	27
15	CMP 4' –pH 3-		20
16	CMP 4' –pH 10.7-		35
17	CMP 5	Mainly TH	51
18	CMP 5'	TH and SS	40
19	CMP 6	Mainly TH	46
20	CMP 6'	Mainly SS	35

Table 3: T_m (° C) of target and reference CMP triple helices. TH/SS equilibrium of target and reference CMPs.

Triple helices with Azp-containing CMPs in the Xaa position (CMP 1-CMP 2-CMP 1'-CMP 2')

As we expected, analyzing **CMP 1** and comparing it with **CMP 2** we observed that the triple helix formed by **CMP 1** is more stable. The (*4R*)-Azp, adopting an *exo*

pucker, for the reason explained above, does not interact with the neighboring Hyp. As it is highlighted in the Figure 8, the C(4)-substituent most likely points outside the triple helix.

Consequently, the triple helix is stabilized most likely due to the beneficial stereoelectronic effect exerted by Hyp.

The results concerning the (4*S*)-containing Azp CMPs are quite surprising: as it is depicted in Figure 8, (4*S*)-Azp adopts an *endo* pucker. Moreover, the C(4)-substituent of Azp and the OH group of the neighboring Hyp point to each other. As a result, a destabilization of the triple helix of **CMP 1'** was found, lowering T_m . Unexpectedly, **CMP 1'** and **CMP 2'** have similar T_m . It could be due to a compensation between the preference of Hyp in Yaa position, having the right pucker, and the destabilizing stereo-electronic interactions of the azido and hydroxyl group.

Triple helices with Amp in the Xaa position (CMP 3-CMP 4-CMP 3'-CMP 4')

As previously reported¹⁷¹, in the case of (C4)-Amp ring pucker flips with the change of pH due to the different stereoelectronic properties of the amino group. We thus performed CD experiments at different pHs.

CMP 3 forms triple helix both under neutral, basic and acidic environment. This behavior is in agreement with the fact that there are not steric or electronic destabilizing effects, because the neighboring (C4)-substituents point outside the triple helix. On the other hand, the proline-containing compound **CMP 4** is less stable in comparison with **CMP 3** in the same pH range.

A different scenario was observed for (4*S*)-Amp **CMP 3'** depending on the pH. In fact, in an acidic environment (4*S*)-Amp adopts an *endo* pucker, whereas under basic conditions, it adopts an *exo* pucker giving a more stable triple helix, according to the literature data¹⁷¹. (Figure 6)

In contrast, it seems that in case of the **CMP 3'**, a stabilizing interaction between the ammonium and the neighboring hydroxyl group competes with the destabilizing transannular H bond (Figure 6), having the reference compound **CMP 4'** a T_m of 20° C (Entry 15, Table 3)

Independently from the pH, the Hyp-containing **CMP 3'** forms more stable triple helices in comparison with reference compound **CMP 4'**. This finding could be probably due to the higher Hyp $K_{tran:cis}$ with respect to the Pro $K_{trans:cis}$.

Triple helices with Acp-containing CMP in the Xaa position (CMP 5-CMP 6-CMP 5'-CMP 6')

The substitution of Pro with Hyp in the Yaa position stabilizes the triple helices in Acp-containing CMP to the same extent, independently for the C(4)-configuration (see entries 17-20, Table 3). These results suggest that there is no interfering or destabilizing interaction between the (C4)-substituent of Acp and the hydroxyl group of Hyp.

Effect of Flp in the Yaa position on the Thermal Stability of Collagen Triple Helices (CMP 7, CMP 7', CMP 8, CMP 8', CMP 9, CMP 9')

As already mentioned, an EWG of the (4*S*)-pyrrolidine ring can interact with the neighboring hydroxyl group of Hyp-containing CMP. In the case of N₃ (**CMP 1'**, entry 2, Table 3) the interaction is destabilizing and in the case of NH₃⁺ (**CMP 3'**, entry 9, Table 3) is stabilizing.

In order to understand the nature of the interaction between the substituents of the two neighboring functionalized prolines (H-bonds or dipole interactions or steric repulsion), fluorine substituent was chosen because of its properties. It is more electronegative and less sterical demanding with respect to the hydroxyl group. Moreover, it's known that fluorine is a poorer H-Bond acceptor in comparison with the hydroxyl group.

As a result, the Hyp in Yaa position was replaced with (4*R*)-Flp and peptides **CMP 7**, **CMP 7'**, **CMP 8**, **CMP 8'**, **CMP 9**, **CMP 9'** were prepared.

CMP	Ac-(Pro-Hyp-Gly)₃-Xaa-(4<i>R</i>)-Flp-Gly-(Pro-Hyp-Gly)₃-NH₂
CMP 7	Ac-(Pro-Hyp-Gly) ₃ -(4 <i>R</i>)Azp-Flp-Gly-(Pro-Hyp-Gly) ₃ -NH ₂
CMP 7'	Ac-(Pro-Hyp-Gly) ₃ -(4 <i>S</i>)Azp-Flp-Gly-(Pro-Hyp-Gly) ₃ -NH ₂
CMP 8	Ac-(Pro-Hyp-Gly) ₃ -(4 <i>R</i>)Amp-Flp-Gly-(Pro-Hyp-Gly) ₃ -NH ₂
CMP 8'	Ac-(Pro-Hyp-Gly) ₃ -(4 <i>S</i>)Amp-Flp-Gly-(Pro-Hyp-Gly) ₃ -NH ₂
CMP 9	Ac-(Pro-Hyp-Gly) ₃ -(4 <i>R</i>)Acp-Flp-Gly-(Pro-Hyp-Gly) ₃ -NH ₂
CMP 9'	Ac-(Pro-Hyp-Gly) ₃ -(4 <i>R</i>)Acp-Flp-Gly-(Pro-Hyp-Gly) ₃ -NH ₂

Table 4: Synthesized CMP containing (4*R*)-Flp in Yaa position.

If the destabilization of **CMPs** containing (4*R*)-Hyp in Yaa position, is caused by an electronic effect, the corresponding **CMPs** containing (4*R*)-Flp in the same position are supposed to form less stable triple helix. On the contrary, if the destabilization is due to steric clashes, the thermal stability of fluorine containing **CMPs** is expected to be higher.

For the triple helices derived from **CMPs** bearing Flp in the Yaa position, T_m values were similar or slightly higher than what we observed for the triple helices derived from our target compounds that bear Hyp in the Yaa position (compare Table 3 with Table 5). Triple helices bearing a (4*R*)-configured residue with an EWG at (C4) position have the same stability. As we can see from the Table 5, triple helix derived from **CMP 7'** (Xaa = 4*S*Azp, Yaa = 4*R*Flp) is slightly more stable than target compound **CMP 1'** (Xaa = 4*S*Azp, Yaa = 4*R*Hyp), indicating that azido and hydroxyl group destabilize the triple helix through steric repulsion.

Entry	CMP	T_m (° C)	$\Delta T_m = T_m(\text{Flp}) - T_m(\text{Hyp})^x$
1	CMP 7	50	0

2	CMP 7'	41	3
3	CMP 8 -pH = 7.4-	51	3
4	CMP 8 -pH = 3-	50	1
5	CMP 8 -pH = 10.7-	51	3
6	CMP 8' -pH = 7.4-	38	0
7	CMP 8' -pH = 3-	32	-1
8	CMP 8' , -pH = 10.7-	46	3
9	CMP 9	52	1
10	CMP 9'	43	3

Table 5: Thermal Stability of triple helices derived from Flp CMPs. ^x Differences in melting temperature between Flp-containing CMP and Hyp-containing CMP

Furthermore, we did not observe differences between the stability of **CMP 8'** (Xaa = 4SAmp; Yaa = 4RFlp) and **CMP 3'** (Xaa = 4SAmp; Yaa = 4RHyp) in acidic environment.

Our hypothesis is that, being the $\Delta T_m = 1$, the stabilization of **CMP 3'** could be due to a H-bond between NH_3^+ and OH, instead for **CMP 8'** could be due to a electrostatic interaction (between NH_3^+ and F).

Thermal Stability of triple helices derived from CMPs of the type –((4SAzp)-Hyp-Gly)_n–

In a next step, we wanted to investigate if the stabilizing effects of Hyp in the Yaa position is additive. For this purpose, we chose the least stable interaction pair, (4S)-Azp and Hyp, and we synthesized **CMP 10** [Ac-((4S)Azp-Hyp-Gly)₇-NH₂]. The recorded CD spectrum showed the maximum at 225 nm and the minimum at 190 nm indicating the presence of a PPII helix. However, GPC confirmed the presence of a single strand at room temperature. Also thermal denaturation studies monitored by CD spectroscopy gave a T_m value smaller than 15 °C. This experiment shows that

the stabilizing effect of Hyp is not additive. As already stated by Raines, unfavorable overall dipole interactions disrupt the collagen triple helix.

In conclusion, in the present study, we have successfully demonstrated that a substitution of Pro in the Yaa position of Ac-(Pro-Hyp-Gly)₃-Xaa-Yaa-Gly-(Pro-Hyp-Gly)₃-NH₂ CMP sequences with Hyp increases triple helix stability, most likely due to pre-organization of the pucker caused by the gauche effect. Triple helices derived from CMPs that contain a (*4R*)-configured proline derivative (X = N₃, NH₂, Ac) in the Xaa position are in general stabilized, if Hyp is present in the Yaa position, because these neighboring C(4)-substituents cannot interact. Instead, if a (*4S*)-configured proline derivatives are installed, the triple helix stability is affected by neighboring interactions. The azido group of (*4S*)-Azp interferes with the neighboring hydroxyl group of Hyp due to steric repulsions. The ammonium group of (*4S*)-AmpH⁺ favorably interacts with the neighboring hydroxyl group of Hyp, most likely through H bonds, and with F, most likely through dipole interactions, in case of CMP containing Flp in Yaa position.

These findings give us very important information about how to design more stable collagen model peptides. It will not be necessary to substitute the Yaa position of CMPs with Pro, but to keep the natural most abundant residue, Hyp, in that position. In the meantime, replacing proline in Xaa of the middle repeat with a selected (C4)-substituted proline could be an idea for stabilizing the CMP triple helix, taking in consideration that unfavorable overall dipole interactions can disrupt the CMP triple helix.

Experimental part

Protocol A - General procedure for swelling

Before automated peptide synthesis, the resin was swelled in CH₂Cl₂ for 15 min. while shaking. Then the resin was drained and washed with dimethylformamide (DMF) (3 x 6 mL) and drained again.

Protocol B - General protocol for microwave-assisted peptide synthesis

For microwave-assisted automated peptide synthesis, a Liberty Blue synthesizer was used. After swelling the resin in DMF on the synthesizer, *i*-Pr₂NEt (8 equiv. 2 M in 1-methylpyrrolidine-2-one (NMP), HATU (4 equiv., 0.5 M in DMF) and the Fmoc-amino acid/Fmoc-tripeptide (4 equiv., 0.2 M in DMF) were added to the resin. The mixture was allowed to react for 15 min. at 70°C, then washed with DMF (4x 6 mL). Fmoc-deprotection was carried out by addition 40% (v/v) piperidine in DMF and reaction for 1 min. This step was repeated 4 times. The resin was then washed with DMF (4x 6 mL). Amino acid couplings/tripeptide couplings and Fmoc deprotections were repeated until the desired peptides were obtained. For the automated synthesis of the collagen model peptides (CMPs), no capping was performed.

Protocol C – On resin N-terminal acetylation and side chain acetylation

Acetylation was performed manually at room temperature on the solid support-bound peptide. Acetic acid (3.0 equiv.), HATU (2.95 equiv.) and *i*-Pr₂NEt (6 equiv.) were dissolved in CH₂Cl₂ (4-5 mL). After pre-activation for 5 min, the coupling mixture was added to the resin. and agitated for 1-2 hrs. The resin was washed with CH₂Cl₂ (3x), DMF (3x), CH₂Cl₂ (3x), and petroleum ether (2x). The reaction was monitored by the qualitative color tests on bead or by LC-MS after test cleavage (see Protocol E).

Protocol D - On resin Staudinger reduction

The resin was swelled for 15 min. in tetrahydrofuran (THF) and washed with THF (3x). To the solid phase bound peptide, H₂O (0.65 mL/g resin) and P(CH₃)₃ (5.0 equiv./azide, 1 M in THF) in 2 mL THF were added. The reaction was shaken at room temperature for 1 hr. The resin was washed with THF (5x), CH₂Cl₂ (5x), DMF (3x), i-PrOH (2x), CH₂Cl₂ (3x), and petroleum ether (3x).

Protocol E - Cleavage from the resin

The resin was shaken for 1 hr in a mixture of trifluoroacetic acid (TFA)/(i-Pr₂)₃Si-H/H₂O (92.5:2.5:2.5). The peptide in solution was collected by filtration in a conical flask. Addition of ice-cold Et₂O afforded the peptide as a white precipitate. The solid was isolated by centrifugation followed by decantation. The solid was suspended in Et₂O, sonicated, centrifuged again and the supernatant was decanted. The residual white solid was dissolved in water/CH₃CN, frozen, and lyophilized to obtain a white foam.

Protocol F – Purification and analysis by RP HPLC

CH₃CN (A) and H₂O containing 1% CH₃CN and 0.1% TFA (B) were used as eluents. For semi-preparative HPLC a flow rate of 5 mL/min., for analytical HPLC a flow rate of 1 mL/min and for LC-MS a flow rate of 0.5 mL/min. were used. The column oven was heated to 65 °C to prevent triple helix formation, except for LC-MS it was at 50 °C. After the semi-preparative HPLC purification all collected fractions were analyzed by analytical HPLC or LC-MS and only pure fractions were combined. Aminoproline containing CMPs were desalted with a VariPure cartridge prior to lyophilizing.

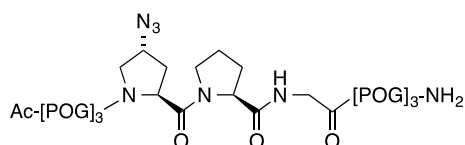
Preparative Columns: Phenomenex, Jupiter 4u, Proteo 90Å, 250 x 10 mm, 4 micron (1); Phenomenex, Jupiter 5 μm, 300Å, 250 x 10 mm (2).

Analytical Columns: Phenomenex, Jupiter 4u, Proteo 90Å, 250 x 4.6 mm, 4 micron (3); Phenomenex, Jupiter 5 μm, 300Å, 250 x 4.6 mm (4)

LC-MS: Reprosil Gold C18, 125 x 3mm (5).

Protocol G – Gel permeation chromatography: Nanopure H₂O was used as eluent. A flow rate of 0.1 mL/min. was used. The column was kept at left at room temperature.

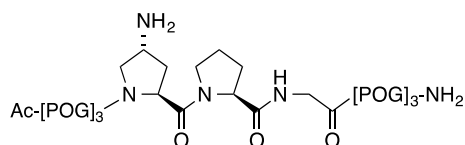
Ac-[ProHypGly]₃-(4R)AzpProGly-[ProHypGly]₃-NH₂



Analytical reverse-phase HPLC on column (3): 98% to 5% B over 30 min, t_R = 8.8 min.; 91% to 60% B over 20 min., t_R = 8.1 min. Purity determined by analytical HPLC using UV detection at 214 nm: >99%.

HRMS (MALDI): m/z calcd for $[C_{86}H_{124}N_{25}O_{28}]^+$: 1954.9021, found $[M+H]^+$ = 1954.9021, found $[M+Na]^+$ = 1976.8862, $[M+K]^+$ = 1992.8601.

Ac-[ProHypGly]₃-(4R)AmpProGly-[ProHypGly]₃-NH₂

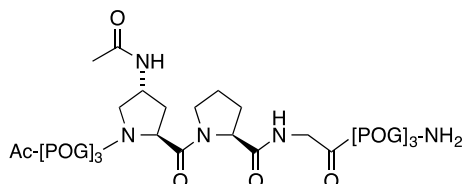


Analytical reverse-phase HPLC on column (3): 98% to 5% B over 30 min, t_R = 7.980 min.; 91% to 60% B over 20 min., t_R = 6.090 min. Purity determined by analytical HPLC using UV detection at 214 nm: >99%.

HRMS (MALDI): m/z calcd for $[C_{86}H_{126}N_{23}O_{28}]^+$: 1928.9137, found $[M+H]^+$ = 1928.9155, found $[M+Na]^+$ = 1950.8973, $[M+K]^+$ = 1966.8708.

Analytical gel permeation chromatography: 100% mQ water over 25 min, $t_R = 16.050$ (triple helix), $t_R = 16.903$ (single strand).

Ac-[ProHypGly]₃-(4R)AcpProGly-[ProHypGly]₃-NH₂

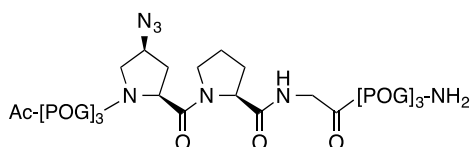


Analytical reverse-phase HPLC on column (3): 98% to 5% B over 30 min, $t_R = 8.9$ min.; 91% to 60% B over 20 min., $t_R = 6.4$ min. Purity determined by analytical HPLC using UV detection at 214 nm: >99%.

HRMS (MALDI): m/z calcd for $[C_{88}H_{128}N_{23}O_{29}]^+$: 1970.9243, found $[M+H]^+ = 1970.9250$, found $[M+Na]^+ = 1992.9070$, $[M+K]^+ = 2008.8814$.

Analytical gel permeation chromatography: 100% mQ water over 25 min, $t_R = 11.417$ (triple helix), $t_R = 13.197$ (single strand).

Ac-[ProHypGly]₃-(4S)AzpProGly-[ProHypGly]₃-NH₂

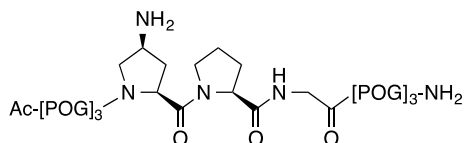


Analytical reverse-phase HPLC on column (3): 98% to 5% B over 30 min, $t_R = 8.6$ min.; 91% to 60% B over 20 min., $t_R = 7.4$ min. Purity determined by analytical HPLC using UV detection at 214 nm: >99%.

HRMS (MALDI): m/z calcd for $[C_{86}H_{124}N_{25}O_{28}]^+$: 1954.9042, found $[M+H]^+ = 1954.9063$, found $[M+Na]^+ = 1976.8885$, $[M+K]^+ = 1992.8615$.

Analytical gel permeation chromatography: 100% mQ water over 25 min, $t_R = 11.573$ (triple helix), $t_R = 13.360$ (single strand).

Ac-[ProHypGly]₃-(4S)AmpProGly-[ProHypGly]₃-NH₂

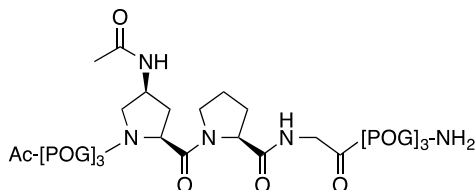


Analytical reverse-phase HPLC on column (3): 98% to 5% B over 30 min, $t_R = 7.9$ min.; 91% to 60% B over 20 min., $t_R = 6.2$ min. Purity determined by analytical HPLC using UV detection at 214 nm: >99%.

HRMS (MALDI): m/z calcd for $[C_{86}H_{126}N_{23}O_{28}]^+$: 1928.9137, found $[M+H]^+ = 1928.9149$, found $[M+Na]^+ = 1950.8970$, $[M+K]^+ = 1966.8681$.

Analytical gel permeation chromatograph: 100% mQ water over 25 min, $t_R = 16.513$ (triple helix), $t_R = 17.733$ (single strand).

Ac-[ProHypGly]₃-(4S)AcpProGly-[ProHypGly]₃-NH₂

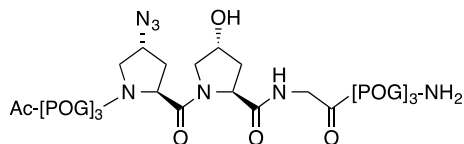


Analytical reverse-phase HPLC on column (3): 98% to 5% B over 30 min, $t_R = 8.2$ min.; 91% to 60% B over 20 min., $t_R = 6.6$ min. Purity determined by analytical HPLC using UV detection at 214 nm: >99%.

HRMS (MALDI): m/z calcd for $[C_{86}H_{128}N_{23}O_{29}]^+$: 1970.9243, found $[M+H]^+ = 1970.9264$, found $[M+Na]^+ = 1992.9077$, $[M+K]^+ = 2008.8795$.

Analytical gel permeation chromatography: 100% mQ water over 25 min, $t_R = 11.423$ (triple helix), $t_R = 13.260$ (single strand).

Ac-[ProHypGly]₃-(4R)AzpHypGly-[ProHypGly]₃-NH₂

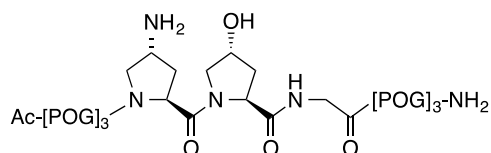


Analytical reverse-phase HPLC on column (3): 98% to 5% B over 30 min, $t_R = 8.4$ min.; 95% to 70% B over 20 min., $t_R = 10.7$ min. Purity determined by analytical HPLC using UV detection at 214 nm: >97%.

HRMS (MALDI): m/z calcd for $[C_{86}H_{124}N_{25}O_{29}]^+$: 1970.8991, found $[M+H]^+ = 1970.9007$, found $[M+Na]^+ = 1992.8826$, $[M+K]^+ = 2008.8557$.

Analytical gel permeation chromatography: 100% mQ water over 25 min, $t_R = 11.667$ (triple helix), $t_R = 13.327$ (single strand).

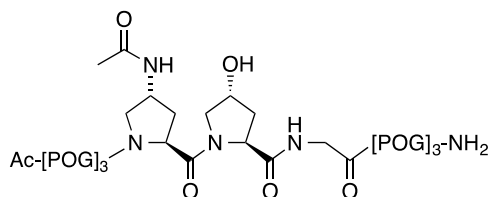
Ac-[ProHypGly]3-(4R)AmpHypGly-[ProHypGly]3-NH₂



Analytical reverse-phase HPLC on column (3): 98% to 5% B over 30 min, $t_R = 7.6$ min.; 91% to 60% B over 20 min., $t_R = 5,9$ min. Purity determined by analytical HPLC using UV detection at 214 nm: >99%.

HRMS (MALDI): m/z calcd for $[C_{86}H_{126}N_{23}O_{29}]^+$: 1944.9086, found $[M+H]^+ = 1944.9098$, found $[M+Na]^+ = 1966.8930$, $[M+K]^+ = 1982.8651$.

Ac-[ProHypGly]3-(4R)AcpHypGly-[ProHypGly]3-NH₂

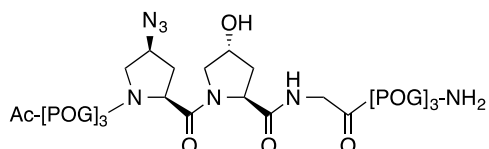


Analytical reverse-phase HPLC on column (3): 98% to 5% B over 30 min, $t_R = 7.9$ min.; 91% to 60% B over 20 min., $t_R = 5,9$ min. Purity determined by analytical HPLC using UV detection at 214 nm: >99%.

HRMS (MALDI): m/z calcd for $[C_{88}H_{128}N_{23}O_{30}]^+$: 1986.9192, found $[M+H]^+ = 1986.9189$, found $[M+Na]^+ = 2008.9016$, $[M+K]^+ = 2030.8812$.

Analytical gel permeation chromatography: 100% mQ water over 25 min, $t_R = 11.483$ (triple helix), $t_R = 13.243$ (single strand).

Ac-[ProHypGly]₃-(4S)AzpHypGly-[ProHypGly]₃-NH₂

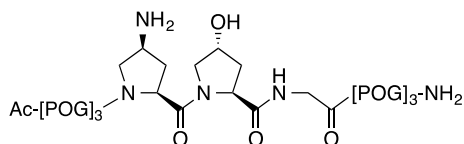


Analytical reverse-phase HPLC on column (3): 98% to 5% B over 30 min, $t_R = 8.4$ min.; 91% to 60% B over 20 min., $t_R = 7.0$ min. Purity determined by analytical HPLC using UV detection at 214 nm: >99%.

HRMS (MALDI): m/z calcd for $[C_{86}H_{124}N_{25}O_{29}]^+$: 1970.8991, found $[M+H]^+ = 1970.9001$, found $[M+Na]^+ = 1992.8812$, $[M+K]^+ = 2008.8542$.

Analytical gel permeation chromatography: 100% mQ water over 25 min, $t_R = 11.500$ (triple helix), $t_R = 13.357$ (single strand).

Ac-[ProHypGly]₃-(4S)AmpHypGly-[ProHypGly]₃-NH₂

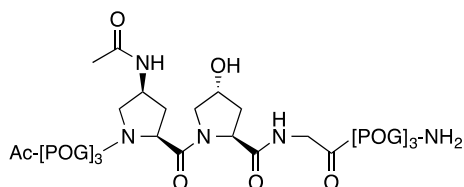


Analytical reverse-phase HPLC on column (3): 98% to 5% B over 30 min, $t_R = 3.4$ min.; 91% to 60% B over 20 min., $t_R = 6.0$ min. Purity determined by analytical HPLC using UV detection at 214 nm: >99%.

HRMS (MALDI): m/z calcd for $[C_{86}H_{126}N_{23}O_{29}]^+$: 1944.9086, found $[M+H]^+ = 1944.9093$, found $[M+Na]^+ = 1966.8923$, $[M+K]^+ = 1982.8634$.

Analytical gel permeation chromatography: 100% mQ water over 25 min, $t_R = 15.9$ (triple helix), $t_R = 16.5$ (single strand).

Ac-[ProHypGly]₃-(4S)AcpHypGly-[ProHypGly]₃-NH₂

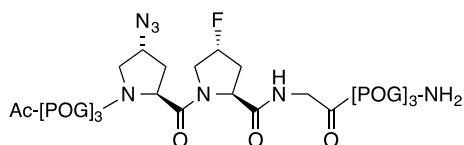


Analytical reverse-phase HPLC on column (3): 98% to 5% B over 30 min, $t_R = 7.9$ min.; 91% to 60% B over 20 min., $t_R = 6.2$ min. Purity determined by analytical HPLC using UV detection at 214 nm: >99%.

HRMS (MALDI): m/z calcd for $[C_{86}H_{128}N_{23}O_{30}]^+$: 1986.9192, found $[M+H]^+ = 1986.9202$, found $[M+Na]^+ = 2008.9033$, $[M+K]^+ = 2024.8757$.

Analytical gel permeation chromatograph: 100% mQ water over 25 min, $t_R = 11.457$ (triple helix), $t_R = 13.257$ (single strand).

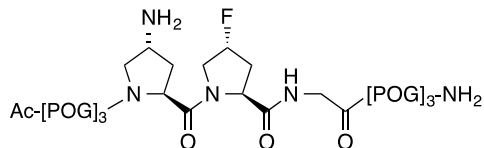
Ac-[ProHypGly]₃-(4R)AzpFlpGly-[ProHypGly]₃-NH₂



Analytical reverse-phase HPLC on column (3): 98% to 5% B over 30 min, $t_R = 8.8$ min.; 91% to 60% B over 20 min., $t_R = 7.8$ min. Purity determined by analytical HPLC using UV detection at 214 nm: >99%.

HRMS (MALDI): m/z calcd for $[C_{86}H_{123}FN_{25}O_{28}]^+$: 1972.8948, found $[M+H]^+ = 1972.8947$, found $[M+Na]^+ = 1994.8777$, $[M+K]^+ = 2010.8565$.

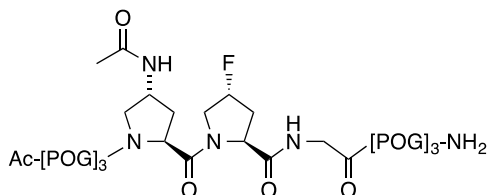
Ac-[ProHypGly]₃-(4R)AmpFlpGly-[ProHypGly]₃-NH₂



Analytical reverse-phase HPLC on column (3): 98% to 5% B over 30 min, $t_R = 8.0$ min.; 91% to 60% B over 20 min., $t_R = 6.2$ min. Purity according to HPLC: >99%

HRMS (MALDI): m/z calcd for $[C_{86}H_{123}FN_{25}O_{28}]^+$: 1946.9043, found $[M+H]^+ = 1946.9051$, found $[M+Na]^+ = 1968.8863$, $[M+K]^+ = 1984.8600$.

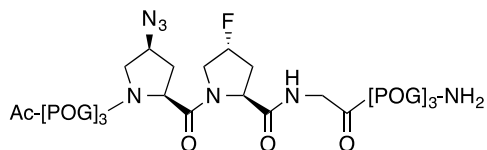
Ac-[ProHypGly]₃-(4R)AcpFlpGly-[ProHypGly]₃-NH₂



Analytical reverse-phase HPLC on column (3): 98% to 5% B over 30 min, $t_R = 8.0$ min.; 91% to 60% B over 20 min., $t_R = 6.4$ min. Purity determined by analytical HPLC using UV detection at 214 nm: >99%.

HRMS (MALDI): m/z calcd for $[C_{88}H_{127}FN_{23}O_{29}]^+$: 1988.9194, found $[M+H]^+ = 1988.9150$, found $[M+Na]^+ = 2010.8962$, $[M+K]^+ = 2026.8701$.

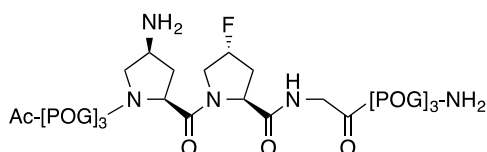
Ac-[ProHypGly]₃-(4S)AzpFlpGly-[ProHypGly]₃-NH₂



Analytical reverse-phase HPLC on column (3): 98% to 5% B over 30 min, $t_R = 8.3$ min.; 91% to 60% B over 20 min., $t_R = 7.3$ min. Purity determined by analytical HPLC using UV detection at 214 nm: >99%.

HRMS (MALDI): m/z calcd for $[C_{86}H_{123}FN_{25}O_{28}]^+$: 1972.8948, found $[M+H]^+ = 1972.8949$, found $[M+Na]^+ = 1994.8765$, $[M+K]^+ = 2010.8513$.

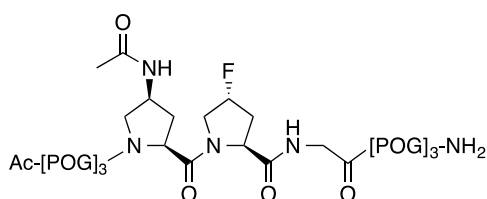
Ac-[ProHypGly]3-(4S)AmpFlpGly-[ProHypGly]3-NH₂



Analytical reverse-phase HPLC on column (3): 98% to 5% B over 30 min, $t_R = 8.0$ min.; 95 % to 70% B over 20 min., $t_R = 9.5$ min. Purity determined by analytical HPLC using UV detection at 214 nm: >99%.

HRMS (MALDI): m/z calcd for $[C_{86}H_{125}FN_{23}O_{28}]^+$: 1946.9043, found $[M+H]^+ = 1946.9035$, found $[M+Na]^+ = 1968.8855$, $[M+K]^+ = 1984.8598$.

Ac-[ProHypGly]3-(4S)AcpFlpGly-[ProHypGly]3-NH₂



Analytical reverse-phase HPLC on column (3): 98% to 5% B over 30 min, $t_R = 8.0$ min.; 95% to 70% B over 20 min., $t_R = 9.9$ min. Purity determined by analytical HPLC using UV detection at 214 nm: >99%.

HRMS (MALDI): m/z calcd for $[C_{88}H_{127}FN_{23}O_{29}]^+$: 1988.9194, found $[M+H]^+ = 1988.9131$, found $[M+Na]^+ = 2010.8972$, $[M+K]^+ = 2026.8699$.

Bibliography

1. Schueler-Furman, O.; Wang, C.; Bradley, P.; Misura, K.; Baker, D. *Science* (80) 2005, 310, 638–642.
2. Gellman, S. H. *Acc Chem Res* 1998, 31, 173–180.
3. Schreiber, J. V; Frackenkohl, J.; Moser, F.; Fleischmann, T.; Kohler, H.-P. E.; Seebach, D. *ChemBioChem* 2002, 3, 424.
4. Geueke, B.; Namoto, K.; Seebach, D.; Kohler, H. P. E. *J Bacteriol* 2005, 187, 5910–5917.
5. Heitz, F.; Morris, M. C.; Divita, G. *Br J Pharmacol* 2009, 157, 195–206.
6. Foged, C.; Nielsen, H. M. *Expert Opin Drug Deliv* 2008, 5, 105–117.
7. Lakshmanan, A.; Zhang, S.; Hauser, C. A. E. *Trends Biotechnol* 2012, 30, 155–165.
8. Panda, J. J.; Chauhan, V. S. *Polym Chem* 2014, 5.
9. Aleman, C.; Bianco, A.; Venanzi, M. *Peptide Materials: From Nanostructures to Applications*; Wiley, 2013.
10. Dasgupta, A.; Mondal, J. H.; Das, D. *RSC Adv* 2013, 3, 9117–9149.
11. Mondal, S.; Gazit, E. *ChemNanoMat* 2016, 2, 323–332.
12. Mandal, D.; Nasrolahi Shirazi, A.; Parang, K. *Org Biomol Chem* 2014, 12, 3544–3561.
13. Hintermann, T.; Seebach, D. *Chim Int J Chem* 1997, 51, 244–247.
14. Banerjee, A.; Balaram, P. *Curr Sci* 1997, 73, 1067.
15. Qiu, J. X.; Petersson, E. J.; Matthews, E. E.; Schepartz, A. *J Am Chem Soc* 2006, 128, 11338–11339.
16. Cheng, R. P.; Gellman, S. H.; DeGrado, W. F. *Chem Rev* 2001, 101, 3219–3232.
17. Seebach, D.; Jacobi, A.; Rueping, M.; Gademann, K.; Ernst, M. *Helv Chim Acta* 2000, 83, 2115–2140.
18. Appella, D. H.; Christianson, L. A.; Karle, I. L.; Powell, D. R.; Gellman, S. H. *J Am Chem Soc* 1996, 118, 13071–13072.
19. Appella, D. H.; LePlae, P. R.; Raguse, T. L.; Gellman, S. H. *J Org Chem* 2000, 65, 4766–4769.
20. Juaristi, E.; Soloshonok, V. A. *Enantioselective synthesis of Beta-Amino Acids*, Second Edi.; 2005.

21. Bode, K. A.; Applequist, J. *Macromolecules* 1997, 30, 2144–2150.
22. Appella, D. H.; Barchi, J. J.; Durell, S. R.; Gellman, S. H. *J Am Chem Soc* 1999, 121, 2309–2310.
23. Appella, D. H.; Christianson, L. A.; Klein, D. A.; Powell, D. R.; Huang, X.; Barchi, J. J.; Gellman, S. H. *Nature*. 1997, pp 381–384.
24. Wang, X.; Espinosa, J. F.; Gellman, S. H. *J Am Chem Soc* 2000, 122, 4821–4822.
25. Vasudev, P. G.; Chatterjee, S.; Narayanaswamy, S.; Padmanabhan, B. *Chem Rev* 2011, 111, 657–687.
26. Seebach, D.; Abele, S.; Gademann, K.; Guichard, G.; Hintermann, T.; Jaun, B.; Matthews, J. L.; Schreiber, J. V.; Oberer, L.; Hommel, U.; Widmer, H. *Helv Chim Acta* 1998, 81, 932–982.
27. Aurora, R.; Creamer, T. P.; Srinivasan, R.; Rose, G. D. *J Biol Chem* 1997, 272, 1413–1416.
28. Claridge, T. D. W.; Goodman, J. M.; Moreno, A.; Angus, D.; Barker, S. F.; Taillefumier, C.; Watterson, M. P.; Fleet, G. W. J. *Tetrahedron Lett* 2001, 42, 4251–4255.
29. Abele, S.; Seiler, P.; Seebach, D. *Helv Chim Acta* 1999, 82, 1559–1571.
30. Yang, D.; Qu, J.; Li, B.; Ng, F. F.; Wang, X. C.; Cheung, K. K.; Wang, D. P.; Wu, Y. D. *J Am Chem Soc* 1999, 121, 589–590.
31. Krauthauser, S.; Christianson, L. A.; Popwel, D. R.; Gellman, S. H. *J Am Chem Soc* 1997, 119, 11719–11720.
32. Bestian, H. *Angew Chemie Int Ed English* 1968, 7, 278–285.
33. Glickson, J. D.; Applequist, J. *J Am Chem Soc* 1971, 93, 3276–3281.
34. Yuki, H.; Okamoto, Y.; Taketani, Y.; Tsubota, T.; Marubayashi, Y. *J Polym Sci Polym Chem Ed* 1978, 16, 2237–2251.
35. Chen, F.; Lepore, G.; Goodman, M. *Macromolecules* 1974, 7, 779–783.
36. López-Carrasquero, F.; Alemán, C.; Muñoz-Guerra, S. *Biopolymers* 1995, 36, 263–271.
37. Bella, J.; Alemán, C.; Fernández-Santin, J. M.; Alegre, C.; Subirana, J. A. *Macromolecules* 1992, 25, 5225–5230.
38. Daura, X.; Gademann, K.; Sch?fer, H.; Jaun, B.; Seebach, D.; Van Gunsteren, W. F. *J Am Chem Soc* 2001, 123, 2393–2404.
39. Yong Jun Chung; Christianson, L. A.; Stanger, H. E.; Powell, D. R.; Gellman, S. H. *J Am Chem Soc* 1998, 120, 10555–10556.

40. Krauthäuser, S.; Christianson, L. A.; Powell, D. R.; Gellman, S. H. *J Am Chem Soc* 1997, 119, 11719–11720.
41. Seebach, D.; Ciceri, P. E.; Overhand, M.; Jaun, B.; Rigo, D.; Oberer, L.; Hommel, U.; Amstutz, R.; Widmer, H. *Helv Chim Acta* 1996, 79, 2043–2066.
42. Huck, B. R.; Fisk, J. D.; Gellman, S. H. *Org Lett* 2000, 2, 2607–2610.
43. Chung, Y. J.; Christianson, L. A.; Stanger, H. E.; Powell, D. R.; Gellman, S. H. *J Am Chem Soc* 1998, 120, 10555–10556.
44. Maron, D. M.; Ames, B. N. *Mutat Res Mutagen Relat Subj* 1983, 113, 173–215.
45. Hook, D. F.; Bindschädler, P.; Mahajan, Y. R.; Šebesta, R.; Kast, P.; Seebach, D. *Chem Biodivers* 2005, 2, 591–632.
46. Huck, B. R.; Langenhan, J. M.; Gellman, S. H. *Org Lett* 1999, 1, 1717–1720.
47. Bonetti, A.; Pellegrino, S.; Das, P.; Yuran, S.; Bucci, R.; Ferri, N.; Meneghetti, F.; Castellano, C.; Reches, M.; Gelmi, M. L. *Org Lett* 2015, 17, 4468–4471.
48. Bucci, R.; Das, P.; Iannuzzi, F.; Feligioni, M.; Gandolfi, R.; Gelmi, M. L.; Reches, M.; Pellegrino, S. *Org Biomol Chem* 2017, 6773–6779.
49. Koglin, N.; Zorn, C.; Beumer, R.; Cabrele, C.; Bubert, C.; Sewald, N.; Reiser, O.; Beck-Sickinger, A. G. *Angew Chemie - Int Ed* 2003, 42, 202–205.
50. Pellegrino, S.; Tonali, N.; Erba, E.; Kaffy, J.; Taverna, M.; Contini, A.; Taylor, M.; Allsop, D.; Gelmi, M. L.; Ongeri, S. *Chem Sci* 2017, 8, 1295–1302.
51. Ko, E.; Raghuraman, A.; Perez, L. M.; Ioerger, T. R.; Burgess, K. *J Am Chem Soc* 2013, 135, 167–173.
52. Horne, W. S.; Johnson, L. M.; Ketas, T. J.; Klasse, P. J.; Lu, M.; Moore, J. P.; Gellman, S. H. *Proc Natl Acad Sci U S A* 2009, 106, 14751–14756.
53. Clerici, F.; Erba, E.; Gelmi, M. L.; Pellegrino, S. *Tetrahedron Lett* 2016, 57, 5540–5550.
54. Kar, S.; Huang, B.-H.; Wu, K.-W.; Lee, C.-R.; Tai, Y. *Soft Matter* 2014, 10, 8075–8082.
55. Goel, R.; Gopal, S.; Gupta, A. *J Mater Chem B* 2015, 3, 5849–5857.
56. Parween, S.; Misra, A.; Ramakumar, S.; Chauhan, V. S. *J Mater Chem B* 2014, 2, 3096–3106.
57. Sorrenti, A.; Illa, O.; Pons, R.; Ortuño, R. M. *Langmuir* 2015, 31, 9608–9618.
58. Gorrea, E.; Nolis, P.; Torres, E.; Da Silva, E.; Amabilino, D. B.; Branchadell, V.; Ortuño, R. M. *Chem – A Eur J* 2011, 17, 4588–4597.
59. Torres, E.; Puigmarti-Luis, J.; del Pino, A.; Ortuno, R. M.; Amabilino, D. B. *Org*

- Biomol Chem 2010, 8, 1661–1665.
60. Bucci, R.; Bonetti, A.; Clerici, F.; Contini, A.; Nava, D.; Pellegrino, S.; Tessaro, D.; Gelmi, M. L. *Chem - A Eur J* 2017, 23, 10822–10831.
 61. Chakrabarti, P.; Bhattacharyya, R. *Prog Biophys Mol Biol* 2007, 95, 83–137.
 62. Bernabeu, M. C.; Díaz, J. L.; Jiménez, O.; Lavilla, R. *Synth Commun* 2004, 34, 137–149.
 63. Liljeblad, A.; Kanerva, L. T. *Tetrahedron* 2006, 62, 5831–5854.
 64. Berkessel, A.; Jurkiewicz, I.; Mohan, R. *ChemCatChem* 2011, 3, 319–330.
 65. Liljeblad, A.; Kavenius, H.-M.; Tähtinen, P.; Kanerva, L. T. *Tetrahedron: Asymmetry* 2007, 18, 181–191.
 66. Martinelli, J. R.; Watson, D. A.; Freckmann, D. M. M.; Barder, T. E.; Buchwald, S. L. *J Org Chem* 2008, 73, 7102–7107.
 67. Shiotani, S.; Hori, T.; Mitsuhashi, K. *Chem Pharm Bull (Tokyo)* 1967, 15, 88–93.
 68. Tessaro, D. *Cascade Biocatalysis : Integrating Stereoselective and Environmentally Friendly Reactions*; 2014.
 69. D'Arrigo, P.; Cerioli, L.; Servi, S.; Viani, F.; Tessaro, D. *Catal Sci Technol* 2012, 2, 1606–1616.
 70. Nicolaou, K. C.; Zou, B.; Dethe, D. H.; Li, D. B.; Chen, D. Y.-K. *Angew Chemie* 2006, 118, 7950–7956.
 71. Bonetti, A.; Beccalli, E.; Caselli, A.; Clerici, F.; Pellegrino, S.; Gelmi, M. L. *Chem - A Eur J* 2015, 21, 1692–1703.
 72. Sladojevich, F.; Guarna, A.; Trabocchi, A. *Org Biomol Chem* 2010, 8, 916–924.
 73. Von Roedern, E. G.; Lohof, E.; Hessler, G.; Hoffmann, M.; Kessler, H. *J Am Chem Soc* 1996, 118, 10156–10167.
 74. Crisma, M.; De Zotti, M.; Moretto, A.; Peggion, C.; Drouillat, B.; Wright, K.; Couty, F.; Toniolo, C.; Formaggio, F. *New J Chem* 2015, 39, 3208–3216.
 75. Smith, J. A.; Pease, L. G.; Kopple, K. D. *Crit Rev Biochem* 1980, 8, 315–399.
 76. Toniolo, C.; Benedetti, E. *Crit Rev Biochem* 1980, 9, 1–44.
 77. Rose, G. D.; Glerasch, L. M.; Smith, J. A. *Turns in Peptides and Proteins*; 1985; Vol. 37.
 78. Vass, E.; Hollósi, M.; Besson, F.; Buchet, R. *Chem Rev* 2003, 103, 1917–1954.
 79. Crisma, M.; Formaggio, F.; Moretto, A.; Toniolo, C. *Pept Sci* 2006, 84, 3–12.
 80. Milner-White, E. J.; Ross, B. M.; Ismail, R.; Belhadj-Mostefa, K.; Poet, R. *J Mol*

- Biol 1988, 204, 777–782.
81. Burland, P. A.; Osborn, H. M. I.; Turkson, A. *Bioorganic Med Chem* 2011, 19, 5679–5692.
 82. Tonan, K.; Ikawa, S. *Spectrochim Acta Part A Mol Biomol Spectrosc* 2003, 59, 111–120.
 83. Steinke, D.; Kula, M. R. *Angew Chemie* 1990, 102, 1204–1206.
 84. Ryakhovskii, V.; Agafonov, S.; Kosyrev, Y. *Usp Khim* 60, 1817–1836.
 85. Seebach, D.; Beck, A.; Capone, S.; Deniau, G.; Grošelj, U.; Zass, E. *Synthesis (Stuttg)* 2009, 2009, 1–32.
 86. Szakonyi, Z.; Fülöp, F. *Amino Acids* 2011, 41, 597–608.
 87. Mikami, K.; Fustero, S.; Sánchez-Roselló, M.; Aceña, J.; Soloshonok, V.; Sorochinsky, A. *Synthesis (Stuttg)* 2011, 2011, 3045–3079.
 88. Hart, D. J.; Ha, D. C. *Chem Rev* 1989, 89, 1447–1465.
 89. Goodman, J. L.; Petersson, E. J.; Daniels, D. S.; Qiu, J. X.; Schepartz, A. *J Am Chem Soc* 2007, 129, 14746–14751.
 90. Balamurugan, D.; Muraleedharan, K. M. *Chem - A Eur J* 2012, 18, 9516–9520.
 91. Gademan, K.; Hintermann, T.; Schreiber, J. V. *Curr Med Chem* 1999, 6, 905–925.
 92. Dobrev, A.; Ivanov, C. *Chem Ber* 1971, 104, 981–985.
 93. Patgiri, A.; Joy, S. T.; Arora, P. S. *J Am Chem Soc* 2012, 134, 11495–11502.
 94. Pilsl, L. K. A.; Reiser, O. *Amino Acids* 2011, 41, 709–718.
 95. Mándity, I. M.; Wéber, E.; Martinek, T. A.; Olajos, G.; Tóth, G. K.; Vass, E.; Fülöp, F. *Angew Chemie* 2009, 121, 2205–2209.
 96. Bonetti, A.; Clerici, F.; Foschi, F.; Nava, D.; Pellegrino, S.; Penso, M.; Soave, R.; Luisa, M. *European J Org Chem* 2014, 3203–3209.
 97. Zerbe; Bader. *Peptide/Protein NMR*; pp 1–27.
 98. *Bioorg Med Chem* 2009, 17, 2950–2962.
 99. Jiang, X. C.; Gao, J. Q. *Int J Pharm* 2017, 521, 167–175.
 100. Bilensoy, E. *Expert Opin Drug Deliv* 2010, 7, 795–809.
 101. Mokhtarzadeh, A.; Alibakhshi, A.; Hashemi, M.; Hejazi, M.; Hosseini, V.; de la Guardia, M.; Ramezani, M. *J Control Release* 2017, 245, 116–126.
 102. Carmona-Ribeiro, A. M.; de Melo Carrasco, L. D. *Int J Mol Sci* 2013, 14, 9906–9946.

103. Nativo, P.; Prior, I. a; Brust, M. 2008, 2, 1639–1644.
104. Arvizo, R. R.; Miranda, O. R.; Thompson, M. A.; Pabelick, C. M.; Bhattacharya, R.; David Robertson, J.; Rotello, V. M.; Prakash, Y. S.; Mukherjee, P. *Nano Lett* 2010, 10, 2543–2548.
105. Ghosh, P.; Han, G.; De, M.; Kim, C. K.; Rotello, V. M. *Adv Drug Deliv Rev* 2008, 60, 1307–1315.
106. Ramos, J.; Forcada, J.; Hidalgo-Alvarez, R. *Chem Rev* 2014, 114, 367–428.
107. Tashima, T. *Bioorganic Med Chem Lett* 2017, 27, 121–130.
108. Arruebo, M.; Valladares, M.; González-Fernández, Á. *J Nanomater* 2009, 2009.
109. Sajeesh, S.; Choe, J. Y.; Lee, T. Y.; Lee, D. J. *J Mater Chem B* 2015, 3, 207–216.
110. Blanco, E.; Shen, H.; Ferrari, M. *Nat Biotechnol* 2015, 33, 941–951.
111. Nitta, S. K.; Numata, K. *Int J Mol Sci* 2013, 14, 1629–1654.
112. Eskandari, S.; Guerin, T.; Toth, I.; Stephenson, R. J. *Adv Drug Deliv Rev* 2017, 110, 169–187.
113. Mallamace, D.; Corsaro, C.; Vasi, C.; Vasi, S.; Dugo, G.; Mallamace, F. *Phys A Stat Mech its Appl* 2014, 412, 39–44.
114. Zhang, Z.; Feng, S. S. *Biomaterials* 2006, 27, 4025–4033.
115. Lin, Y.-C.; Boone, M.; Meuris, L.; Lemmens, I.; Van Roy, N.; Soete, A.; Reumers, J.; Moisse, M.; Plaisance, S.; Drmanac, R.; Chen, J.; Speleman, F.; Lambrechts, D.; Van de Peer, Y.; Tavernier, J.; Callewaert, N. *Nat Commun* 2014, 5, 4767.
116. Yao, W.; Yan, Y.; Xue, L.; Zhang, C.; Li, G.; Zheng, Q.; Zhao, Y. S.; Jiang, H.; Yao, J. *Angew Chemie - Int Ed* 2013, 52, 8713–8717.
117. Torabi, S. F.; Lu, Y. *Curr Opin Biotechnol* 2014, 28, 88–95.
118. Langenhan, J. M.; Guzei, I. A.; Gellman, S. H. 2003, 2504–2507.
119. Ranganathan, D.; Haridas, V.; Kurur, S.; Thomas, A.; Madhusudanan, K. P.; Nagaraj, R.; Kunwar, A. C.; Sarma, A. V. S.; Karle, I. L. *J Am Chem Soc* 1998, 120, 8448–8460.
120. Nowick, J. S.; Smith, E. M.; Ziller, J. W.; Shaka, A. J. *Synthesis (Stuttg)* 2002, 58.
121. Hibbs, D. E.; Hursthouse, M. B.; Jones, I. G.; Jones, W.; Malik, K. M. A.; North, M. *J Org Chem* 1998, 3263, 1496–1504.
122. Wagner, G.; Feigel, M. *Tetrahedron* 1993, 49, 10831–10842.
123. Nowick, J. S.; Insaf, S. *J Am Chem Soc* 1997, 119, 10903–10908.
124. Skar, M. L.; Svendsen, J. S. *Tetrahedron* 1997, 53, 17425–17440.

125. Chitnumsub, P.; Fiori, W. R.; Lashuel, H. A.; Diaz, H.; Kelly, J. W. *Bioorganic Med Chem* 1999, 7, 39–59.
126. Fisk, J. D.; Gellman, S. H. *J Am Chem Soc* 2001, 123, 343–344.
127. Nowick, J. S. *Acc Chem Res* 2008, 41, 1319–1330.
128. Antzutkin, O. N.; Balbach, J. J.; Leapman, R. D.; Rizzo, N. W.; Reed, J.; Tycko, R. *Proc Natl Acad Sci* 2000, 97, 13045–13050.
129. Hughes, R. M.; Waters, M. L. *Curr Opin Struct Biol* 2006, 16, 514–524.
130. Norman, B. H.; Gruber, J. M.; Hollinshead, S. P.; Wilson, J. W.; Starling, J. J.; Law, K. L.; Self, T. D.; Tabas, L. B.; Williams, D. C.; Paul, D. C.; Wagner, M. M.; Dantzig, A. H. *Bioorganic Med Chem Lett* 2002, 12, 883–886.
131. Bailey, T. R.; Diana, G. D.; Kowalczyk, P. J.; Akullian, V.; Eissenstat, M. A.; Cutcliffe, D.; Mallamo, J. P.; Carabateas, P. M.; Pevear, D. C. *J Med Chem* 1992, 35, 4628–4633.
132. Baruchello, R.; Simoni, D.; Marchetti, P.; Rondanin, R.; Mangiola, S.; Costantini, C.; Meli, M.; Giannini, G.; Vesce, L.; Carollo, V.; Brunetti, T.; Battistuzzi, G.; Tolomeo, M.; Cabri, W. *Eur J Med Chem* 2014, 76, 53–60.
133. Brough, P. a; Aherne, W.; Barril, X.; Borgognoni, J.; Boxall, K.; Cansfield, J. E.; Cheung, K.-M. J.; Collins, I.; Davies, N. G. M.; Drysdale, M. J.; Dymock, B.; Eccles, S. a; Finch, H.; Fink, A.; Hayes, A.; Howes, R.; Hubbard, R. E.; James, K.; Jordan, A. M.; Lockie, A.; Martins, V.; Massey, A.; Matthews, T. P.; McDonald, E.; Northfield, C. J.; Pearl, L. H.; Prodromou, C.; Ray, S.; Raynaud, F. I.; Roughley, S. D.; Sharp, S. Y.; Surgenor, A.; Walmsley, D. L.; Webb, P.; Wood, M.; Workman, P.; Wright, L. *J Med Chem* 2007, 51, 196–218.
134. Padwa, A. *Synthetic applications of 1, 3-dipolar cycloaddition chemistry toward heterocycles and natural products; 2003; Vol. 59.*
135. Jones, R. C. F.; Bhalay, G.; Carter, P. a.; Duller, K. a. M.; Dunn, S. H. *J Chem Soc Perkin Trans 1* 1999, 1999, 765–776.
136. Mukaiyama, T.; Hoshino, T. *J Am Chem Soc* 1960, 82, 5339–5342.
137. Jones, R. H.; Robinson, G. C.; Thomas, E. J. *Tetrahedron* 1984, 40, 177.
138. Ko, S. sung; Confalone, P. N. *Tetrahedron* 1985, 41, 3511.
139. Jurczak, J.; Gryko, D.; Kobrzycka, E.; Gruza, H.; Prokopowicz, P. *Tetrahedron* 1998, 54, 6051–6064.
140. Myers, a G.; Zhong, B.; Kung, D. W.; Movassaghi, M.; Lanman, B. a; Kwon, S. *Org Lett* 2000, 2, 3337–3340.
141. Jones, R. C. F.; Bullons, J. P.; Law, C. C. M.; Elsegood, M. R. *J. Chem Commun (Cambridge, England)* 2014, 50, 1588–1590.

142. Padwa, A.; Smolanoff, J. *J Am Chem Soc* 1971, 93, 548–550.
143. Iwashita, T.; Kusumi, T.; Kakasawa, H. *Chem Lett* 1979, 1337–1340.
144. Wang, C. J.; Ripka, W. C.; Confalone, P. N. *Tetrahedron Lett* 1984, 25, 4613–4616.
145. Estrada, A. A.; Shore, D. G.; Blackwood, E.; Chen, Y.-H.; Deshmukh, G.; Ding, X.; DiPasquale, A. G.; Epler, J. A.; Friedman, L. S.; Koehler, M. F. T.; Liu, L.; Malek, S.; Nonomiya, J.; Ortwine, D. F.; Pei, Z.; Sideris, S.; St-Jean, F.; Trinh, L.; Truong, T.; Lyssikatos, J. P. *J Med Chem* 2013, 56, 3090–3101.
146. Vellemae, E.; Stepanov, V.; Maeorg, U. *Synth Commun* 2010, 40, 3397–3404.
147. Jacquemard, U.; Beneteau, V.; Lefoix, M.; Routier, S.; Merour, J. Y.; Coudert, G. *Tetrahedron* 2004, 60, 10039–10047.
148. Just, G.; Grozinger, K. *Synthesis (Stuttg)* 1976, 475–476.
149. Bergeron, R. J.; McManis, J. S. *J Org Chem* 1988, 53, 3108–3111.
150. Zerella, R.; Evans, P.; Ionides, J.; Packman, L.; Trotter, B.; Williams, D. *Protein Sci* 1999, 8, 1320–1331.
151. Smith, L. J.; Bolin, K. A.; Schwalbe, H.; MacArthur, M. W.; Thornton, J. M.; Dobson, C. M. *J Mol Biol* 1996, 255, 494–506.
152. Kim, B. H.; Kim, S. W. *Bull Korean Chem Soc* 1994, 9, 807–808.
153. Fields, G. B.; Prockop, D. J. *Biopolym - Pept Sci Sect* 1996, 40, 345–357.
154. Shoulders, M. D.; Raines, R. T. *Annu Rev Biochem* 2009, 78, 929–958.
155. Fields, G. B. *Org Biomol Chem* 2010, 8, 1237.
156. Martin, P. *Science (80-)* 1997, 276, 75–81.
157. Tanrikulu, I. C.; Forticaux, A.; Jin, S.; Raines, R. T. *Nat Chem* 2016, 8, 1008–1014.
158. Przybyla, D. E.; Chmielewski, J. *Biochemistry* 2010, 49, 4411–4419.
159. Neri, D.; Supuran, C. T. *Nat Rev Drug Discov* 2011, 10, 767–777.
160. Okuyama, K.; Hongo, C.; Fukushima, R.; Wu, G.; Narita, H.; Noguchi, K.; Tanaka, Y.; Nishino, N. *Biopolym - Pept Sci Sect* 2004, 76, 367–377.
161. Erdmann, R. S.; Wennemers, H. *Angew Chemie - Int Ed* 2011, 50, 6835–6838.
162. Kotch, F. W.; Guzei, I. A.; Raines, R. T. *J Am Chem Soc* 2008, 130, 2952–2953.
163. Holmgren, S. K.; Taylor, K. M.; Bretscher, L. E.; Raines, R. T. *Nature* 1998, 392, 666–667.
164. Bretscher, L. E.; Jenkins, C. L.; Taylor, K. M.; DeRider, M. L.; Raines, R. T. *J Am Chem Soc* 2001, 123, 777–778.

165. Eberhardt, E. S.; Panasik, N.; Raines, R. T. *J Am Chem Soc* 1996, 118, 12261–12266.
166. Sonntag, L.-S.; Schweizer, S.; Ochsenfeld, C.; Wennemers, H. *J Am Chem Soc* 2006, 128, 14697–14703.
167. PANASIK, N.; EBERHARDT, E. S.; EDISON, A. S.; POWELL, D. R.; RAINES, R. T. *Int J Pept Protein Res* 1994, 44, 262–269.
168. Bretscher, L. E.; Jenkins, C. L.; Taylor, K. M.; DeRider, M. L.; Raines, R. T. *J Am Chem Soc* 2001, 123, 777–778.
169. Erdmann, R. S.; Wennemers, H. *Bioorganic Med Chem* 2013, 21, 3565–3568.
170. Erdmann, R. S.; Wennemers, H. *Org Biomol Chem* 2012, 10, 1982.
171. Egli, J.; Siebler, C.; Maryasin, B.; Erdmann, R. S.; Bergande, C.; Ochsenfeld, C.; Wennemers, H. *Chem - A Eur J* 2017, 23, 7938–7944.
172. Hodges, J. A.; Raines, R. T. *J Am Chem Soc* 2005, 127, 15923–15932.
173. Barth, D.; Milbradt, A. G.; Renner, C.; Moroder, L. *ChemBioChem* 2004, 5, 79–86.
174. Furthmayr, H.; Wiedemann, H.; Timpl, R.; Odermatt, E.; Engel, J. *Biochem J* 1983, 211, 303–311.